




**ADVERTIMENT.** L'accés als continguts d'aquesta tesi queda condicionat a l'acceptació de les condicions d'ús establertes per la següent llicència Creative Commons:  [http://cat.creativecommons.org/?page\\_id=184](http://cat.creativecommons.org/?page_id=184)

**ADVERTENCIA.** El acceso a los contenidos de esta tesis queda condicionado a la aceptación de las condiciones de uso establecidas por la siguiente licencia Creative Commons:  <http://es.creativecommons.org/blog/licencias/>

**WARNING.** The access to the contents of this doctoral thesis it is limited to the acceptance of the use conditions set by the following Creative Commons license:  <https://creativecommons.org/licenses/?lang=en>



Universitat Autònoma de Barcelona

ESCOLA D'ENGINYERIA

Departament d'Enginyeria Electrònica

---

# Short Range Device platform for NFC and RFID wireless Telecommunications

---

Ph.D. thesis

**Author:** Josep Ignasi Cairó i Molins

**Supervisors:** Dr. Ferran Martín Antolín and Dr. Jordi Bonache Albacete

Programa de Doctorat en Enginyeria Electrònica i de Telecomunicació  
Universitat Autònoma de Barcelona  
Escola d'Enginyeria  
Departament d'Enginyeria Electrònica



Bellaterra (Cerdanyola del Vallés), July 2020



The undersigned, Ferran Martín Antolín, and Jordi Bonache Albacete, Professors of the Electronics Engineering Department (Engineering School) of the Universitat Autònoma de Barcelona,

CERTIFIES: that the thesis entitled Short Range Device platform for NFC and RFID wireless Telecommunications,"has been written by Josep Ignasi Cairó Molins under their supervision.

And hereby to acknowledge the above, sign the present.

J.I. Cairó Molins      F. Martín Antolín      J. Bonache Albacete

Programa de Doctorat en Enginyeria Electrònica i de  
Telecomunicació  
Universitat Autònoma de Barcelona  
Escola d'Enginyeria  
Departament d'Enginyeria Electrònica

Bellaterra (Cerdanyola del Vallés), July 2020





# Contents

<b>1</b>	<b>Introduction and Objectives</b>	<b>10</b>
1.1	Brief Introduction to short range devices (SRD) . . . . .	10
1.2	Objectives of the thesis . . . . .	11
<b>2</b>	<b>Budget Link and interference Analysis</b>	<b>13</b>
2.1	Introduction . . . . .	13
2.2	Type of tags and relation with the project . . . . .	14
2.3	UHF radio regulations . . . . .	15
2.4	RFID system read range . . . . .	16
2.4.1	Path Loss in long-range RFID . . . . .	17
2.4.2	Tag-limiting read range . . . . .	20
2.4.3	Reader-limiting read range . . . . .	23
2.4.4	Tag-Reader matching reading range . . . . .	25
2.5	Radio channel impairments . . . . .	27
2.5.1	Self-leakage (Self-Jammer) and interference from other radios . . . . .	28
2.5.2	Range degradation due to noise at the input . . . . .	33
2.5.3	Range correlation on phase noise . . . . .	33
2.5.4	Range reduction caused by mobile phone and other readers . . . . .	37
2.5.5	Read range reduction caused by proximity tags . . . . .	38
2.5.6	Detection circuit for non-desirable signals . . . . .	42
2.5.7	Read range influenced by material close to the tag . . . . .	44
2.6	RFID tag load modulation influence on read range . . . . .	45
2.7	System co-simulation . . . . .	53
2.7.1	Simulation results considering output filter . . . . .	54
2.7.2	Antenna modeling . . . . .	58
2.7.3	Complete UHF-RFID system . . . . .	58
2.8	Conclusions . . . . .	59

<b>3</b>	<b>HF antenna and charging circuit design</b>	<b>61</b>
3.1	Introduction . . . . .	61
3.2	HF-RFID system design . . . . .	61
3.2.1	Propagation Antenna Field Regions . . . . .	62
3.2.2	Coil antenna design . . . . .	63
3.2.3	Coil coupling effects . . . . .	69
3.2.4	HF-transmitter design . . . . .	71
3.2.5	Causes for reduction of coupling factor between coils . . . . .	76
3.3	Wireless Power Transfer (WPT) . . . . .	82
3.3.1	Resonance peak analysis . . . . .	82
3.3.2	Power transfer efficiency . . . . .	86
3.4	Conclusions . . . . .	98
<b>4</b>	<b>NFC to RFID circuit implementation</b>	<b>99</b>
4.1	Introduction . . . . .	99
4.2	UHF-RFID architecture . . . . .	99
4.2.1	Gen2 Protocol introduction . . . . .	99
4.2.2	EPC Global Class3 Protocol introduction . . . . .	100
4.2.3	UHF-RFID transceiver technologies . . . . .	100
4.2.4	UHF-Tag . . . . .	102
4.3	UHF-RFID electronics design . . . . .	104
4.4	UHF-RFID Compact antenna design . . . . .	105
4.5	NFC and WPT circuit design . . . . .	107
4.5.1	Power versus communication trade-off . . . . .	109
4.5.2	Bandwidth and efficiency tuning circuit . . . . .	109
4.5.3	Designing the tuning circuit and integration in NFC circuit . . . . .	112
4.6	Conclusions . . . . .	115
<b>5</b>	<b>Application in NFC and RFID sensing</b>	<b>116</b>
5.1	NFC and UHF-RFID sensor nodes with WPT . . . . .	116
5.2	System energy requirements . . . . .	116
5.2.1	Powering the RFID sensor . . . . .	116
5.2.2	RFID and NFC energy requirements . . . . .	117
5.3	Measurements . . . . .	120
5.4	Conclusions . . . . .	122
<b>6</b>	<b>Conclusions</b>	<b>123</b>

<b>A ANNEX: Commercial RFID tag performance</b>	<b>125</b>
<b>B ANNEX: Magnetic field in coil structures</b>	<b>126</b>
<b>C ANNEX: Losses in a HF-coupled loop-based system</b>	<b>129</b>
<b>D ANNEX: Probability Distribution functions</b>	<b>132</b>
<b>E ANNEX: DC induced voltage</b>	<b>134</b>



# List of Constants

## Constants

$k$	—	Wave number	—	$2\pi/\lambda$ .
$\mu_0$	—	Magnetic permeability	—	$4\pi \cdot 10^{-7} \text{ N/A}^2$ .
$\sigma_{Cu}$	—	Copper conductivity	—	$5.8 \cdot 10^6 \text{ S/m}$ .
$K$	—	Boltzmann constant	—	$1.32 \cdot 10^{-23} \text{ J/K}$ .
$c$	—	Light speed	—	$3 \cdot 10^8 \cdot \text{m/s}$ .

## Parameter definitions

$j$	—	Square root of minus 1 ( $\sqrt{-1}$ )
<i>Tesla</i>	—	Magnetic flux density unit $\frac{Wb}{m^2} = \frac{N \cdot s}{m \cdot C} = \frac{N}{A \cdot m} = 10^4 Gauss$
<i>dBm</i>	—	Power in milliwatt (P(mW)) at dB scale: $10 \cdot \log(P(mW))$
$erfc(\frac{x}{\sqrt{(2)}})$	—	Complementary erfc(x) function: $\frac{\sqrt{(2)}}{\sqrt{\pi i}} \int_x^\infty e^{-\frac{x^2}{2}} dx$
<i>Q-function</i>	—	$2Q(\sqrt{2}x) = erfc(x)$

# Acknowledgments

I would like to thanks specially to Dr. Ferran Martín and Dr. Jordi Bonache for providing the means to develop this research within the CIMITEC group at UAB, with their valuable advises to deeply understand some concepts in microwave devices that concern this work. Also, the possibility they provide in getting in contact with a very well knowledge group in the microwave community of researchers such as Dr. Ferran Paredes, Dr. Gerard Zamora or Dr. Gerard Sisó, and allowing me to use their facilities and laboratory.

My most special thanks to my wife Silvia, for believing in me, and being very comprehensive and patient for all the time that I have dedicated to this research at home. Also to my son Albert and my daughter Claudia, who have not been so much critical on their father dedication to this thesis, thank you!.

Last but certainly not least, I would like to heartfully thank my parents, for giving me support from the very beginning in this challenging task. In special to my father Dionís Cairó, who encouraged me to work hard to pursue my objectives. He would had been very proud if he could have seen this research finished, thank you!

# Summary

In this thesis, it is analyzed in detail aspects related to compact RFID radio communications design, and its interaction with different sort of elements starting from passive tags, the most widely used interface in RFID world. Ending with application of RFID sensor semi-passive tags, where a new sort of technologies are emerging in this interesting field.

With the idea of facilitating the introduction of such RFID sensing new technologies, we have developed and RFID reader that is very compact in design, and uses the mobile phone as the main human interface. For that purpose, the reader has to comply with compact small factor, such as small planar integrated antennas, very low power consumption and compact front end. Also must take special care of interference. The mobile phone is a device that includes so many radio sources, that we must ensure our radio can coexist with them, without being affected by their interference and, without affecting them.

In addition to the previous interference analysis, and design demonstration for RFID front-end, we have include some new concepts to mention:

- Analysis of limitations in read ranges for UHF-RFID technologies.
- Apply HF-RFID (such as NFC) not only for communications, but also for energy transfer.
- Optimization of NFC front-end when using radio for both communication (with mobile phone) and sending energy to remote sensors (charge remote battery).
- Prove of concept using our designed RFID sensing devices.
- Demonstrate new concepts of NFC-energy transfer for RFID sensors.

In order to help better understand the presented concepts, there are some analytical demonstrations explained in detail, with particular numerical examples being applied to our design, that have the intention to be taken as reference formulation and values for design.

Some concepts are explained based on simulations. In particular chapter 2 includes a system simulation that faces with different temporal and frequency effects. There are electromagnetic simulations (for antenna simulation), with electrical simulation (front-end devices) and system simulations (include RFID modulation and coding aspects). In chapter 3 many interaction effects between coils and RFID antennas are evaluated in detail. Also include the new concept that is used to optimize simultaneously communications and energy transfer between our NFC device and a new made RFID sensor tag.

There are many explanations on how the energy transfer circuit works, based on different configurations between primary and secondary circuits (transmitter and receiver), and optimization techniques. While chapter 4 and 5 are dedicated to hardware design, for reader in HF and UHF frequencies, as well as passive-sensor tag design. Measurements are taken not only showing the possibility to use NFC as a means for very short distance communications between our designed reader with the mobile phone, but also to transfer energy to new ultra-low power RFID sensors.



# 1 Introduction and Objectives

## 1.1 Brief Introduction to short range devices (SRD)

Radiofrequency identification (RFID) and near field communications (NFC) are wireless technologies that have experienced an exponential growth in recent years. Nowadays, RFID is a technology of use in several fields, such as item tracking, inventory, access control, etc., with RFID tags that can operate at several bands including, high-frequency (HF) band (13,56 MHz), ultra-high-frequency (UHF) band (860-915 MHz), and microwave bands (typically operating at 2.4 GHz). RFID is becoming very popular and widespread. The radio technology is improving time by time, system integration into the Radio Frequency Integrated Circuit (RFIC) is becoming more dense, antenna is more compact, the price lowers, and the performance improves. As an example, efforts to improve the RFIC performance in RFID tags such as sensitivity and the input impedance, allows for longer read ranges and wider operation bandwidth. For those reasons, it becomes feasible the possibility to integrate the radio in mobile or portable devices, which opens the possibility for its use in even more different situations and environments such as wireless sensors [1]. The number of applications where RFID is deployed is increasing, and so the number of reader transceivers and tag antennas.

With the advent of Internet of Things (IoT), there is a forecast that a larger number of RFID tags will be deployed with sensor functionality and data logging requirements. Also larger number of readers will be required with extended capabilities. RFID transceiver design is then a topic of interest to create higher performance readers with lower costs and more compact size.

RFID tags mainly use an identification code (ID) called Electronics Product Code (EPC), that is used by an external system to retrieve more information of the object from a back-end database. RFID tags come with additional memory in the form of Electrically Erasable Programmable Read-Only Memory (EEPROM), which can store more information than just the ID. The type of data format has been a topic of investigation for [2], such as Extensive Markup Language (XML) or Comma Separated Values (CSV), also there is the way to find methods on how to increase the memory on a tag.

- Passive tags can reach up to a maximum of 2KB memory or 32 KB for UHF-RFID [3]
- Active tags have memory between 16 bytes and 128 KB [4]

NFC is a technology that has been progressively growing in application such as mobile payment, contact-less payments, public transport, museum services, etc. It applies in the short range contact-less range, operating at the near field (inductive coupling) in the HF frequency band (13.56MHz). With the idea of using such technologies in every time more and more applications, there is a need also to increase integration, so to reduce radio architecture complexity, sometimes developing radio parts into the digital domain, named Software Defined Radio (SDR), having compact, simple and low cost radio transceiver designs that can be widely used. In the case of short distance communications links, the environment components do not affect so much to radio system performance. So while in RFID reading range can reach various meters, the surrounding environment has higher effects in the radio,

but in NFC where reading range is of few centimeters, and the surrounding conditions do not affect so much.

With the aim of extending the UHF RFID functionality into the Internet of Things (IoT) sensing field, in combination with the mobile phone or device equipped with NFC technology, with special focus on increasing the read range and tag reading technologies, the goal of this work is to design a compact RFID to NFC reader capable to communicate with mobile phones, integrating a low-profile patch antenna for an UHF RFID module, able to operate in contact with a mobile phone. The communication between the mobile phone and such a module is achieved by means of NFC technology, since most smartphones, tablets etc. are equipped with NFC capability

When performing mid-long range communications, the surrounding effects may influence the quality of signals, so it becomes necessary to be able to analyze and diagnose possible impairments effects caused in the radio link parameters. With the aim of being able to produce a tool that enables to work on these two previous standards, it is of importance to investigate several of the system requirements that can be critical for their radio performance. In the following section the main objectives of the system investigated in this work will be presented.

## 1.2 Objectives of the thesis

To expand the use of RFID passive or semi-passive technologies, there are several issues to be solved, either on the technology side as well as for the system part. Since most common applications are hand-held devices, compactness and long battery lasting are mandatory conditions to consider in the design phase. In that sense, we emphasize the importance of providing compact antenna design, perfectly matched and integrated with the RFIC or active part of the architecture for general performance optimization, as well as multi-standard functionality in the case that more than one protocol are desirable. A particular aspect considered here is the design of compact low profile microstrip patch antenna to operate in contact with a mobile phone, in addition to the design of a NFC antenna, that is intended to communicate with the NFC antenna already being used by actual mobile phones.

Aspects related to UHF and NFC antenna integration will be considered; compatibility with wireless power transfer for recharging the batteries of RFID or NFC sensors that require energy harvesting, or study possible interference caused by the own radio or external devices; spurious emissions caused by different radios and determined by local regulations such as ETSI in Europe [5] or FCC in US [6]. Other effects are self-leakage, local oscillator phase noise or other radios transmitting at adjacent channels are also relevant when evaluating performance degradation by an RFID system. Also strong coupling effects between antennas, and analysis on how they influence on communication range.

A main goal of this thesis is then, analyzing system performances of NFC and RFID as Short Range Devices (SRD) operating in the ISM bands (mainly 13.56 MHz and 868 MHz) with their peculiarities in terms of link budget analysis. Real implementation using conventional RFIC's supporting both NFC and UHF-Gen2 protocols, looking at common benefits in the ID but mainly for RFID-sensors and other Wireless Sensor Networks (WSN) applications. Such sensors can be battery powered, so in this case a novelty in circuit implementation is presented in this work, by applying the principles of wireless power transfer (WPT) into NFC in order to charge batteries at short distances attached into battery powered (BAP) wireless sensors.

In Fig. 3.30 we show the block diagram of all parts of the system that will be developed, and part of them analyzed and studied in detail in order to demonstrate feasibility of the system.

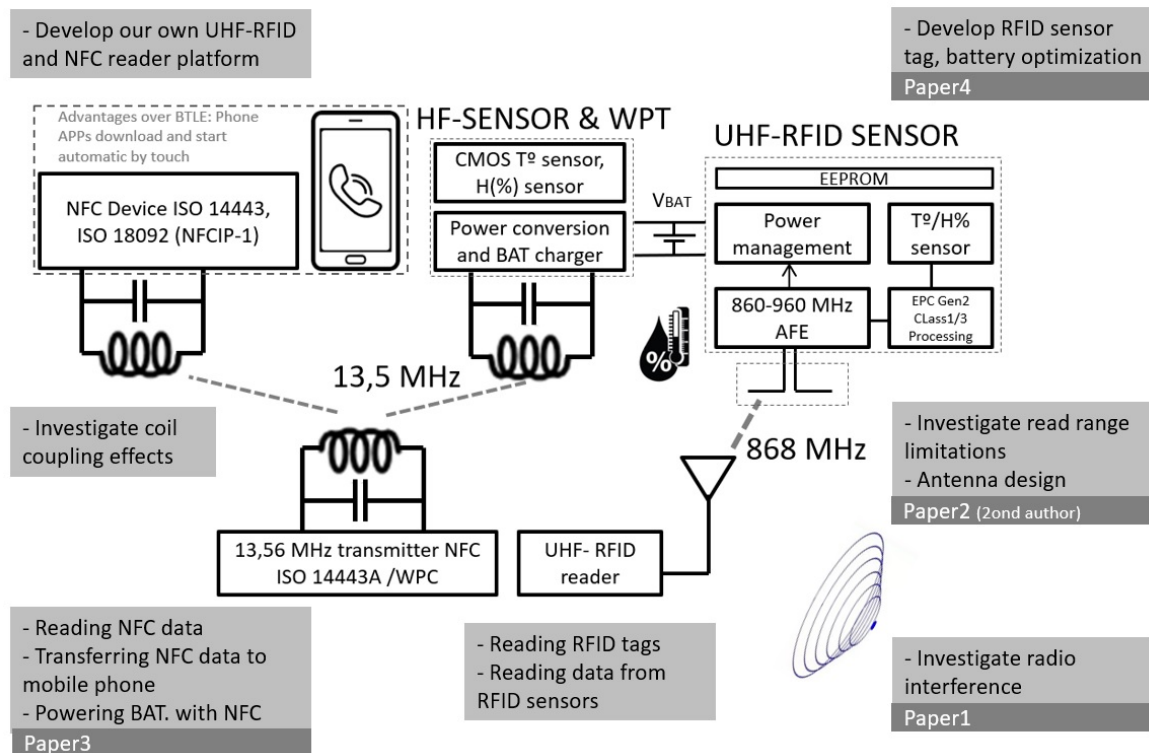


Figure 1.1: Bloc diagram of the system under investigation, highlighting special contributions of this work .

- Paper 1: "Review of interference sources in congested environments and its effects in UHF-RFID systems" [7]
- Paper 2: "Compact design of UHF RFID and NFC antennas for mobile phones" [8],
- Paper 3: "Reconfigurable system for Wireless Power Transfer (WPT) and Near Field Communications (NFC)" [9]
- Paper 4: "NFC system optimization for simultaneous powering and communication with wireless sensors" [10]

## 2 Budget Link and interference Analysis

### 2.1 Introduction

With the increasing number of applications where RFID tags are being considered, there is an interest in pushing its capabilities into the limits to expand its potential applications even further. This is sometimes equivalent as being able to use them in longer range communications links such as wireless sensor networks (WSN), where low consumption sensors are attached to an RFID tag, and the reader takes the measurement after powering the tag. Also means, being more prone to radio interference, couplings, or secondary effects due to design uncertainties. Transponders (or tags) that operate at the low-frequency (LF) band of 125 kHz [11] and HF 13,56 MHz have already been deployed for a number of years with the disadvantage of limited range typically less than 1 m, normally in the centimeter range. The maximum read range for passive RF tags at UHF frequencies is typically from 2 to 10 m [12], with either tag and reader optimized for the link. Actual mobile phones include NFC, by expanding mobile radio from NFC to RFID has direct influence on read range.

There are several effects influencing radio performance such as self-leakage, happening when continuous carrier is sent by the reader while receiving circuit is activated and, may lower receiver sensitivity. Due to its strong influence, some authors [13] are proposing methodologies for its compensation within the own chip. Local oscillator phase noise, is also influencing read range, since it will leak to the receiver passing through the power amplifier and isolator, overshadowing thermal noise component from receiver. This effect can be minimized, such as in [14], thanks to the short time difference between RFID transmitter and backscattering signal. The range correlation effect can further reduce such unwanted influence. Finally other important causes of range reduction are the ones caused by other radios, in adjacent channels or also propagating strong signals in nearby frequency bands.

From our knowledge there is no work dealing with a wide range of possibilities for interference issues that nowadays RFID readers are prone to, so in this work, are listed and analyzed in detail several sources of interference that may affect the RFID systems when coexisting with various sort of other radios mainly in the UHF band. Also the analytic expressions for such influences are detailed, introducing new aspects for such evaluation, such as the mutual tag antenna influence or new radio sources such as LTE (4G) that are penetrating in the UHF band. All of them are analyzed and some analytic examples are presented for a better understanding.

In our low power radio system application, long radio range is combined with low power consumption and multi-protocol application, so an study of range performance versus different sort of parameters is of much interest in order to evaluate the limitations of the radio. Several effects, internal and external from the radio, are analyzed.

Firstly a review of different standard wireless technologies being used nowadays, some applied already for WSN applications are being listed in table 2.1, with the most relevant indicators of its performance. Such metrics will be compared with the ones related to RFID-NFC technology in terms, for example, of sensitivity and power consumption, so one can justify design decisions in the use of most appropriate technology for a particular application.

Table 2.1: CONSUMPTION FROM TAG IC'S AND OTHER SRD'S RADIOS

Param.	Bluetooth	UWB	ZigBee	WiFi	BLE
IEEE spec.	802.15.1	802.15.3a	802.15.4	802.11a/b/g	
Freq. Band	2.4 GHz	3.1-10.6 GHz	868/915 MHz; 2.4 GHz	2.5; 5 GHz	2.4 GHz
Max. Rate	1-3 Mbps	114 Mbps	250 kbps	54 Mbps	1 Mbps
Nom. Range	10 m	10 m	10-100 m	100 m	
TX power	0-10 dBm	-41.3 dBm/MHz	-25;0 dBm	15;-20 dBm	10 dBm
N° channels	79	1-15	1/10; 16	14(2.4GHz)	40
Channel BW	1 MHz	0.5-7.5 GHz	0.3-0.6-2 MHz	22 MHz	2 MHz
Modulation	GFSK	DS-UWB, MB-OFDM	DSSS	DSS,CCK, OFDM	GFSK
$I_{TX}$	57 mA	227 mA	25 mA	300 mA	18 mA
$I_{RX}$	47 mA	227 mA	27 mA	280 mA	15 mA
$I_{Sby}$	20 $\mu$ A		3 $\mu$ A	20 $\mu$ A	1 $\mu$ A
Sensitivity	-90 dBm	-84 dBm	-92 dBm(2.4GHz) -102 dBm-UHF	-90 dBm(4Mbps) -74 dBm(54Mbps)	-87 to -93dBm
Chisep	BlueCore2	XS110	CC2430	CX53111	CC2540
VDD	1.8 V	3.3 V	3.0 V	3.3 V	3 V

## 2.2 Type of tags and relation with the project

In many applications, the read range of actual RFID tags at UHF and microwave is adequate, however, there are applications where an increase of read range would be appreciated. For that reason, it would be required to increase power consumption of few microamps from actual passive tags Fig. 2.1 (a).

Active tags such as the one in Fig. 2.1 (b), have the disadvantage of needing a battery with small form factor, so they do not need to rely on backscatter modulation, and use the battery instead to activate the circuit. That poses again a challenge in the low power radio design. Active and semi-active tags enable more sophisticated applications at the price of increasing cost, and typically limited lifetime.

In normal tag design, sensitivities range between -10 to -18 dBm, which makes clear the idea that in evaluating the reading range of tags, the limiting factor will be the tag. In [15] sensitivity increase is done, achieving an improvement of 9 dB by using a small battery. As the technology is pushed into the limits with better designs, one can reach very high sensitivity tag designs. This is the case of the design [16] that avoids using an internal regulator, neither a VCO, since it extracts the required clock signal from the downlink data. In [17] uses an active rectifier RF front-end biased in deep subthreshold near the saturation/linear boundary, to be able to operate at lower voltages, having effect on range.

The Surface-Acoustic-Wave (SAW) RFID technology, is also used to increase the reading range from passive tags, since it uses much less reader power to meet the reading requirements in non-ideal conditions. They normally operate with a spread-spectrum signal at 2.44 GHz, limited in data capacity and more tolerant to temperature variation than silicon IC tags. With a reader antenna gain of 15 dB it is possible to read tags at 18 m distance [18]. Those tags convert microwave electromagnetic signal into elastic Rayleigh waves via a piezoelectric effect, which are scattered by the electrodes on the surface of the crystal, wave reflectors that produce a uniquely encoded acoustic wave pulses, which are then reconverted to electrical signals at the antenna. Global SAW tag (GST) were first introduced in 2001.

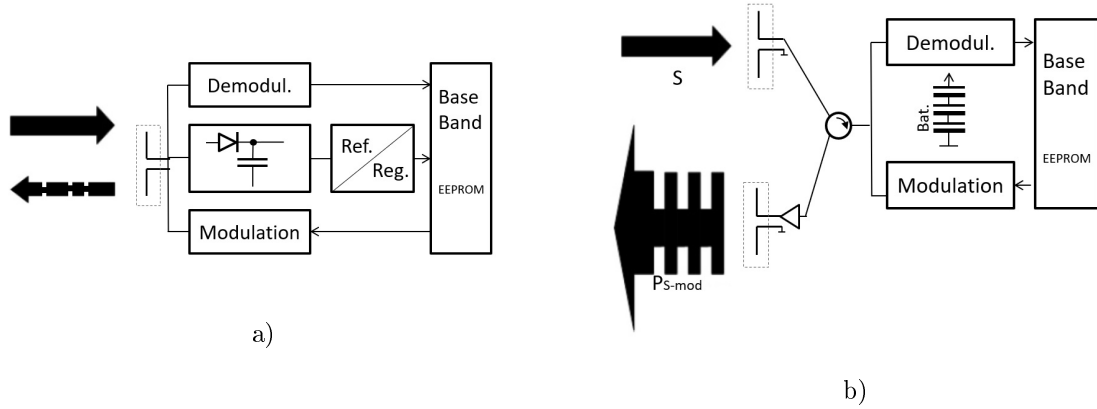


Figure 2.1: (a) A typical architecture of a passive tag IC, where antenna is connected directly to the receiver first stage (rectifying circuit), the demodulator and transmitter output, (b) Battery Assisted Passive tag providing better sensitivity in forward link and amplification in backscattering.

Very low power consumption is also achieved by [19], in a WSN applications at 2 GHz. In this case the design is based on new protocol that controls duty cycle, uses a radio with "uncertain-IF" architecture, which combines MEMS-based high-Q filtering and a free-running CMOS ring oscillator as the RF LO.

Table 2.2: LIST OF TAG IC'S POWER CONSUMPTIONS AND OTHER SRD'S RADIOS

Work	Power ( $\mu$ W)	Sensit. (dBm)	Energy/bit (pJ/bit)	Technology	year
[20]	NA	-14	NA	0.13 $\mu$ m CMOS	2007
[21]	240	-18.5	1600	0.35 Ti/Al/Ta/Al-Si	2009
[22]	2.6	-17	NA	0.18 $\mu$ m CMOS	2011
[16]	14	-21.2	98.6	0.18 $\mu$ m CMOS	2014
[23]	29R 71W	-12	NA	0.13 $\mu$ m CMOS	2014
[24]	(*)			0.13 $\mu$ m CMOS	2019

\* Features 55 dB TX leakage suppression

## 2.3 UHF radio regulations

In this work we will treat in more detail the different requirements to achieve an optimum read range, describing the different parameters that are influencing the reading range, and analyzing how it is possible to improve such performance always fulfilling radio regulations. Different properties of an RFID radio system will be presented, that are affecting its performance in major degree, so being able to understand properly the tuning peculiarities from the system. Some limitations are physical limitations, and many apply in the design, so they must be considered.

One parameter that affects the radio link and is fixed by regulation, is the transmit output power, to avoid harm to human health and frequency interference. In Europe, there is a limitation for the use of RFID in the UHF frequency band, being limited to the frequencies between 865 and 868 MHz, having to be compliant with the ETSI standard EN 302 208 [25] (updated version from the previous EN 300 220), with an equivalent radiated power shown in Fig. 2.2 ( $2 W^{ERP} = 3.2 W^{EIRP}$ ). In the United States, the equivalent exists with the FCC part 15 [6], a reader carrier frequency must be at one of the 50 channels spread evenly between 902.75 MHz and 926.25 MHz, hopping to each one and

dwelling no more than 400 ms. While readers can be manufactured to operate in only one region, at one frequency specified, the tags are designed for matching and backscattering across the entire 860 MHz to 960 MHz band.

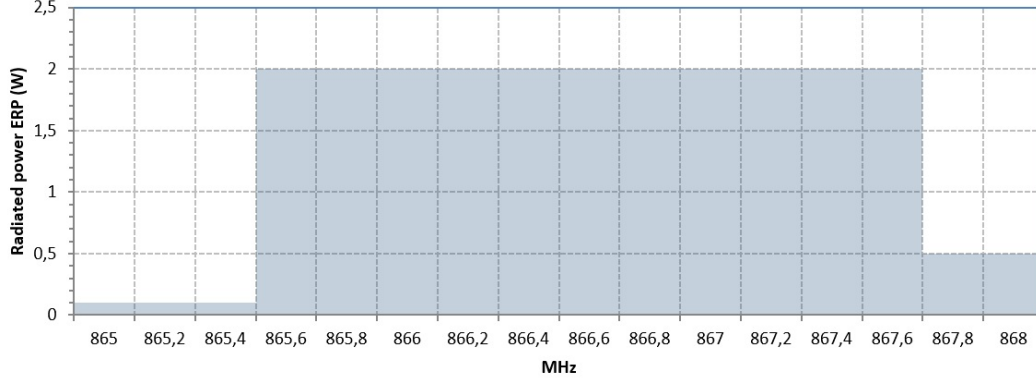


Figure 2.2: Equivalent radiated power allowed by the standard EN 302 208.

In other countries, other values are applied as an example: Argentina 902-928 MHz @ 4  $W^{ERP}$ ; China 920,5-924,5 @ 2  $W^{ERP}$ ; Australia 902-926 MHz @ 4  $W^{ERP}$ .

Table 2.3: COMPARISON OF RFID READ RANGE ACCORDING TO FREQUENCY BAND

	Frequency	Range	Ex. Standard
LF	125 kHz	< 40 cm	ISO 18000-6A
HF	13.56 MHz	up to 10 cm	ISO 14443
	13.56 MHz	up to 1 m	ISO 18000-3
HF-NFC	13.56 MHz	1 to 1.5 m	ISO 15693
UHF	850 to 950 MHz	10 m	ISO 18000-6C
Microwave	2.4 to 2.45 GHz	100 m	ISO 18000-4

Table 2.4: ASSIGNED UHF FREQUENCIES FOR DIFFERENT REGIONS

Region	Freq. band	Bandwidth
Europe	866-869 MHz	3 MHz
America	902-928 MHz	26 MHz
Asia	950-956 MHz	6 MHz

## 2.4 RFID system read range

In a link budget analysis, where the operating frequency is fixed, and supposing a fixed transmit power, the maximum reading range of an RFID system for a determined environment, is mainly limited by antenna gain, space losses, and receiver sensitivity. Having a reader transmitter and a tag receiver that backscatters the demodulated signal back to the reader, the range by this RFID system may

be classified into tag-limiting and reader-limiting read range. Due to the passive nature of the tags, the link will be mainly limited by the tag. But since we open the filed to RFID sensor tags and semipassive tags, it is of interest to contemplate other possibilities

In the case of RFID systems, the radio range is limited by some factors that differ from other radio systems due to the fact that the receiver (tag) has to power itself from the incoming signal, and use a very simple modulation (ASK, OOK). The reader varies the transmit power and thus the power available by the tag; the tag therefore needs some shunted power supply capacitance to sustain power for up to about 10  $\mu s$  during modulation, enabling data rates between 40 kbps and 640 kbps.

Read ranges of passive UHF-RFID tags are limited by the tags ability to power itself from the incoming continuous wave (CW) signal from the reader, rectifying it into the DC supply. While for HF tags the field strength of the magnetic field at zero distance is between 1.5 and 7.5 A/m, for UHF tags we specify transmitted power of 1 to 0.5 W maximum. High efficiency rectifying designs are normally required to optimize the energy capture, they range in efficiency between 15% to 80% [12]. In some cases even the reader transmitted waveform has been optimized in order to increase tag efficiency when powering from the incoming electromagnetic field [26]. Other possibilities that affect positively in increasing read-range are the increase in antenna gain or the matching network.

In addition to the limitation of self-powered receiver, when considering long range RFID systems, the losses in the path from reader to tag, back to the reader, should be also considered, similarly as in other communications systems when the radio range starts to increase. Path loss is strongly dependent on propagation environment [27], and position of surrounding objects, so the characterization of such objects is of importance.

### 2.4.1 Path Loss in long-range RFID

In the case of UHF-RFID, where high power can be transmitted at high operating frequency, long to medium range electromagnetic waves can suffer from multiple reflections inducing severe path losses, due to dynamic channel conditions (varying soil types) that also attenuate the electromagnetic waves due to absorption by bricks, rocks, soil, and liquids. Such environment variations in the communication channel, does not happen when using high frequency (HF) and low frequency (LF) bands, where the draw-back is the need for using large antennas. In fact, multipathing (relaying) can be used in magnetic induction communication as an advantage. Furthermore, the magnetic permeability of earth and water are similar to that of air, even so, there are also path losses (PL), since magnetic fields can penetrate water, sediments and rocks and are very well shielded by metallic objects.

A good interesting point to evaluate PL in RFID systems, is to consider other telecommunication systems such as cellular, where PL has been vastly evaluated. In fact one can use several models present in the literature to estimate PL. Since path link is much longer (1-10 m) than the wavelength ( $\lambda = 0.3m @ 900MHz$ ), between the transmitter and receiver it is possible to have a clear line-of-sight (LOS) path, and some reflection paths, so path can be modeled using **Rician channel**. For more multipath environments it can be used the **Rayleigh** channel model. One model that is very well suited for modeling LOS radio channel is the **Two-Ray-model** that uses the two-ray theory, using the contributions of the two plane waves as depicted in Fig. 2.3. In this case the path loss model becomes represented by the following expression [28]:

$$L_p = -10 \log \left( \frac{\lambda}{4\pi} \right)^2 - 10 \log \left[ \left| \frac{1}{r_1} e^{-jkr_1} + \Gamma(\theta) \frac{1}{r_2} e^{-jkr_2} \right|^2 \right] \quad (2.1)$$

- $r_1$  is the direct distance from the transmitter to the receiver;  $r_1 = \sqrt{(h_1 - h_2)^2 + r^2}$
- $r_2$  is the distance after reflection into the ground;  $r_2 = \frac{h_1}{\cos \alpha} + \frac{h_2}{\cos \alpha}$



- $k$  is the wave number or the number of waves that exist over a specified distance  $k = \frac{2\pi}{\lambda}$ , and  $\lambda$  is the wavelength.
- $\Gamma(\theta)$  is the reflection coefficient at the angle direction  $\theta$

$$\Gamma(\theta) = \frac{\cos(\theta) - a\sqrt{\epsilon_r - \sin^2\theta}}{\cos(\theta) + a\sqrt{\epsilon_r - \sin^2\theta}} \quad (2.2)$$

The reflection coefficient depends on the angle of incidence  $\theta$ , and the polarization. Where the angle  $\theta = 90^\circ - \alpha$ , and  $a = 1/\epsilon_r$  for vertical polarization, or  $a = 1$  for horizontal polarization (Fig. 2.3 (a),  $\epsilon_r$  being the relative permittivity of the media).

It is interesting to note from Fig. 2.3 (b) how the two-ray causes variation in attenuation with respect to the ideal path loss where attenuation decreases 20 dB/dec steadily. For the particular case of the long range RFID system operating at the UHF band, with particular antenna height, the model may present strong deeps at certain distances where both waves interact destructively. When considering antenna polarization we see that, in the locations where  $|\Gamma(\theta)|$  is larger in horizontal polarization, in vertical polarization is of opposite sign, they change alternatively versus distance.

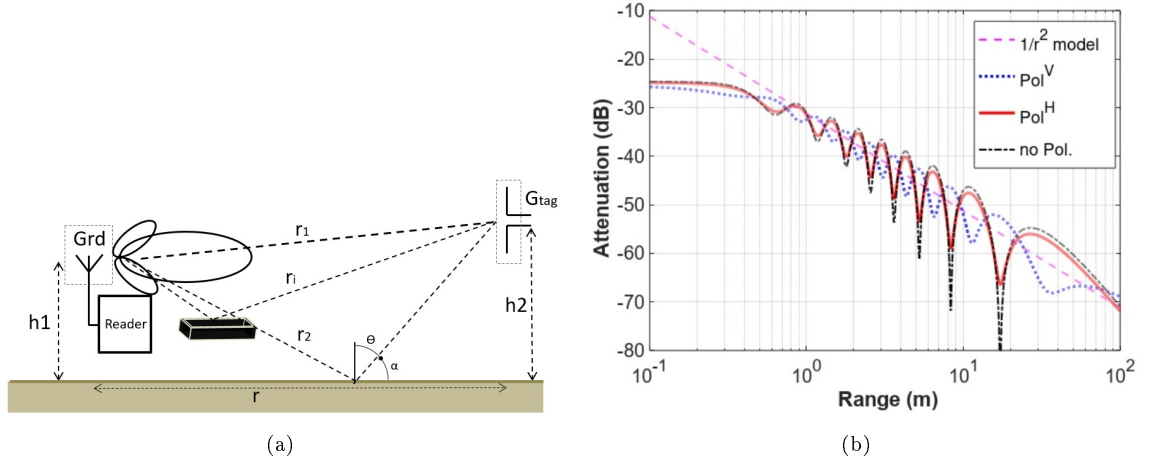


Figure 2.3: (a) Two-ray model representing the path loss between two antennas separated a distance  $r_1$ . (b) Free Space Attenuation for  $h_1 = 1.5$  m,  $h_2 = 2$  m, ground  $\epsilon_r = 15-j60$ ,  $\sigma = 5\mu\Omega/\text{m}$  [29]

In addition to the case of long-range RFID, we introduce the possibility of having more than two ray model for the propagation of radio waves from reader to the tag. We can introduce here the possibility of having several paths due to the presence of different walls or obstacles in the line-of-sight (LOS) of the incident radio wave, so in that case one can define a **multi-path model** for the path loss [30];

$$L_p = -10\log\left(\frac{\lambda}{4\pi}\right)^2 - 10\log\left[\left|G_1^{1/2}\frac{1}{r_1}e^{-jkr_1} + G_i^{1/2}\sum_{i=1}^n\Gamma_i(\theta)\frac{1}{r_i}e^{-jkr_i}\right|^2\right] \quad (2.3)$$

where the antennas are considered to be isotropic (antenna gains independent of the propagation direction ( $G(\theta_i) = G_i$ );

- $G_1$  accounts for the receiver and transmitter antenna gain at the LOS direction,

- $G_i$  accounts for the receiver and transmitter antenna gain of the propagation way numbered  $i$  and,
- $\Gamma(\theta)$  is the reflection coefficient of each ray

From the electromagnetic wave power density incident to the tag antenna in free space  $S_{tag}$ , the power absorbed by the antenna is the maximum power that can be delivered to the matching conjugate load  $P_{RX_{tag}}$ . Using the expression of effective area of the antenna, given by  $A_{tag}$  [31], and being  $P_{TX_{rd}}$  the transmit power of the reader, and  $S_{tag}$  the tag sensitivity:

$$P_{RX_{tag}} = S_{tag} \cdot A_{tag}; \quad A_{tag} = \frac{\lambda^2}{4\pi} G_{tag}; \quad \rightarrow \quad P_{RX_{tag}} = \frac{P_{TX_{rd}} G_{rd}}{4\pi r^2} \frac{\lambda^2}{4\pi} G_{tag} \quad (2.4)$$

Performing an RF link analysis, where the electromagnetic wave transmitted by the reader antenna radiates to the tag through the air, and then is backscattered or reversely propagated back to the reader, carrying the information stored in the tag, one can start with the modification of the Friis transmission equation in order to represent the budgeted analysis [32]. In the ideal case that all the RF energy caught by the tag is re-radiated back to the reader (100% RF to DC efficiency and perfect match), the maximum distance that a reader can reach is obtained first looking at the power received by the tag:

$$P_{RX_{tag}} = \frac{P_{TX_{rd}} G_{rd}}{4\pi r^2} A_{tag} = P_{TX_{rd}} G_{rd} G_{tag} \left( \frac{\lambda}{4\pi r} \right)^2 \quad (2.5)$$

where

- $P_{RX_{tag}}$  is the tag receiving power,
- $A_{tag} = G_{tag} \lambda^2 / (4\pi)$  is the equivalent aperture of tag antenna, and
- $P_{TX_{rd}}$  is the power being transmitted by the reader and
- $G_{rd}, G_{tag}$  are reader and tag antenna gain respectively.

To become more realistic one should introduce several phenomena that degrades or influence the range performance tag-reader and are found in reality such as:

- $\Delta G$ : antenna gain penalty due to detuning or close proximity of tag antenna with materials.
- $L_p$ : a more realistic path model such as *multi-path model*
- $\rho$ : reflection coefficient of the tag given by

$$\rho = \frac{Z_{ant} - Z_{ic}^*}{Z_{ant} + Z_{ic}} \quad (2.6)$$

where  $Z_{ant}$  is the impedance of the antenna, and  $Z_{ic}$  is the input impedance presented by the tag IC. Expressing in dB the previous expression:

$$P_{RX_{tag}}(dBm) = P_{TX_{rd}}(dBm) + G_{rd}(dB) + G_{tag}(dB) + 10 \log(1 - |\rho|^2) + \Delta G(dB) - L_p(dB) \quad (2.7)$$

with  $L_p$  being path loss term expressed as  $L_p = \left( \frac{\lambda}{4\pi r} \right)^2$ .

Some authors define additional losses named Modulation Losses that can vary from 6 dB to 12 dB, defined from previous expressions as:

$$ML = 10\Delta\log(1 - |\rho|^2) + \Delta G(\text{dB}) \quad (2.8)$$

From this received power at the tag, and with the previous assumption of having 100% RF to DC conversion efficiency, the returned power at the reader can be found to be:

$$P_{RX_{rd}} = \frac{P_{RX_{tag}} G_{tag}}{4\pi r^2} A_{rd} = P_{TX_{rd}} G_{rd}^2 G_{tag}^2 \left( \frac{\lambda}{4\pi r} \right)^4 \quad (2.9)$$

Introducing the before mentioned non idealities, the received power can be expressed as;

$$P_{RX_{rd}}(\text{dBm}) = P_{TX_{rd}}(\text{dBm}) + 2G_{rd}(\text{dB}) + 2G_{tag}(\text{dB}) + 20\log(|\rho'|) + 2\Delta G(\text{dB}) - 2L_p(\text{dB}) \quad (2.10)$$

where  $\rho'$  is the differential reflection coefficient of tag ( $\rho' = \rho_1 - \rho_2$ , where  $\rho_1$  and  $\rho_2$  are the 0 and 1 states of the chip reflection coefficient, which depends on the chip tag).

If we would like to double the reading range, then the transmit power, the antenna gain, or the sensitivity of the receiver should increase at least 12dB their effect, which becomes a very challenging goal to achieve. Since that means for an antenna gain to increase by 6 dB, or for the reader transmitter, to increase power by 12 dB, which might imply introduce external power amplifier (PA), or in some case radiating outside the regulated limits (FCC, ETSI,...).

The slope of the path loss for the complete link versus distance is  $n=4$  (40 dB/dec). For real path loss it can behave with lower exponential factor than in free space. In fact from Fig. 2.3 one can see that for a one way link, the path loss in the range between 1 to 3 meters (typical RFID), between -30 to -48 dB attenuation, so for the complete path, the worst case would be -60 to -96 dB attenuation.



#### How to double read range?

If we intend to double the read range, using Eq.(2.9) we can see that we need extra 12 dB ( $10 \cdot \log(2^4)$ ). One possibility would be to use a 6 dB higher antenna gain, or 12 dB higher transmit power.

### 2.4.2 Tag-limiting read range

For RFID radio link, the most common case scenario to evaluate range performance is when the tag is limiting the reading range in the whole link. This is due to the fact that for passive tags, the device needs to obtain energy from the same carrier that provides communication data, and during short time intervals to power-up the IC to supply enough energy for sending back (backscattering) its information. Typical IC require of few tens of microwatts at somewhat more than 1 Volt [33]. The energy supplied to do so is small, since much losses occur when converting the energy (electric signals into radiating waves and back to electric signals), so that will penalty the reading range.

As it is shown in chapter 4, there are some examples of tag sensitivities from high performance IC's that can be found nowadays in the market or are in design phase. A very high tag sensitivity is reached as -21 dBm, for passive tags. There are other examples found in research papers, as in the

case of [19] which combines MEMS-based high-Q filtering and a free-running CMOS ring oscillator as the RF LO in 90 nm, that allows to power the radio at 0.5 V, consuming 52  $\mu$ W and reaching a sensitivity of -72 dBm. Another example of extremely low power consumption receiver is cited in [17]. In this case, it uses as a first stage, a self-biased rectifier with DTMOs device in deep-subthreshold with sensitivity of -41 dBm.

The powering function in passive tags is performed by means of voltage multiplier rectifier, converting the low RF input power signal into DC supply voltage. The element for rectifying the RF voltage and convert to DC, is a diode P-N junction, that needs large forward break-over voltage, so the powering needs are high. Such penalty can be reduced by using other diodes such as hot carrier diodes and Schottky. So a critical factor to perform such function will be the availability of Schottky diodes with low drop voltage  $V_s \leq 0.3V$ , because the antenna input voltage needs to overcome such voltage. Also large saturation current  $I_s$  and small series resistance  $R_s$  are needed. The voltage at radiofrequency ( $V_{rf}$ ) at the input of the rectifying circuit, and the rectification efficiency becomes:

$$V_{rf} = \sqrt{\frac{P_{rf}}{Re\{I_{in}\}}} \quad E(\%) = \frac{V_{BAT} \cdot I_{DC}}{P_{rf}} \cdot 100 \quad (2.11)$$

The rectifying circuit is used to store energy into a capacitor or small battery ( $V_{BAT}$ ). Its efficiency will depend on the input power RF level  $P_{rf}$ .

Other factors that influence the power conversion are the losses in the IC. Large junction and substrate capacitances may dominate power losses, not only in rectifying stage design but also in the RFIC. They are determining factor of total power losses, since for standard CMOS process used to build RFIC, there is a quadratic dependency of substrate loss on capacitance ( $C_{sub}$ ) as well as on frequency ( $\omega = 2\pi f$ ), which explains why there is much lower efficiency of the front-end at 2.45 GHz compared with the 868 or 915 MHz design. In Eq.(2.12) the losses at the CMOS substrate are expressed proportional to the square of  $C_{sub}$  and  $freq$ .

$$P_{sub} = \frac{1}{2}v^2 \frac{R_{sub}}{R_{sub}^2 + (\omega C_{sub})^{-2}} \approx \frac{1}{2}v^2 R_{sub}(\omega C_{sub})^2 \quad (2.12)$$

approximation valid for typical low-resistivity CMOS substrates where  $R_{sub}\omega C_{sub} \ll 1$ ;

- $v$  is the device RF peak voltage with respect to substrate
- $R_{sub}$  is the series resistance of substrate layer,
- $C_{sub}$  is the substrate capacitance

Technology limitations for devices conforming the front-end IC are then also considered in the design phase of RFID systems, basic effects to take into account are frequency operation and chip area. The ideal technology would support Schottky diodes with an affordable channel length for cost reasons. In [33] a tag IC using 0.18  $\mu$ m is designed, consuming only 7.4  $\mu$ W with a sensitivity of -12 dBm. It integrates a 600 pF capacitor as storage, and uses 0.3 V Schottky diode. In [21] uses 90 and 140 mV turn-on Schottky diodes, fabricated with Ti/Al/Ta/Al 0,35  $\mu$ m CMOS. The sensitivity is -14.8 dBm.

In addition to RFIC technology, and RF-to-DC energy conversion losses (some values of power conversion efficiency range as 65% [34], 42.7% as in [35]), the main factors contributing to range limitation are tag sensitivity ( $P_{RX_{tag}}$ ), determined by RFIC stages, power consumption ( $V_{BAT}$ ,  $I_{DC}$ ), and typically from RFID systems, the tag **back-scattering efficiency** ( $\chi$ ). These parameters influence system characteristics, such as forward and reverse tag read range.

Other non idealities can be included in the tag reception, making it possible to represent some effects that also will influence the receiving power before reaching the tag-IC such as:

- $\tau_M$  The **impedance matching coefficient** [36], that will account for the losses due to reflections between antenna and IC.
- $\tau_p$  The **polarization mismatch** or polarization efficiency.
- $G_{tag}$  The tag antenna gain,

By including the previous mentioned effects, the basic range estimation is obtained by:

$$P_{RX_{tag}} = P_{TX_{rd}} G_{rd} G_{tag} \left( \frac{\lambda}{4\pi r} \right)^2 \tau_M \tau_p; \rightarrow r = \frac{\lambda}{4\pi} \sqrt{\frac{P_{TX_{rd}} G_{rd} G_{tag} \cdot \tau_M \cdot \tau_p}{P_{RX_{tag}}}} \quad (2.13)$$



### Technology limitations

Read range depends on technology such as availability of Schotcky diodes for the RF to DC converter, substrate losses Eq.(2.12), tag sensitivity Eq.(2.13), or possible mismatches between tag-IC and tag antenna impedance.

For the tag limiting factors we define the two main factors that contribute to such limitations, one is the *Tag sensitivity* ( $P_{RX_{tag}}$ ), which corresponds the the minimum incident power needed at the tag antenna to properly read (or write with different sensitivity than read operation) to the tag IC. Another is the  $P_{ic}$  that it is linked to chip sensitivity and tag antenna parameters by

$$P_{ic} = \tau_M \cdot P_{RX_{tag}}; \quad (2.14)$$

Let us determine the impedance mismatch effect on the tag receiving power. From the receive tag equivalent circuit (see Fig. 2.4) where  $U_a$  is the open circuit voltage generated in the tag,  $Z_{tag}$  is the internal impedance of the tag, the power  $P_{ic}$  applied into the load  $Z_{ic}$  is given by  $P_{ic} = 1/2 \Re\{v_a^* \cdot i_{ic}\} = 1/2 \Re\{Z_{ic} \cdot |I_{ic}|^2\}$ , where  $I_{ic}$  is the current into the load. Taking the load power as stated in Eq.(2.15) the maximum power into the load will occur for  $Z_{ic} = Z_{tag}^*$ , so when  $R_{ic} = R_s$  and,  $X_{ic} = -X_{tag}$ , that coincides with the available power from the antenna Fig. 2.4;

- $Z_{tag} = jX_{tag} + (R_{tag} + R_r) = jX_{tag} + R_s$ ; is the Tag antenna impedance with  $R_s = R_r + R_{tag}$ .
- $Z_{ic} = R_{ic} + jX_{ic}$ ; is the impedance seen at the tag IC terminals to be switched during modulation (Annex B).

$$P_{ic} = \frac{1}{2} |I_{ic}|^2 \Re\{Z_{ic}\} = \frac{1}{2} \left| \frac{U_a}{Z_{ic} + Z_{tag}} \right|^2 R_{ic} = \frac{1}{8} \frac{|U_a|^2}{R_s} \left( \frac{4R_{ic}R_s}{|Z_{ic} + Z_{tag}|^2} \right) = P_{RX_{tag}} \cdot \tau_M \quad (2.15)$$

where

$$P_{avl} = P_{RX_{tag}} = \frac{1}{8} \frac{|U_a|^2}{R_s} \quad \text{and} \quad \tau_M = \frac{4R_s R_{ic}}{|Z_{ic} + Z_{tag}|^2} \quad (2.16)$$

being  $P_{avl}$  the input available power that can be extracted from the antenna into the IC. Once considered mismatch caused by possible polarization effects between reader and tag antennas, as well as mismatch effects between tag antenna and tag IC, the read range will be limited by the transmitted power of the reader  $P_{TX_{rd}}$  and tag sensitivity  $P_{RX_{tag}}$ .

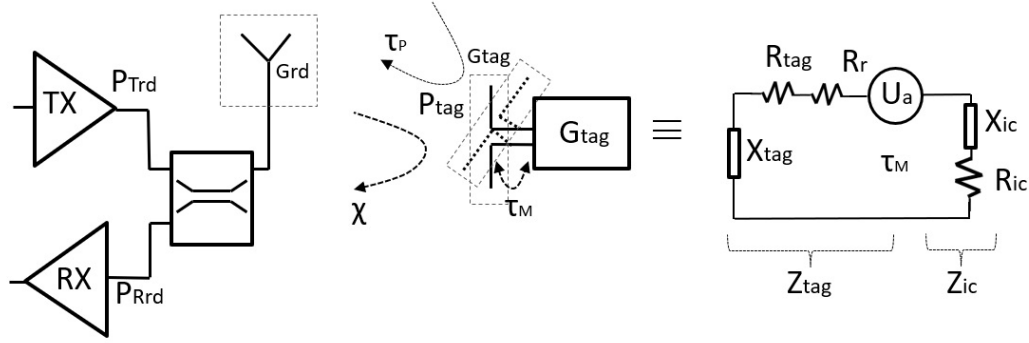


Figure 2.4: Tag equivalent circuit, showing some of the parameters that affect the reading range between a reader and a tag antenna (dipole  $R_{tag} = 72 \Omega$ ),  $\chi$  represents backscattering power.



### Environment parameters degrading read range

In Eq.(2.7) one introduces  $\Delta G$ : as antenna gain penalty due to detuning for materials in close proximity to antenna. Also in Eq.(2.13) is introduced  $\tau_M$ , the impedance matching coefficient accounting for losses due to reflections, similar to  $\Delta G$ : mismatch Eq.(2.16), and polarization losses Eq.(2.3).

### 2.4.3 Reader-limiting read range

In the case the reader is limiting the read range, there will be enough strength back-scattered signal from the tag reaching the reader receiver antenna ( $P_{RX_{rd}}$ ), that it is able to demodulate correctly the signal according to the minimum SNR required, until one level where the received signal reaches the receiver sensitivity ( $S_{rd}$ ). In that case, it is needed to include both paths from reader to the tag, back to the reader in the analysis:

$$r = \frac{\lambda}{4\pi} \sqrt[4]{\frac{P_{TX_{rd}} G_{rd}^2 G_{tag}^2}{P_{RX_{rd}}}} \quad (2.17)$$

In Fig. 2.5 are illustrated the results, for a link performance considering both cases, tag-limiting and reader-limiting reading range using the parameters summarized in the following case. Anyhow, since tag technology is commonly passive, range is commonly limited by the tag. In the case that tag technology improves, or active tags are being used, the reader sensibility will be a concern.

When including IC mismatches in the tag, or demodulation effects in the detection circuit, efficiencies of the RF to DC converters and internal losses in the tag, all such effects can be included in what is known as Modulation Losses (ML). In our cases we include such realistic or practical losses in one term, break down previously in different terms, but that for practical reasons can be considered between 6 dB and 12 dB:

$$r = \frac{\lambda}{4\pi} \sqrt[4]{\frac{P_{TX_{rd}} G_{rd}^2 G_{tag}^2 \cdot ML}{P_{RX_{rd}}}} \quad (2.18)$$

**Case:** Evaluation of the optimum reader sensitivity for a read range of 1.8 m with tag and reader antenna gains of  $G_{tag} = 2.15 \text{ dB}$  and  $G_{rd} = 2 \text{ dB}$ .

- Using Eq.(2.17) with a reader sensitivity of  $S_{rd} = -50 \text{ dBm}$ , one can reach 1.8 m distance.
- Using Eq.(2.5) we need a tag with a sensitivity of  $S_{rd} = -17.5 \text{ dBm}$  in order to reach the 1.8 m reading range.

The values presented for tag sensitivity are close to commercial values, so  $-17 \text{ dBm}$  as achieved by Alien Higgs [37], other are lower such as  $S_{tag} = -9 \text{ dBm}$  from Impinj Monza tag. These are other values of tag sensitivities referred in table 2.2 (Annex A).

Including the factor of  $ML = 6 \text{ dB}$ , the required tag sensitivity should improve by  $6 \text{ dB}$  down to  $-24 \text{ dBm}$ , while in the cases of the reader should be  $-56 \text{ dBm}$ .

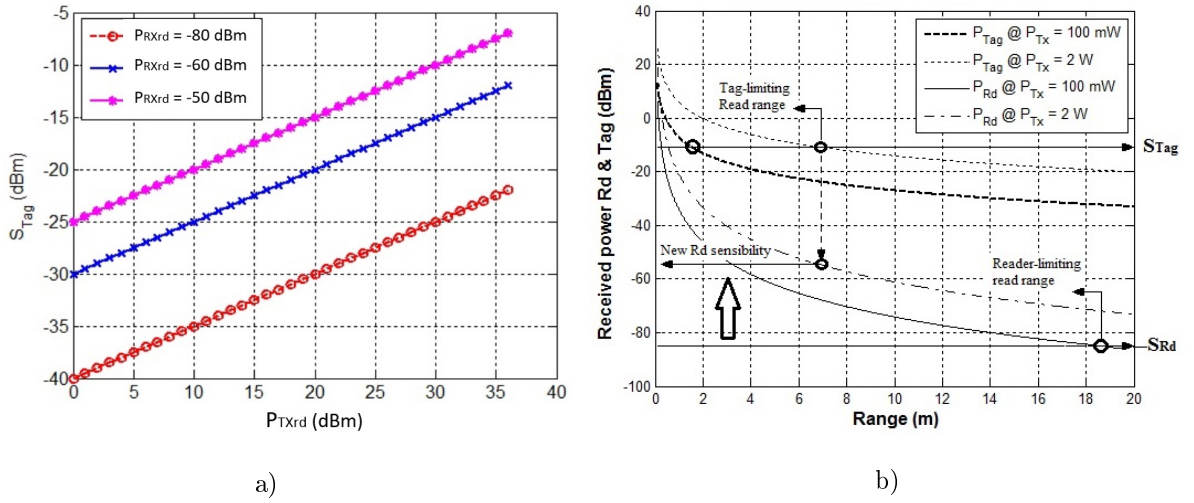


Figure 2.5: RFID Reader-tag link analysis: (a) Tag sensitivity as a function of Reader transmit power for different reader sensitivities. (b) Tag-limited and Reader-limited read range for  $G_{rd} = 2 \text{ dB}$  and  $G_{tag} = 2.15 \text{ dB}$

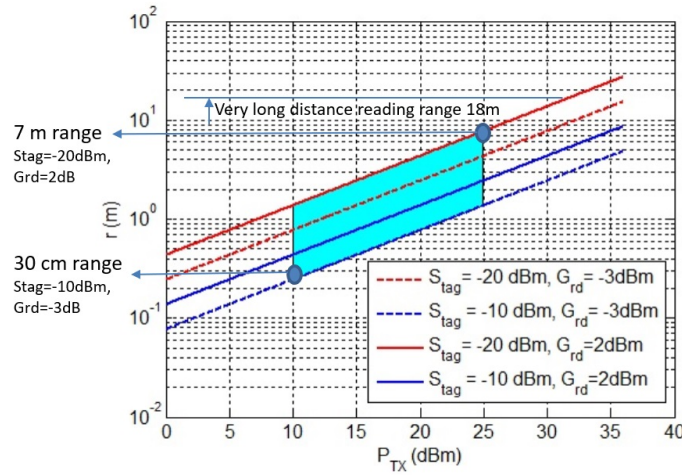


Figure 2.6: Reading range for different tag sensitivities in case of  $G_{tag} = 2$  dB and for  $G_{rd} = -3$  dB and  $+2$  dB. Shadow area is read range for low power reader ( $10 < P_{TX} < 25$  dBm).

#### 2.4.4 Tag-Reader matching reading range

To get a better understanding of the capabilities of RFID systems in the optimization of the power range, one can consider the tag and reader as two separate radios, with their limitations that need to be optimized as a whole in the system. According to what has been observed so far, the optimal operation distance would be the one that, with the power transmitted by the reader, there is just enough energy to power-up the tag and reach threshold sensibility for correct demodulating incoming signal, and back-scatter its information to the reader with enough power, to reach the sensitivity of reader receiver, and to properly demodulate the information, which is determined by the minimum SNR (acceptable Bit Error Rate -  $BER_{th}$ ).

The examples mentioned before on technology improvement, show a tendency towards increase IC sensitivities, so one can expect in the future, an increase on read-range limited only by the available technology. Looking at Fig. 2.5 there is still a lot of room to achieve an ideal performance, where the reader-limiter range would coincide with tag-limiting range. In such ideal matching situation one should accomplish:

$$S_{tag} = \sqrt{P_{TXrd} \cdot S_{rd}} \quad (2.19)$$



**Case:** Evaluation of the reading range for tag-reader matching conditions, in the case that reader transmit power is  $P_{TX_{rd}} = 20 \text{ dBm}$  and antenna gains of:  $G_{rd} = 2\text{dB}$ ,  $G_{tag} = 2, 15\text{dB}$ . Looking at Fig. 2.5 (a):

- With a reader with a very good sensitivity of  $-90 \text{ dBm}$ , the required tag sensitivity would need to be  $S_{tag} = -35 \text{ dBm}$ , and the range 25 m.
- With a reader sensitivity of  $-80 \text{ dBm}$ , the required tag sensitivity would need to be  $S_{tag} = -30 \text{ dBm}$ , and the range 14 m.
- With a reader sensitivity of  $-60 \text{ dBm}$ , the required tag sensitivity would need to be  $S_{tag} = -20 \text{ dBm}$ , and a range of 4 m.

However it is difficult to design a reader with sensitivity below  $-80 \text{ dBm}$  due to self-leakage effects for imperfect isolation of circulator, that degradates sensitivity to  $-50$  and  $-60 \text{ dBm}$ , and even more difficult to achieve passive RFID IC's with  $-35 \text{ dBm}$  sensitivities. The last case, seems to be the more reasonable in terms of state of the art tag technology. In such a case, and with a reader with pour antenna gain characteristics such as  $G_{rd} = -3 \text{ dB}$ , due to for example integration into small hand held devices such as our case, and a tag antenna with gain  $G_{tag} = 2, 15 \text{ dB}$ , the accomplished reading range that would match the one from direct link and direct plus back-scattered link would be **2.5 m**. If one includes a margin factor of  $10 \text{ dB}$  (mismatch, reflections in materials, polarization effects) the range would lower to **1.4 m**.

Due to the possibility of applying several design improvements in the reader side, the limitations will come from the IC-tag technology. As the tag increases sensitivity the reading range will increase. That will be the main limiting factor.

### Introducing Radar Cross Section (RCS)

Using the equivalent model of the tag shown in Fig. 2.4, it is possible to represent link parameters as a function of such model and use the concept of Radar Cross Section (RCS) to perform link analysis, because for each impedance state of the tag integrated circuit (tag-IC), the tag presents a certain RCS. Due to the nature of the tag passive functionality, RCS is another well established concept for the evaluation of tag technologies. Let us start presenting the power that is re-radiated by the tag in the direction to the reader, which will correspond to the part of the power dissipated at the antenna resistance ( $K \cdot P_{RX_{tag}}$ ) multiplied by the gain, in matching conditions:

$$P_{TX_{tag}} = K P_{RX_{tag}} G_{tag} = \frac{4R_{tag}^2}{|(Z_{tag} + Z_{ic})|^2} P_{RX_{tag}} G_{tag} \quad (2.20)$$

by applying the results of Eq.(2.4), it is possible to represent:

$$P_{TX_{tag}} = \frac{4R_{tag}^2}{|(Z_{tag} + Z_{ic})|^2} \frac{P_{TX_{rd}} G_{rd}}{4\pi r^2} \frac{\lambda^2}{4\pi} G_{tag}^2 \quad (2.21)$$

and the RCS ( $\sigma$ ) from the tag antenna, using [31], and knowing that  $S_{tag} = \frac{P_{RX_{tag}}}{A_{tag}} = \frac{P_{TX_{rd}} \cdot G_{rd}}{4\pi r^2}$ :

$$\sigma = \frac{P_{TX_{tag}}}{S_{tag}} = \frac{K P_{RX_{tag}} G_{tag}}{S_{tag}} = K A_{tag} G_{tag} = \frac{4R_{tag}^2}{|(Z_{tag} + Z_{ic})|^2} \frac{\lambda^2}{4\pi} G_{tag}^2 \quad (2.22)$$

$$\sigma = \frac{\lambda^2 G_{tag}^2 R_{tag}^2}{\pi |Z_{tag} + Z_{ic}|^2} \quad (2.23)$$

In this expression the chip impedance  $Z_{ic}$  will depend on the input power level. Also to mention that in case of any polarization mismatch between transmitter and receiver antennas the coefficient  $\tau_p$  should be considered. Using an anechoic chamber, and by using the method exposed in [31], with the two measurement of scattering parameters, it is possible to find RCS for a particular tag antenna, by calculating the backscattered power  $P_{RX_{rd}}$  from the tag. The return loss is approximated by:

$$|S_{11}|^2 \approx \frac{P_{RX_{rd}}}{P_{TX_{rd}}} \quad (2.24)$$

and by using the radar equation [38], the RCS of the tag can be experimentally determined as:

$$P_{RX_{rd}} = \frac{P_{TX_{rd}} G_{rd} \lambda^2 \sigma}{(4\pi)^3 r^4}; \quad \rightarrow \quad \sigma = |S_{11}|^2 \frac{(4\pi)^3 r^4}{G_{rd}^2 \lambda^2} \quad (2.25)$$

So by measuring magnitude of  $S_{11}$  parameter, one can determine SCR and have an idea of the tag reading range.

## 2.5 Radio channel impairments

There are different causes that produce the RFID radio system range to be influenced by. Some causes are environmental, surrounding materials, as described before, but in other cases the influences are from other radios coexisting in the vicinity of our radio system. In such a case we can study the following four cases of interference to be analyzed in RFID system namely:

- self-reader interference,
- reader-to-reader interference,
- tag-to-tag interference, and
- reader-to-tag interference.

The RFID system has the peculiarity of being a backscattering system which compared to conventional radio transceivers, it includes large amount of colored phase noise about the RF carrier [39], coming from local-oscillator (LO leakage) through direct down-conversion receiver's mixer, coupling between TX-RX antenna, antenna mismatch or unmodulation cluttered reflections.

The techniques used in conventional receivers to mitigate this noise such as, increase receiver sensitivity, higher antenna gains, higher transmit power, reduce bit rate (enhance signal bandwidth) or low noise receive amplifiers, do not improve necessarily the performance of decoder, because the interference is present before the signal reaches the receiver hardware, and the colored noise spectrum accumulates more power density at lower frequencies.

Let us start by analyzing some of these causes that become part of any RFID system, and evaluate how do they affect into the reading range.

### 2.5.1 Self-leakage (Self-Jammer) and interference from other radios

In a RFID system, since the reverse modulated signal that the reader receives from the tags are very weak (antenna size very small with radar cross-section (RCS) between 0.02 and 0.07  $m^2$  [40]), and due to the continuous carrier wave that reader needs to transmit to the tag to ensure energy supply, this can lead to problems. The reason is because of weak tag information will be received by the reader, while the receiver can be saturated by the transmit carrier leakage, reducing reading range.

Also affecting the read range in RFID systems are the effects caused by other radios in close proximity, working at close frequency bands. In a communication channel, it is very common to share it with several radio systems that are interconnected aiming at inter-changing information among them in a non-deterministic manner. So there are time intervals that the radios broadcast to the medium in order to interrogate for a possible presence of other radios, in the same band or, a band close to our transmitting-band. There is the possibility that the radio that is transmitting higher power level, may interfere with the receiving radio, so they can incur in:

- Presence of other readers that are requested to transmit high power, due to low tag sensitivity and may interfere with our radio.
- De-sensitization, due to the presence of strong signal from other radio systems (phone, WSN, others) at the receiver, that causes the low noise amplifier (LNA) to saturate and operate wrongly.

Gen-2 protocol specifies that, when the  $TX$  launches command information, the receiver is in non working state. After the command information is sent, a continuous carrier wave is transmitted and the receiver circuit starts to work simultaneously. For a transmit power of 0.5 W (27 dBm) and a circulator with 22 dB isolation, the carrier leakage will be 5 dBm to the receiver input, which would saturate the receiver first stage ( $S_{sj}$  in Fig. 2.8). Such receiver desensitizing signal is known as simply carrier leakage, or leaking carrier. The interference produced by the transmitter in the receiver, can be one of the big problems in the radio performance, degrading the radio range considerably. Several designs to suppress carrier have been tried to reduce this problem [41–43], where they use carrier leakage suppressor after circulator in the receiving path looking at phase and amplitude of the signal, or apply a balanced topology and special suppression IC design. This is one of the main causes of possible problems limiting RFID performance on the real field.

In a dense reader environment, where several readers share several channels, the readers must include the schemes defined in the EPC GEN 2 [44] specification to minimize mutual interference, and should confine their spurious emissions as shown in Fig. 2.13. In multiple or dense reader environment, the interfering signals are spurious and residual out-of-band modulated signals of the uplink. By applying the Central Limit Theorem to the interference, it can be approximated by Gaussian noise, being uncorrelated with the tag backscattered signal and noise, so the effective average signal-to-interference-plus-noise ratio (SINR)  $\bar{\gamma}$  is given by;

$$\bar{\gamma} = \frac{S}{N + I} = \frac{1}{\frac{1}{SNR} + \frac{1}{CIR}} \quad (2.26)$$

where  $I$  is the average interference power and  $CIR$  the carrier-to-interference ratio, which can be calculated from the difference between the reader receive power by the tag, and the interference power  $P_I = P_{TX_{int}} - ACPR + G_{int} + G_{Rd} - L_{p_{int}}$ , where  $P_{TX_{int}}$  and  $G_{int}$  are the power transmitted by the interfering reader and its antenna gain in the direction of the interfered reader. ACPR is Adjacent Channel Power Ratio coming from transmitter mask and  $L_{p_{int}}$  is the path loss from interfere to reader.

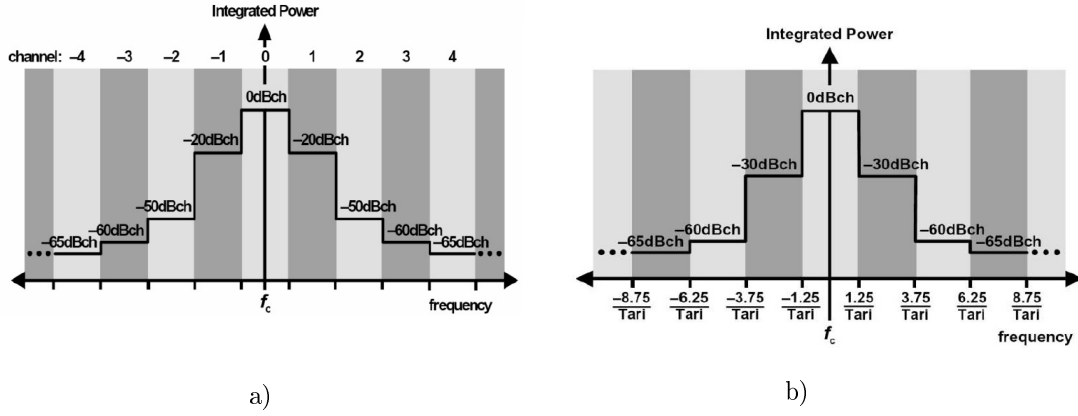


Figure 2.7: Reader transmit mask for EPCglobal Gen2. (a) Multiple reader environment with bandwidth according to local regulations (pg.30 version 2.01 April 2015) and, (b) dense reader environment where bandwidth  $R_{BW} = 2,5/Tari$ .

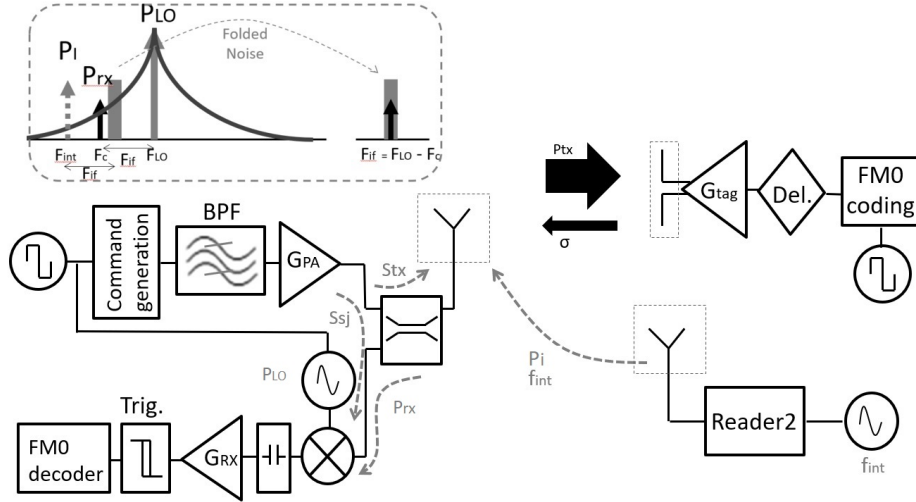


Figure 2.8: Interference caused by other RFID radios in the nearby.

In the case that the direct current (DC) offset due to TX leakage to the receiving antenna is removed by the baseband Band Pass Filter (BPF), the phase noise of the TX-LO leakage on the receiver bandwidth, can not be removed by the filter and may have much stronger level than thermal noise present at receiver input. This will overshadow the noise in a manner that the reverse link interrogation range mainly depends on the phase noise of the TX leakage. Such effect is evaluated at the end of this chapter, and presented in Fig. 2.8.

In the radio developed in our work, a solution for the receiver front-end consist on including a mixer first receiver stage, instead of LNA (see Fig. 2.12), this solution is provided by the IC supplier with reference **AS3993**. In case of overloading the RX mixer due to reflecting carrier, power can be detected by the system by triggering a measurement of RF input level. This is done by downconverting RF input level on the two RX mixers inputs into a proportional DC level of I and Q channel known as Receive Signal strength Indicator (RSSI). The 1 dB desensitization level, is the RF input power of interference that causes the small-signal conversion loss to increase by 1 dB. This value is typically 2

to 5 dB above the compression point level.

There are two values monitored by the RSSI, one is the pilot and another the data. There is the possibility to define a threshold value for the RSSI, to indicate to the microcontroller unit that interference is present at mixers input, so an action can be taken to avoid desensitivation, or interference from other radios. By fixing mixer gain  $G_{MX}$ , this possible interference signals can be detected, by monitoring the argument of the signal in the mixer path.

$$|MX_{DC}| = \sqrt{I_{DC}^2 + Q_{DC}^2}; \quad P_{in}(dBm) = 20 \log \left( \frac{|MX_{DC}|}{G_{MX}} \right) \quad (2.27)$$

where  $G_{MX}$  is the mixer gain that can vary depending on the input power from 17 to 286 [45].

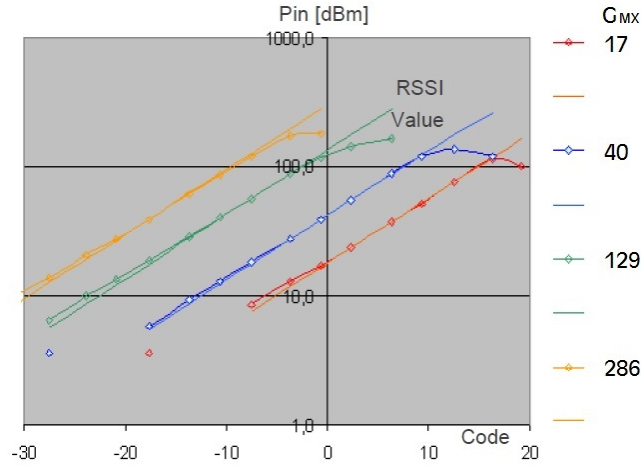


Figure 2.9: Mixer output measurement proportional to Pin(dBm).

Some solutions such as [13], use an on-chip feedback based solution to eliminate the self-jammer. To evaluate its influence, one must include the non-linearities effects of the receiver into the self-jammer signal, so the output noise will include such effects when evaluating the signal quality.

Let us name  $A_{isol}$  the isolation between the circulator ports and the output power of the PA  $P_{out}$ , the leakage signal from the output of the PA to MX input (self-jammer) is  $S_{SJ}(t)$  Fig. 2.8. The third order Input Intercept Point (IIP3) is used to investigate the effects of the receiver non-linearities into the  $S_{SJ}(t)$  signal and also interference signal  $S_I(t)$  that may be present at an interference frequency of  $f_I$ . Describing the output of a receiver as:

$$y_{mx,out}(t) = \alpha_1 x(t) + \alpha_3 x^3(t) \quad (2.28)$$

with  $\alpha_1$  representing the small signal gain and  $\alpha_3 < 0$  the nonlinear behavior of the receiver, with  $x(t)$  the input signal defined as:

$$x(t) = s_{RX}(t) + s_{SJ}(t) + s_I(t) = A_{RX} \cdot \cos[(\omega_c \pm \omega_{RX})t] + A_{SJ} \cdot \cos(\omega_c t + \theta_{SJ}) + A_I \cdot \cos[(\omega_c \pm \omega_I)t + \theta_I] \quad (2.29)$$

After substituting Eq.(2.29) into Eq.(2.28) and removing the components out of the band, rejected by the internal IC LPF, the minimum amplitude of the in-band signal (when  $\theta_{SJ} = \theta_I = 0$ ) at the output of the receiver will be;

$$|Y_{m_{out}}| = A_{RX} \left( \alpha_1 - \frac{3}{4} A_{RX}^2 - |\alpha_3| \left( \frac{9}{4} A_{SJ}^2 + 3 A_I^2 \right) \right) \quad (2.30)$$

which for  $A_{SJ} \gg A_I, A_{RX}$  the putput signal becomes;

$$|Y_{m_{out}}| = \alpha_1 A_{RX} \left( 1 - \frac{9}{4} \left| \frac{\alpha_3}{\alpha_1} \right| A_{SJ}^2 \right) \quad (2.31)$$

So the signal-to-noise ratio at the receiver output is [13]:

$$SNR_{RX} = 10 \log \left( \frac{|S_{out}|^2}{N_{RX}} \right) = 10 \log ((\alpha_1 A_{RX})^2) - N_{RX}(dB) + 20 \log \left( 1 - \frac{9}{4} \left| \frac{\alpha_3}{\alpha_1} \right| A_{SJ}^2 \right) \quad (2.32)$$

The last term shows the receiver sensitivity degradation, which is directly related with the non-linearity level of the receiver, which corresponds to:

$$IIP3 = 10 \log \left( \frac{4}{3} \left| \frac{\alpha_1}{\alpha_3} \right| \right) \quad (2.33)$$

As can be seen in Fig. 2.10, having a sensitivity degradation of 1 dB, the IIP3 requirements can range from -5 dBm, for a self-jammer of -20 dBm, up to +25 dBm in case of a strong self-jammer as high as +10 dBm.

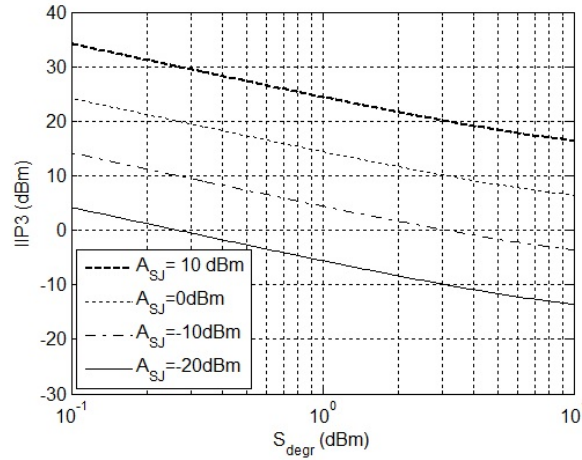


Figure 2.10: Requirement for the radio IIP3 due to self-jammer.

The non-linear performance of the mixer as first stage will limit the performance regarding sensitivity degradation. Due to high IIP3, the radio will be less sensible to self-jammer. When combining expressions (2.32) and (2.33), we can obtain that the receiving power including the effect of self-jammer will become:

$$R_{RX} = SNR + N_{RX}(dB) - 20 \log \left( 1 - \frac{3 \cdot a_{SJ}^2}{iip_3} \right) \quad (2.34)$$

As can be seen in Fig. 2.11, the range degradation is shown for a radio with maximum read range of 14 m and for ultra-long reading range of 23 m, in the case of three different radio specifications of IIP3. For low IIP3 (-10 dBm) the degradation in range can be very high, even with small self-jammer interference.

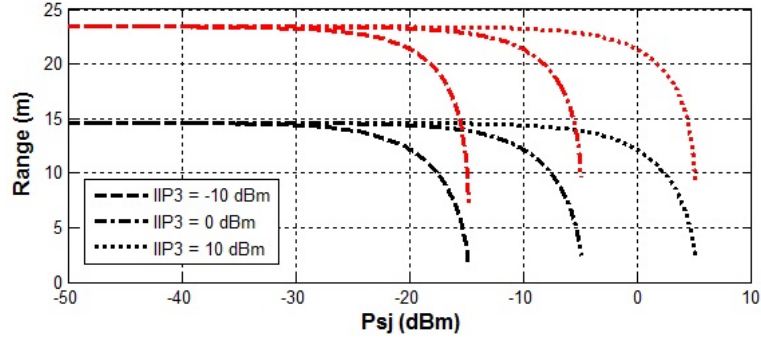


Figure 2.11: Read range reduction caused by self-jammer effects, and improved effects caused by Range Correlation (red).

To obtain maximum read range (at  $BER_{th}$ ), the distance between signal and noise (SNR) needs to be maximized, so one must get maximum Spurious Free Dynamic Range (SFDR). The receiver must comply with having low noise and high linearity [46]. It is possible to achieve low noise by using the traditional LNA-first structure, but in RFID that has large jammer noise, this one will be amplified and the receiver will be de-sensitized. In the case of AS3993 with a mixer-first structure, it provides high linearity. Though it is at the cost of conversion loss, the amplification can be postponed to IF ([47] shows  $IIP3 = 2.96$  dBm,  $NF = 21.9$  dB,  $SNR = 15$  dB at  $BW = 100$  kHz).

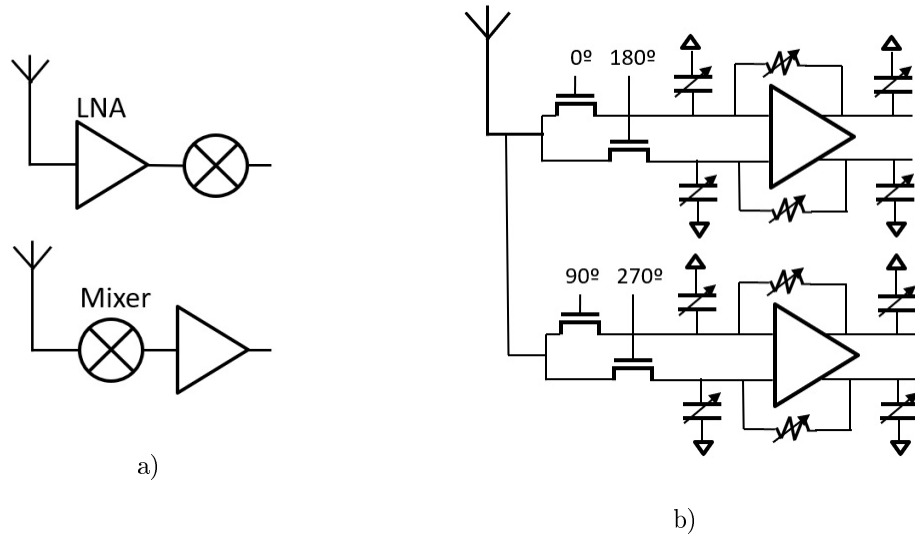


Figure 2.12: Difference between (a) LNA-first and Mixer-first structure. (b) Included example of Mixer-first implementation in CMOS [47].

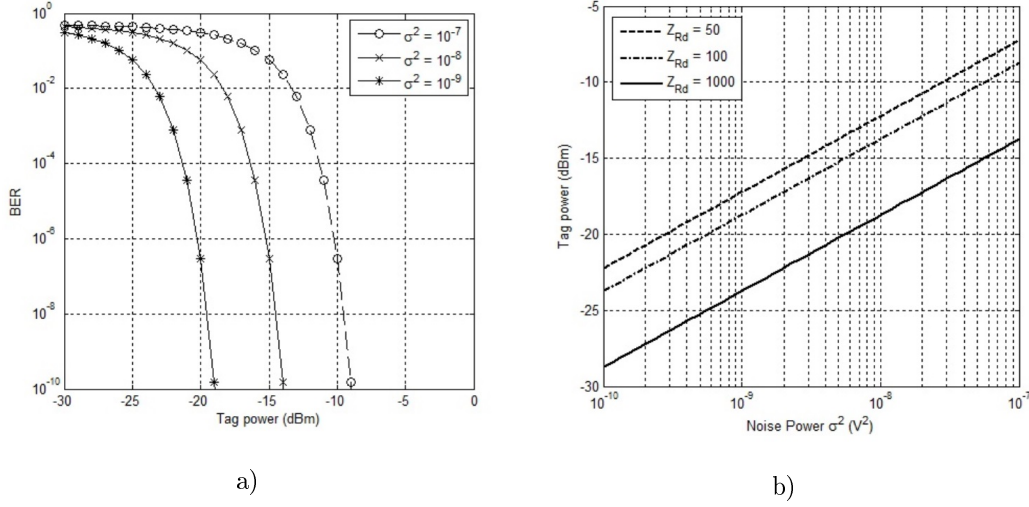


Figure 2.13: (a) BER at reader as a function of the power received by the tag, for different noise power at the reader receiver ( $Z_{Rd} = 1k\Omega$ ) (b) Required tag power for the reader to demodulate properly ( $BER_{th} = 10^{-3}$ ) the back-scattered signal with three different reader input impedance levels.

### 2.5.2 Range degradation due to noise at the input

The noise at the reader input is a determining parameter that influences reader performance. Noise may be caused by the fact that the reader being close to a thermal source, such as another electronic device, a heater, or close to a source generating interference that influence the reader noise such as some RF signals Fig. 2.8 (LO leakage from TX).

Noise at the input of reader receiver is critical in this respect as it is shown in Fig. 2.13. In case we would need to achieve a  $BER = 10^{-5}$ , the required sensitivity for the tag could vary from  $P_{Tag} = -17.5$  dBm when having a noise power at the reader input of  $\sigma^2 = 10^{-9}$  until a sensitivity of  $P_{Tag} = -7.5$  dBm for a noise power 20 dB above  $\sigma^2 = 10^{-7}$ . In the case of having two different tag technologies, with a difference in sensitivity of 10 dB, the optimum read range would have been decreased by 10 m (from 14.6 m down to 4.6 m, with  $P_{Rd} = 2$  W), with ideal propagation and reflection conditions. The detailed analytical expressions for BER performance are described later in this chapter.

### 2.5.3 Range correlation on phase noise

As stated, read range depends on sensitivity of the reader, which is related to the noise and interference levels at the receiver terminals. The larger the noise and the effects of the interference, the larger the required received signal power to satisfy with SNR. Lets analyze noise due to interference effect.

In an ideal receiver, the noise floor is caused by thermal noise only. However since the isolation between transmitter and receiver antennas is not perfect, we can start by considering the primary performance limiting on the uplink, which is the local oscillator (LO) phase noise ( $\Theta_{LO}$ ), leaking from the transmitter circuit through the circulator or directional coupler (with isolation ratio of  $A_{isol}$ ), to the receiver circuit (see Fig. 2.8). This will overshadow the thermal noise component at the receiver input, that is the leaking power ( $P_{leak} = P_{TX} - A_{isol}$ ) a fundamental limitation in terms of reader sensitivity.

$$x_{LO}(t) = A_{LO} \cdot \cos[\omega t + \Theta_{LO}(t)] \quad (2.35)$$



$x_{LO}(t)$  is the LO signal amplified by the PA and, passed through the circulator to the receiver. This signal is transmitted to the air receiving later the backscattered from the tag. The backscattered signal  $x_M(t)$  in the case of PSK modulation at the receiving antenna can be expressed as:

$$x_M(t) = \cos[\omega(t - \frac{2r}{c}) + \Theta_s(t) + \Theta_{LO}(t - \frac{2r}{c})] \quad (2.36)$$

where  $r$  is the tag-reader distance, and  $c$  is the wave propagation velocity,  $\Theta_s(t)$  denotes the phase signal representing the binary data ("0" or "1") of the tag. At the receiver the backscattering signal and the LO signal are mixed, and the output is low-pass filtered. The resulting in-phase baseband signal will be:

$$x(t) = \cos \left[ \Theta_0 + \frac{2r}{c} + \Theta_s(t) + \Delta \Theta(t) \right] + n_0(t) + n_{PN}(t) \quad (2.37)$$

where  $\Theta_0 + \frac{2r}{c}$  is the constant phase shift dependent on the tag-reader distance,  $\Delta \Theta(t)$  is the residual phase noise,  $n_0(t)$  is the thermal noise at the receiver, and  $n_{PN}(t)$  is the sum of additive phase noise of the receiver, that do not affect the tag's signal phase which contains information data, so they are not considered. The residual phase term in (2.37) is given by

$$\Delta \Theta(t) = \Theta_{LO}(t) - \Theta_{LO} \left( t - \frac{2r}{c} \right) \quad (2.38)$$

When having the same LO for transmitter and receiver, the phase noise of the received signal is correlated with the LO, depending on the time difference between the two signals. For small time difference, the effect greatly abbreviates the phase noise spectrum at baseband, effect known as **range correlation** [14]. A quantitative characterization of the relation between range and phase noise can be done in the frequency domain. The PSD of  $\Delta \Theta(t)$ ,  $S_{\Delta\Theta}(f_0)$  at an offset frequency,  $f_0$  is given by:

$$S_{\Delta\Theta}(f_0) = S_{\Theta_{LO}}(f_0) \cdot |1 - e^{-j2\pi f_0 \frac{2r}{c}}|^2 = S_{\Theta_{LO}}(f_0) \cdot \left[ 4 \sin^2 \left( 2\pi \frac{rf_0}{c} \right) \right] \quad (2.39)$$

So for a low offset frequency, the baseband noise spectrum will increase proportional to the square of the distance between tag and reader. The correlation level between the phase noise of the received tag signal with that of the LO, is inversely proportional to the time difference between the two signals (very small  $\sim$  nsec, for the case of RFID due to short distances), and so the phase noise is reduced by correlation effect. For the case of having values for  $r$  and  $f_0$  of 8 m and 160 kHz, respectively, the value of  $rf_0/c$  will be on the order of  $10^{-3}$ . So the range correlation effect will reduce the PSD dramatically.

Working the previous expressions, one can find the expression for the noise power at the receiver input considering the effects of LO phase noise;

$$\sigma^2 = P_{TX} - A_{isol} + \Theta_{LO} + C_{PA} + 10 \cdot \log(BW) \quad (2.40)$$

where  $C_{PA}$  is a factor used to convert phase noise into amplitude phase noise [12] required in order to be able to work on equivalent amplitude noise at the receiver.

The phase noise of the LO, will depend on the ACPR specification at the offset frequency from the carrier. In the case of the EPC Global specification for the transmit mask, and looking at the 1st and 2nd adjacent channel, it is already possible to estimate the power noise that would leak into the receiver.

Table 2.5: LEAKING POWER FROM THE LO TO RECEIVER

ACPR (dB)	$\Theta_{LO}$	Isol+ $C_{PA}$	$\sigma^2$ (dBm)
20	-124	65	-101
50	-94	65	-71
60	-84	65	-61



### Specifications for the RFID-UHF radio transceiver

Gathering data from previous analysis, one can detail the following system specifications for the RFID reader: IIP3 = 3 dBm, NF = 22 dB, SNR = 15 dB, CBW = 100 kHz. BER =  $10^{-3}$ , ACPR = 30 dB,  $\Theta_{LO}$  = -114 dBc/Hz,  $NF_{RX}$  = 29 dB,  $NF_{MX}$  = 12 dB.

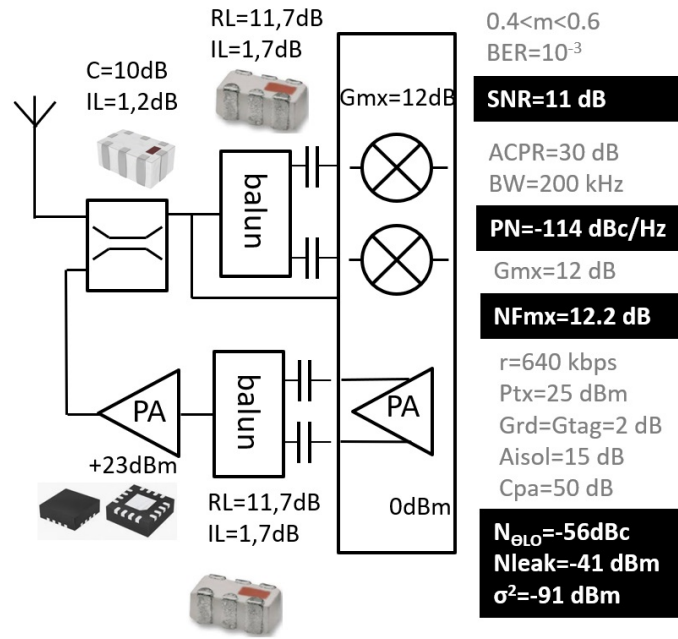


Figure 2.14: Block diagram of the front-end for the UHF-RFID reader, including computed values as per previous Case

**Case:** To determine the interference effects, we look at Fig. 2.13 where shows the Adjacent Channel Power Ratio  $ACPR = 30 \text{ dB}$ . Considering a receiver with a sensitivity of  $P_{RX,min} = -80 \text{ dBm}$  and a Channel Bandwidth  $CBW = 200 \text{ kHz}$ , we will find the phase noise requirements and noise figure of the receiver assuming a mixer gain of  $G_{MX} = 12 \text{ dB}$ . From Fig. 2.27 using modulation index  $m$  between 0.4 and 0.6, the  $SNR = 11 \text{ dB}$  for a  $BER = 10^{-3}$ .

- Noise power at the receiver, considering the phase noise and interferer is;  $P_N(\text{dBc/Hz}) = P_I + \Theta_{LO}(\Delta\omega) + 10\log(BW)$ . We know also that SNR must comply with the condition of accepting ACPR for the  $SNR_{min}$ , in which case the phase noise needs to be  $-114 \text{ dBc/Hz}$ :

$$\frac{P_{RX,min}}{P_I \cdot \Theta_{LO}(\Delta\omega) \cdot CBW} \geq SNR_{min}; \quad \Theta_{LO}(\Delta\omega) \leq P_{RX,min} + ACPR - SNR_{min} - 10\log(CBW) \quad (2.41)$$

- To find the NF of the mixer, let's first estimate the NF of the whole receiver. In our case we have

$$NF_{RX} = 174 \text{ dBm} + P_{RX,min} - 10\log(BW) - SNR_{min} = 29.4 \text{ dB} \quad (2.42)$$

Taking the Noise Figure cascading equation for the receiver, including LNA and Mixer one has the following:

$$NF_{RX} = NF_{LNA} + 4 \frac{NF_{MX} - 1}{G_{LNA}^2} + 4G_{MX}^2(NF_{MX} - 1) \quad (2.43)$$

But because the NF is mainly defined by the NF and gain of the mixers, with its noise appearing at the LNA input directly, the last term is the predominant, so we end up with:

$$NF_{MX} = \frac{NF_{RX}}{4G_{MX}^2} + 1 = 12.2 \text{ dB}. \quad (2.44)$$

- Evaluation of the reading range versus data rate that, in accordance with FM0 modulation EPC standard [44] will be between  $r_{max} = 640 \text{ kbps}$  and  $r_{min} = 40 \text{ kbps}$ , to comply with  $BER = 10^{-3}$ . Reader transmit power is  $P_{TX,rd} = +25 \text{ dBm}$ , antenna gains of:  $G_{rd} = 2 \text{ dB}$ , and  $G_{tag} = 2, 15 \text{ dB}$ . In the reader side one can make the assumption that isolation between transmitter and receiver is  $A_{isol} = 15 \text{ dB}$  [48].

1. A typical phase noise power spectral density from [12] is  $-115 \text{ dBc/Hz}$  relative to the CW signal power at the offset of the subcarrier frequency of  $640 \text{ kHz}$ . So relative to the CW signal we have:
2. Total LO phase noise power  $N_{\Theta_{LO}} = \Theta_{LO} + 10 \cdot \log(R(\text{bps})) = -115 + 10 \cdot \log(640 \cdot 10^3) = -56 \text{ dBc @ } 640 \text{ kbps}$ .
3. The phase noise power of the input leaking component at the receiver for a transmit power  $P_{TX} = 30 \text{ dBm}$ , will be:  $N_{leak} = P_{TX} - A_{isol} + N_{\Theta_{LO}} = 30 \text{ dBm} - 15 \text{ dB} - 56 \text{ dBc} = -41 \text{ dBm}$ .
4. With a conversion factor of  $C_{pa} = 50 \text{ dB}$  from phase to amplitude phase noise, the equivalent phase noise at the receiver will be:  $\sigma^2 = N_{leak} + C_{pa} = -41 \text{ dBm} - 50 \text{ dB} = -91 \text{ dBm}$

### 2.5.4 Range reduction caused by mobile phone and other readers

The radio system under analysis, is intended to be used in conjunction with the mobile phone. The data gathered via UHF-RFID, is being transferred to the mobile phone APP via NFC, so interference between radio operating in near bands is to be considered.

In order to expand the number of frequencies available to mobile operators, the World Radiocommunications Conference (WRC-07) allocated in 2007 in Region 1 the 790-862 MHz frequency band to mobile services. This new band referred as Digital Divident band, while will allow deploying advanced cellular systems that use high speed broadband LTE, but there is a concern on potential interference to low power SRD operating in adjacent band 863-870 MHz [49].

Considering mobile phones a source of interference, there exist two mobile phone bands that are close to RFID-UHF system, such as 800 Band, that in the case of Spain, is becoming the 20 band (B20) for 4G LTE (this band has disappeared from TDT channels) also in use in other European countries, and the 900 Band, being used by 3G GSM (3G rural areas, corresponds to B8). Other bands are being used in other countries such as LTE band 5 at 850 MHz, used in Corea and Israel and LTE Band 6 of 800 MHz being used in LTE Japan. Due to the proximity to the UHF bands used for the SRD such as our RFID system, there may exists some effects of interference, that could degrade the behavior of the radio, mostly in the upper adjacent band, because of high level of Out-Of-Band (OOB) emissions produced by very wide bandwidth LTE signals Fig. 2.16.

Table 2.6: FREQUENCIES AND LTE BANDS (SPAIN)

Frequency (MHz)	LTE Band	Uplink Freq.	Downlink Freq.	RFID (EU)	Actual use
800	20	832-862	791-821	865-868	Nowadays used for TDT, from 31 March 2015 used for LTE

In the work done by Arnaud [50], there are some test performed introducing a RFID system at 868 MHz which is interfered by a GSM phone working at 880.2 MHz. The GSM radio located at 1 m from the RFID reader that transmits at 2 W, and changes its transmit power from 33 dBm (2 W) maximum level down to 5 dBm. The Fig. 2.15 shows how the radiated field by the GSM signal affects the reading range of the RFID reader, there is a strong reduction of maximum reading range.

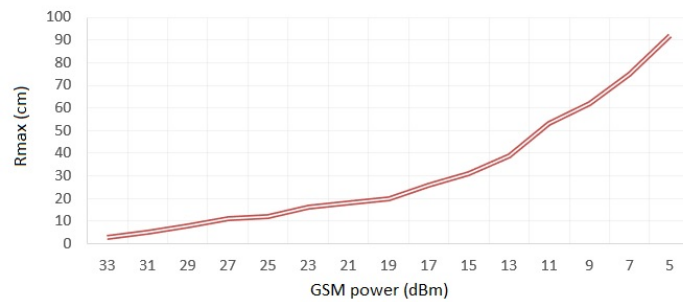


Figure 2.15: Maximum reading distance by an RFID reader located at 1 m distance form a 2 W GSM radio.

In the case of other readers close to each other, there is also the possibility of interference. Lets imagine a reader transmitting 1 W output power with antenna gain 6 dBi and a reader located at a distance "r" receiving in a 1 dBi antenna. In case both are tuned to the same channel, the power received at different distances would be:

- $P_{RX} = -3.5\text{dBm}$  at  $r = 5$  m.
- $P_{RX} = -9.5\text{dBm}$  at  $r = 10$  m.
- $P_{RX} = -23.5\text{dBm}$  at  $r = 50$  m.

For the situation of being in a Multiple reader environment (Fig. 2.8), using the EPC Global Gen.2 dense interrogation mode, with the reader transmitting in the adjacent channel, will transmit with 1% of the total energy of the principal channel (20 dB down), so at 10 m distance, the received power by the reader at central channel will be;  $P_{RX}^I = -9.5\text{ dBm} - 20\text{ dB} = -29.5\text{ dBm}$ , sufficient power such as to block tags at 1 or 2 m distance.

Fig. 2.16 shows how the output spectrum mask of a UE transmitter is divided in three components: occupied or channel bandwidth (with 99% of the total integrated mean power), out of band (OOB), and the out of spurious emission domain [51]. In (b) and example of 5 devices measuring the in-band and out-of-band power (one WiFi router with LTE backhaul and three 4G USB dongles), when transmitting maximum power (23 dBm) in 16QAM, on all 50 resource blocks within a 10 MHz channel centered on 857 MHz [52]. LTE emission mask is also included [51].

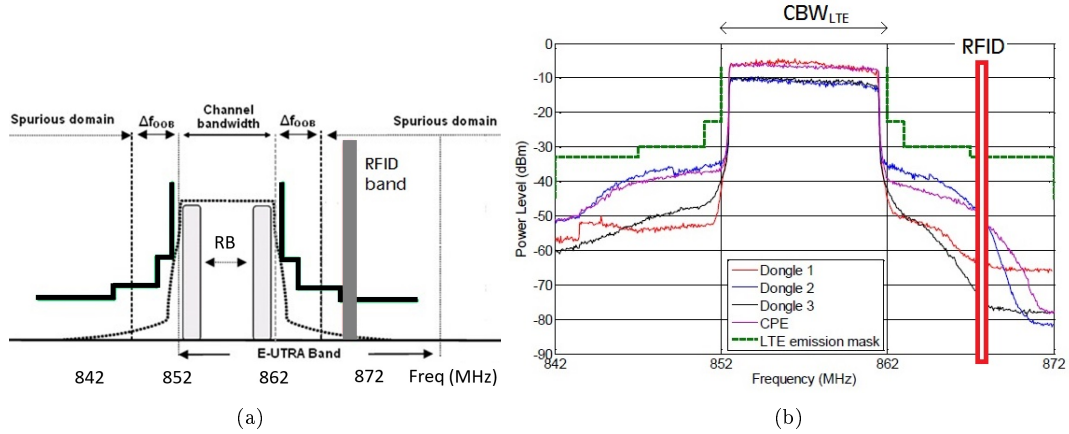


Figure 2.16: (a) Transmitter RF spectrum masks and, (b) RMS signal of four LTE devices (RBW = 10 kHz)

### 2.5.5 Read range reduction caused by proximity tags

Now it is time to consider the case of having several tag antennas close to each other, and evaluate their mutual effects, in terms of power influence. It is supposed that electromagnetic coupling will affect each other antennas, so the matching between antennas and active parts will be influenced represented by the impedance matching coefficient  $\Delta G$ , introduced in section 2.4.1, or the antenna gain penalty  $\tau_M$  in section 2.4.2. In practical situations large number of tag antennas may be present in close proximity when many articles or sensors are to be tagged. In such circumstances, collective scattering modulation in certain type of tags may lead to confusion or failures in anti-collision procedure in the protocol.

While Gen2 EPC ID tags already incorporate anti-collision protocols by means of some commands (kill command), for RFID sensors this can be a problem, because they need to be operating all the time, so an study such as considered here may bring important inputs on how to deploy such devices in the field.

From the optimal design of power antenna transfer, with matching conditions between the antenna and the IC, there can be a deviation from the optimal impedance design caused by electromagnetic coupling of antennas when, for example, two tags are close together, so a mismatch will cause a decrease in read range. As stated by [53] when dipole antennas are close, mutual impedance arises at each antenna. In multiple arrayed tags, there is also antenna interference that causes a reduction in the radar cross section [32, 54, 55]. To experimentally visualize such effect, one can take measurements by examining the two port S-parameters matrix  $\mathbf{S}$ , presenting the power wave reflection coefficient  $S$  with the associated power reflection coefficient  $|S|^2$ :

$$\mathbf{S} = \frac{Z_L - Z_a^*}{Z_L + Z_a} \quad |S|^2 = \left| \frac{Z_L - Z_a^*}{Z_L + Z_a} \right|^2 \quad (2.45)$$

$|S|^2$  represents the fraction of the maximum power available from the generator that is not delivered into the load. For an easy interpretation of mutual impedance effects between the antennas, it is recommended converting to  $\mathbf{Z}$  parameters as:

$$\mathbf{Z} = \frac{\mathbf{I} + \mathbf{S}}{\mathbf{I} - \mathbf{S}} = \begin{bmatrix} 1 + S_{11} & S_{12} \\ S_{21} & 1 + S_{22} \end{bmatrix} \begin{bmatrix} Z_{11} & Z_{12} \\ Z_{21} & Z_{22} \end{bmatrix} \quad (2.46)$$

where the mutual effects between tag antennas will be represented in the measurement of the mutual components  $Z_{12}$  and  $Z_{21}$ , and the equivalent normalized (in this case normalized to 50  $\Omega$ ) antenna impedance considering mutual effects from other antennas will be [56]:

$$\overline{Z_{in}} = 50 \left[ Z_{11} - \frac{Z_{12}Z_{21}}{Z_{22} + Z_{IC}} \right] = 50 \left[ \frac{Z_{11}^2 + Z_{11}Z_{IC} - Z_{12}^2}{Z_{11} + Z_{IC}} \right] \quad (2.47)$$

For two tags with similar geometry and characteristics,  $\mathbf{Z}$  will be symmetrical (that is to say,  $Z_{11} = Z_{22}$ ,  $Z_{12} = Z_{21}$ ).

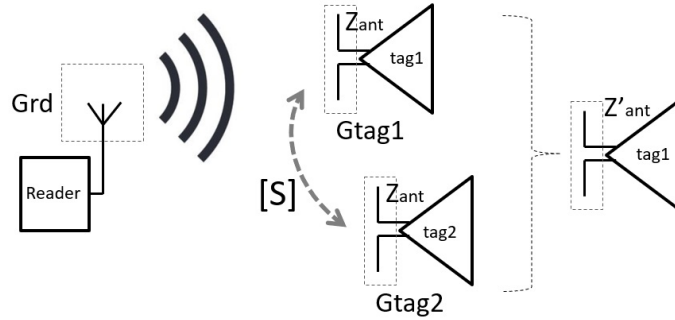
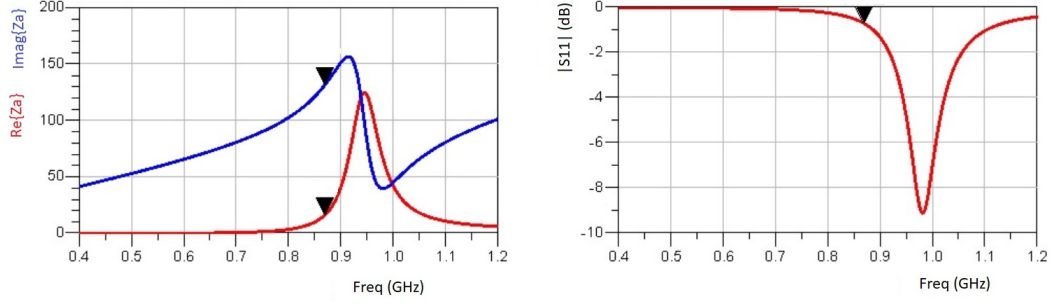


Figure 2.17: Electromagnetic coupling effects between two tags in close proximity.

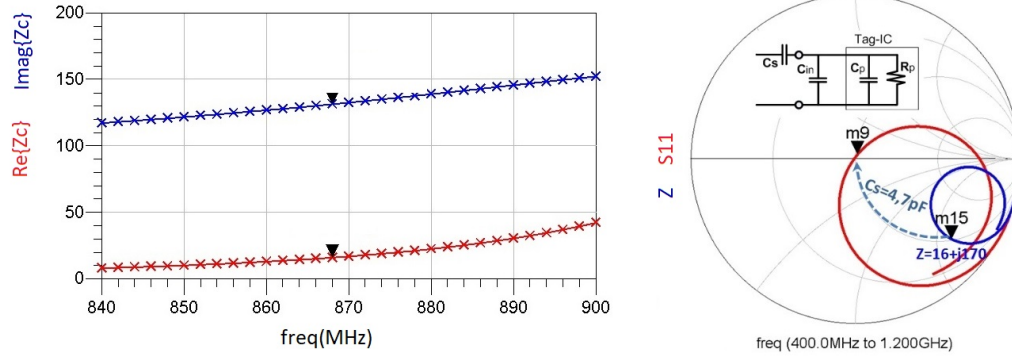
To show this effect, a tag dipole antenna has been designed shown in Fig. 2.18, using an electromagnetic 2.5D solver from Agilent(*Momentum*). It matches an Impinj Monza 5 IC, similar as would have a sensor tag ( $C_p = 0.825$  pF,  $R_p = 1.8$  k $\Omega$  and  $C_{in} = 0.245$  pF). The simulation results for the tag antenna and the matching are shown in Fig. 2.19. In order to perfectly match the tag antenna, with IC, a series capacitor ( $C_s$ ) is placed between both as shown in Fig. 2.19. Total input tag antenna impedance, is monitored during the simulations in order to analyze the influence of proximity tags.



Figure 2.18: Parts of the designed dipole type RFID tag antenna.



(a) Wideband tag impedance



(b) Working frequency band tag impedance.

Figure 2.19: Impedance characteristics for the dipole type tag antenna. Matching of the tag antenna with impinj Monza 5 IC, showing equivalent circuit. ( $R_{dip} = 72\Omega$ ).

The effects on the influence on mutual tags, has been analyzed based on close proximity in the horizontal and vertical plane axis as shown in Fig. 2.20. In such cases, looking at the impedance presented at the tag antenna terminals, there is a clear decrease of the impedance by placing both tags together, so at the extreme of 5 mm distance, the impedance shift is from the original  $Z_i = 16 + j133$ , down to  $Z_f = 9.6 + j9$ .

The tags influence can be understood as a shadowing effect on the read range. One effect that was represented by including the Gain Penalty factor in the Friis equation. On the other hand, such gain penalty factor, can be analyzed when evaluating the influence that such mismatch produced by proximity tags, would have on the voltage induced in the tag. As a matter of fact, if we consider the modulation of the incident electromagnetic field in the antenna by the tag-IC, such effect is presented in the back-scattering signal affected by nearby tags.

The signal to noise ratio at the receiver is proportional to the energy of the bit, so to the distance between bits in the constellation diagram for the particular modulation scheme. According to minimum

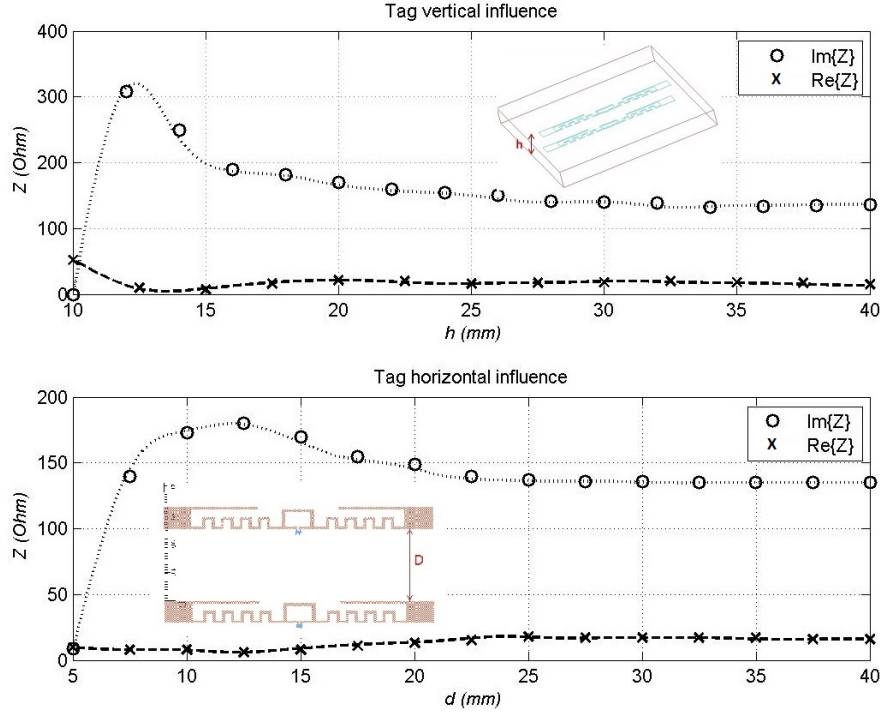


Figure 2.20: Simulation results for the influence over tag impedance on the influence of horizontal and vertical close proximity tags.

detection distance as represented in Fig. 2.26  $d_{min} = 2V_0$ , will determine the minimum detection threshold to resolve between all the received bits. Assuming ideal, matched-filter demodulation and Additive White Gaussian Noise (AWGN) with standard deviation  $\sigma$  at the detector input, the BER for both PSK and ASK (OOK) will be determined based on such energy distance between received bits. The effect on the back-scattering of the tag antennas, can then be introduced by the reflection coefficient between load and antenna impedance affected by proximity tags.

The proximity tags affect the impedance values from the different modulation states,  $Z_1 = R_1 + jX_1$  and  $Z_2 = R_2 + jX_2$  to  $Z_1'$  and  $Z_2'$ . Since for both ASK and PSK, it is possible to express the BER depending on the modulation index ( $m$ ) as;  $m = \frac{|\rho_1 - \rho_2|}{2}$ , being  $\rho_{1,2}$  the reflection coefficient at the tag antenna terminals [33, 57], it will be possible to include such proximity tag effects into the BER expression.

$$\begin{aligned}
 BER &= \frac{1}{2} \operatorname{erfc} \left( \frac{|V_{R1} - V_{R2}|}{4\sqrt{2}\sigma} \right) = \\
 &\frac{1}{2} \operatorname{erfc} \left( \frac{|V_0| \cdot |\rho_1 - \rho_2|}{4\sqrt{2}\sigma} \right) = \frac{1}{2} \operatorname{erfc} \left( \frac{|V_0| \cdot m}{2\sqrt{2}\sigma} \right)
 \end{aligned} \tag{2.48}$$

Considering ASK modulation, the two possible states will depend on the modulation depth, which will be conditioned also by the mismatch between antenna and modulation impedances;  $|V_{R1} - V_{R2}| = |V_0| \cdot |\rho_1 - \rho_2| = |V_0| 2m$ . Taking as example the case where two tags are located at a distance of 20 mm one on top of the other, the simulation results from the mutual coupling, shows that  $m = 0.54$ . The results of BER degradation due to imperfect matching between antennas shows a degradation of SNR of 3 dB, due to this only effect as shown in Fig. 2.22. Such modulation effect, will degrade reading range. Same figure part b) shows the corresponding BER degradation for different distances between



tags, as seen in case  $h = 10$  mm the SNR degradation is so high that such effect would degrade much the reception of any tag (situation where one tag sits on top the other just 1 cm apart).

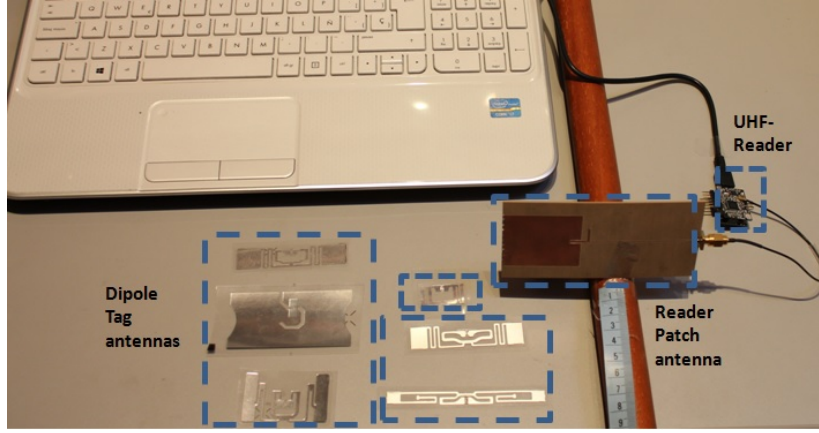


Figure 2.21: Measurement set-up for inter-tag interference.

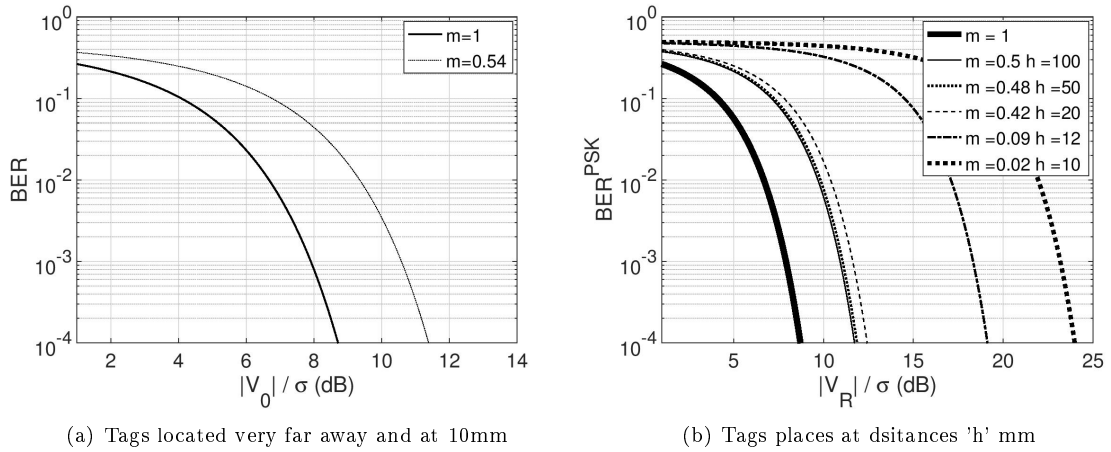


Figure 2.22: BER degradation for different distances between tags ( $0 < h < 100$  mm).

One can conclude that in order to see a clear effect of inter-tag interference, they must be located very close one to another. Since RFID is becoming very spread used for item identification, it is an effect to consider.

As it has been shown, there are many effects that are prone to influence link quality so to reduce reading range in RFID systems. Some of them caused by the radio itself, other radios being in close proximity, or the accumulation of tags. For the first two cases, it is here proposed a method for detecting interference sources based on RSSI, which would allow to act on the radio in order to reduce the tagging time to the slots where low interference is detected. In such a case, radio interrogation time can be reduced to the optimal time slots and therefore also the power consumption.

### 2.5.6 Detection circuit for non-desirable signals

It is though that Receive Signal Strength Indicator (RSSI) would provide information on the level of signal-to-interference plus noise ratio (SINR), and was not related to external interference. However, as

it is shown here, it is possible to use RSSI indicator also for prediction on other source of interference, since it can be used to measure the strength of the signal as it is mend to do, but also link status.

Considering this new advantageous feature, it is possible to build a link-aware protocol to improve RFID radio system performance in a hostile wireless environment. Some previous work have already analyzed similar feature but for other radio systems such as [58], where the strong correlation between BER and RSSI is used to predict interference, or [59] where they show that link reliability in a wireless network, depends on an intraframe SINR distribution and not on RSSI. In our case, there is an RSSI indication covering wide input power range through mixer gain selection. The measurement of RSSI values for the RFID radio are shown in Fig. 2.23, where  $G_{MX}$  corresponds to mixer gain. Table 2.7 presents different RSSI curve limits, based on selected gain, as well as the maximum sensitivity levels depending on the desired reading distance (in this case for a reader with  $P_{TX} = 20$  dBm,  $G_{rd} = G_{tag} = 2.1$  dB).

Two areas are indicating the regions where one could shut down the radio due to the potential presence of interference. So in the case of an application where tag reading distance would be longer than 1 m, it is proposed to shut down the radio (EN=0) for measurements of RSSI included in the small area of Fig. 2.23 (gains  $G_{MX}=53, 62$ ). For reading ranges longer than 2 m, one could establish the bigger indicated area as the one to shut down the radio ( $G_{MX}=53, 62, 71$ ). Such a procedure presented, would provide means for detecting strong interference signal, that would for sure overshadow the faint tag signal at the reader input. So by means of this detection system, it is possible to avoid turning on the whole radio system and transmit the carrier for tag inventory, which is the highest power hungry sequence.

Table 2.7: SENSIBILITY VERSUS GAIN AND DISTANCE, BEING  $G_{MX}$  THE MIXER GAIN IN DB'S.

$G_{MX}$	Available $S_{Rd}$ Min/max		Dist. (m)	Max. $S_{Rd}$ (dBm)
53	-50	-22	1	> -35
62	-59	-31	2	> -50
71	-68	-40	3	> -55
80	-77	-49	4	> -60

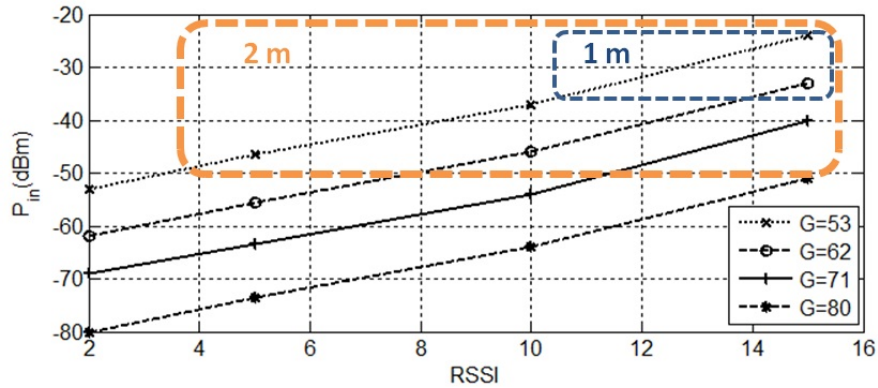


Figure 2.23: RSSI measurement versus input power.

In our front-end that uses mixer first stage receiver, in case of overloading the RX mixer due to reflecting carrier, power can be detected by triggering a measurement of RF input level. This is done by downconverting RF input level on the two RX mixers inputs into a proportional DC level of I and Q channels [60].

$$|MX_{DC}| = \sqrt{I_{DC}^2 + Q_{DC}^2} \quad (2.49)$$

$$P_{in}(dBm) = 10 \cdot \log \left( \frac{|MX_{DC}|}{G_{MX}} \right) \quad (2.50)$$

$G_{MX}$  is the mixer gain that can vary depending on the input power from 17 up to 286. The receive power level reflected indication comes from (2.50). By proper examining  $MX_{DC}$  level it is possible to adjust the tag interrogation time to the slot where input level is lower than the minimum sensitivity level corresponding to the read range.

### 2.5.7 Read range influenced by material close to the tag

In common applications, the RFID tag is located close to different objects or attached to them, to accomplish with its identification or tracking function on the particular object. The electromagnetic characteristics of such an object will affect the performance of the tag antennas, even in some cases may cause the communication to vanish totally, so it is of maximum interest to consider such elements when designing an RFID system. There are several works that have investigated those influences, such as the measurement taken in [12, 61], where they already introduce the variation of resonant frequency due to proximity to metal canes or, the return losses made by plastic bottle among others. Also to mention studies conducted by simulation [62] showing the effect of a folded dipole over a ground plane on radiation pattern, antenna impedance, directivity or front to back ratio.

In the analysis of the consequences carried out by the presence of influencing objects close to the tag antenna, one possibility is to include a factor into the Friis equation, such as the gain penalty [63]:

$$P_{R_{tag}} = P_{T_{rd}} G_{rd} \left( \frac{\lambda}{4\pi d} \right)^2 G_{tag} L_{sys} G_P \quad (2.51)$$

where

- $L_{sys}$  are the losses in the system
- $G_P$  is the Gain Penalty due to objects close or attached to tag antenna

There are some previous works that already present interesting results based on measurements with and without the material close ( $d \approx 1/50\lambda_0$ ) or attached to the tag:  $G_P(dB) = G_{tag, freespace}(dBi) - G_{tag, material}$ . As can be seen in table 2.8,  $G_P$  increases with the increasing of loss tangent. In the case of attaching a tag into aluminum slab, one with the highest  $G_P$  associated, it is of interest to note how the reading range is modified Fig. 2.24

Table 2.8: GAIN PENALTIES FOR 915 MHz HALF-WAVE DIPOLE TAG PLACED CLOSE TO MATERIALS

	Cardboard Sheet	Acrylic Slab	Pine Plywood	De-ionized Water	Ethylene Glicol	Ground Beef	Aluminum Slab
Gain Penalty, GP(dB)	0.9	1.1	4.7	5.8	7.6	10.2	10.4
Relative Permittivity, $\epsilon_r$	1	2.6	1.7	77.3	33	50	-
Loss Tangent, tg $\delta$	0	0.0061	0.036	0.048	0.4	0.7	-

Permittivity and loss tangent interpolated from [64]

For comparison, Fig. 2.24 depicts the difference in the reader receive power, using Eq.(2.9), from the path attenuation shown using basic model or using the two-ray model (including Eq.(2.1) and Eq.(2.2)), with vertical polarization antennas attached close to aluminum slab, susceptible to Gain Penalties due to electrical conductivity of material. For a reader with sensitivity of -70 dBm, the penalty translates into a reading range decrease from 5 m, to 1.2 m. So this is a very important phenomenon to consider, and in the case of such proximity, the tag antenna should be designed to mitigate such effects.

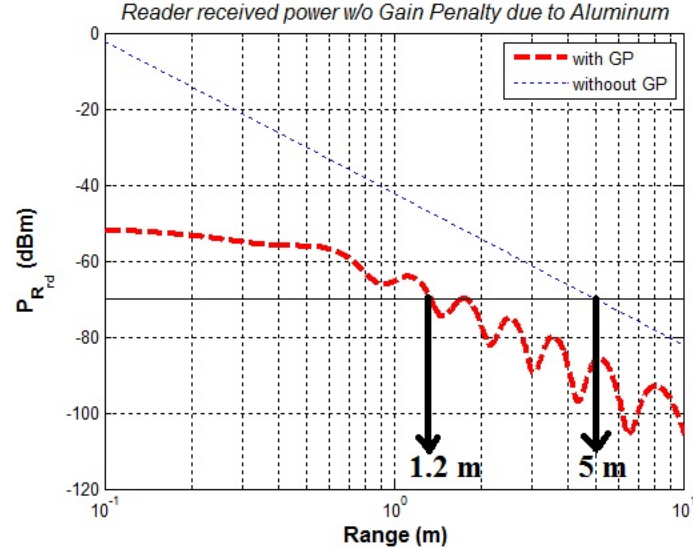


Figure 2.24: Two ray versus basic attenuation propagation model influence in reading range for a tag attached to aluminum slab.

## 2.6 RFID tag load modulation influence on read range

The system under study, consists of an UHF-RFID reader in communication with a remote tag antenna IC. Since our frequency band comprises 868 MHz, from the ISO/IEC 18000 RFID Air Interface Standards, the ones that will affect to us will be comprised in the 18000-6 Part 6. The RFID class structure, depicted in the following, provides a framework to classify tags according to their primary functional characteristics:

- **Class 1:** Read-only passive identity tags, no battery.
- **Class 2:** Passive tags with additional functionality, such as memory or encryption.
- **Class 3:** Semipassive tags (battery assisted); may support broadband communication
- **Class 4:** Active or ad hoc tags, that may be capable of broadband peer-to-peer communication with other active tags, in the same frequency band and, with readers.
- **Class 5:** Reader tags; they can power other Class 1, 2, and 3 tags and also communicate with Class 4 tags and with each other wirelessly.

Developed by the EPCglobal industry group, the EPC Generation 2 standard [44] defines the physical and logical requirements for a passive-backscatter, interrogator-talks-first (ITF), RFID system operating

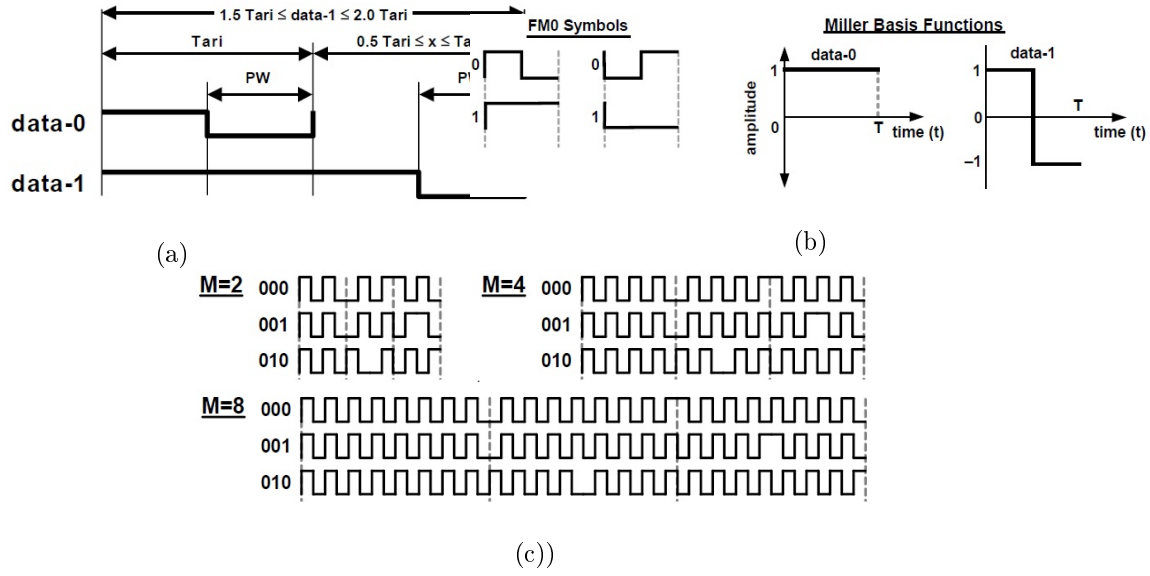


Figure 2.25: (a) PIE data-0/1 symbols, with  $6.25 \mu\text{s} \leq T_{\text{ari}} \leq 25 \mu\text{s}$ . (b) FM0 and Miller basis functions. (c) Example of Miller code for  $M = 2, 4, 8$ .

in the 860 to 960 MHz frequency range. EPC Gen 2 is a new standard for RFID tags, specifying the operation of the tag and the communication protocol for interoperability with EPC readers worldwide [65].

For a deeper understanding of the whole system proposed in this thesis, some tools will be set up (Matlab, Agilent ADS) to perform system level simulations of the RFID and NFC architectures. Different radio building blocks will be modeled. Special attention will be paid on the analog/RF interface. Since the work uses commercial radios, the system will not include the different elements that define radio design (RFIC design), but the elements that interface with the RF front-end part such as Low-Noise Amplifier, antenna, switches, amplifiers, reflections with environment or AWGN noise.

One way to evaluate the system performance of any radio system, consists on analyzing how the signal and the noise are performing at the receiver, so it is possible to validate the correct performance of the radio system, by looking at the variation of such parameters. In particular read range can be evaluated based on the SNR required by the radio, that will be determined according to threshold BER required.

There are two major protocols adopted for UHF passive RFID field, EPCglobal specifications and ISO 18000-6, which identify the interaction between tags and readers. An RFID reader can use in the uplink, Double-Side Band Amplitude Shift Keying (DSB-ASK), Phase-Reversal ASK (PR-ASK) and Single-Side Band ASK (SSB-ASK). The EPC GEN 2 specification defines a number of options for the physical layer in both downlink and uplink (table 2.9), the reader uses Pulse Interval Encoding (PIE). The length of Data-0 is given in  $T_{\text{ari}}$ , where a  $T_{\text{ari}}$  is the time reference unit of signaling and takes values between  $6.25 \mu\text{s}$  and  $25 \mu\text{s}$ . The length of Data-1 takes values between 1.5 and 2  $T_{\text{ari}}$  (see Fig. 2.25).

Demodulation from tag to reader is unique because of the backscattering demodulation technique. As the electromagnetic wave is reflected toward the antenna, a transistor is switched rapidly between one of two impedance states. Because each impedance state has both a complex and imaginary characteristic, the resulting RF signal shows changes in both phase and amplitude. Thus, backscattered information from an RFID tag uses a modulation scheme that is a combination of phase-shift keying

(PSK) and amplitude shift keying (ASK).

While varying the IC terminal impedance, the field is modulated and the induced reader voltage ( $V_R$ ) at the antenna will vary between  $V_{R1}$  and  $V_{R2}$ , enough levels to be demodulated correctly, above  $BER_{th}$ . It is conceptually understood that by using the two values further away of  $V_R$ , the demodulator can differentiate more clearly the two values, so in this case would be the more suitable to reduce transmission error but higher power is required. For the evaluation on maximum reading distance, it will be considered two modulation schemes ASK and PSK, in each situation the interrogation range will be determined based on link quality (BER).

The terminal IC impedance can also be affected by electromagnetic coupling during the radio link. This is due to close proximity of metal objects, other antennas, or other type of material objects, that may interfere not only in the signal, but also produce variations in tag antenna impedance  $Z_{tag}$ , and change the resonance characteristic, such as becoming relatively narrower [66]. Such effects, not only influence reading range, due to mismatch and reduced input power, but also affect both amplitude and phase distortion, so the modulation depth [57], which will affect either the tag and the reader receiver. Anyhow this will affect the modulation schemes typically used in RFID; ASK, or in particular OOK adopted by standards, or PSK [33].

Table 2.9: SUMMARY TABLE EPC GEN2

Uplink modulation			Reader data encoding	Tag data encoding
DSB-ASK	PR-ASK	SSB-ASK	length Data0: 1 Tari length Data1: 1.5-2 Tari ( $6.25 \leq \text{Tari} \leq 25 \mu\text{s}$ )	FM0 Miller subcarrier encoding 2-4 or 8 cycles/encoded sym.
Link Freq. (LF) = $\frac{DR}{T_{Real} + R}$ , ( $5 \text{ kbps} \leq \text{LF} \leq 640 \text{ kbps}$ )				
5 kbps: Miller M=8, $T_{Real} = 200 \mu\text{s}$ , DR=8 (Divide Ratio)				
640 kbps: FM0, $T_{Real} = 33.3 \mu\text{s}$ , DR=64/3				

Tag communicates with reader using FM0 or Miller sub-carrier encoding, where Miller code can be spread to reduce the rate by multiplying the encoded symbols by a sequence that can include 2, 4 or 8 cycles per encoded symbol. The general form for BPSK signal with amplitude will be:

$$A = \sqrt{\frac{2E_b}{T_b}}; \quad s_n(t) = A \cos(2\pi f_c t + \pi(1 - n)), \quad n = 0, 1. \quad (2.52)$$

The constellation diagram of BPSK signal consists only of two signals that can be represented by  $\sqrt{E_b}\phi(t)$  for "1", and  $-\sqrt{E_b}\phi(t)$  for "0", where  $\phi(t)$  is the *basis function*:

$$\phi(t) = \sqrt{\frac{2}{T_b}} \cos(2\pi f_c t) \quad (2.53)$$

The received signal will be;  $r_1 = s_1 + n$ , and  $r_2 = s_2 + n$ , with the noise  $n(t)$  that follows the power density function of:

$$p(x) = \frac{1}{\sqrt{2\pi\sigma^2}} e^{-\frac{(x-\mu)^2}{2\sigma^2}} \quad (2.54)$$

where the standard noise deviation at the input of the receiver relates with the power noise by;  $\sigma^2 = \frac{N_0}{2}$ . The probability of having an error in the received signal  $r$  when transmitting  $s_1$  is;

$$P(e|s_1) = \int_{-\infty}^0 P(r|s_1) \cdot dr = \frac{1}{\sqrt{\pi N_0}} \int_{-\infty}^0 e^{-\frac{(r - \sqrt{\frac{E_b}{N_0}})^2}{N_0}} dr = \frac{1}{\sqrt{\pi}} \int_{\sqrt{\frac{E_b}{N_0}}}^{\infty} e^{-z^2} dz = \frac{1}{2} \operatorname{erfc} \left( \sqrt{\frac{E_b}{N_0}} \right) \quad (2.55)$$

where  $\operatorname{erfc}(x)$ <sup>1</sup> is the complementary error function;

The ratio between signal to noise is an expression that helps in specifying radio performance by means of the ratio between the number of bits that can be received erroneously, compared to the total transmitted number of bits, so the Bit Error Rate (BER).

$$SNR = \gamma_b = \frac{E_b}{N_0} = \frac{V_0^2}{N_0} = \frac{V_0^2}{2\sigma^2} = \frac{d_{min}^2}{8\sigma^2} \quad (2.56)$$

where the energy of the bit voltage is related to the distance between the bits in the constellation diagram for the particular modulation scheme Fig. 2.26, according to minimum distance between constellation detection voltages  $d_{min} = 2V_0$ , which will determine the minimum detection threshold to resolve between all the received bits in the analog to digital conversion system of the demodulator.

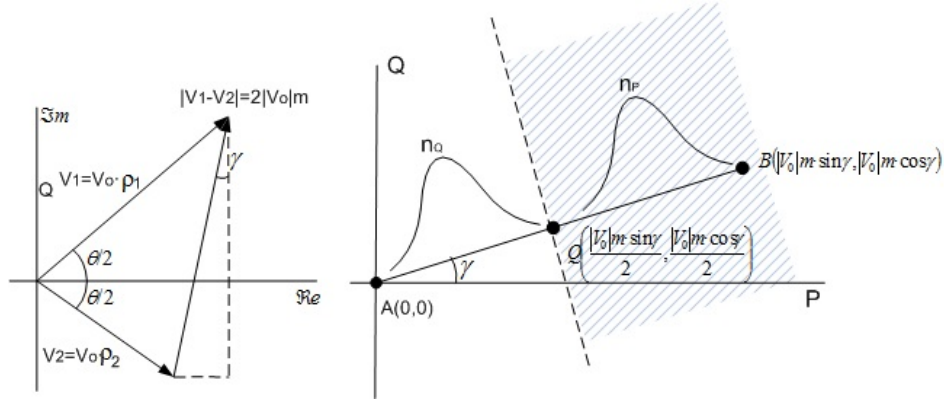


Figure 2.26: Amplitude and phase mixed modulation, with  $\mathbf{m}$  modulation index. In the right side, detector threshold separation between binary input levels with AWGN.

A coherent receiver can be used for both ASK and BPSK modulation, the only adjustment will need to be done for the threshold detection. Both modulations also use unipolar Return-to-Zero (RZ) codification, where the modulation of alternative "0" and "1" will deliver a square wave with amplitude varying from " $\frac{V_{R1} - V_{R2}}{2}$ " and "0". In this case, for an antenna resistance equal to  $R_{ant}$ , the modulated or effective power will be [57]  $P_U = \frac{(V_{R1} - V_{R2})^2}{8R_{ant}}$ .

In ASK the power reflection coefficient would be 0 in case of data "0" and  $\rho$  for data "1". For PSK in both cases would be  $\rho$ . So the time averaging absorption power of the tag is:

$$PA^{ASK} = \left(1 - \frac{\rho}{2}\right) P_R; \quad PA^{PSK} = (1 - \rho) P_R \quad (2.57)$$

where  $P_R = \left(\frac{\lambda}{4\pi r}\right)^2 P_T G_T G_R$  is the power received by the tag antenna.

---

<sup>1</sup>  $\frac{1}{2} \operatorname{erfc} \left( \frac{x}{\sqrt{2}} \right) = \frac{1}{\sqrt{2\pi}} \int_x^{\infty} e^{-\frac{x^2}{2}} dx$

Assuming ideal, matched-filter demodulation and Additive White Gaussian Noise (AWGN) with standard deviation  $\sigma$  at the detector input, the BER for both PSK and ASK (OOK) will be determined based on such energy distance between received bits.

With this RFID system, the maximum demodulation distance will be found depending on the load modulation and the back-scattering signal affected by nearby objects. Such effects need to be introduced in the reflection coefficient between load (subject to the modulation) and antenna impedance (subject to environmental effects) [67];

$$\rho = \frac{Z_L - Z_{ant}^*}{Z_L + Z_{ant}}; \quad \rho_{1,2} = \frac{Z_{1,2} - Z_{ant}^*}{Z_{1,2} + Z_{ant}} \quad (2.58)$$

when the modulation takes place by switching the impedances values from  $Z_1 = R_1 + jX_1$  and  $Z_2 = R_2 + jX_2$ . For both ASK and PSK, the BER will be able to be expressed depending on the **modulation index (m)** as;  $m = \frac{|\rho_1 - \rho_2|}{2}$ , being  $\rho_{1,2}$  the reflection coefficient at the tag antenna terminals [33, 57].

$$BER = \frac{1}{2} \operatorname{erfc} \left( \frac{|V_{R1} - V_{R2}|}{4\sqrt{2}\sigma} \right) = \frac{1}{2} \operatorname{erfc} \left( \frac{|V_0| \cdot |\rho_1 - \rho_2|}{4\sqrt{2}\sigma} \right) = \frac{1}{2} \operatorname{erfc} \left( \frac{|V_0| \cdot m}{2\sqrt{2}\sigma} \right) \quad (2.59)$$

- ASK modulation: the two states have different voltage  $V_{R1}$  and  $V_{R2}$  associated, depending on modulation depth. The minimum distance will be:  $d_{min} = (V_{R1} - V_{R2})/2$ . Extreme case is for  $V_{R2} = 0$  for OOK modulation, with  $d_{min} = (V_{R1}/2)$ . In this case as can be seen in the Fig. 2.27 is the more easy demodulating one, presenting the less errors.

$$BER^{ASK} = \frac{1}{2} \operatorname{erfc} \left( \frac{|V_{R1} - V_{R2}|}{4\sqrt{2}\sigma} \right); \quad BER^{OOK} = \frac{1}{2} \operatorname{erfc} \left( \frac{|V_{R1}|}{4\sqrt{2}\sigma} \right) \quad (2.60)$$

In one state  $|\rho_1| = 1$  ( $Z_1 = 0$  or  $Z_2 = \infty$ ), and in the other state  $|\rho_2| = 0$  ( $Z_2 = Z_{ant}^*$ ).

- PSK Modulation: the two states ("0" and "1") values have the same voltage  $V_{R1} = V_{R2} = V_R$ , differing in phase and angle  $\theta$  that can be determined by the tag back-scattering field.

$$\theta = |\arg(V_{R1}) - \arg(V_{R2})|; \quad BER^{PSK} = \frac{1}{2} \operatorname{erfc} \left( \frac{|V_R| \sin(\theta/2)}{2\sqrt{2}\sigma} \right) \quad (2.61)$$

In PSK, when  $Z_{tag}$  and  $Z_{ic}$  are such that  $\Re\{\rho_{1,2}\} = 0$ , and the phase angle;  $\Im\{\rho_1\} = jm$  and  $\Im\{\rho_2\} = -jm$ ; then  $\theta = 2\arctg(m)$  [68]. It is interesting to observe how the receiver performs when modifying the modulation index. The Fig. 2.27 shows how for several phase-difference between the two states of the incoming received voltage, the radio demodulates differently the information. For higher modulation index (m), the modulation becomes more efficient and BER improves. But if we increase "m", the power absorption coefficient lowers, so the deactivation tag range (to turn off the tag) also decreases.

### Using encoding

The UHF reader in addition to setting the uplink data rate (between 40 to 640 kbps), it is also setting the coding scheme, namely FM0, Miller-2, Miller-4 or Miller-8. Because FM0 is highly susceptible to noise and interference, then Miller-8 is more robust to errors than Miller-2, but also the link rates are reduced. Two expressions of BER are compared in order to analyze the behavior of RFID system in an AWGN channel [69], and also in a multipath channel, following a Rayleigh distribution [70] and including the effect of the coding scheme.



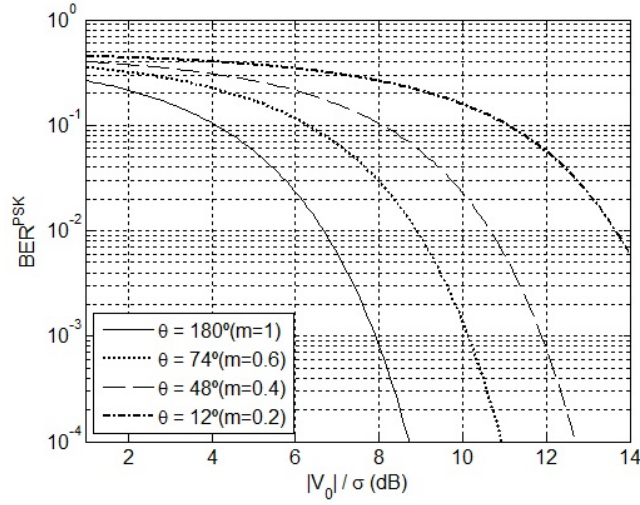


Figure 2.27: BER versus SNR according to Eq.(2.59).

- **AWGN channel:** the BER with  $E_s$  the symbol energy (or bit energy in our case),  $N_0/2$  the noise power spectrum density of an AWGN channel,  $M$  the Miller-code order, and  $Q(x)$  the Q-function<sup>2</sup>, is the following:

$$BER^{AWGN} = 2Q\left(\sqrt{\frac{ME_s}{N_0}}\right) \left[1 - Q\left(\sqrt{\frac{ME_s}{N_0}}\right)\right] \quad (2.62)$$

- **Rayleigh channel:** In the case of considering the RFID in a multipath channel, assuming that noise bandwidth is approximately equal to  $\frac{1}{T_s}$  ( $T_s$  symbol duration) so the Signal to Noise ratio and the BER correspond to the following expressions:

$$SNR = \gamma \simeq \frac{E_s/T_s}{N_0/T_s} = \frac{E_s}{N_0} \quad (2.63)$$

$$BER^{Ray} = \frac{1}{2} - \frac{1}{\sqrt{1+2/(M\gamma)}} + \frac{2}{\pi} \frac{\tan^{-1}\left[\left(\sqrt{1+2/(M\gamma)}\right)\right]}{\sqrt{1+2/(M\gamma)}} = \frac{1}{2M\gamma} \quad (2.64)$$

In Fig. 2.28 it is compared the BER performance of FM0 and Miller codes in ideal AWGN and Rayleigh channels. Within Gaussian Noise channels the BER decreases faster than in Rayleigh channels for large SNR. Also BER decreases with the increase of the Miller sub-carrier order (but data rate decreases). Four different cases have been represented that include the influence of self jammer into the radio, by means of the IIP3 specification. When lowering the IIP3 from +15 dBm to 0 dBm, we appreciate the lowering of performance both, in Rayleigh and Gaussian channels. The relation between self-jammer, IIP3 and SNR is obtained by combining Eq.(2.32), Eq.(2.33) into Eq.(2.62) and Eq.(2.64).

<sup>2</sup> $Q(x) = \int_x^\infty \frac{1}{\sqrt{2\pi}} e^{-y^2/2} dy$ , to note the relation with the erfc(x) function which is the following;  $erfc(x) = 2Q(\sqrt{2}x)$  and with erf(x);  $erf(x) = 1 - 2Q(\sqrt{2}x)$ .

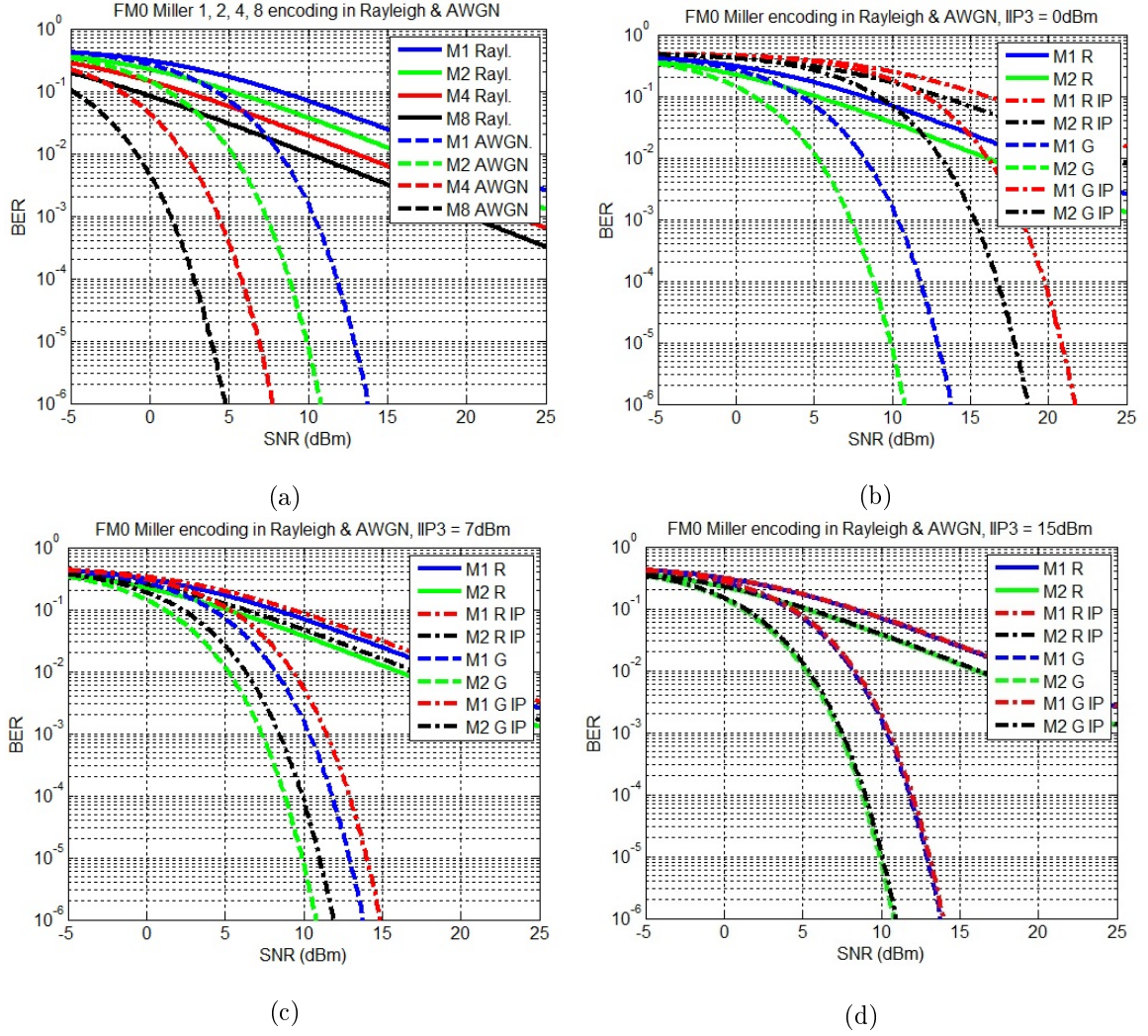


Figure 2.28: BER for radio RFID Miller FM encoding, with Gaussian and Rayleigh channel conditions. In the case of (b), (c) and (d) it is imposed some SNR degradation due to selfjammer.

In general if the real and imaginary part of a Phase Modulated signal are corrupted by Gaussian noise, then the statistics of the signal will follow Rician distribution. The difference from the case of Rayleigh distribution is described next.

### Rayleigh Distribution

Considering a noise process  $n(t) = r(t)e^{j\Phi(t)} = x(t) + jy(t)$ , where  $r(t)$  is the magnitude or envelope and  $\Phi(t)$  the phase,  $x(t)$  is the in-phase, and  $y(t)$  is the quadrature component. If both random processes  $x(t)$  and  $y(t)$  are statistically independent Gaussian distributed, with the same variance and zero mean, then their joint probability density function is:

$$P(x, y) = P(x)P(y) = \frac{1}{2\pi\sigma^2} e^{-\frac{x^2+y^2}{2\sigma^2}} \quad (2.65)$$

Transforming differential areas by using  $dx dy = r dr d\Phi$ , gives the joint probability density function of  $r(t)$  and  $\Phi(t)$  as;

$$P(r) = \int_{-\pi}^{\pi} \frac{r}{2\pi\sigma^2} e^{-\frac{r^2}{2\sigma^2}} d\Phi = \boxed{\frac{r}{\sigma^2} e^{-\frac{r^2}{2\sigma^2}}} \quad \text{Rayleigh distribution} \quad (2.66)$$

$$P(\Phi) = \int_0^{\infty} \frac{r}{2\pi\sigma^2} e^{-\frac{r^2}{2\sigma^2}} dr = \boxed{\frac{1}{2\pi}} \quad \text{Uniform distribution} \quad (2.67)$$

with the random variables  $t$  and  $\Phi$  that are statistically independent,  $P(r, \Phi) = P(r)P(\Phi)$ .

### Rice Distribution

In a noise process  $n(t) = r(t)e^{j\Phi(t)} = x(t) + jy(t)$ ;  $X$  is from  $N(\mu_x, \sigma^2)$ , and  $Y$  is from  $N(\mu_y, \sigma^2)$ . If both processes are statistically independent Gaussian distributed, with the same variance  $\sigma^2$  and means  $\mu_x$  and  $\mu_y$ , then the probability density function of  $r$  is the Rician probability density function;

$$p(r) = \frac{r}{\sigma^2} e^{-\frac{r^2 + m^2}{2\sigma^2}} I_0\left(\frac{rm}{\sigma^2}\right) \quad (2.68)$$

where  $m^2 = \mu_x^2 + \mu_y^2$  and  $I_0$  is the modified 0-th order Bessel function of the first kind given by:

$$I_0(x) \equiv \frac{1}{\pi} \int_0^{\pi} e^{x \cos \theta} d\theta \quad (2.69)$$

While Rayleigh and Nakagami distributions are used to model dense scatters, the Rician, models fading with a stronger LoS component. This can be more close to the case of RFID, where distance is not so big, a direct vision path is established and no so many scatters are expected when reader and tag are located not so close to the floor. A parameter to describe the expected scattering is the  $K$  value, that defines the importance of the LoS component between transmitter and receiver, defined as:

$$K = \frac{\text{LoS component}}{\text{multipath scattered power}} = \frac{m^2}{2\sigma^2}; \quad m = \sqrt{\frac{K}{K+1}}; \quad \sigma = \sqrt{\frac{1}{2(K+1)}} \quad (2.70)$$

The value of the Rician  $K$  factor is a measure of the severity of fading, with  $K=0$  ( $-\infty$  dB) being the most severe fading case (Rayleigh fading), and  $K = \infty$  representing no fading (for  $K \gg 1$ , tends to Gaussian distribution).

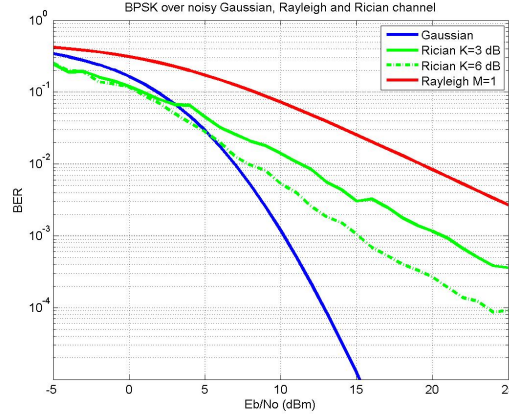


Figure 2.29: Comparison of BER for different channel noise models.

## 2.7 System co-simulation

When analyzing complete systems that include physical elements, hardware components in RF, analog and digital blocks, and the analysis requires time and frequency domain responses, we need to implement a simulation environment allowing the analysis of a complete RFID EPCglobal Gen2 system, from base band to the radio part at the UHF frequencies. It considers phenomena such as the radio IC transceiver interacting with other components, or stages of the radio (such as self-jammer effect between transmitter and receiver). Also incorporating real models of antennas with their PCB layout, allowing to study the influence of real antenna geometry in the RFID system by means of co-simulation capabilities; multiple path propagation effects that can be modeled by means of different analytical models and including physical dimensions of objects and obstacles as well as their reflection of absorbing properties, or the interaction between various tags responding to various readers at the same time.

It is proposed, based on channel path models, the interaction of several readers synchronized at different channels and distances over the pad, including different filter topology. So that, such simulating environment allows to be a useful tool for the interference analysis proposed in RFID, allowing to allocate possible sources for range limitation before installing real devices in the field such as antenna location for the readers and propose filter solutions. In Fig. 2.30, it is possible to see two of the proposed scenarios, with the interactions between tags and readers. In the case of the scenario b) it is normally used some sort of anti-collision techniques for the management of the multiple reading, so having available a simulation environment can be of help when designing anti-collision algorithms.

For the simulation of the RFID system, it has been used the simulation tool from Keysight ADS Ptolemy which includes two basic motors, one is RF and analogue simulator and the other is the digital signal processing simulator Ptolemy based in the discrete sampling concept, with a processing done in a similar way as the one that would be done with a DSP. Here the co-simulation is used to simulate in the same digital environment parts of RF/analogue (antenna, modulator) with the Envelope controller, that allows a fast circuit analysis when using complex signals such as the RF digitally modulated, with representation in the frequency-time domain. Even when considering a not very complex modulation scheme as defined by EPCglobal Gen2 (ASK-PSK) with its coding schemes, it is necessary the use of such Envelope controller.

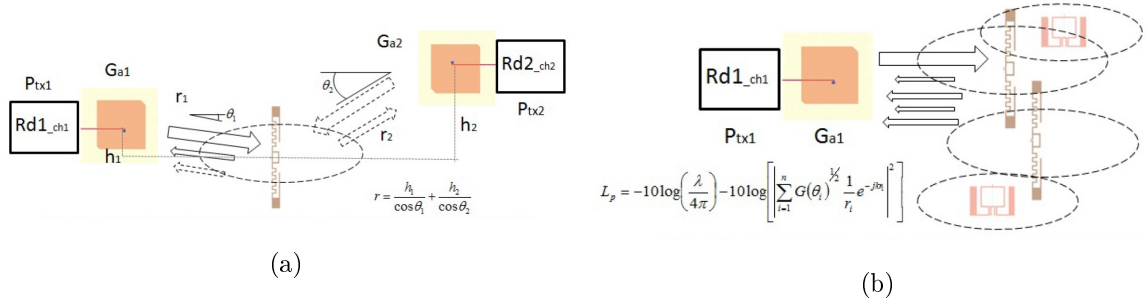


Figure 2.30: Scenarios attributed to (a) the interference's caused by various readers in different positions to one tag or (b) various tags interfering with each other, backscattering to a unique reader (anti-collision required).

### 2.7.1 Simulation results considering output filter

In Fig. 2.31 it can be seen the results of superposition of two spectral responses from tags into the reader in adjacent channels, that could correspond to first use case in Fig. 2.30, where two readers illuminate the tags. It is mandatory to keep the radiated spectrum signal within the limits indicated by the spectral masks specified by the standard. Such test can be included in this simulation for one or various readers. As specified by the standard which includes spectral mask for low and dense operation mode. It is also shown (bottom right) the spectral mask limiting the allowed zone for high density readers areas, where the bandwidth is  $RBW = 2.5/T_{\text{ari}}$ . The limiting mask is used to define the permissible filter that must be used for the RFID transmitter. The result depicted in Fig. 2.31 corresponds to the case of using an order 5 Chebyshev filter, so its effect is reflected into such spectrum. Another possibility is using a Rise Cosine filter with alpha of 1, as seen in Fig. 2.32, also showing the effect over the digital information time signal of such filtering effect. Such filter is normally being used to reduce the Inter-symbol Interference (ISI) and avoid synchronization problems. As shown in the Fig. 2.32, the filter pulse shape generation is implemented in the reader transmitter side, in order to satisfy the requirements fixed by the standard EPCglobal Gen2 (0,05 (A-B) V/m), that can be accomplished using before mentioned Rise Cosine with roll-off factor of 1. Other filter type such as Butterworth has also been tested.

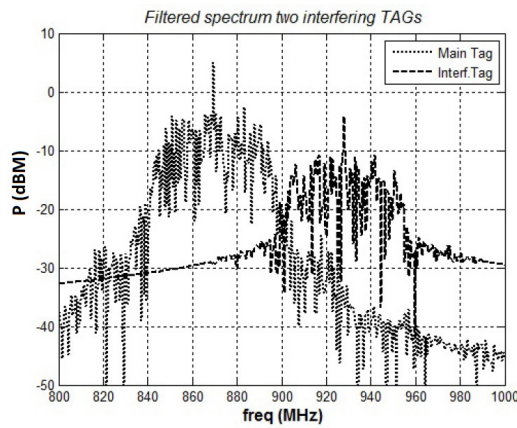


Figure 2.31: Superposition of two tags responses to readers transmitting in adjacent channels

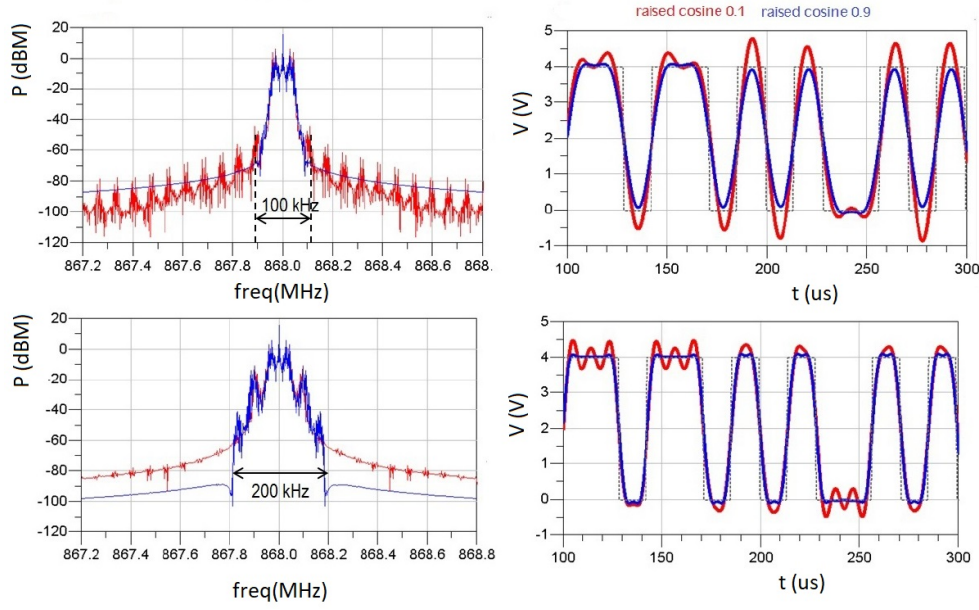


Figure 2.32: Frequency and time response to the codification with filter responses in different bandwidths

In the simulation results presented in Fig. 2.33, it can be seen how, a way of measuring tag 1 sensitivity, can be done by sending a sentence Query to the tag and hearing its response. Under different conditions, for example, channel use cases, distances, antenna positions and so, one can detect the reader response, for an specific gain settings. The value for which the receive signal has enough level for decoding (code RN16), determines the tag sensitivity. Such simulation helps on defining the receiver stage gain settings, in our case corresponds to the setting detailed in Fig. 2.33. For these systems, where the noise of the own receiver is so strong as the one it is defined by self-jammer conditions, it is not common to place a low noise amplifier (LNA) at the entrance of the receiver, so the Noise Figure (NF) is determined by the LNA as a first stage of the receiver, instead of the mixer. The conditions for Mixer and other receiver blocks (filters, gain stages) can be evaluated by such system simulations including the models of transistors, or real passive parts or the block with its electrical specifications.

A second set of simulation results shown here, consider only one tag under the influence of two synchronized readers in adjacent channels. The power received by the tag would correspond with the one presented in Eq. (2.71), where  $P_{tag}$  is the power received by the tag that represents its sensitivity:

$$P_{tag} = P_{min} G \left( \frac{\lambda}{4\pi r} \right)^2 \quad (2.71)$$

$G$  is the antenna reader gain,  $r$  is the distance between reader and tag and  $P_{min}$  is the minimum power being transmitted by the reader. Under a configured reader-tag situation, a sensitivity analysis is done based on considerations for channel attenuation and antenna gain settings. Fig. 2.33 at the bottom, shows the time domain receive signal at the reader, after being backscattered by the tag. One can observe that after the Query command that illuminates the tag antenna, a very weak signal is being detected by the reader after traveling all the way back from tag to reader. The filtering (including DC block) and receive gain setting will be determined based on this signal. So one can define such blocks based on this simulated signals. At the top of Fig. 2.33 one can see how the signal

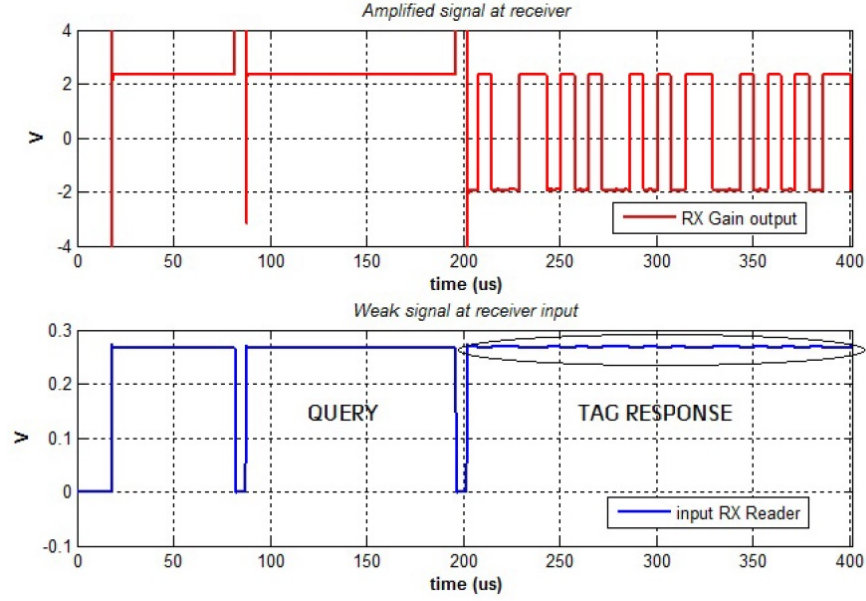


Figure 2.33: Receiver sensitivity measurement, after sending a continuous carrier and listening the receiver result.

looks like, after being filtered and amplified according to the settings mentioned before. Such settings conditions can be seen also at Fig. 2.33.

In reference to the tag, this one receives a continuous wave (CW) and generates a reflection or backscattering with modulation in amplitude or phase (AM o PM) and FM0 or Miller codification, modulating a subcarrier (40 kHz a 640 kHz). The data rates may vary for FM0 (40 - 640 kbps) or subcarrier modulation (5 - 320 kbps). In our case the tag modulation is AM with FM0 coding. In Fig. 2.34 can be seen the system blocks used for generating either the FM0 coding or decoding in the ADS simulation blocks.

In comparison with other works such as [71], that includes only electric field solvers providing a powerful tool for such purpose, this work intends to complement further in the analysis including analog and digital parts. It has been analyzed for example different sort of filters and receive sensitivities based on signal responses such as shown in Fig. 2.33 one can define the settings parameters for the receiver chain for example, to adequate receive gain stage in order for the decoder and demodulator to be able to demodulate the receive signal properly and detect, in our case EPC information.

In the model developed for this Fig. 2.33, the reader generates a CW that illuminates the tags close to it, and also, will be used to simulate the effect of carrier injection, from the transmitter side to the receiver, passing over a circulator or duplexor (in our case duplexor with 30 dB isolation). The tag responds by AM modulating the carrier according to FM0 (schema Fig. 2.34). From this base model, the system has been grown to include the effects of other radios over some tags, also similar to the ones shown in the Fig. 2.31, and transmitting in adjacent channels, since it is supposed a channel discrimination corresponding to a robust system.

In the DL the reader uses Pulse Interval Encoding (PIE). The data length for "0" comes in T<sub>aris</sub> (time reference unit for signaling) that can comprise values between 6.25 ms and 25 ms, used normally to obtain the transmission data rate. The data "1" length can take values between 1.5 and 2 T<sub>ari</sub>. This information is modeled in the transmitter side of the reader. In Fig. 2.35 one can see the modeling detail both for the coding and decoding, as well as the bit pattern with and without coding. Such bit



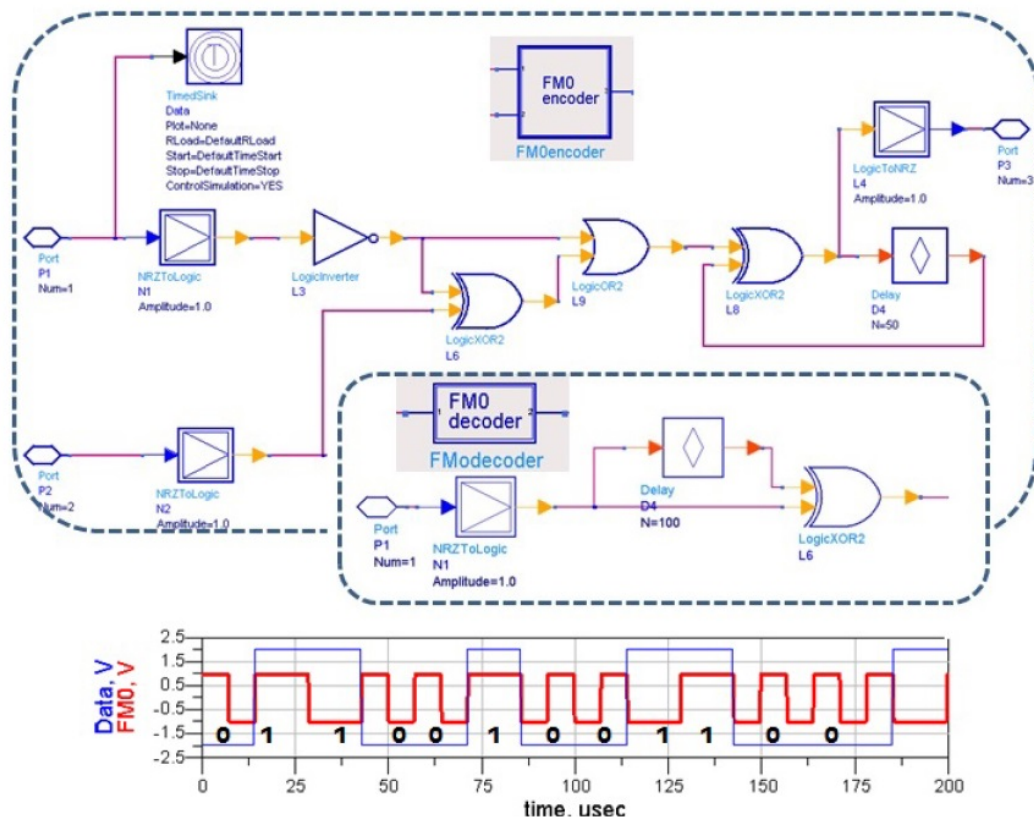


Figure 2.34: Graphical representation and Block scheme for the coder and decoder in the case of FM0 coding, including at the bottom its physical implementation in ADS.



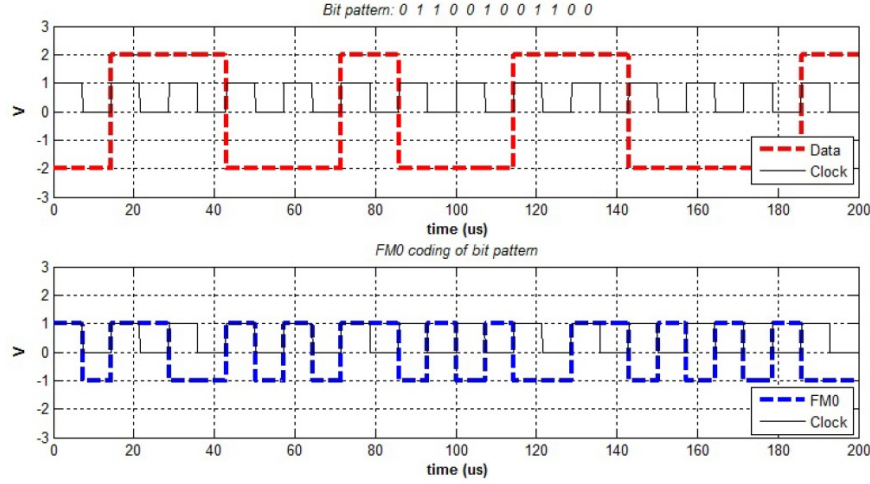


Figure 2.35: Time signal at the transmitted bit pattern including clocking of the signal after FM0 encoding.

pattern representing the information data bits, modulates the carrier and is received, after passing the channel, by the Momentum modeled receiving antenna and mixer first stage receiver.

### 2.7.2 Antenna modeling

Both for the reader and the tag, antenna models have been created using Momentum from ADS, which allows a 2.5D element simulation. The properties of the material used for the antennas are the ones from RO3010 with dielectric constant 10.2 and thickness of 1.27 mm. This allows for a good compromise between size and performance at the working frequency of 868 MHz. As can be seen in Fig. 2.36, the reader antenna corresponds to a two layer patch antenna, with two lateral cuts to provide with circular polarization and appropriate gain. The tag is composed by a dipole with adaptation in T, dipole "Meandered" and "Tip loading" Fig. 2.17.

EPCglobal Class 1 Gen 2 standard, specifies a variety of options to code the information in the UL from tag to reader, being the most simple the FM0 code, with a transition at the end of each period, and with an additional transition at the middle of the bit for the bit "0" [72]. This codification has also memory, so that the FM0 sequences depend on the previous ones. In the image of Fig. 2.35 one can see the components that define the coding part (located in the tag) and the decoding (in the reader) for the FM0 case. The presented system, designs both, the tag coding and the reader decoding in order to be able to compare responses in the digital base band side. Both coding schemes used in Gen2; FM0 and Miller, use the same base functions, so that, they have the same Bit Error Rate (BER) response, that corresponds to Eq.(2.62). With such expression and simulation set-up, it is possible to evaluate the error probability of the transmission versus different situations of noise channel, transmitted power, filtering design, information coding or other parameters to consider.

### 2.7.3 Complete UHF-RFID system

Fig. 2.37 represents the simulation model for the complete blocks of the system. In this case it is shown the reader, with the tag models and the channel, defined in both directions of the radio link for clarity of the picture. It is omitted the replicas of other reader and tags model, that are used for the case of multiple dense reader simulations. Also other possible radio models (SRD, LTE, GSM and so)

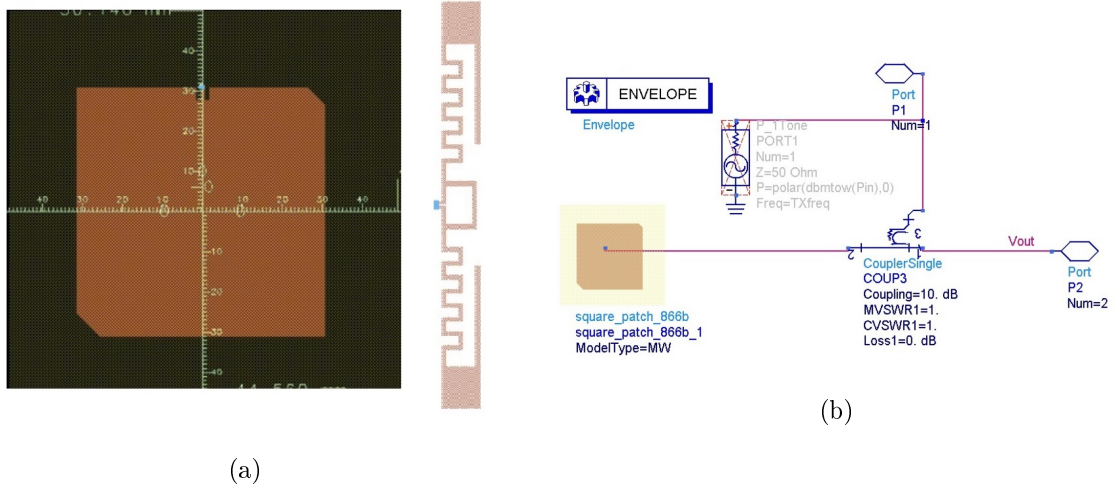


Figure 2.36: Incorporating the Momentum model of the patch antenna for the reader, and the dipole tag antenna (a), for the co-simulation (b), which uses the engine "Envelope".

can be included in the model, so their effects with the RFID system can also be analyzed. Some of the blocks shown in the figure include sub-models with their corresponding real parameters, for close proximity to reality, allowing a maximum of accuracy for the component that integrates the system.

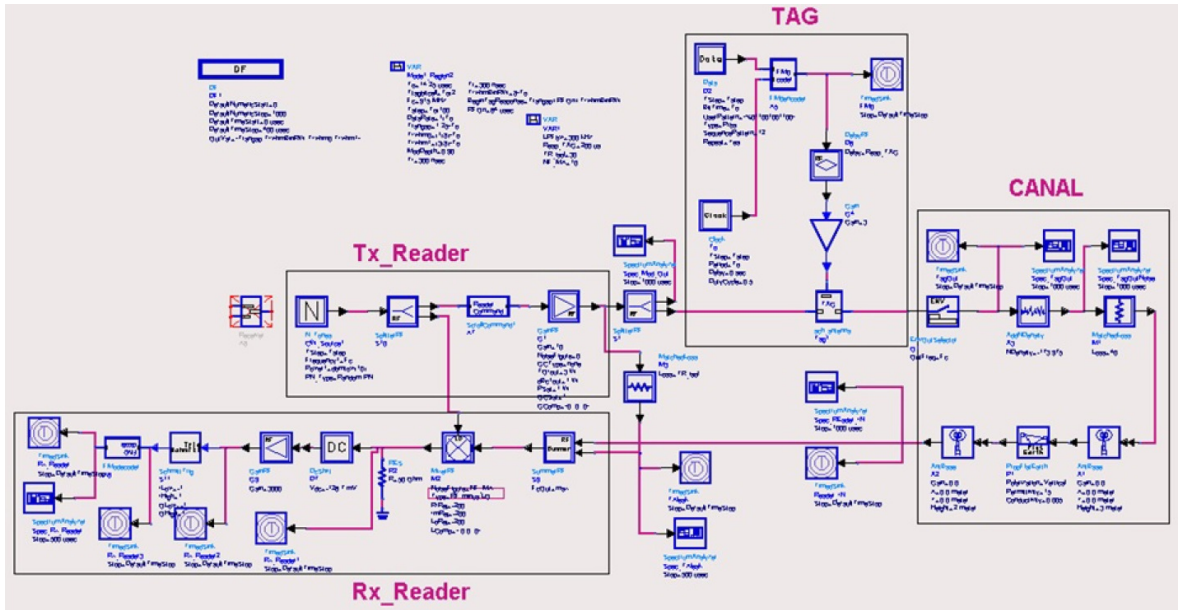


Figure 2.37: ADS model of the RFID system including, reader transmitter with its antenna layout, tag, channel with attenuation and noise and receiver reader.

## 2.8 Conclusions

Due to the nature of the RFID systems, very weak back-scattering signal must be detected. This system study has provided with significant parameters of the different blocks that constitute it, showing

that it is prone to interference from many sources. After looking in detail all possible undesirable effects that may incur in actual RFID systems, considering tag or reader limiting factors, it is concluded that incorporating a detection circuit based on RSSI to scan for such effects would be advantageous. Such circuit is described and the benefits are evaluated as being good contributions for future RFID readers, mainly in hostile environments or where dense population or tags is present. Such analysis can be extended when designing an RFID co-simulation environment, and the RSSI detection circuit in the receiver after the mixer, as in Fig. 2.37, with the detection power from Eq.(2.72) will indicate best mixer gain settings  $G_{MX}$ .

$$P_{in}(dBm) = 10 \cdot \log \left( \frac{\sqrt{I_{DC}^2 + Q_{DC}^2}}{G_{MX}} \right) \quad (2.72)$$

It is out of the scope of this work, but by using different antenna, RF front-end models, and channel conditions, one can analyze in detail the system. So with this works it helps to set up the basis for RFID analysis to better understand system performance. A superposition method for Ptolemy co-simulation can be applied in order to extend the use cases. Different filter settings are tested to verify spectrum masks, while modifying physical parameters of RF front end such as antenna layout, IIP3, P1dB, gains and sensitivities.

New conclusions have been obtained based on studies of two tag interaction, showing some configurations where the detection is basically reduced or not possible based on SNR threshold limitations.

Finally it is shown an interesting system co-simulation tools that allows the system simulation, including different sort of interference, as well as different environments with their channel models and physical components coming from layout data.

## 3 HF antenna and charging circuit design

### 3.1 Introduction

There are two different technologies that use HF in RFID applications; HF-RFID and NFC both operating at 13.56 MHz band. In this work we will focus on the Near Field Communication (NFC), used in mobile phones. Some actual applications for NFC include the possibility to open a communication link, to authenticate, or to implement payment by bringing two NFC devices close to each other. Devices with NFC interface operate at 13.56 MHz via inductive loop antennas. One possibility of operating environment is when the antenna is close to the battery pack of a mobile phone. In this case, the loop coils of NFC antennas are constructed on a ferrite layer, to magnetically isolate them from metal (typical with relative permeabilities of  $\mu'_r > 80 \dots 160$  and low losses  $\mu''_r < 3 \dots 5$  [73]).

For certain applications, which demand relatively low data rate (106 kbps) and a small read out distance ( $< 1\text{m}$ ), the HF 13.56 MHz band is the preferred choice [74] because of two main reasons.

- First, since this band is internationally allocated for unlicensed (ISM) use worldwide, the designed system has the possibility to perform anywhere in the world.
- Second, the magnetic field propagation at HF (HF-RFID) penetrates dielectric materials with high permittivity, such as water and ground, better than the EM waves at UHF (UHF-RFID) in short range applications.

The inductive link established between two antennas is weak and performed by resonating antennas. That means that can be implemented by one of the four possible combinations of series or parallel tuned typologies.

Some authors have studied how to enhance mutual coupling between antennas and, have studied the H-field from the reader antenna. With the optimal antenna size design, the internal area of the coil can be exploited to enhance the H-field as is done by the authors in [75], with an unequal spacing between turns of the coil that allows adjusting the  $L$  without de-tuning its resonance ( $f_r$ ). In this work our proposal is to use NFC, not only for communication, but also for transferring power into a HF sensor node, describing an innovative circuit presented for this purpose, so detailed coupling analysis between coils needs to be performed in detail.

### 3.2 HF-RFID system design

Here we will introduce our NFC system used for communication and energy transfer. Magnetic or inductive coupling at radio frequencies for wireless power and data transfer is a known solution for some devices. An inductive link consists of two weakly coupled resonant circuits that can be misaligned, where coil coupling conditions can be very small due to large coil separation or a very small pick-up

coil diameter. From the inductive element, a way to transfer power of near-field RFID, is to add a parallel capacitor to create a resonance circuit. In the case of very short distances, high power transfer efficiencies can be achieved (on the order of 90% for very short lengths; 1-3 cm) [76]. However, the efficiency of such techniques drops drastically for higher distances decaying at a relation of  $1/r^6$ .

Electromagnetic resonance coupling involves creating an LC resonance, and transferring the power with electromagnetic coupling without radiating electromagnetic waves. According to ISM band, the bandwidth of the resonance for 13.56 MHz range is  $13.56 \text{ MHz} \pm 7 \text{ kHz}$ , so probably a tuner must be used to match the resonance. Some authors have been using strongly coupled magnetic resonance (SCMR) already for RFID (in the case of [77] at 60 cm distance). These are non-radiation methods operating in the reactive near-field, that include between transmitter and receiving loop an helix close to each loop, achieving a wireless-to-wireless efficiency of 40% and 60% in air, for a distance of 2 m [78, 79].

Either for communicating HF radios or for wirelessly power transfer (WPT), one crucial part of the design is the matching circuit. Through proper impedance matching circuits, the transfer power efficiency or reading range are improved. Since the impedances of reactive components in the matching circuits are frequency dependent, the impedance can only be matched at a single operating frequency, or a small frequency band, depending on the  $Q$ .

Driving the matching network, there must be a high efficiency power amplifier (PA) such as "Class E" PA, also known as switched mode PA, because the transistor acts as a switch instead of current source, in order to improve efficiency (theoretical 100%) [80]. Also they offer high capability to drive relatively high AC current through the transmitter coil from a relatively low DC input current and voltage. With the transistor operating as on/off switch, the load network shapes the voltage and current waveforms [81], in such a way that simultaneously high voltage and high current are avoided in the transistor. Minimum voltage-current product during the switching in the transitions is avoided. The RF output amplitude is almost linearly proportional to the DC supply voltage. An important element for such PA is the switch, since it must have a low ON resistance, in the case of the common MOSFET process the  $R_{DS(ON)}$ . However, reducing ON resistance, usually results in an increase in gate capacitance as well as an increase in gate voltage. On the contrary, decreasing gate capacitance increases rise and fall times [82]. Such features are important when designing coil driving stage and filtering blocs.

### 3.2.1 Propagation Antenna Field Regions

Once a transmitting device is wireless sending propagation waves on the media, depending on the distance that a receiving antenna is located from the transmitter, the propagation waves present different characteristics. To electromagnetically efficiently radiate a signal, the linear dimension of the antenna must be comparable with the operation frequency wavelength. However in the case of HF-RFID, dimensions are much less in the order of  $0,002\lambda$  where  $\lambda=22\text{m}$  @ 13.56 MHz, therefore it is difficult to form a true antenna for RFID applications. Alternatively a small loop antenna, with current flowing into the coil, radiates a near-magnetic-field that falls with  $1/r^3$ . This type of antenna is called *magnetic dipole antenna* widely used in RFID. When an antenna is transmitting electromagnetic waves, it is exposed to changes in its boundary conditions, so in its transmitting characteristics, due to conducting, or non-conducting material (with a dielectric constant and/or a permeability constant greater than 1), located in the reactive near-field region.

One can divide the space around an antenna (or other radiating element) into the near-field region and the far-field region. The near-field region is further divided into the reactive-field region and the radiating-field region (Fresnel)[83]. Further away there is the far field (Fraunhofer) region. In the reactive near field region, the energy is oscillating and stored in space, so it is not radiating. When the resonant evanescent fields of two antennas overlap, they are strongly coupled to each other. This coupling can be modeled by using the couple mode theory (CMT).

- **Reactive Near Field:** The region immediately surrounding the antenna where the reactive field (stored energy - standing waves) is dominant. If  $D$  is the longitude or diameter of the antenna:

$$r \leq 0.62\sqrt{\frac{D^3}{\lambda}} \quad (3.1)$$

- **Near Field (Fresnel region):** The region between the reactive near-field and the far-field where the radiation field (propagating waves) is dominant, and the field distribution is dependent on the distance from the antenna. Very close to the antenna, we have the reactive near field region, that surrounds the antenna wherein the reactive field predominates. Such boundary is defined as follows:

$$0.62\sqrt{\frac{D^3}{\lambda}} \leq r_2 \leq \frac{2D^2}{\lambda} \quad (3.2)$$

- **Far Field (Fraunhofer region)** In the far field region, the relative angular distribution does not vary with distance and the radiated power decays according to the inverse square of the distance ( $1/r^2$ ), so the field distribution is essentially independent of the distance from the antenna. The Fraunhofer region is defined for

$$r \geq \frac{2D^2}{\lambda} \quad (3.3)$$

### 3.2.2 Coil antenna design

We start by explaining the design of loop antenna for reader in NFC applications, to later expand it for WPT. In HF-RFID applications, at 13.56 MHz for passive tags, some hundreds of  $nH$  to few  $\mu H$  of inductance and few  $pF$  of resonant capacitor are typically used. The reader coil and the tag coil, form a transformer with air-gap where the voltage is transferred through inductive coupling. The efficiency of the voltage transfer ratio can be increased significantly with high  $Q$  circuits. The antenna coil design in such systems is mainly influenced by low cost, low profile, and electrically small size. Whereas the bandwidth ( $BW$ ) requirement for tag coils is not so critical in most RFID applications. That is not true when coming to apply the antenna for NFC communications, where data is transferred at higher data rate.

There are several publications which describe different approaches for loop antenna design, starting with Maxwell [84], who gives analytic equations for inductance estimation, to [85] which provides several useful approximations for practical cases in RFID applications [86]. For the antenna design, the main parameter is the inductance, less important are the parasitic capacitance, and the antenna losses ( $R_{loss}$ ), so one can consider designing and inductance and focusing on geometry to get the desired values. The design parameter for the reader coil antenna are the coil shape and size, the section of the wire, and the number of loops. These parameters determine relevant system performance quantities such the coupling coefficient ( $k$ ) between the reader and tag coils, H-field ( $H$ ) at the receiving tag coil, inductance  $L$ , and unloaded quality factor  $Q$  of the antenna. To obtain major reading range one wants to maximize induced voltage in the tag that will activate the chip for tag response. Some approaches to do so are described:

- A first approach is to improve  $k$  maintaining  $L$  [87, 88]; so it implies improved coverage and antenna size reduction due to increase in induced voltage  $V_{ind}$  as a function of  $I$  current in the reader:

$$V_{ind} = j\omega M_{12}I = j\omega k\sqrt{L_{Tag}L_{Rd}} \cdot I \quad (3.4)$$

As shown in [87], an optimum  $k$  design while keeping  $L$  constant results in 25% reduction in  $Q$ -factor, that implies an increase in antenna loss and reduced efficiency.

- A second approach is to improve the propagating H-field between reader and tag, so following Faraday's law, the induced voltage is increased as:

$$V_{ind} = -\frac{d\Phi(t)}{dt} = \Phi \cdot j\omega = B \cdot A_{Tag} \cdot j\omega = j\omega\mu_0 N_{Tag} A_{Tag} H \quad (3.5)$$

Where we have not considered the  $90^\circ$  phase shift of the carrier signal from the derivative of  $B(t)$ <sup>1</sup>. However, the  $H$  improvement (increase number of loops and space between the elements that form the coil) in the coil surely improves  $V_{ind}$  but it will lower  $Q$  of the reader coil (this assumes a constant  $L$ , since  $Q = \omega L/R$ ) [87, 89].

- Also one could want to design smaller antennas. If the loop area is reduced by half, this could be compensated by an increase in the number of turns by 2 to achieve the same induced voltage Eq.(3.5). But since the chip has fixed capacitance, at resonance we need to maintain inductance, so such condition does not fit.

### Coil design

For the antenna geometry, normally for this kind of antennas the squarer the better. Bearing in mind this is magnetic coupled data and one should be looking for a loop with as much inductance as possible, but not so much that it's self resonant frequency is lower than (say) 15MHz. As a simple idea about inductance can be defined as the total flux produced per ampere. The bigger the cross sectional area, the more flux is produced per ampere. A long thin loop however has less inductance than a square loop of the same area.

There are many studies related to the calculation of planar multi-layer coils [90, 91] that cover the design from different approaches, and methodologies. One important aspect considered in this work is the search for an analytic expression that presents, based on basic geometrical and physical properties, an estimation for the coil design. From that approach, we will construct a model, and using the Method of Moments implemented in ADS (Agilent) simulation tool, electromagnetic simulations is conducted to complement the calculations and finally be measured.

Firstly, we estimate the inductance analytically. After several approaches the method used takes the following considerations.

- Convert the square or rectangular loop in a single turn geometry. The rectangular cross-section with track width  $w$  and thickness  $t$ , is approximated by a circular cross-section of equal area:

$$d = 2\sqrt{\frac{t \cdot w}{\pi}} \quad (3.6)$$

- With the square mean, we calculate the average length  $a$  and the average width  $b$  of a single turn loop, out of the maximum length  $a_0$  and the maximum width  $w_0$  of the  $N$  turn antenna.

$$a = \sqrt{\frac{a_o^2 + [a_o - 2N(g + w)]^2}{2}}; \quad b = \sqrt{\frac{b_o^2 + [b_o - 2N(g + w)]^2}{2}} \quad (3.7)$$

$g$  specifies the gap between conductor tracks.

---

<sup>1</sup>  $\mu_0 = 4\pi \cdot 10^{-7} \text{Vs/Am}$

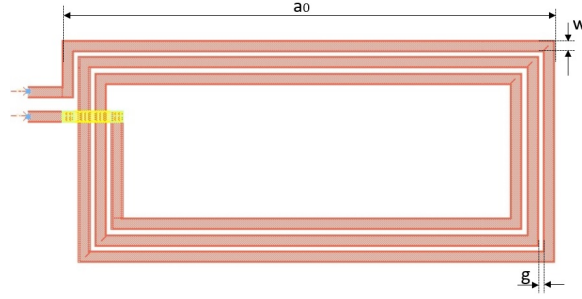


Figure 3.1: Single layer multi-turn coil size definition

- We must find the contributions from the self-inductance  $L_1$  and  $L_2$  given in Eq.(3.8), and the mutual inductance  $M_1$  and  $M_2$  between all parallel conductor parts given in Eq.(3.9) and (3.10),

$$L_1 = \frac{\mu_0 \cdot a}{16\pi}; \quad L_2 = \frac{\mu_0 \cdot b}{16\pi} \quad (3.8)$$

$$M_1 = \frac{\mu_0}{2\pi} \left[ a \cdot \ln \left[ \frac{2ab}{d(a + \sqrt{a^2 + b^2})} \right] - 2b + \sqrt{a^2 + b^2} \right] \quad (3.9)$$

$$M_2 = \frac{\mu_0}{2\pi} \left[ a \cdot \ln \left[ \frac{2ab}{d(b + \sqrt{a^2 + b^2})} \right] - 2a + \sqrt{a^2 + b^2} \right] \quad (3.10)$$

- The final inductance value is obtained by adding the contributions from the previous self and mutual inductance values, including the number of turns  $N$  and, to compensate the edge effects and bridge crossing, it is considered the exponent  $E$  set to 1.64, [92]:

$$L_{ant} = (2M_1 + 2M_2 + 2L_1 + 2L_2)N^E \quad (3.11)$$

- Find the equivalent series resistance of the antenna, by finding the DC-resistance where a *factor* (close to  $0.9 \cdot 10^{-3}$ ) is considered to take into account edge radius and mechanical tolerances. In addition the skin effect losses are also included. From this value one can also obtain directly the quality factor of the antenna  $A_{ant}$

$$R_{DC} = \frac{2N(a_0 + b_0) - 2(N-1)(w + g)}{\sigma \cdot t \cdot w \cdot factor} \quad (3.12)$$

$$R_{AC} \approx R_{DC} \left[ 1 + \frac{(d \cdot 10^{-3})^2 \cdot f \pi \mu_0 \sigma}{4 \cdot 48} \right] \quad (3.13)$$

and then converting the series into parallel equivalent resistance, that should be at least a magnitude smaller than chip losses ( $R_{DC}$ )

$$R_{ant} = \frac{(2\pi f L_{ant} \cdot 10^{-6})^2}{R_{AC}}; \quad Q_{ant} = \frac{R_{ant}}{2\pi f_r L_{ant}} \quad (3.14)$$

In order to find the requirements for the coil antenna, it is interesting to consider both cases, coil design for a tag or for a reader. The previous expressions are serving as a first estimation for the design, edge effects, skin depth, distributed parasitic capacitance (influences parameter  $E$ ), are difficult to estimate. Also there has been no consideration on the substrate definition such as dielectric permittivity ( $\epsilon_r$ ) or the dielectric losses ( $\tan\delta$ ).



For the analysis of the whole front-end, one has to consider the coil with the rest of the circuitry. In the case of an RFID reader, there is a matching network adapting the coil to the reader impedance, which will be normally the output impedance from a class D or E amplifier, which switches between the internal positive supply and GND, so that the output carrier frequency is a rectangular wave. The PA will then feed just a small amount of effective power  $P_E$  that will compensate damping losses. The major contribution of the antenna current is the reactive power of the oscillating energy  $W_M$ . The quality factor responsible for this relation is:

$$Q = \frac{W_M}{P_E} \omega = \frac{I^2 L}{I^2 \cdot R_s} \omega = \frac{L \omega}{R_s} \quad (3.15)$$

For a high Q factor, less power needs to be fed into the antenna to achieve the same field strength H-field.

In the case of a tag, there is the impedance of the chip to be considered as well as the assembly circuitry that tie together the IC with the antennas like welding, crimping or soldering Fig. 3.2.

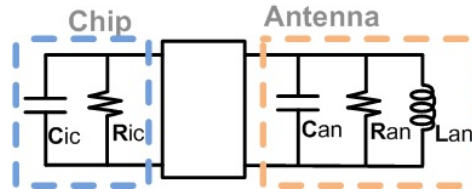


Figure 3.2: Equivalent circuit for tag-IC and Coil antenna

- $R_{ic}$  and  $C_{ic}$  are the equivalent resistance of the chip, representing its losses and the input capacitance seen at the input of the chip, that depends on technology and number of transistor gates.
- $R_{as}$  and  $C_{as}$  represents the assembly of the chip (bonding wires, flip-chip assembly), that will depend on chip package
- $L_{an}$  and  $C_{an}$  represent the antenna inductance and capacitance as resonant circuit
- $R_{an}$  represent antenna losses

Table 3.1: COIL ANTENNA PARAMETERS.

Design	outline (a x b)	thickness (t)	Permittivity ( $\epsilon$ )	track gap (g)	track width (w)	turns (N)
$L_A$	30 x 30	0.8	3.55	0.3	0.7	3
$L_B$	93 x 60	1.6	6	0.3	0.7	2

All dimensions in (mm), metal conductivity  $\sigma = 5.8 \cdot 10^7$  [S/m], FR4  $\tan \delta = 0.02$ .

From the simulation point of view, to comment that using Momentum there is the possibility to compute the S-parameters of the coils and obtain directly the equivalent lumped parameters using the Port1 single 50  $\Omega$  and Port2 ground port referenced to Port1. In such case the following expressions are used to determine L and Q values:

$$Z_{eq} = 50 \cdot \frac{1 + S_{11}}{1 - S_{11}}; \quad L(nH) = 10^9 \cdot \frac{Im\{Z_{eq}\}}{2\pi f}; \quad Q = \frac{Im\{Z_{eq}\}}{Re\{Z_{eq}\}} \quad (3.16)$$

Also, there is the possibility to use the same layout but with the two ports being  $50 \Omega$  single ports. In such a differential case, the determination of the inductor parameters can be done using the following transformations and equations [93]. The admittance  $Y$  parameters, are obtained from the conversion of the  $S$  using normalized  $50\Omega$  impedance. The same for the impedance  $Z$  parameters.

$$L_Y(nH) = 10^9 \cdot \frac{Im\{-1/Y_{21}\}}{2\pi f}; \quad Q = \frac{Im\{-Y_{22}\}}{Re\{Y_{22}\}} \quad (3.17)$$

$$Z_e = Z_{11} - \frac{Z_{12} \cdot Z_{21}}{Z_{22}}; \quad L_Z(nH) = 10^9 \cdot \frac{Im\{Z_e\}}{2\pi f}; \quad Q = \frac{Im\{Z_e\}}{Re\{Z_e\}} \quad (3.18)$$

The difference in using any of the above mentioned methods is very small. The higher difference comes from the determination of the self-resonance of the coil, probably due to the computation of the equivalent distributed capacitance of the coil tracks. As the HF antenna has its first and fundamental parallel self-resonance well above the carrier frequency, it can be assumed a complex inductive load.

Table 3.2: COIL DESIGN COMPARISON: ANALYTIC AND SIMULATIONS

Sample	ADS		Analytic	
	L (nH)	Q	L (nH)	Q
$L_A$	586	86	578	117
$L_B$	1080	81	994	118

Finally, it is of interest to determine the antenna model in order to be used in the whole transceiver design. The single loop antenna with length  $l$  and conductor cross section  $A$  provides Ohmic losses for DC currents that are defined by

$$R_{DC} = \frac{l}{\sigma A} \quad (3.19)$$

For the AC currents, one has to consider the *skin effect* that determines the effective cross section for the current following in the conductor, since it penetrates just a depth inside the conductor defined by the skin depth:

$$\delta = \sqrt{\frac{2}{\omega \mu \sigma}} \quad (3.20)$$

where the conductivity and permeability of the conductor are presented by  $\sigma$  and  $\mu$  respectively (in Cooper that  $\sigma_{Cu} = 5.8 \cdot 10^6 S/m$ , the skin depth at 13.56 MHz is  $\delta_{Cu} = 18 \mu m$ ). In order to compute the effective AC resistance, it can be assumed that the entire current flows in the conductor skin with the thickness determined by the skin depth  $\delta$ , which is only valid for a single conductor with a circular cross section. In case of a spiral coil, current in the adjacent coil wires causes a magnetic field resulting in an asymmetric current distribution, and making AC resistance calculation a tedious method, that in some cases is resolved by using numerical methods [86].

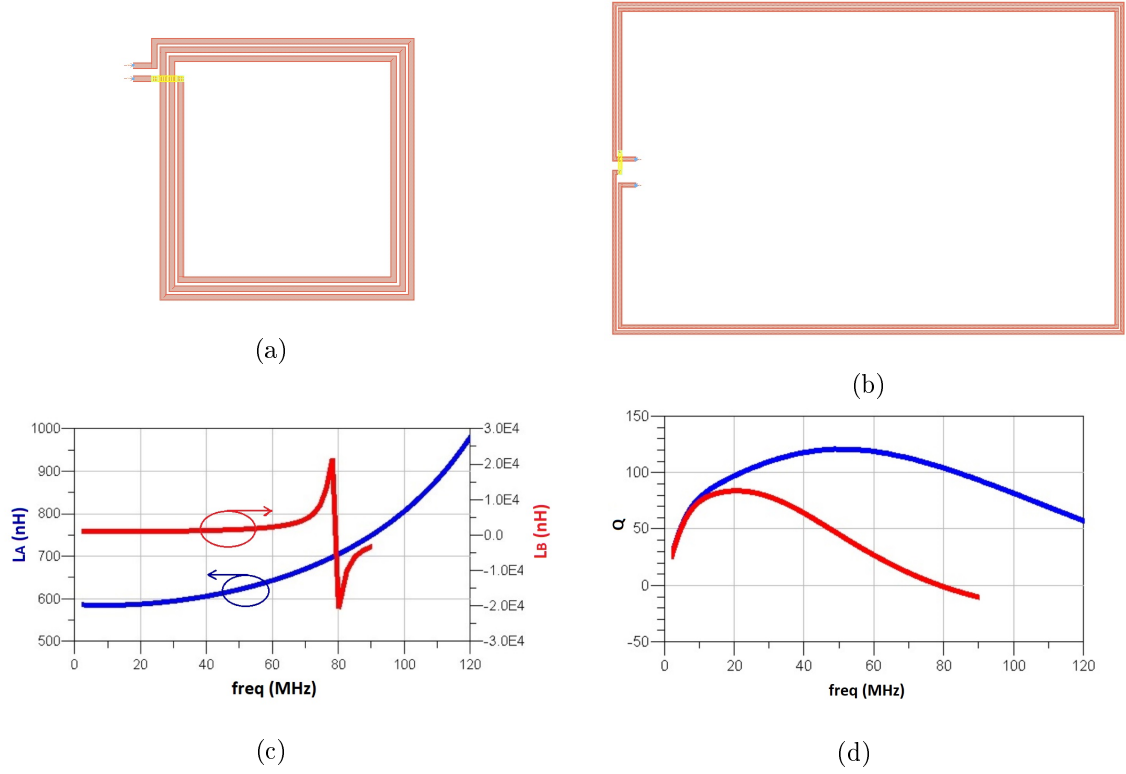


Figure 3.3: Layout of two implemented coils. (a)  $L_A=580\text{nH}$ ,  $N=3$  in blue, (b)  $L_B=1\mu\text{H}$ ,  $N=2$  in red, with their respective simulation results, showing inductance in [nH], self-resonance, and quality factor.

### Coil equivalent circuit

It is determined the equivalent parallel AC resistance of the coil ( $L_B = L_1$ ), based on the Momentum simulations computed in ADS, that defines the antenna quality value:

$$R_{eq} = L_1 \omega \cdot Q = 1080 \cdot 10^{-9} \cdot 2\pi \cdot 13.56 \cdot 10^6 \cdot 81 = 7.4 \text{ k}\Omega \quad (3.21)$$

which is composed by the equivalent parallel resistance between the DC series loop resistance  $R_{DC}$  (measured to 470 mΩ) converted in parallel, to  $R_p = \frac{X_{L1}^2 + R_{DC} X_{L1}}{R_{DC}}$  (in our case can be approximated by  $R_p = \frac{X_{L1}^2}{R_{DC}}$ ,  $R_p = 18 \text{ k}\Omega$ , see Fig. 3.4), and the loop AC resistance that would be measured at the working frequency  $R_{AC}$ , see Fig. 3.4:

$$R_{eq} = \frac{R_p R_{AC}}{R_p + R_{AC}}; \quad R_{AC} = \frac{R_p R_{eq}}{R_p - R_{eq}} = 12.5 \text{ k}\Omega \quad (3.22)$$

Such resistance would be the equivalent at the working frequency. If one would want to measure it at another frequency (loop self-resonance) it should be multiplied by the frequency dependence factor

$$\sqrt{\frac{f_{SelfRes}}{f_{rfid}}}.$$

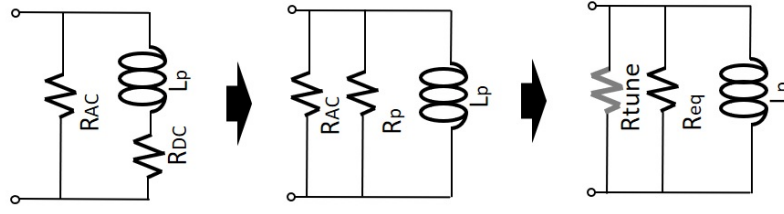


Figure 3.4: Loop antenna equivalent circuit. To reduce  $Q$  we place  $R_{tune}$

Another aspect to take into account in the antenna design is the real quality factor that the reader expects from the antenna, when considering the specific RF system. For such case, concrete standardize specifications are needed, that must specify the channel occupancy and data rate, so the available bandwidth required by the system in order to comply with the signal-to-noise ratio.

In the case of Mifare ISO 14443A specification, it provides a data rate of 105.9 kbps (length of a bit frame is  $9.44 \mu s$ ), with 100% ASK Modified Miller Code from reader to card, and OOK, Manchester code load modulation with a sub-carrier of 847.5 kHz (since Manchester coded data modulates a sub-carrier as  $f_{SUB} = \frac{f_R}{16} = 847.5 \text{ kHz}$ ). Generates side-bands of  $\frac{1}{9.44 \mu s} = 106 \text{ kHz}$  at both sides of the sub-carrier. In the case of ISO 14443B the modulation is BPSK. We consider here then a sub-carrier spacing of 848 kHz, so the required quality factor from the antenna should be:

$$Q = \frac{f_r}{B\omega} = \frac{13.56 \text{ MHz}}{848 \text{ kHz}} = 16 \quad (3.23)$$

It is necessary then to reduce the antenna  $Q$  value from 81 to a value lets say 20. In order to do so, the driver circuit should be seeing at the antenna terminals a parallel resistance of value;  $R_T = Q \cdot X_L = 20(2\pi f 1080 \text{ nH}) = 1.8 \text{ k}\Omega$ , so, to do so, the resistance to place in parallel with the coil should be;  $R_1 = \frac{R_T R_{eq}}{R_{eq} - R_T} = 2.3 \text{ k}\Omega$ .

A clear compromise arises for the optimization of coil antennas for both NFC and WPT. The question is how to optimize communication and power transfer using a single coil. The next sections aims at showing one technique that can be used on improving both objective simultaneously, considering circuit design parameters. Also presents some analytic expressions for better understanding the adopted solution.

### 3.2.3 Coil coupling effects

For the communication or energy transfer between two transceivers using near-field coupling, the communication is performed using two antennas located close to each other, so their magnetic fields are interacting and mutual induction generates a current to flow from the generator antenna to the coupled antenna. The magnetic field generated by a coil with a current  $i_1$  on a loop with area  $S$  is given by Biot and Savart law:

$$\mathbf{B} = \frac{\mu_0 i_1}{4\pi} \oint_C \frac{d\mathbf{S} \mathbf{x}}{|\mathbf{x}|^3} \quad (3.24)$$

$\mathbf{x}$  is the distance at which to calculate  $\mathbf{B}$ . Much easier to handle is the mutual coupling between the two antennas:

$$M = \iint_{A_2} \frac{B(i_1)}{i_1} \cdot dA_2; \quad k = \frac{M}{\sqrt{L_1 L_2}} \quad (3.25)$$

In the case of a tag, with the antenna designed at the resonant frequency, it would consume energy from the field generated by the reader antenna. This energy consumption in the tag, used to send data back to the reader, has a feedback effect as a voltage drop in the reader. Due to small coupling factor between reader and tag antennas, the tag response is up to 60 dB below the voltage generated by the reader. In NFC systems the standard [94] defines for Europe a maximal field strength for a transmitter at a distance of 10 m. For a carrier frequency of 13.56 MHz, a maximal field strength of 60 dB $\mu$ A/m is allowed, and the bandwidth is  $\pm 900$  kHz. The limit of field strength for different frequencies is depicted in Fig. 3.5.

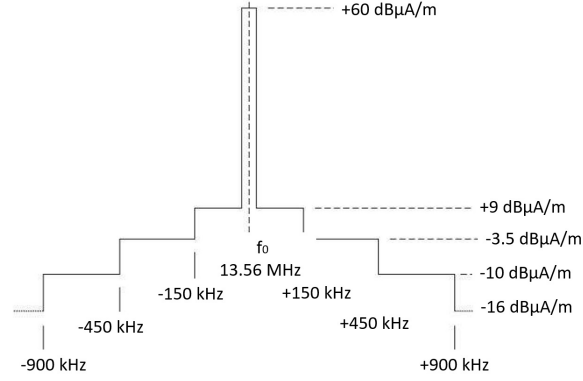


Figure 3.5: Spectral mask for NFC system.

In coil coupling, coil dimensions and shape substantially affect the magnitude of the magnetic field in the near-field region. When a loop is placed in a magnetic field that can be generated by another coil, an induced voltage is generated, and is calculated as:

$$V_t = \oint_C \mathbf{E} \cdot d\mathbf{l} = \frac{\partial}{\partial t} \iint_S \mathbf{B} \cdot d\mathbf{s} \quad (3.26)$$

where:

- $C$  is the length of the loop curve, and  $S$  is the area of the loop
- $\mathbf{E}$  is the electric field vector
- $\mathbf{l}$  is the tangent direction of the loop curve, and
- $\mathbf{s}$  is the normal direction of the loop surface.

Since the loop will be small compared to the wavelength ( $D=0.002 \lambda$ ), the magnetic field  $\mathbf{B}$  can be considered constant on the location of the coil. Because the induced voltage in each and every turn of the coil is serially connected, for an antenna with  $N_t$  turns, the induced voltage will be transforming into Laplace:

$$V_t \approx -j\omega B \sum_{i=1}^{N_t} S_i = -j\omega I_0 K \sum_{i=1}^{N_t} S_i \quad (3.27)$$

Inductive coupling connects the reader with the tag via their loop antennas. The functionality and performance of the RFID system will depend greatly in such coupling effect, that through the air will

perform influenced by nearby objects. In the presence of no objects, it is of interest to discuss about the main factors that define coupling performance.

In Annex B, it has already been obtained the expression for the magnetic field generated by a loop antenna B.11. In order to find the voltage induced in a second loop antenna (tag), one has to find which part of such magnetic field crosses the loop of the second antenna and from here, it is direct to deduce the voltage induced in such receiving antenna.

The mutual coupling between the two antennas is related according to the following expression, where  $R_1$  is the radius of the reader loop,  $N_2$  and  $A_2$  is the number of turns and area of the tag coil, located at a distance  $r$  from the reader coil:

$$M_{21} = \frac{B_z A_2 N_2}{I_0} = \frac{\mu_0 A_2 N_2}{2R_1} \left( \frac{R_1^2}{R_1^2 + r^2} \right)^{3/2} \quad (3.28)$$

The coupling coefficient relates with the mutual induction coefficient through the inductance values of each coil by;  $k = M/\sqrt{L_1 L_2}$ . In the case that both inductance have the same value ( $L_1 = L_2 = L$ ), then  $k = M/L$ . so;

$$L = N \frac{\mu_0 A \cdot N}{2R_2}; \quad \text{then} \quad M_{21} = L \left( \frac{R_1^2}{R_1^2 + r^2} \right)^{3/2}; \quad \text{and} \quad k = L \left( \frac{R_1^2}{R_1^2 + r^2} \right)^{3/2} \quad (3.29)$$

In this particular case, the coupling coefficient between the two identical coils, will depend only on geometrical properties. As shown in Fig. 3.6, for distances between coils of 1 to 10 cm, the bigger the coil radio, the better the coupling. Otherwise the difference in radius does not affect so much.

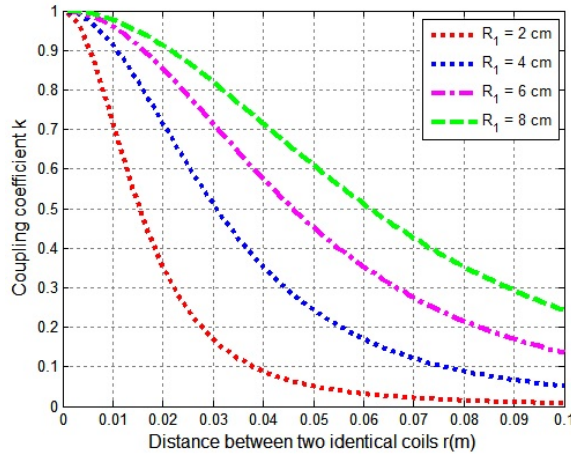


Figure 3.6: Coupling coefficient for different antenna radius  $R_1$  plotted at varying distances  $r$ .

### 3.2.4 HF-transmitter design

In the transmitter section, after the modulation block and driver output, there is the necessity to design final transmitter parts such as filter, matching network and resonance circuit. For this purpose it is necessary to consider bandwidth adjustment to feed the apparent power into the antenna, where the major part is reactive power and the minority is effective power. We must include our idea of including an element in the tuning circuit of the coil that adapts the transmitter to become optimum

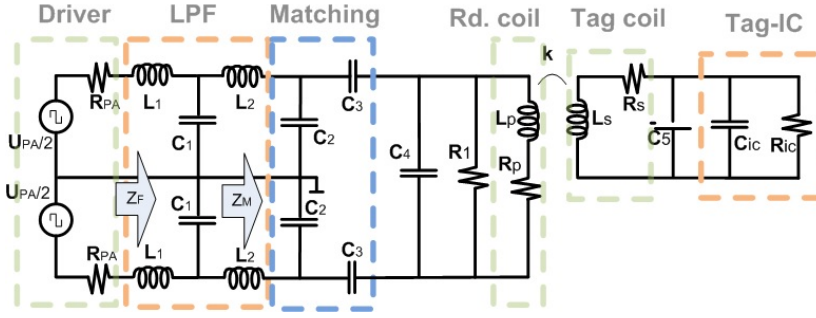


Figure 3.7: Differential driven circuit for the RFID transmitter.

for NFC communications and at the same time, also optimum for transferring power into a receiver for purposes such as charging batteries of an NFC or RFID sensor.

In the case of the matching network normally composed of two capacitors, it will adapt the output impedance of the IC driver, ( $R_{PA}$ ) which, depending on the chip may vary from 2 to 5  $\Omega$ , to the antenna impedance, in order to transfer maximum power from the IC to the antenna. Tuning capacitors are also represented in parallel with the coil inductance in order to tune to the resonance frequency of the NFC system helping in maintaining the resonance frequency versus deviation in the antenna environment.

The IC used for this work (**AS3911**) from AMS manufacturer), tunes the loop antenna by switching between capacitors in parallel with the antenna. To do so, it measures the reflection coefficient and, measures the antenna impedance at 13.56 MHz. It is done comparing the measurement with a 50  $\Omega$  resistor using a Wheatstone bridge. The measuring bridge's DC source is replaced with a waveform generator providing 13.56 MHz sinusoidal signal. The measure of the antenna impedance takes the reflection coefficient and, makes the decision to switch between capacitors in parallel with the antenna for tuning purposes.

The use of such tuning mechanism is very much justified in our case, since the NFC antenna operates in a difficult environment such as smartphone, in close proximity to other devices, and where some parasitic effects due to unknowns within the mobile phone are present. In the context of contact-less proximity communication standards, such effects are known as "card loading", which refers to a de-tuning of the reader antenna resonant circuit, for example affecting  $f_{res}$  and  $Q$ . To compensate for such negative effects caused by the tolerances and coupling, such tuning mechanism can help in the adaptation of antenna impedance matching, and contributes to the reduction of power consumption for the device.

The two branches of the differential network which connects the PCB antenna to the driver output are identical Fig. 3.7. Because in the IC the voltage is limited to low voltages, and the  $R_{ON}$ -resistance of the driver switches cannot be neglected, the differential driver output allows to have an output voltage of almost double the supply, so this reduces the power losses in the output. Furthermore, a differential stage always means better noise suppression. So the voltage at the output is split up into two sources  $V_{PA/2}$ , which drive the output signal in phase opposition.

For our particular design case, using the transceiver IC AS3911, the different stages are designed according to the following components representation:

Knowing values are the driver impedance from the IC which corresponds to  $R_{PA} = 2 \Omega$ , also antenna equivalent circuit represented by the series combination of  $L_p = 1080 \text{ nH}$  and the DC resistance of  $R_p = 470 \text{ m}\Omega$ . From these values it is direct to determine the parallel capacitance value that would resonate the coil at the working frequency of 13.56 MHz, which would be  $C = \frac{1}{\omega^2 L_p} = 128 \text{ pF}$ .

In the determination of parallel capacitance value, we must also consider the rest of capacitance that

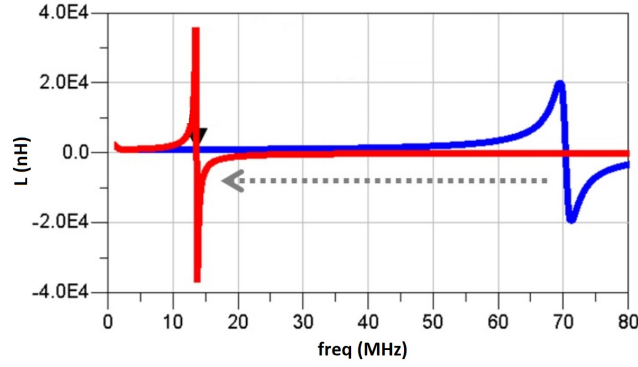


Figure 3.8: Adjustment of antenna self-resonance to the working frequency.

lay in parallel with the loop antenna. Such capacitance are the ones coming from voltage capacitance voltage divider, responsible for sensing the received voltage at the antenna terminals ( $C_{div} = 18 \text{ pF}$ ) and, half capacitance value from the tuning capacitors also applied in each parallel output driver branch ( $C_{tune} = 56 \text{ pF}$ ). A good explanation on the tuning performance for such capacitors can be found in [95, 96].



#### Loop antenna components

$L_p$  1080 nH, Circuit for optimal Q (for NFC where  $Q = 20$ , and for WPT where  $Q = 80$ ) by placing  $R_1 = 1,2 \text{ k } \Omega$ ,  $C_{tune} = 56 \text{ pF}$ .

### Filter and matching network design

In the following, we are representing the low-pass filter (LPF) used to comply with Electromagnetic Compatibility (EMC) rules, and also to convert the square output signal into a sine-wave of low harmonic distortion. Such filter will affect the bandwidth and time-domain properties of the modulation signal from the HF transmitter, and also now we should consider the antenna resonance in combination with the filter resonance, so the RF behavior cannot be simply modeled by one equivalent resonance circuit and its quality factor. A second order LC circuit is being implemented and the LPF simulation results representing the low pass characteristics are also shown in Fig. 3.9.

Since the PA output is an square wave, it can be represented by a Fourier series by:

$$v_o(t) = \frac{4A}{\pi} \left[ \sin(\omega t) + \frac{1}{3} \sin(3\omega t) + \frac{1}{5} \sin(5\omega t) + \dots \right] = \frac{4A}{\pi} \sum_{m=1}^{\infty} \frac{\sin[(2m-1)\omega t]}{2m-1} \quad (3.30)$$

consisting of a fundamental sine-wave and several harmonics to be filtered. This filter will influence the matching impedance  $Z_M$ , transforming it onto  $Z_F$  (see Fig. 3.7) which can be obtained from:

$$Z_F = L_1 s + \frac{\frac{1}{C_1 s} (L_2 s + Z_M)}{\frac{1}{C_1 s} + L_2 s + Z_M} = \frac{-jL_1 L_2 C_1 \omega^3 - \omega^2 L_1 C_1 Z_M + j\omega(L_1 + L_2) + Z_M}{(1 - L_2 C_1 \omega^2) + j\omega Z_M C_1} \quad (3.31)$$



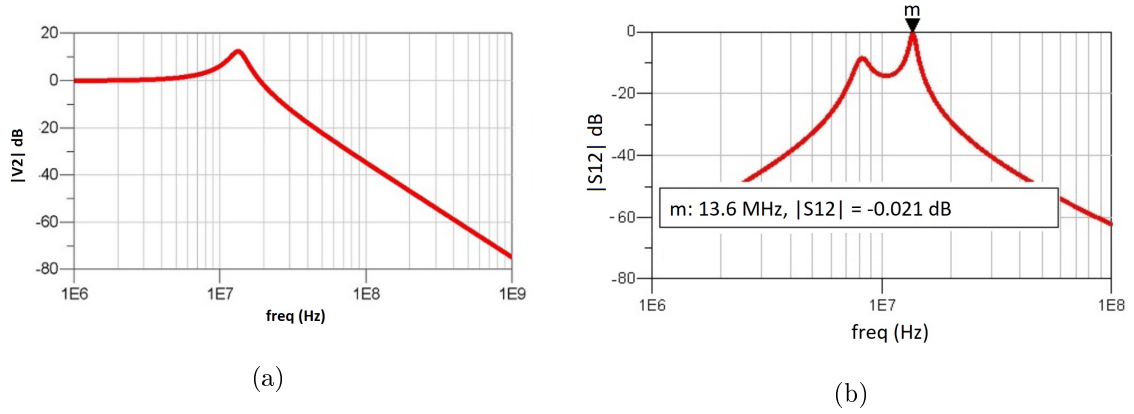


Figure 3.9: Frequency response of the implemented LPF at the HF reader input. Wide bandwidth matching frequency response.

The transfer function of the filter, has the very well-known expression, which corresponds to a second-order transfer function. The cut-off frequency from the LPF corresponds to  $\omega_0 = \frac{1}{\sqrt{LC}} = 13.5 \text{ MHz}$ , for the design values of  $L_1 = 100 \text{ nH}$ , and  $C_1 = 1.4 \text{ nF}$ . But for the final adjustment of the filtering functions the matching circuit must be included, which also acts as a filter, so the adjusted values that match with the rest of the transmit circuit correspond to the following  $L_1 = 10 \text{ nH}$ , and  $C_1 = 47 \text{ pF}$ .

$$H(s) = \frac{V_2(s)}{V_1(s)} = \frac{1 - \frac{L_1 s}{Z_F}}{L_2 s + Z_M} \cdot Z_M = \frac{Z_M}{-j\omega^3 L_1 L_2 C_1 - \omega^2 L_1 C_1 Z_M + j\omega(L_1 + L_2) + Z_M}; \quad (3.32)$$

The whole frequency response for the transmitter part, including all the effects before mentioned corresponds to the one depicted in Fig. 3.11, showing good matching conditions for two frequencies one of which is 13.6 MHz.

The working circuit schematic, corresponds to the equivalent single ended circuit. Since our interest is driving the antenna in differential mode in order to extract the maximum power with the minimum supply voltage, such schematic will need to be converted in the layout corresponding values. Single ended schematic is depicted in Fig. 3.10.

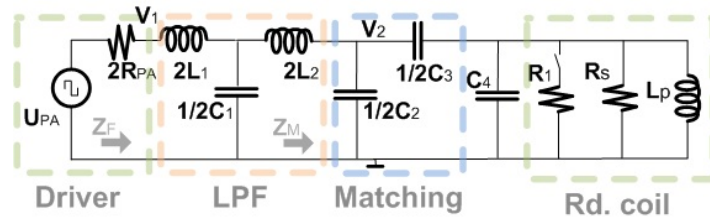


Figure 3.10: Equivalent single ended circuit for the RFID transmitter.

Impedance matching is necessary in RF circuit design to guaranty maximum power delivery between a source and its load, and improve the signal to noise ratio of the system. In the Fig. 3.10 an LC-matching network is used, very common due to its simplicity and low loss, also since antenna have inductive performance, it allows to use a simplified L-topology matching network with two capacitors, which is advantageous for power efficiency since a capacitor can be fabricated nearly loss-less for HF (type COG or NPO). Since the NFC antenna has its first and fundamental parallel self-resonance

well above the carrier frequency (Fig. 3.8), we can assume it is a complex inductive load, so a simplified matching with only two "L" shape capacitors is used, in addition to series inductance. From manufacturing data the drive stage can be assumed to have an impedance of  $2\ \Omega$ .

Including the effect of the input LPF, it can be seen how the center frequency of the matching is shifted from 13.55 MHz to 13.49 MHz. Such small change does not suppose a compromise so our first assumption was correct, see Fig. 3.11. Table 3.3 shows the design parameters for this part of the circuit.

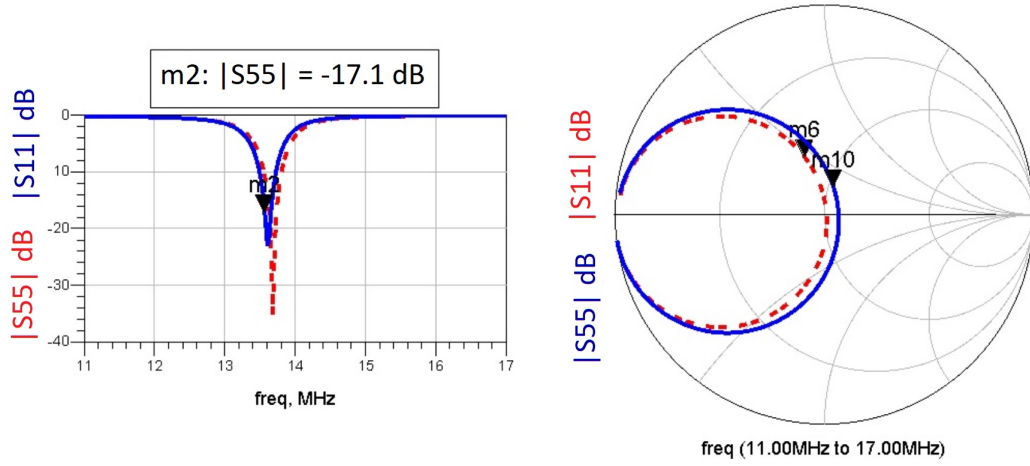


Figure 3.11: Frequency response of matching network w (blue) and w/o (red) the LPF.

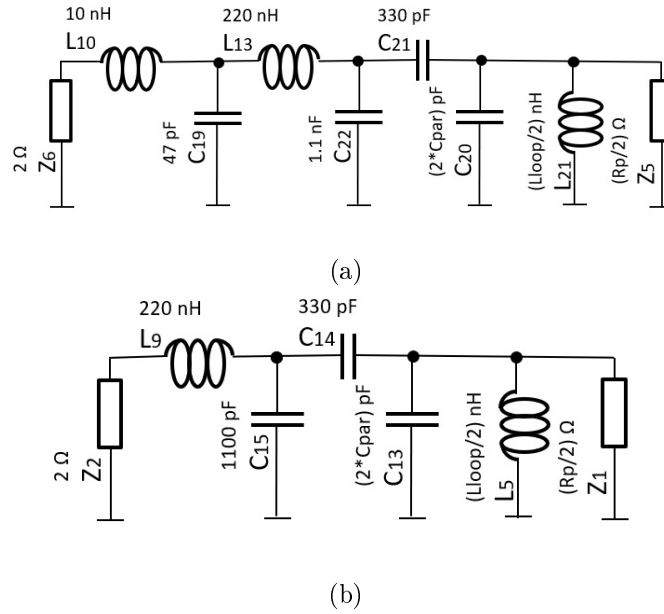


Figure 3.12: Circuit of matching network with and without the LPF:  $C_{par} = 45$ ,  $L_{loop} = 940$ ,  $R_p = 2200$ ,  $f_{eq} = 13.56$  MHz.

Table 3.3: COIL ANTENNA, FILTER AND MATCHING NETWORK PARAMETER VALUES.

$R_{PA}$	$L_1(nH)$	$C_1(pF)$	$L_2(nH)$	$C_2(pF)$	$C_3(pF)$	$R_{eq}(\Omega)$	$C_{eq}(pF)$	$L(nH)$
2	10	47	220	1100	330	2200	45	940

### 3.2.5 Causes for reduction of coupling factor between coils

#### Simulation results for lateral miss-alignment

In any NFC device, for an optimum transfer of data between coils, they must be aligned and close together. In order to obtain the coupling coefficient for different configurations, a set of simulations have been performed with two coupled rectangular shape antennas, the same ones as simulated in Fig. 4.2 (b). The results of the four presented cases of different overlapping conditions are presented in the plots shown in table 3.4, including the 3D representation for better understanding.


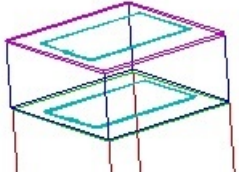
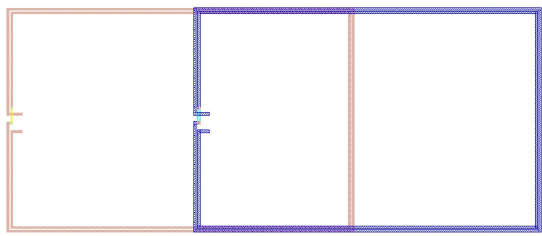
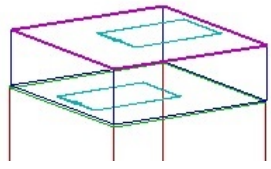
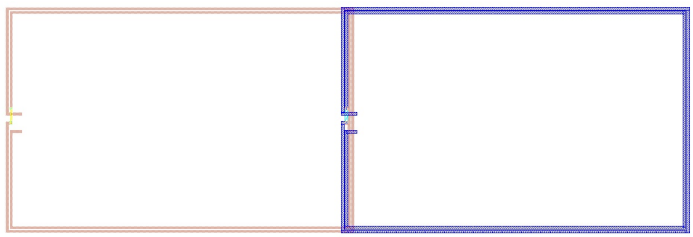
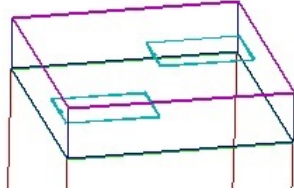
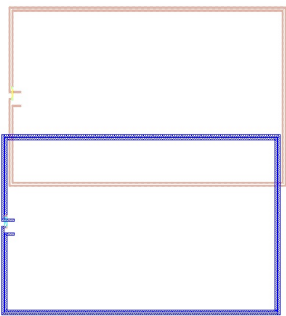
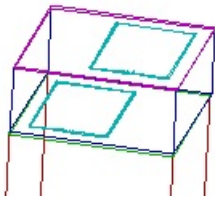
Basically the presented results correspond, into a situation which can be real in practice, since for example in a small size device with NFC inside, lets say a mobile phone, the user is unaware of the position of the coil. So in this case, when wanting to establish a communication channel, the link performance will depend on the relative position between the two coils that form it. In this case, it is assumed that the coils are at a fixed distance (5 cm) and are shifted in both directions "x" and "y".

The simulation results are comparing the mutual coupling between the two identical coils, which is computed using the conversion from  $S$  to  $Z$  parameters. From  $Z_{21}$  one can obtain the mutual coupling as stated in eq.(3.33), and the results are plotted versus frequency in Fig. 3.13. At the frequency of interest, with perfect overlapping antennas with the same size, and separated by a distance of  $x = 5$  mm, the mutual coupling is maximum reaching 400 nH. This corresponds to maximal overlapping area plotted of  $5400 \text{ mm}^2$ .

When shifting one of the coils in the  $y$  direction, the coupling between the two identical coils is lower when overlapping area is  $1800 \text{ mm}^2$ , corresponding to a 1/3 shift of the "b" dimension (case b) in Table 3.4). The reason for this performance, could be attributed to the fact that the magnetic flux, crossing both areas of the coil, the one overlapped with the primary coil and the second outside the limits of this coil, are compensating the currents that induce in the different parts of the coil. This is an interesting phenomena to note. Using  $Z$  the transformation from  $S$  parameters:

$$M(nH) = 10^{-9} \frac{Z_{21}}{f} \quad (3.33)$$

Table 3.4: CONFIGURATION FOR LATERAL MISS-ALIGNMENT OF RECTANGULAR ANTENNAS

Case	Coil location	3D representation
a) $x=y=0$		
b) $x=a/2,$ $y=0$		
c) $x=a, y=0$		
d) $x=0,$ $y=a/4$		

*Two separated antennas on FR4 substrates ( $\epsilon_r = 6, tg\delta = 0.02$ ), in air separation of 5 cm*

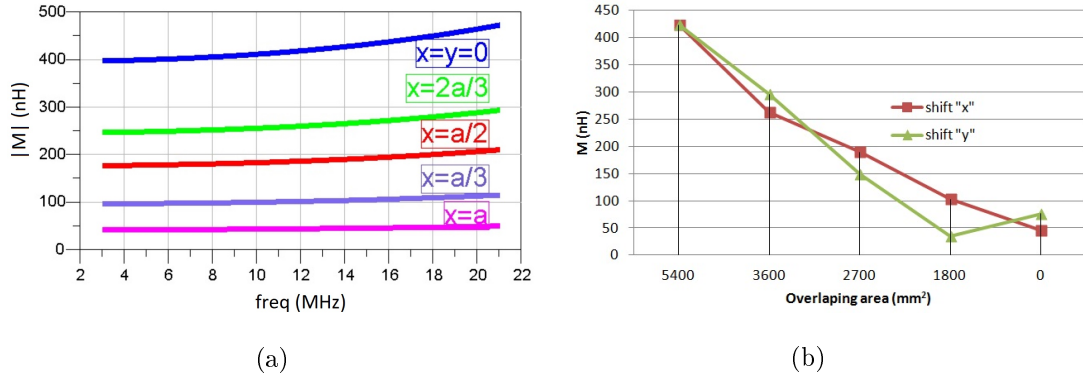


Figure 3.13: Coupling effects for two parallel rectangular loops ( $N=2$ ) at a distance  $x = 5$  mm for different geometrical positions (Table 3.4). (a) Shifting two antennas in "x" direction. (b) Shift in "x" and "y" direction.

### Mutual coupling for different area coils

In many real situations the coil of transmitter and receiver will be of different area because of different manufacturers, with their need to fit in very small and limited spaces. In such case, it is of interest to investigate the performance of the system when having two concentric rectangular antennas parallel placed at a fixed distance  $x = 5$  mm, one (the reader) fixed at the same dimensions as previously simulated, and the second (tag) changing in size. Our investigation considers ranging the outer loop from 15 mm outside the perimeter of the reader loop, until 15 mm inside the reader loop. The simulation results of the mutual coefficient is also shown in Fig. 3.14. The maximum coupling happens for the case of equal inductance area as expected, with the mutual inductance being almost 450 nH.

The simulated results also arises the fact that there is almost no difference, in the case of having a big loop antenna exceeding the transmitter antenna, or a smaller loop one, it just collects less number of flux magnetic field lines. In both cases the mutual inductance is diminishing in a similar manner at the ratio of 0,25  $\mu\text{H}/\text{cm}$  for  $\Delta < 0$ , or 0,5  $\mu\text{H}/\text{cm}$  for  $\Delta > 0$  ( $\Delta$  is the direction of area increase).

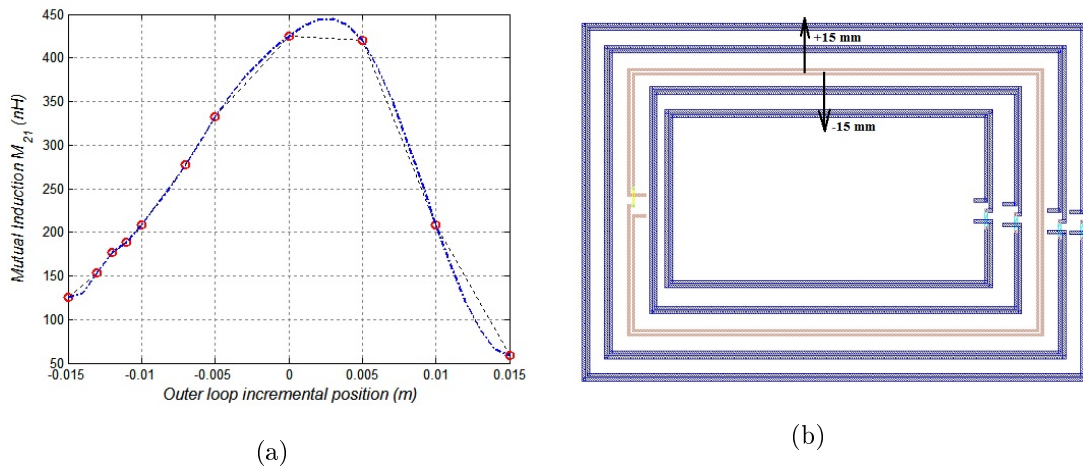


Figure 3.14: Mutual induction between two concentric different size rectangular coils.

### Analytic results for the optimal mutual coupling

The coupling coefficient is computed for an equivalent circular loop antenna, having the same area as would have the rectangular loop antenna, (equivalent radius of 43 mm using Eq. 3.28). The mutual coupling in the case of having identical size rectangular loop antenna, is obtained, using the computation of the magnetic field generated along the  $x$  axis by a rectangular loop antenna with edge length  $a \times b$  according to [68]:

$$H(x)|_{rect.} = \frac{NI_0ab}{4\pi\sqrt{a^2 + b^2 + x^2}} \left( \frac{1}{a^2 + x^2} + \frac{1}{b^2 + x^2} \right) \quad (3.34)$$

Since the direct relationship applies for the magnetic flux intensity  $\mathbf{B} = \mu\mathbf{H}$ , the mutual coupling can be found, independently of the current flowing in the loop  $I_0$ , as:

$$M(x) = \frac{B(x)ab}{I_0} = \frac{\mu H(x)ab}{I_0} \quad (3.35)$$

which is represented in the Fig. 3.15 in both scales, linear and logarithmic, to represent the strong variability versus the distance. The simulation results follow very well the analytic results up to 10 mm distance from the two coils, with a decay of 60 dB/dec (power level). For close proximity coupling the simulations show a much greater coupling factor. For the case of one coil over each other, that is  $x = 0$ , the magnetic field and mutual coupling are expressed as:

$$H(x=0)|_{rect.} = \frac{NI_0ab(a^2 + b^2)}{16\pi[(a/2)^2 + (b/2)^2]^{3/2}}; \quad M_{21}(x=0) = \frac{N(ab)^2}{4\pi\sqrt{(a/2)^2 + (b/2)^2}} \quad (3.36)$$

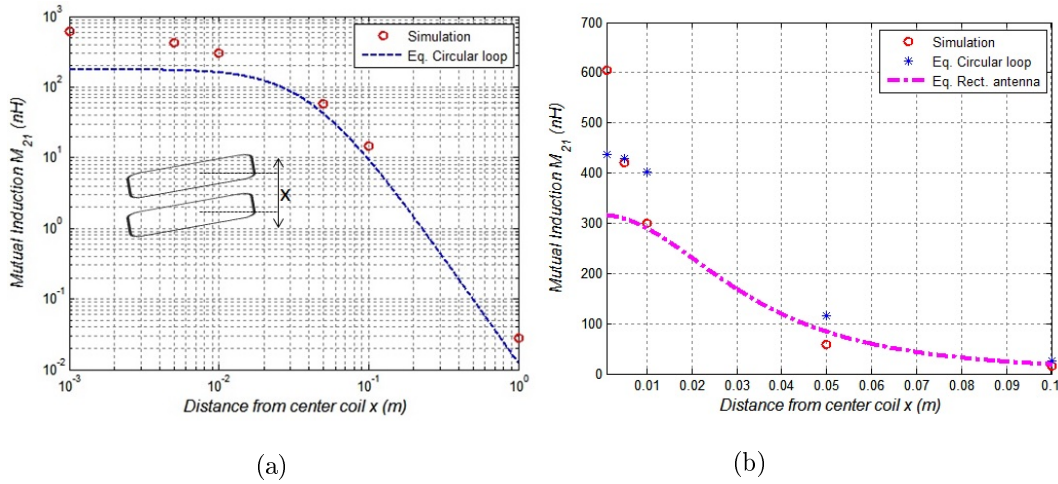


Figure 3.15: Mutual coupling : (a) Simulation of square loops and theoretical values for equivalent circular loop. (b) Same as a) in linear scale, including theoretical rectangular loop results.

If we maintain unchangeable one dimension of the rectangular antenna ( $b = 60 \text{ mm}$ ) and modify the other dimension ( $a$ ), it is interesting to see that there exist one antenna dimension that optimizes the coupling of the antennas for different locations ( $x$ ) between antennas (plotted in circles in Fig. 3.16). This is very interesting if our main purpose consist of, based on a fixed position of the antennas, to perform a optimal design in order to optimize the mutual coupling between antennas as would be expected.

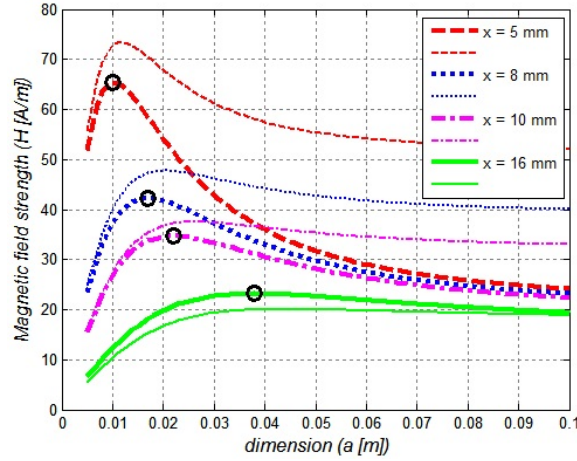


Figure 3.16: Magnetic field generated by a rectangular loop antenna with  $b = 60 \text{ mm}$  (thick lines) and  $b = 20 \text{ mm}$  (thin lines), with  $N = 2$  and  $I = 1A$ . Variation of opposite side is made to find optimal size (circle)  $a_{op}$ .

The optimal points can be found by taking the derivative of (3.34) and making it equal to zero:  $\delta H(x)/\delta x = 0$ . Since the fields are calculated over short distance from the axes of the loop, the optimal sizes are small.

**Our Case:** In our case, where antennas will be close to each other, an small antenna size is enough to communicate with the receiving antenna. We can see in Fig. 3.16 that in the case of looking the field at higher distance, then the small antenna ( $b = 20 \text{ mm}$ ) reduces the field compared with the bigger loop.

From Fig. 3.13, assuming a shift of distance between the two antennas of  $1/3$  from the side edge, the mutual coupling estimated is  $M = 300 \text{ nH}$ , which corresponds to a coupling coefficient  $k=0.3$   $\left( \frac{M}{\sqrt{L_1 L_2}} = \frac{300 \text{ nH}}{994 \text{ nH}} \right)$ .

### Metallic objects between coils

Another possible situation interesting to investigate corresponds to the case where there are some metallic objects in between the coils. This corresponds to real situations, since the NFC system (mobile phone) is subject to be located at any place, with the possibility that some objects are in between the NFC transmitter and a possible receiver.

Since the system operates using the magnetic field, this will induce currents in the metallic objects, and will cause a loss in the communications efficiency, because part of the field will be used to create such parasitic currents and the rest will be arriving to the receiver coil. In Fig. 3.17, it is shown the co-simulation results, using Momentum electromagnetic computation results and computing currents when the two coils are resonating.

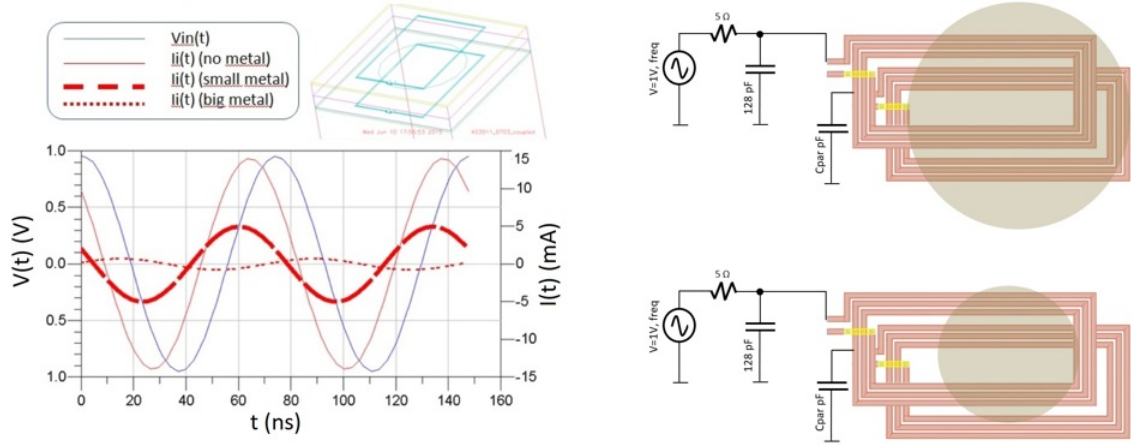


Figure 3.17: Circular metallic object included between the coupled coils represented in shadow.

In addition, as can be seen in Fig. 3.19, the resonance frequency of the coils will be shifted due to the same effect. The induced currents in the metal object, will circulate through the metallic surface and such currents varying at the same frequency as the induced one, will couple with the other fields and vary the resonance frequency of the main magnetic field. Such variation of resonance frequency can be seen by monitoring the  $S_{11}$  parameter on the test simulation set-up presented in the Fig. 3.19. This effect could correspond to the fact of having a shift in the self-inductance measured by:

$$S'_{11}(f) = |S_{11}|e^{j\Theta_{11}} \quad Z'_{eq} = 50 \frac{1 + S'_{11}}{1 - S'_{11}} \quad L'(nH) = 10^9 \cdot \frac{Im\{Z'_{eq}\}}{2\pi f} \quad (3.37)$$

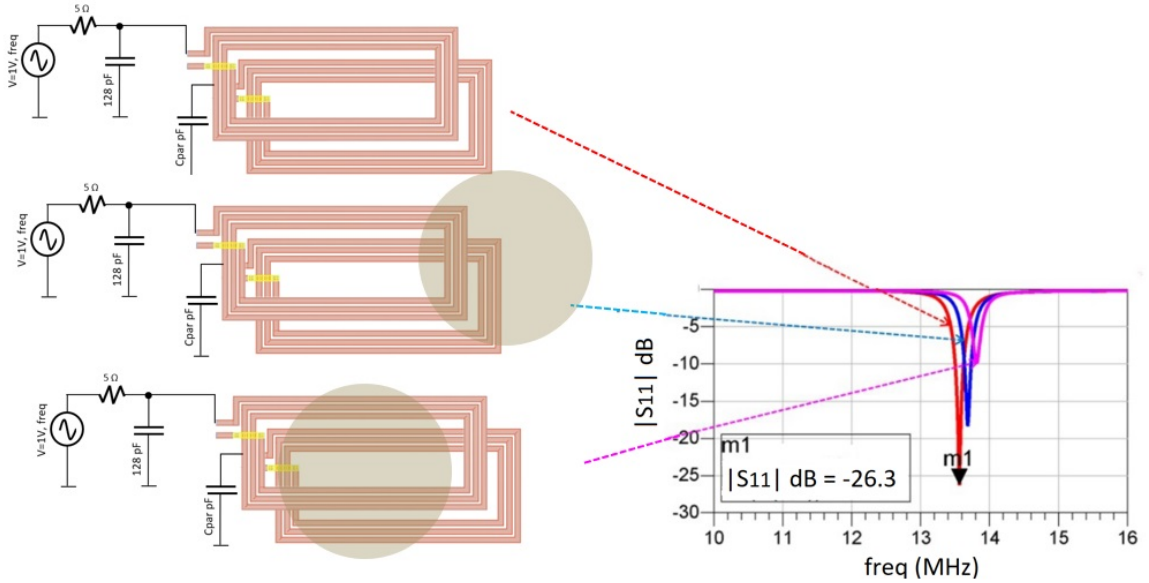


Figure 3.18: Resonant frequency shift caused by induced currents in metallic object.



### 3.3 Wireless Power Transfer (WPT)

After the analysis attributed to the NFC system used for communicating two proximity devices, there are several situations where there is a need for implementing a wireless charging circuit, such as trans-cutaneous devices, covered systems, or underground electronic sensors (no connectors). In the case of this study, since NFC communications already uses the transmitter carrier to power-up the remote tag, we propose using the same energy coming from the mobile phone, or external battery pack in the form of HF electromagnetic fields for charging external systems.

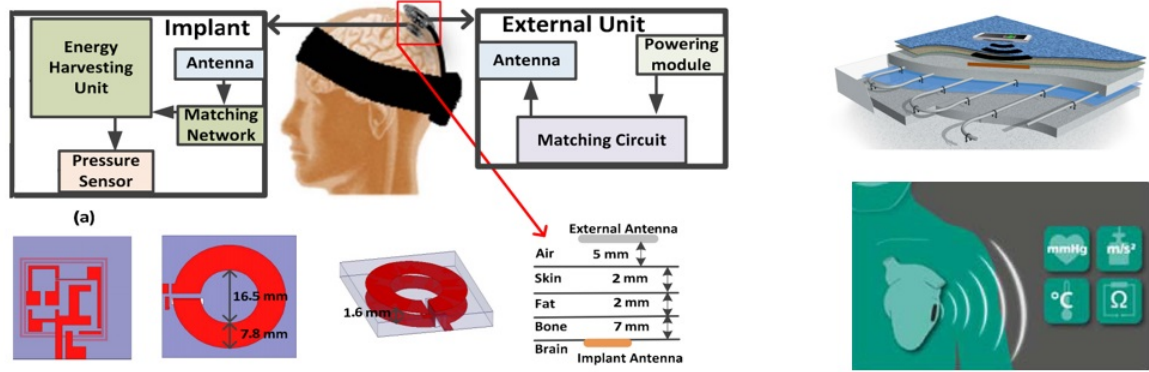


Figure 3.19: Some examples of implantable devices [97] and application in underground sensors requiring wireless communications and power.

In WPT, unlike the case of the coils of a transformer where they are wound around a magnetic core to attain tight coupling, the coils for WPT are usually loosely coupled, due to the absence of a common magnetic core to confine and guide most of the magnetic flux. One can state that a WPT system is formed by two leakage inductance transformer model tank and series resonant capacitors, which has a current-source characteristic, so it should be connected to a capacitive filter having a voltage-source characteristic. In our case a full-bridge rectifier with a capacitive output filter that provides a DC voltage at the output load resistance  $R_L$ .

#### 3.3.1 Resonance peak analysis

One topic of interest from the resonance circuits, is the analysis of the different resonance peaks that can be generated in the energy transfer circuits, due to the modification of several factors. Sometimes between primary and secondary coils, there can be the presence of metallic objects that influence the transfer of energy from one side to the other, or a changing load at the receiving circuit that may also alter the resonance frequency. The effect may be seen as a modification of the resonance condition. In some cases the frequency of maximum power transfer may be shifted or it may appear more than one resonance peaks. Some optimization has already been seen previously.

In the case of tight magnetic coupling between the coils that perform power transfer, the resonant peak of the input impedance is divided into several peaks due to the increase of mutual inductance between the coils. This also will depend on the type of source that drives the coil. For tight magnetic coupling with constant voltage or current source the peaks will be different [98].

Even though in our case for the NFC system, the primary coil design consists of a primary parallel resonance, the circuits devoted to wireless power transfer, similar to the commercial standard known as  $Q_i$ , consist of series resonance either at the primary and secondary [99]. In this analysis we are

going to use this situation (series-series resonance Fig. 3.20), an over it the main focus will be in the appearance of possible resonance peaks. Firstly let us find the input impedance variation versus frequency:

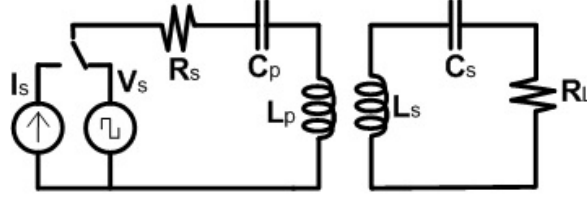


Figure 3.20: Simplified equivalent circuit for the series resonance coils

$$Z_s = \frac{V_s}{I_s} = \frac{(j\omega C_s R_s + 1 - \omega^2 L_s C_s)(j\omega C_L R_L + 1 - \omega^2 L_L C_L) - \omega^2 M^2 C_s C_L}{j\omega C_s (j\omega C_L R_L + 1 - \omega^2 L_L C_L)} \quad (3.38)$$

To simplify the resonant frequency analysis we can omit  $R_s$  and  $R_L$  and focus on the parallel resonance (input impedance should be infinity  $f_{par} = 1/(2\pi\sqrt{L_p C_p})$ ) and series resonance (input impedance should be zero) [98]. For  $\omega_p^2 = 1/(L_p C_p)$  and  $\omega_L^2 = 1/(L_L C_L)$ , then:

$$f_{ser}^L = \frac{\sqrt{\omega_s^{-2} + \omega_p^{-2} - \sqrt{(\omega_s^{-2} - \omega_p^{-2})^2 + 4k^2\omega_s^{-2}\omega_p^{-2}}}}{2\pi\sqrt{2(1-k^2)\omega_s^{-2}\omega_p^{-2}}} \quad (3.39)$$

$$f_{ser}^H = \frac{\sqrt{\omega_s^{-2} + \omega_p^{-2} + \sqrt{(\omega_s^{-2} - \omega_p^{-2})^2 + 4k^2\omega_s^{-2}\omega_p^{-2}}}}{2\pi\sqrt{2(1-k^2)\omega_s^{-2}\omega_p^{-2}}} \quad (3.40)$$

In the case that both coils are totally tuned ( $\omega_s = \omega_L$ ), with  $k=0.3$ ,  $L_s = L_p = 1080 \text{ nH}$ , and  $C_s = C_p = 128 \text{ pF}$ , we would have for both encountered resonance frequencies the following values.

$$f_{ser}^L = \frac{\omega_s \sqrt{1-k}}{\sqrt{1-k^2}} = 11.8 \text{ MHz} \quad f_{ser}^H = \frac{\omega_s \sqrt{1+k}}{\sqrt{1-k^2}} = 16.2 \text{ MHz} \quad (3.41)$$

Which correspond to the simulated values in Fig. 3.21.

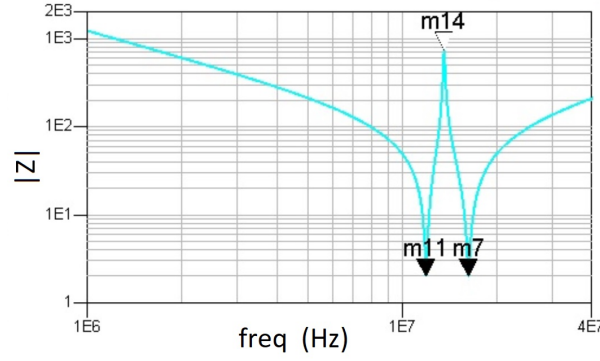


Figure 3.21: Simulation results for the resonant peak produced in the series resonant circuit used for energy transfer for  $C_{par} = 3150$ : m11 @ 11.87 MHz, m14 @ 13.54 MHz, and m7 @ 16.18 MHz.

As was mentioned earlier, the coupling factor may vary due to external factors. If that is the case, it is of interest to show what is the dependence on such factor for the energy transfer in order to try to obtain maximum energy transfer efficiency. Fig. 3.22) shows how as the coupling factor  $k$  increases, the peaks of the series resonance characteristics, move toward distant frequencies from the central resonance.

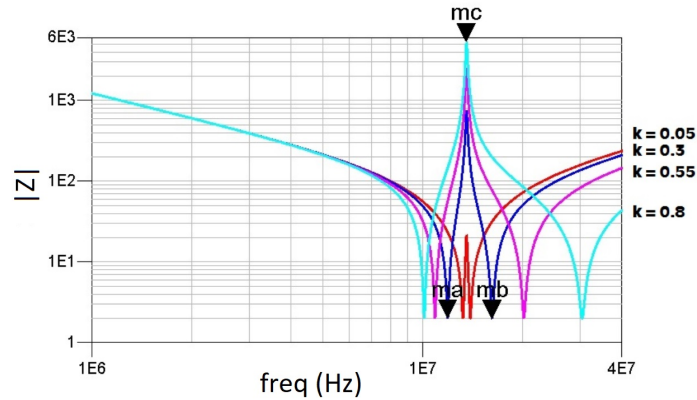


Figure 3.22: Dependence of resonance peaks versus coupling factor  $k$ , where ma, mc and mb, correspond respectively to m11, m14 and m17 of Fig. 3.21.

Finally in Fig. 3.23 it is shown the level of transmitted power to the secondary circuit. Since we may have a series or parallel resonance, what is shown is the effect when introducing a voltage or current source shown in Fig. 3.20. With a voltage source of 1 V feeding the primary coil, since the input impedance presents two resonance frequencies, the power will be transferred ideally at the same two optimal frequencies (for  $V_s = 1$  V, the power at the  $R_L = 1 \Omega$  is of 120 mW), while in the case of having a current source at the input, there will be just one optimal frequency for transferring power to the load (for  $I_s = 15$  mA, will be 85 mW, while with 150 mA would be 8.8 W for the same  $1 \Omega$  load), corresponding to the parallel resonance with infinite input impedance Fig. 3.23.

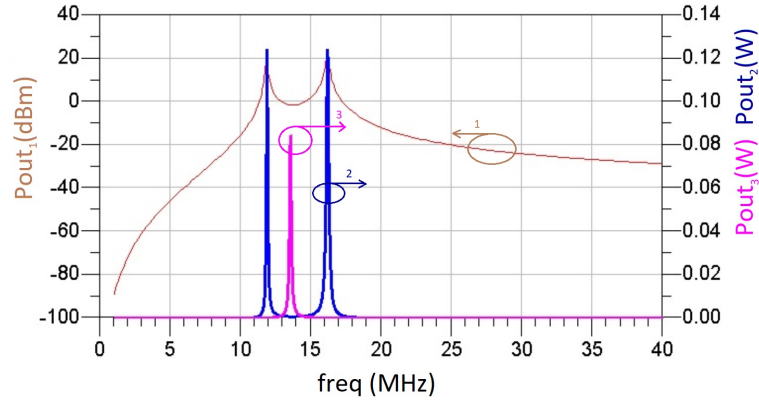


Figure 3.23: Blue( $P_2$  linear scale) and brown ( $P_1$  log. scale in dBm) line show the transferred power to the load when having a voltage source feeding the primary. In pink color ( $P_3$  in linear scale) is the power transferred for a current source.

The load of the charging device can be different, not only due to influencing external devices that come closer to the coupled coils, but also due to secondary load variability, for the connected circuit. In our case of series-series resonance at primary and secondary, the influence of the load is important. As we can see in Fig. 3.25 the amplitude of the resonant peaks can vary due to different loads presented in the secondary ( $R_{LL}$  from 5 to 150  $\Omega$ , in Fig. 3.24). By lowering the load, it arrives at one point that the central resonant peak is split into two of similar amplitude, and at the resonant frequency, the input admittance presents a minimum instead of maximum magnitude.

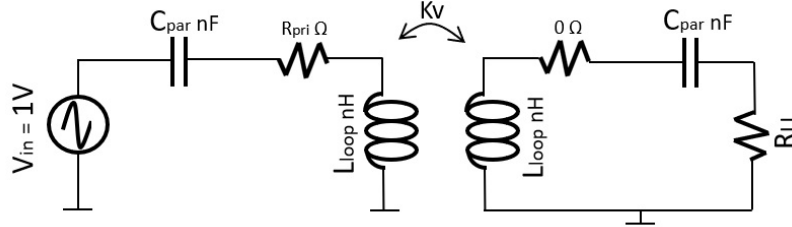


Figure 3.24: Equivalent schematic of the transfer inductive circuit.

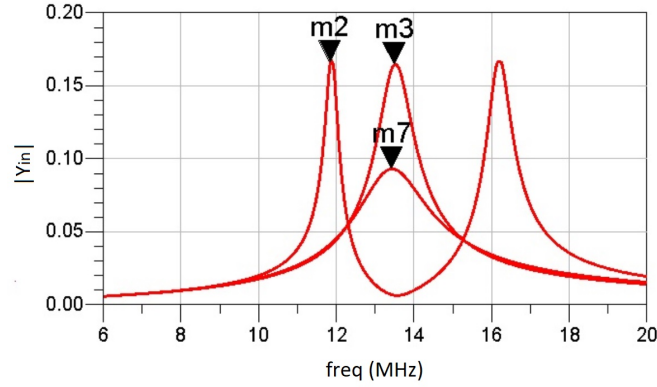


Figure 3.25: Admittance of the primary circuit when having variable loads (m2 @ 11.83 MHz, m3 and m7 @ 13.4 MHz).

### 3.3.2 Power transfer efficiency

One way to evaluate the efficiency of a wireless charging system is by looking at the losses in the magnetic circuit. At this low working frequencies, radiation losses can be neglected. Losses in the magnetic circuit are reflected by ohmic losses in the winding, determined by the coil's magnetic coupling factor  $k$  and the quality factor  $Q$ . The coupling factor will determine the amount of magnetic flux penetrating the receiver in comparison to the flux generated by the transmitter winding, mainly determined by the coil arrangement. For  $k = 0$  the coils are completely decoupled, while for  $k \rightarrow 1$ , all the transmitted magnetic flux reaches the receiver coil.

In Fig. 3.26 it is shown the equivalent circuit of the HF reader operating at 13.56 MHz coupled with a receiver, both using inductive loop antennas and including the different parts of the transmitter circuit design considered previously.

In order to be able to evaluate the performance of the circuit in a more simplified manner, it is possible for the analyses of losses and efficiency, to omit the circuitry dedicated to low pass filtering and matching. Also one can convert the differential network into a single ended referenced to ground, making the impedance transformation as indicated below in the same figure, simpler for analysis purposes.

As it is being demonstrated in Annex C, the Loss Factor expressed as the relation between output power to the input power of the transmitter ( $LF_p$ ), in Fig. 3.26 c) corresponds to the expression obtained in C.5 and repeated here eq.(3.42) ( $\gamma = R_L/X_L$ ):

$$LF_p = \frac{P_{To}}{P_{Ti}} = \frac{R'_p}{R_L} \left[ \frac{(R_s + R_L)^2}{X_{Ls}^2} + \frac{(X_{Ls} - X_{Cs})^2}{X_{Ls}^2} \right] = \frac{1}{(Qk)^2} \left( \frac{1}{\sqrt{q\gamma Q}} + \sqrt{q\gamma Q} \right)^2 \quad (3.42)$$

When considering the different parameter definitions in Annex C, and the ideal case of  $X_{Ls} = X_{Cs}$ , then the following expression is obtained for the total loss factor:

$$LF = LF_s + LF_p = \frac{1}{qQ\gamma} + \frac{1}{(Qk)^2} \left( \frac{1}{\sqrt{q\gamma Q}} + \sqrt{q\gamma Q} \right)^2 = \frac{1}{q\gamma Q} + \frac{q}{\gamma Q k^2} \left( \gamma + \frac{1}{qQ} \right)^2 \quad (3.43)$$

Using this expression, some results are presented in Fig. 3.27, where the loss factor is being plotted for different coupling factors between coils. In the case of  $k = 0.2$ , the  $LF = 0.1$  which corresponds to an efficiency of 90%. The coupling of 0.2 according to Fig. 3.6 corresponds to a couple of equal coils

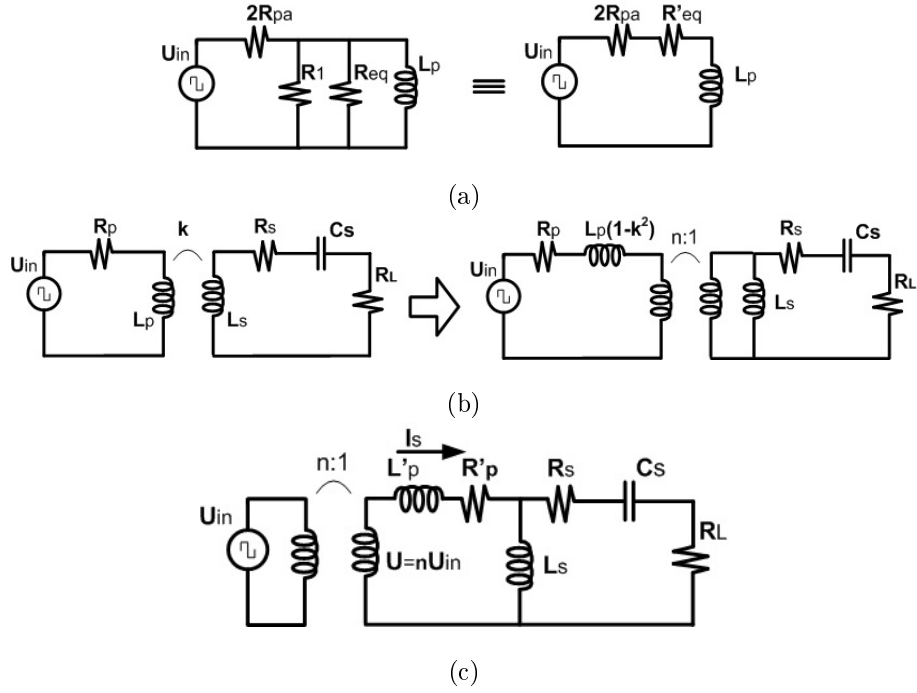


Figure 3.26: (a) Initial transmitter circuit. (b) Equivalent simplified single-ended circuit between charger and reader. (c) Equivalent circuit transformed into the secondary.

with radius  $R_1 = 2 \text{ cm}$  positioned at a distance of  $r = 28 \text{ mm}$ , or for example radius of  $R_1 = 80 \text{ mm}$  at distance  $r = 110 \text{ mm}$ . For the previous obtained equation, the optimum efficiency is also shown by small circles. These values are obtained by doing  $\frac{\delta L F}{\delta \gamma} = 0$ , which corresponds to the optimum for the matching factor defined in Annex C as  $\gamma = \frac{R_L}{L_s \omega}$ .

$$\gamma_{opt} = \frac{1}{qQ} \sqrt{(kQ)^2 + 1}; \quad q = \sqrt{\frac{Q_s}{Q_p}}; \quad Q = \sqrt{Q_p Q_s} \quad (3.44)$$

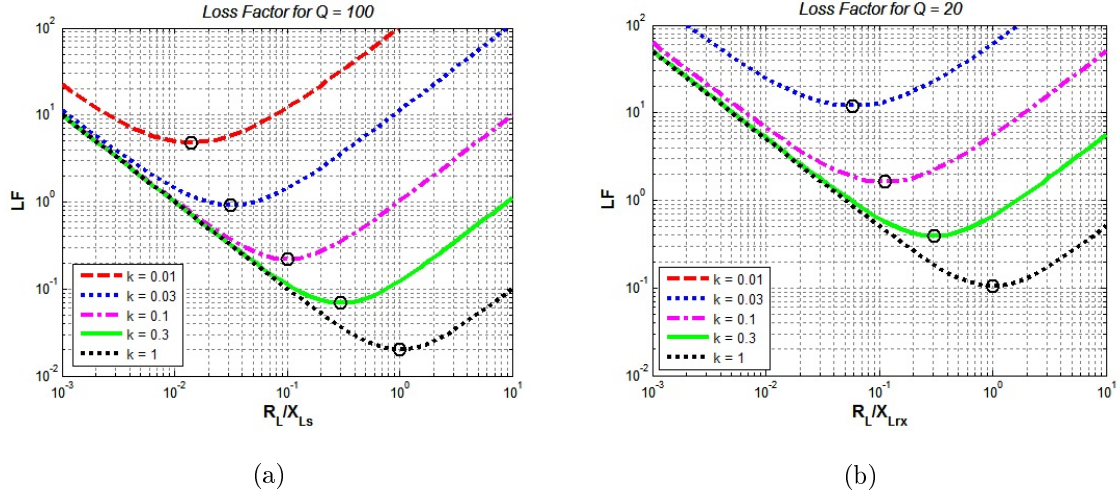


Figure 3.27: Loss Factor for different coupling factors and two realistic inductor quality factors, (a) Loss Factor for  $Q = 100$ , (b) Loss Factor for  $Q = 20$ .

The previous expression, shows that for a good wireless power transfer between the two coils, one needs to optimize the product  $kQ$ . In case of having a bad coupling, it could be compensated by improving the quality factor of the coil. As shown in Fig. 3.28, in the case that the reader has a better quality factor than the receiver coil, there is no much difference between a coupled and non-coupled antenna ( $LF_{X=1} = 4\%$  and  $LF_{X=0} = 6\%$ ). In the opposite case, the difference is much important ( $LF_{X=1} = 4\%$  and  $LF_{X=0} = 18\%$ ). So in general, a much higher freedom exists in the design of the transmitter coil.

In Fig. 3.28 we analyze the effect of perfect resonance in the secondary coil ( $X_{Cs} = X_{Ls}$ , so  $X = 1$ ) and non resonance with  $X \equiv \frac{X_{Cs}}{X_{Ls}} = 0$ .

In our case of having  $Q=20$ , and a  $k = 0.3$ , the optimum value would become  $\gamma_{opt} = 0.3$  corresponding to an efficiency of 60% ( $LF = 40\%$  at  $R_L = 0.3 \cdot 2\pi f \cdot 10^3 nH = 25\Omega$ ,  $R_L/X_L = 0.3$ ). If we had no restriction in regards to the data rate communication transfer, and one could increase the quality factor up to  $Q = 100$ , the transfer efficiency would increase to 90%, so the limiting factor is being shown when using systems that must comply with some communication constraints, and at the same time being able to transfer energy.



#### Limited efficiency

When being limited by  $Q$  (antenna also used for comm's) and  $k$  of the antenna coils, in our case  $k = 0.3$  and  $Q = 20$ , the maximum energy transfer efficiency achieved is 60%. Increasing  $Q$  by 5 would increase efficiency by 1,8 from 50% to 90%.

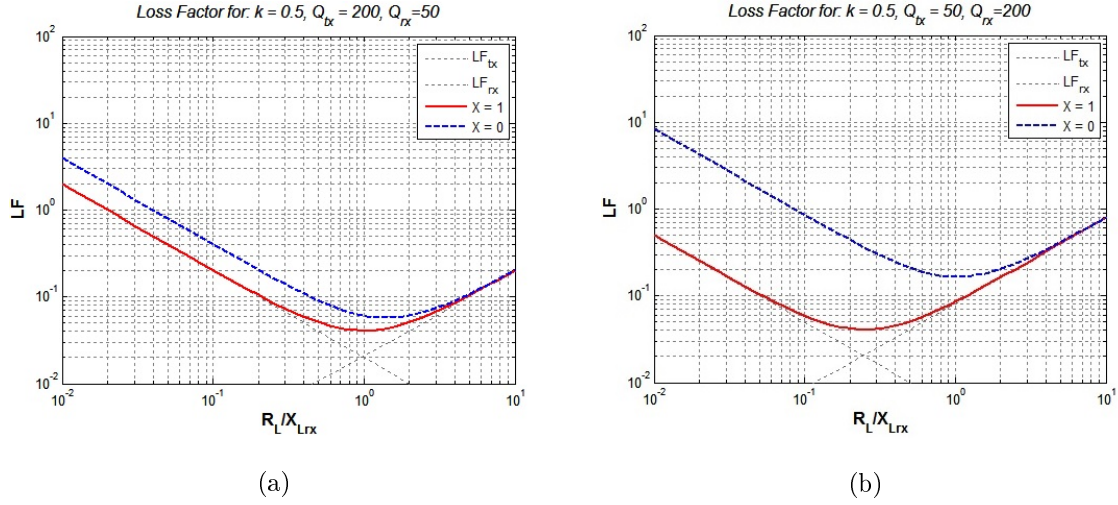


Figure 3.28: Loss Factor in a coupled 2 inductor circuit for different matching conditions and quality factors of receiver and transmitter coils. (a) Transmitter coil with better quality factor, (b) Receiver coil with better quality factor.

In relation to the measurement set-up for such parameters, one way to evaluate the losses is for example by means of measuring the S-parameters. They will help in order to evaluate the efficiency of a wireless power systems as it is used for example in [77]. In that case, the efficiency is computed as:

$$\eta = \frac{P_L}{P_{in}} = \frac{|S_{21}|(1 - |\Gamma_L|^2)}{(1 - |\Gamma_{in}|^2)|1 - S_{22}\Gamma_L|^2} \quad (3.45)$$

where for the case of having matching conditions at the load  $Z_0 = Z_L = 50\Omega$  then,  $\Gamma_L = 0$  and one can write the simplified relation related with the measured values:

$$\Gamma_{in} = \frac{S_{11} + (S_{12}S_{21}\Gamma_L)}{1 - S_{22}\Gamma_L} \quad \text{so} \quad \eta = \frac{|S_{21}|^2}{1 - |S_{11}|^2} \quad (3.46)$$

#### Optimal load for maximum efficiency transfer

Considering the equivalent circuit c) from Fig. 3.26, it is possible to compute the power efficiency in the transfer of power from the reader to the battery charger by considering electrical parameters from the equivalent circuit, including losses  $R_p$  and  $R_s$ . So, as demonstrated in Annex C, the total efficiency, defined as the output power to the load resistor  $R_L$  divided by the real power to the transmitter antenna  $R_p$ , is:

$$\eta_L = \frac{\omega^2 M^2 R_L}{R_p(R_s + R_L)^2 + R_p \left( \omega L_s - \frac{1}{\omega C_{e2}} \right)^2 + \omega^2 M^2 (R_s + R_L)} \quad (3.47)$$

Such efficiency will be optimal for a determined operating load resistance  $R_L$ . The operating conditions are supposed to present a resonance in the coil ( $C_2 = \frac{1}{L_2 \omega^2}$ ). The optimal efficiency provides then maximum output power at the receiving antenna and can be found by doing:  $\frac{\delta \eta_L}{\delta R_L} = 0$ .



$$\begin{aligned}
\omega^2 M^2 (R_p R_s^2 + 2R_p R_s R_L + R_1 R_L^2) + M^4 \omega^4 (R_s + R_L) - \omega^2 M^2 R_L [2R_p (R_s + R_L) + M^2 \omega^2] &= 0; \\
\omega^2 M^2 R_p R_s^2 + M^2 \omega^2 R_p + R_L^2 + M^4 \omega^4 R_s - 2M^2 \omega^2 R_p R_L^2 &= 0; \quad R_p R_s^2 + R_p R_L^2 + M^2 \omega^2 R_s = 0;
\end{aligned} \tag{3.48}$$

solving for  $R_{ic}$  one can find the optimal resistance as:

$$R_{L_{op}} = \sqrt{R_s^2 + \frac{M^2 \omega^2 R_s}{R_p}} = L_2 \omega \sqrt{\frac{1}{Q_s^2} + k^2 \frac{Q_p}{Q_s}} \tag{3.49}$$

The optimum efficiency can be obtained when using optimal load resistance

$$\eta_{L_{op}} = \frac{k^2 Q_p Q_s}{(1 + \sqrt{1 + k^2 Q_p Q_s})^2} \tag{3.50}$$

That can be expressed in terms of the following indicator parameters:

$$Q_p = \frac{L_p \omega}{R_p}; \quad Q_s = \frac{L_s \omega}{R_s}; \quad k = \frac{M}{\sqrt{L_p L_s}}; \tag{3.51}$$

The quality factor of inductances are limited by technology and transmission bandwidth, so we consider the working parameters ( $Q_p = Q_s = 20$ ), and for the different antenna inductance values and coupling coefficients. The optimal load resistance and optimal resistance are represented in Fig. 3.29:

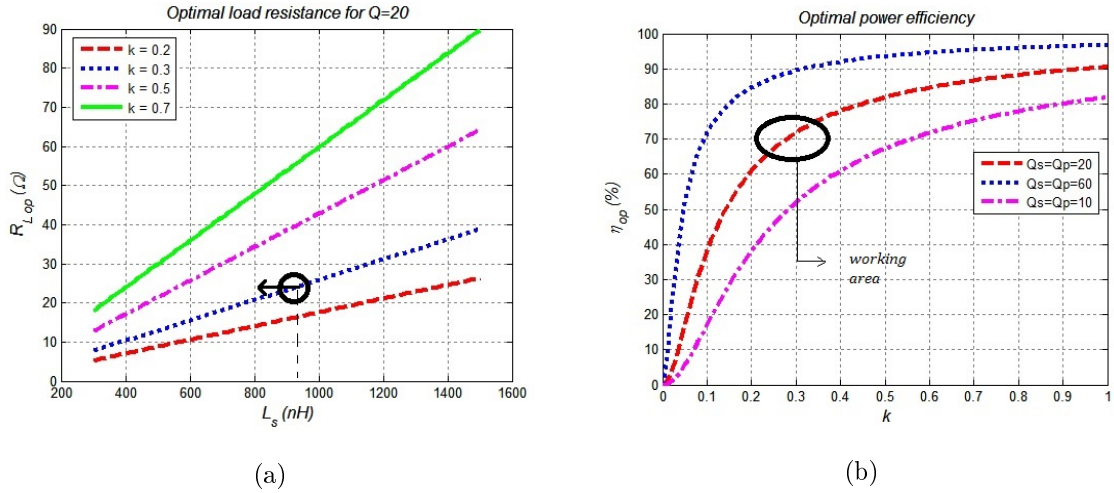


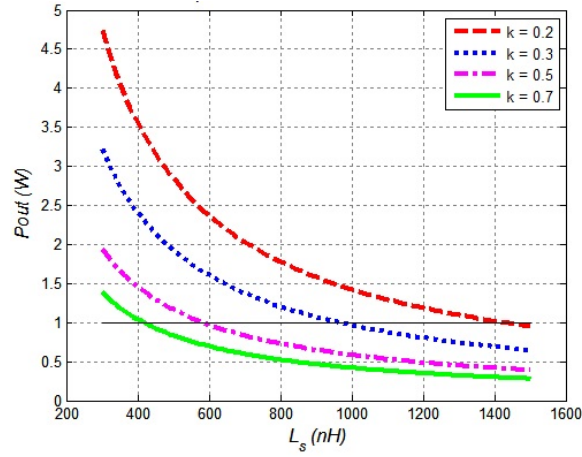
Figure 3.29: Optimal values for load resistance (a) that faces the equivalent circuit of two coupled inductors at resonance frequency. In (b) optimal power efficiency.

Following the discussion on previous section, once found the optimal resistance and the optimal efficiency of the resonant coupling circuit, one has to consider the mission of obtaining from the magnetic field the maximum current to charge a battery. There are different conditions that influence such current induction. One consideration for the charging circuit is limiting the voltage. Here we consider 5V, as the reference voltage used for charging. In the case of optimal load resistance presented to the receiving coil, from the results depicted in Fig. 3.30, for a coupling factor of  $k=0.3$ , the coil

Table 3.5: FEATURES FROM COMMERCIAL NFC READER INTEGRATED CIRCUITS (IC)

IC	Voltage	$I_{sleep}$	$I_{TX}$	Comm's	Compatible
PN512	2.5 - 3.6	10 $\mu A$	100 mA	SPI, UART, $I^2C$	ISO/IEC 14443A/MIFARE
EM4094	3.3 - 5	1 $\mu A$	100 mA	SPI	ISO14443 type A, B
AS3911	2.4 - 5.5	0.7 $\mu A$	600 mA	SPI	ISO 18092 (NFCIP-1), ISO14443A, B and FeliCa

inductance that provides 1 W output power is around 980 mH. With higher coupling factor, to get the same power we require lower inductor, while lower coupling it increase, so for  $k=0.2$ , the inductance can be 1.4  $\mu H$ .

Figure 3.30: Loss Factor for different 'k', for  $Q_s = Q_p = Q = 100$ 

With the previous data, one can look at the induced current in the coil, that corresponds to the magnetic flux field that crosses the coil area. When requiring 5 V at the input of the charging circuit, with  $M = 300$  nH, using Eq.3.4, the current would be:

$$I = \frac{V_{ind}}{j\omega M_{12}} = 196 \text{ mA} \quad (3.52)$$

It has not been possible to use Eq.3.5, because it is only valid for low coupling circuits. The power transfer will be limited by available output power from primary circuit. When using NFC, this power is limited by NFC reader design. Table 3.5 provides information on NFC transmitter circuit, including information of different manufacturers for comparison. In our case AS3911 can provide the higher transmit current.

#### Efficiency analysis including two cases for secondary, series and parallel resonance

In the wireless power transfer circuit, the two coils are normally coupled through low coupling coefficient and a resonant circuit is normally added at the secondary to improve performance. In the primary circuit, in case we want to charge from NFC, the primary circuit will consist on a parallel resonance circuit implemented by the communication circuit design, while for other systems devoted to power transfer energy (Qi), they consider the primary as series resonance circuit. In the secondary we can choose between series and parallel [100], so it is interesting to analyze the different performance characteristics.

In Fig. 3.31 we can see the circuit typologies to implement the resonance in the secondary circuit, which can be series or parallel depending on the capacitor location. For the primary circuit, it is considered parallel resonance. To analyze the efficiency in both cases, it is interesting to transform the secondary into the primary circuit as shown in Fig. 3.32. With that transformation we can obtain the total efficiency as a combination of the efficiency of the primary and secondary circuit:

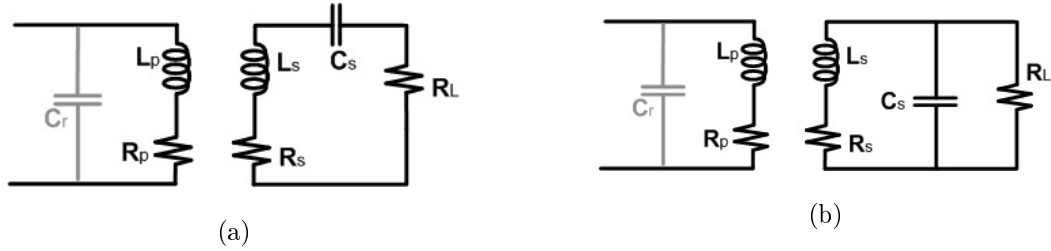


Figure 3.31: All possible resonances at the secondary: (a) Series secondary resonance and (b) Parallel secondary resonance, of the transformer considering series resonance at primary, typical from NFC.

$$\eta = \eta_{pri} \cdot \eta_{sec} \quad \text{where} \quad \eta_{pri} = \frac{\Re\{Z_r\}}{\Re\{Z_r\} + R_p} \quad \text{and} \quad \eta_{sec} = \frac{R_{eq}}{R_{eq} + R_s} \quad (3.53)$$

#### Series resonance in the secondary

Looking the circuit of Fig. 3.31 a) the secondary total impedance can be transformed into the primary by applying the mutual coupling coefficient factor in the following way:

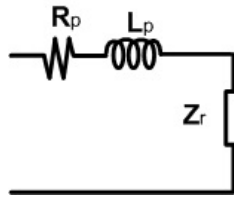


Figure 3.32: Transformation of secondary impedance into the primary.

$$Z_s = R_s + R_L + j \left( L_s \omega - \frac{1}{C_s \omega} \right) \quad (3.54)$$

that converted into the primary side will become (Fig. 3.32):

$$Z_r = \frac{M^2 \omega^2}{Z_s} = \frac{(M\omega)^2 (R_s + R_L)}{(R_s + R_L)^2 + \left(L_s \omega - \frac{1}{C_s \omega}\right)^2} - j \frac{(M\omega)^2 \left(L_s \omega - \frac{1}{C_s \omega}\right)}{(R_s + R_L)^2 + \left(L_s \omega - \frac{1}{C_s \omega}\right)^2} \quad (3.55)$$

taking the real part:

$$\Re\{Z_r\} = \frac{(M\omega)^2 (C_s \omega)^2 (R_s + R_L)}{(L_s C_s \omega^2 - 1)^2 + (C_s \omega)^2 (R_s + R_L)^2} \quad \text{at resonance;} \quad \Re\{Z_r(\omega_0)\} = \frac{(M\omega)^2}{R_s + R_L} \quad (3.56)$$

Then the efficiency of the magnetic circuit when having the series resonance is the following:

$$\eta_{pri}^S = \frac{\Re\{Z_r(\omega_0)\}}{\Re\{Z_r(\omega_0)\} + R_p} = \frac{(M\omega)^2}{(M\omega)^2 + R_p(R_s + R_L)} \quad \text{and} \quad \eta_{sec}^S = \frac{R_L}{R_L + R_s} \quad (3.57)$$

so the total efficiency will be;

$$\eta^S = \eta_{pri}^S \cdot \eta_{sec}^S = \frac{1}{1 + \frac{R_p(R_s + R_L)}{(M\omega)^2}} \cdot \frac{R_L}{R_L + R_s} \quad (3.58)$$

#### Parallel resonance in the secondary

Applying the same reasoning as in the previous case but for the case of having parallel resonance at the secondary as shown in Fig. 3.31 b), we first find the impedance in the secondary considering the inductance series resistance;

$$Z_s = L_s \omega j + \frac{R_L}{R_L C_s \omega j + 1} \quad (3.59)$$

And transforming the impedance into the primary;

$$Z_r = \frac{(M\omega)^2}{Z_s} = \frac{(M\omega)^2 (R_L + R_s)}{(R_L + R_s - \omega^2 R_L C_s L_s)^2 + (\omega L_s)^2} + j(M\omega)^2 \frac{[\omega R_L C_s (R_L + R_s - \omega^2 R_L C_s L_s) - \omega L_s]}{(R_L + R_s - \omega^2 R_L C_s L_s)^2 + (\omega L_s)^2} \quad (3.60)$$

The real part when considering the resonance condition will become;

$$\Re\{Z_r(\omega_0)\} = \frac{(M\omega)^2 (R_L + R_s)}{R_s^2 + (L_s \omega)^2} \quad (3.61)$$

so the efficiency of the magnetic circuit when having the parallel resonance will be the following;

$$\eta_{pri}^P = \frac{\Re\{Z_r(\omega_0)\}}{\Re\{Z_r(\omega_0)\} + R_p} = \frac{(M\omega)^2}{(M\omega)^2 + \frac{R_p}{(R_L + R_s)} [R_s^2 + (L_s \omega)^2]} \quad (3.62)$$

The secondary is constituted by parallel capacitance with the load, the series equivalent resistance in Fig. 3.33 of such parallel circuit is  $R_{eq}$ , which help to compute the efficiency in this secondary circuit as;

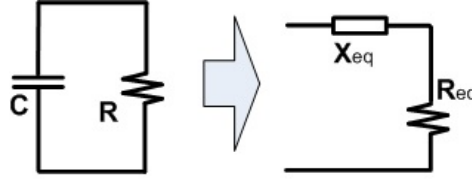


Figure 3.33: Equivalent impedance from the secondary parallel resonance circuit.

$$\eta_{sec}^P = \frac{R_{eq}}{R_{eq} + R_s} = \frac{R_L}{R_L + R_s + R_L^2 R_s C_s^2 \omega^2}; \quad \text{because} \quad R_{eq} = \frac{R_L}{1 + (R_L C_s \omega)^2} \quad (3.63)$$

$$\eta^P = \eta_{pri}^P \cdot \eta_{sec}^P = \frac{1}{1 + \frac{R_p [R_s^2 + (L_s \omega)^2]}{(M \omega)^2 (R_L + R_s)}} \cdot \frac{R_L}{R_L + R_s + R_L^2 R_s C_s^2 \omega^2} \quad (3.64)$$

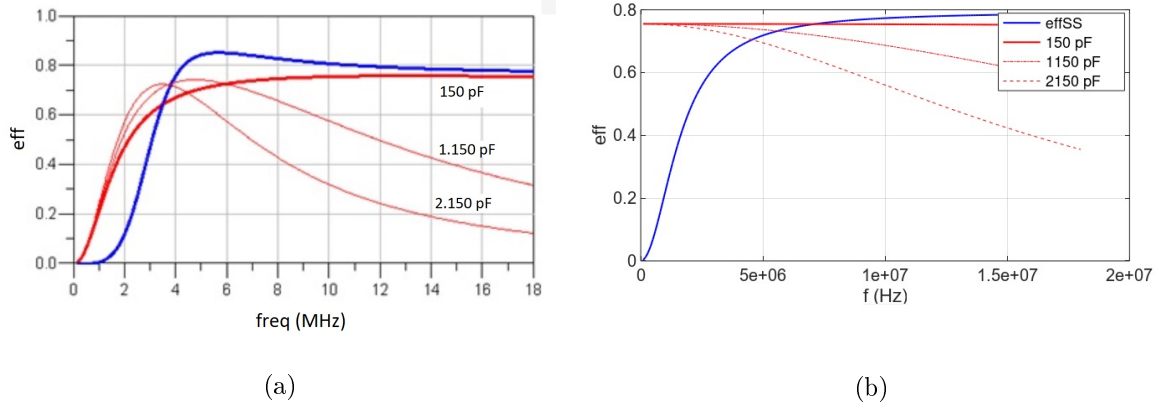
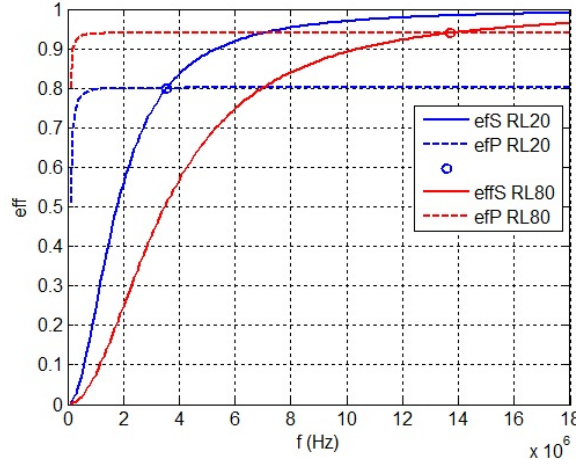


Figure 3.34: Comparison between series series (blue line) and series parallel (red line) resonance between primary and secondary coil inductance. (a) Simulation versus (b) analytic results.

From these expressions, the resistance values are considered ideal components that do not vary with frequency. In this case a slight deviation from ideal resistance values would be expected in the previous figures when computing efficiency versus a wide range of frequencies. Depending on the size of the conductors, a frequency dependency towards increase the resistance by frequency due to skin effect would be expected.

Some interesting conclusions can be extracted from this series-parallel resonance. That is the case where having series resistance at the secondary the efficiency is kept more constant independently of the  $C_s$  value.

Figure 3.35: Effect of  $R_L$  on the power transfer circuit

In relation to the load resistance, as can be seen in Fig. 3.35 when  $R_L$  varies, the effect on efficiency will be lower for parallel resonance, while in the case of series resonance, the variation of efficiency versus frequency will depend much more on this impedance. If one considers a fixed frequency, the variation of efficiency is less in series resonance (5% for series versus 15% for parallel resonance). There is a frequency point where both efficiencies ( $\eta^S, \eta^P$ ) are equal, the frequency where this occurs will be low for lower  $R_L$ . Above such frequency, for a series resonance circuit the efficiency will be always higher.

### Considering driver efficiency

Let us now consider the properties of the power amplifier driving the transmitter coil. This is typically a class E amplifier, which requires just a single switching transistor (can be nMOS), and can achieve a theoretical efficiency of 100%, that in practice becomes 85% [101]. From [102] it is shown that the peak AC voltage on a transmit coil powered by a class E power amplifier operating from a DC voltage supply of  $V_s$  can achieve ideally:

$$V_{T_{pk}} = \frac{2}{\sqrt{\frac{\pi^2}{4} + 1}} Q_p V_s = A_{PA} Q_p V_s \quad (3.65)$$

where  $A_{PA}$  represents the voltage gain of the amplifier, in our case with  $V_s = 5 V_{DC}$  and  $Q_p = 20$ , we have  $V_{T_{pk}} = 39,7$  V. For the total efficiency of the circuit, from the transmitter power amplifier to the power received by the load, one easy option is to transform the circuit to the primary of the coil. Lets first work on the secondary circuit. Converting the inductance series resistance into parallel, which will allow to make equivalences in parallel resistances:

$$Q'_S = \frac{(Q_S^2 R_S) // R_L}{L_S \omega}; \quad Q_P = \frac{\omega_0 L_P}{R_P} \quad (3.66)$$

In addition for the primary circuit, one can decompose the transmitting inductance into the leaking inductance and the magnetizing inductance, see Fig. 3.37. In parallel to the magnetizing inductance, used to transfer power to the receiving or secondary coil, there will be the equivalent capacitance  $C_{Seq}$  and the equivalent resistance  $R_{Seq}$  passed from the secondary to the primary [103].

$$L_{P_{mag}} = k^2 L_P; \quad L_{P_{leak}} = (1 - k^2) L_P \simeq L_P \quad (3.67)$$

$$C_{S_{eq}} = \frac{L_S}{L_P} \frac{C_S}{k^2}; \quad R_{S_{eq}} = k^2 \frac{L_P}{L_S} R_L = k^2 Q_P Q'_S R_P \quad (3.68)$$

with the voltage gain of the amplifier  $A_{PA} \simeq 1.07$ . And the voltage gain from the primary coil to the secondary or receiving coil is given by [102]:

$$A_{wpt} = \frac{V_{S_{pk}}}{V_{P_{pk}}} = k \sqrt{\frac{L_S}{L_P}} Q'_S \quad (3.69)$$

then;

$$\frac{V_{S_{pk}}}{V_S} = A_{PA} k \sqrt{\frac{L_S}{L_P}} Q'_P Q'_S \quad (3.70)$$

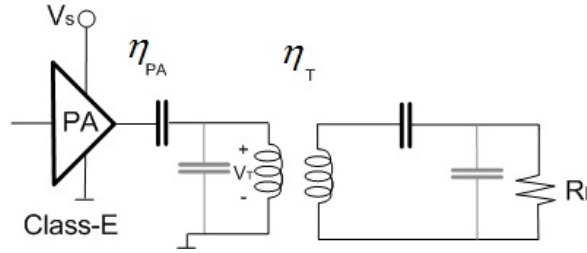


Figure 3.36: Power efficiency balance.

At this point it is possible to consider the total efficiency, from the power amplifier output, to the wireless load charging circuit, or equivalent load resistance. So considering the driven power from the power supply as  $P_{SS} = V_S \cdot I_S$ ;

$$\eta = \frac{P_L}{P_{SS}} = \eta_{PA} \cdot \eta_T \cdot \eta_R = \frac{(R_P + R_{S_{eq}}) I_L^2}{V_S I_S} \cdot \frac{k^2 Q_P Q'_S}{(1 + \sqrt{1 + k^2 Q_P Q'_S})^2} \quad (3.71)$$

assuming the receiving efficiency  $\eta_R \simeq 1$  if the receiving coil without charge has a high  $Q_S$ .

#### Power to the load

For the WPT circuit, the important part is the amount of power that is transferred to the load from the secondary coil, which can be composed of a battery in the case of remote wireless sensors. In this case, it is of interest to be able to deduce an analytical expression that would help in predicting such power. A first step is to use the two-leakage inductance transformer equivalent model Fig. 3.37 b) as used in the efficiency analysis.

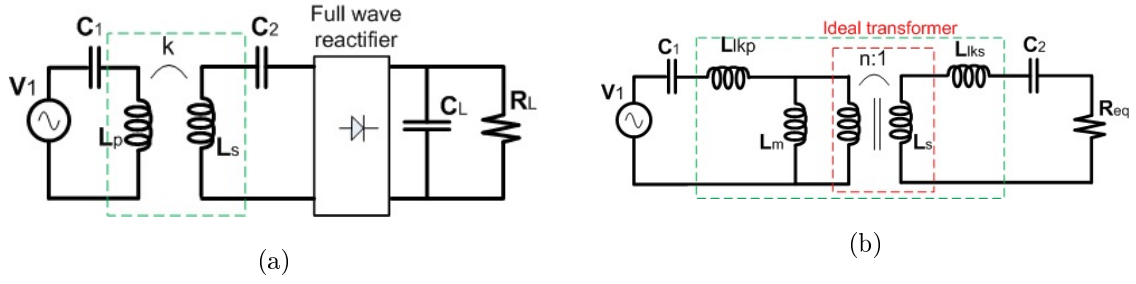


Figure 3.37: Electrical circuit for the WPT system including full-wave rectifier.  $L_{kp} = (1 - k)L_p = (1 - k)n^2L_s$ ,  $L_{ks} = (1 - k)L_s$  and  $L_m = k \cdot L_p$ . (a) WPT circuit with RF/DC rectifier, and (b) Equivalent WPT circuit.

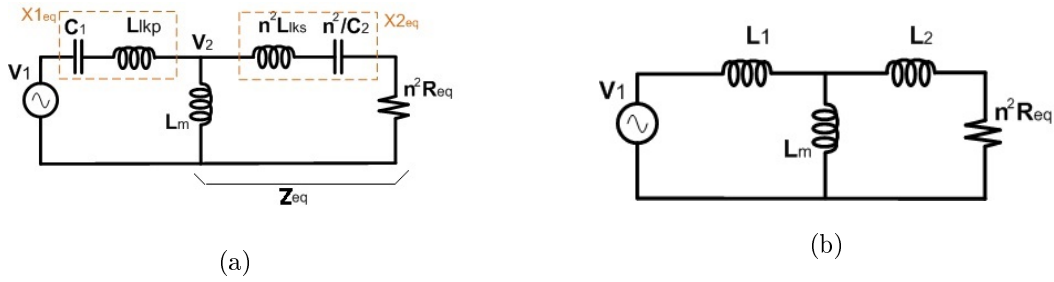


Figure 3.38: Simplification on the previous WPT system.  $L_1 = L_{kp}$ ,  $L_2 = -kn^2L_p$ . (a) First simplified equivalent circuit, and (b) Simplification at resonance frequency.

From this first circuit it is possible even to reduce it further, by transforming the secondary into the primary side such as Fig. 3.38 a), and finally if one is interested at the results when working at the resonant frequency, the one with ideal matching and efficiency conditions, it is possible to reduce even further the circuit to the one depicted in Fig. 3.38 b). In this case the analysis is simplified and shown below:

$$P_L = \frac{V_L^2}{R_L}; \quad \text{where} \quad V_L \Big|_{f_o} = V_2 \frac{n^2 R_{eq}}{|n^2 R_{eq} - j\omega L_p(1 - k - n^2)|}; \quad V_2 = V_1 \frac{Z_{eq}}{|Z_{eq} - j\omega L_p k|} \quad (3.72)$$

$$Z_{eq} \Big|_{f_o} = \frac{j\omega k L_p [(n^2 R_{eq} + j\omega L_p(1 - k - n^2))]}{j\omega k L_p + n^2 R_{eq} + j\omega L_p(1 - k - n^2)} = \frac{j\omega k L_p [n^2 R_{eq} + j\omega L_p(1 - k - n^2)]}{n^2 R_{eq} + j\omega L_p(1 - n^2)} \quad (3.73)$$

$$V_L \Big|_{f_o} = \frac{V_1 \cdot n^2 R_{eq}}{|n^2 R_{eq} + j\omega L_p(1 - k - n^2)|} \cdot \frac{j\omega L_p k [n^2 R_{eq} + j\omega L_p(1 - k - n^2)]}{|j\omega k L_p [n^2 R_{eq} + j\omega L_p(1 - k - n^2)] - j\omega L_p k [n^2 R_{eq} + j\omega L_p(1 - n^2)]|} \quad (3.74)$$

$$V_L \Big|_{f_o} = V_1 \frac{L_p \omega (n^2 + k - 1) + j n^2 R_{eq}}{\omega L_p k} \quad (3.75)$$

where  $V_L$  is the load voltage. In a symmetric WPT circuit, with equal values for the coils in the primary and secondary, the values have been simplified using;  $L_1 = -kL_p$ ,  $L_2 = -L_p(1 - k - n^2)$ , and  $L_m = kL_p$ . In the case  $L_1 = L_2$  we would have  $n = 1$ .



### 3.4 Conclusions

A design of HF communication and power transfer system is analyzed and designed. Based on the coil design a simulation environment is created to investigate filtering and receiver mixer sensitivity.

Some effects of power degradation are investigated, based on non-ideal conditions. Some causes as loss in coupling between primary and secondary coil are investigated considering effects such as proximity of metal objects, miss alignment or, difference in sizes between coils.

Analytical expressions for the efficiency finally provide good insights into the optimum coil design, potential losses, and maximum coupling to accomplish the most remarkable of the HF coupling in NFC circuit. Different resonance configurations are justified in the study, to accomplish a good compromise and design reference.

## 4 NFC to RFID circuit implementation

### 4.1 Introduction

The thesis consist on investigating, and implementing a platform that integrates both systems, NFC and UHF-RFID technologies, which interact with each other, optimizing area, and functionality. It integrates the necessary circuitry to prove the concepts of dual functionality, that is, the use of NFC for communications between NFC devices such as mobile phones, or NFC sensor as usual, and also for charging wireless devices, while being robust to interference.

For simplification on the RFIC design, the "zero-IF" radio architecture with single antenna is chosen for both systems, including a mixer first stage radio as receiver for the RFID part. Such IC's are being provided by ST (recently acquired from AMS - Austria Micro Systems). In regards to NFC, it is used a ST chipset AS3911 with main properties described in table 3.5. The interest of such complete system, resides in providing a tool to mobile phones so, they can power sensors wirelessly, and read recorded data via UHF-RFID at longer distances than NFC.

In the same manner as the NFC and WPT has been designed in chapter 3, with all its building blocks well defined and justified. Here we are going to justify the design of the UHF-RFID design.

### 4.2 UHF-RFID architecture

#### 4.2.1 Gen2 Protocol introduction

For the UHF-RFID communication to take place, the EPCglobal Gen2 protocol specifies that an interrogator will sent the information to the tag/s by modulating the RF carrier in one of the modulation schemes introduced in chapter 2, managing tag populations using three basic commands:

1. **Select:** Choose one or more tags based on a value or values in tag memory, and may use a *Challenge* command to challenge one or more tags, based on tag support for the desired cryptographic suite and authentication type.
2. **Inventory:** After a *Query* command one or more tags may reply. The interrogator detects a single tag reply and requests the tag's EPC. Inventory comprises various multiple commands.
3. **Access:** Communications with an identified tag performing;
  - a core operation such as reading, writing, locking or killing the tag.
  - a security operation such as tag authentication
  - a file-related operation such as opening a particular file

Tags energized by a reader shall be capable of receiving and acting on interrogator commands within a period not exceeding maximum settling time of RF carrier ( $T_s = 1500 \mu s$ ) or rise time ( $T_{hs} = 500 \mu s$ ). The reader may choose to access a tag after acknowledging it. The access commands are *ReqRN*, *Read*, *Write*, *Lock*, *Kill*, *Access*, *BlockWrite*, *BlockErase*, *BlockPermalock*, *Authenticate*, *ReadBuffer*, *SecureComm*, *AuthComm*, *KeyUpdate*, *Untraceable*, *FileOpen*, *FileList* and *FilePrivilege*. Access always begins with an interrogator moving a tag from the **acknowledge** state to either **open** or the **secure** state.

### 4.2.2 EPC Global Class3 Protocol introduction

Since our system must be able to communicate with RFID tags that contain sensor information and have a battery, this tag fits in a new classification out of the regular Class 2 tags with just EPC code. For clarifying purposes, here is a classification of all the RFID tags depending on their functionality:

- Class 0: UHF read-only, preprogrammed passive tag
- Class 1: UHF or HF; write once, read many (WORM)
- Class 2: Passive read-write tags that can be written to at any point in the supply chain
- Class 3: Read-write with onboard sensors capable of recording parameters like temperature, pressure, and motion; can be semipassive or active
- Class 4: Read-write active tags with integrated transmitters; can communicate with other tags and readers
- Class 5: Similar to Class 4 tags but with additional functionality; can provide power to other tags and communicate with devices other than readers

### 4.2.3 UHF-RFID transceiver technologies

The UHF RFID radio reader developed by AMS later ST, is the commercial AS3993 IC, that performs in a single device the receiver and transmitter part. It is an EPC Class 1 Gen 2 [104] RFID reader IC which implements ISO 18000-6C, the ISO 29143 air-interface protocol for mobile RFID interrogators, and ISO 18000-6A/B for operation in direct mode.

The whole integrated CMOS-IC has few external components, one of them is the power amplifier (PA) for high output power. There is a small power integrated PA, but because of the low breakdown voltage, small transconductance and poor passive devices in CMOS technology, it is not a straight forward task to design a fully-integrated CMOS PA with high output power, efficiency and linearity [105], so external PA is required. In addition, with integrated high power PA, there are high spurious emissions generated by the PA that affect the receiver as well as strong components injected into the substrate or induced at the circuit's front end, that demands for a high linearity front-end design. Substrate injection by the PA highly affects the VCO's phase noise (PN). The Fig. 4.1 shows the IC block diagram together with the front end implementations. Instead of selecting high power to the internal PA, which can saturate receiver input sensitivity, due to substrate leakage coupling problem, it is advisable to reduce RF power from the output of the front-end IC, and demand higher power from external PA. In our case we use as external PA the reference RF2172 from RFMD, a 23.5 dBm output power PA with variable gain adjustable from 0 dB to 28 dB, and 45% efficiency. So in this case, the internal PA only requires -5 dBm output power, reducing the risk of coupling and phase noise.

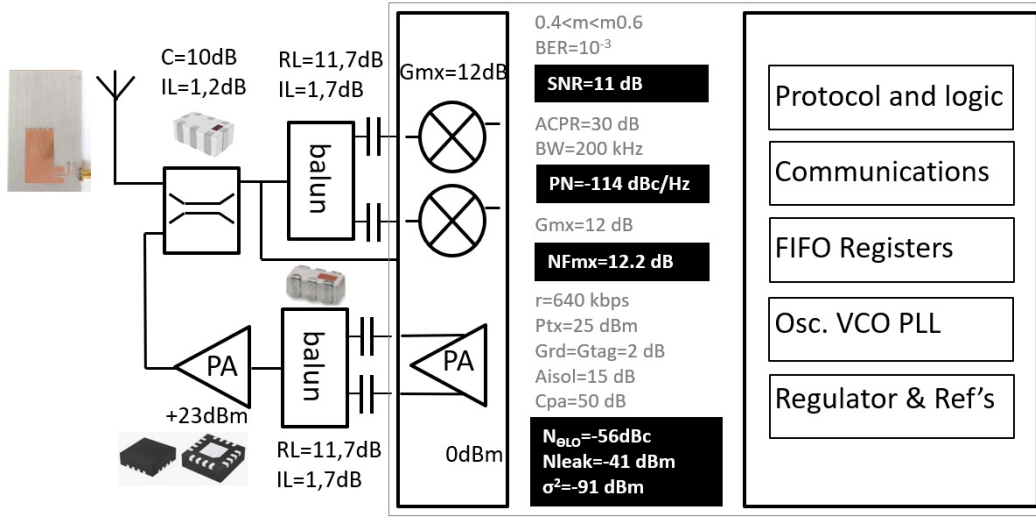


Figure 4.1: Block diagram of the UHF-RFID radio IC, AS3993.

The design has been implemented using FR4 substrate with permittivity of  $\epsilon=4.2$ . Several trials have been needed to improve signal integrity between MCU and front-end due to layout tracing.

The communication between readers and tags is half duplex (R-T and T-R). In forward link, reader sends a modulated carrier to the passive tags. This signal powers up the tags and then tags arbitrates their state and determines which tag responds to the reader. In the return link, the reader sends a continuous-wave (CW) carrier, the tag receives the carrier for powering itself and modulates the backscattered incident wave by varying its input impedance, changing the reflection coefficient of the antenna.

With the intention of integrating RFID radios in compact embedded devices, there is the trend on designing RFIC's in compact size, which implement many functionalities. Some efforts are made in order to improve read range or power consumption, reducing interference desensitization. In table 3.1 there are some examples of RFIC developments for UHF-RFID applications with the achievements on main parameters. Except for [13] that achieves +30 dBm output power and -87.4 dBm sensitivity using an integrated blocker-canceller feedback that eliminates the self-jammer signal, the rest of the solutions present relative low output power. The picture of the IC layout with its sizes is shown in Fig. 4.2.

Table 4.1: PERFORMANCE SUMMARY OF RFID READER ICs

	[106]	[107]	[108]	[109]	[13]	[110]
Technology	0.18 $\mu\text{m}$ SiGe BiCMOS	0.18 $\mu\text{m}$ CMOS	0.18 $\mu\text{m}$ CMOS	0.18 $\mu\text{m}$ CMOS	0.18 $\mu\text{m}$ CMOS	0.18 $\mu\text{m}$ CMOS
Sensitivity, S(dBm)	-85	-77	-85	-90	-95.3	-75
Rx. IIP3 (dBm)	NA	1	NA	-2	-8	NA
Output Power (dBm)	11	7.5	10	10.4	30	22.4
PA on chip	YES	YES	NO	NO	YES	YES
Total power (mW)	1200	203	540	276	92 (no PA)	1089

In the case of the **AS3993**, it has a low power consumption architecture (2.7 V at 65 mA), and small size (QFN-48 7x7 mm), with high sensitivity of -90 dBm. It also includes programmable filters in

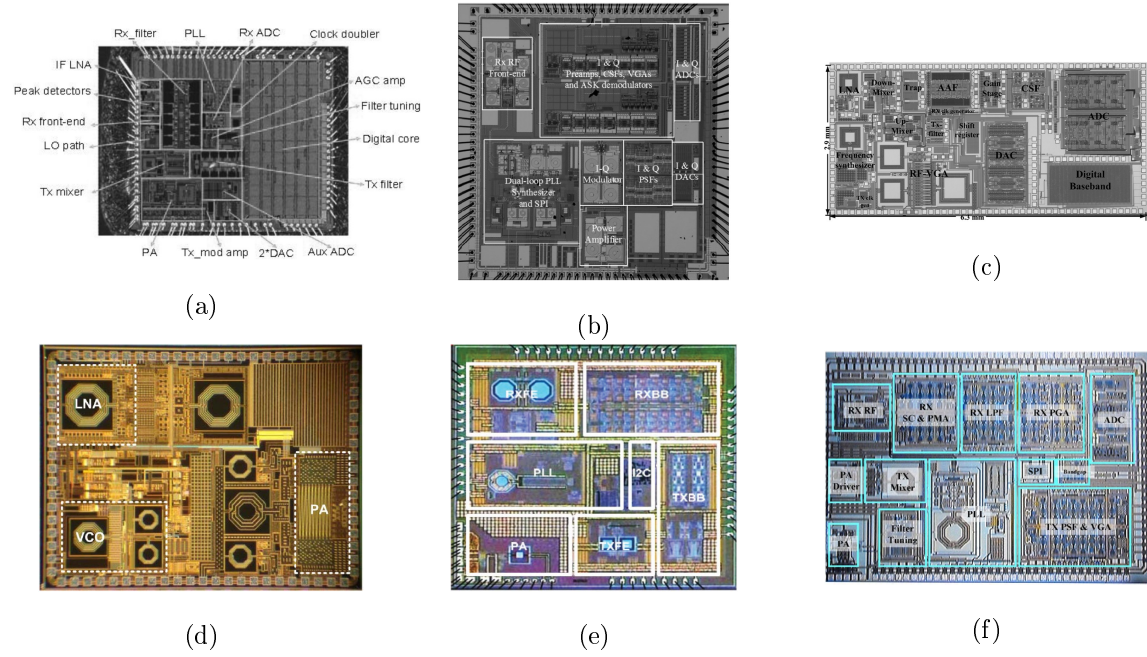


Figure 4.2: Photos of different RFID transceiver CMOS dies. (a) [106] 21  $mm^2$ . (b) [108] 36  $mm^2$ . (c) [109] 18.3  $mm^2$ . (d) [13] 6  $mm^2$ . (e) [110] 16.8  $mm^2$  (f)[111] 13.5  $mm^2$ .

"dense reader" mode, that avoids possible conflicts in environments with many readers. Internal PA can provide up to 20 dBm output power, but for the reasons above mentioned we use the 0 dBm differential output and external PA. Also has internal VCO generating -124 dB/Hz phase noise.

The reader includes some diagnostic features such as RSSI measurement or reflected power. This one is a measurement taken after the mixer, that can be used when activating the transmitter, as stated before, for interference avoidance due to channel occupation. It complies with EPC class 1 Gen2 (ISO 18000-6C), also with ISO 29143 and with ISO 18000-6A/B (direct mode). The configuration can be done accessing the control registers via SPI from a simple MCU. A picture of the blocks for this IC can be seen in Fig. 4.1.

#### 4.2.4 UHF-Tag

There are two operations of the compact RFID to NFC reader, a basic one for inventorying using standard RFID tag, and for sensing applications, a more novel application.

Among the most popular commercial tag manufacturers one can find, Alien with their Higgs series of tags, or Impinj with their Monza series. In all cases, as the time passes by, the improvement in sensitivity is increasing but slowly with technology, so longer reading distances are achievable, reaching -19.5 dBm for the MONZA 4, or -20.5 dBm for the Higgs-EC or Higgs 9. Fig. 4.3 shows some of the most remarkable RFID tag layouts found in literature, including also their sizes.

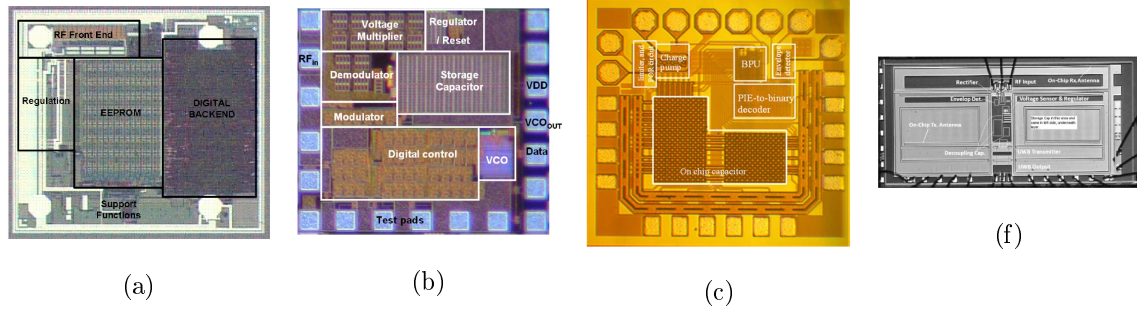


Figure 4.3: Photos of different RFID tag CMOS ICs. (a) [20]  $0.55 \text{ mm}^2$ . (b) [21]  $0.64 \text{ mm}^2$ . (c) [16]  $0.89 \text{ mm}^2$ . (d) [112]  $4.5 \text{ mm}^2$ .

Table 4.2: EPC GEN 2 UHF RFID ICs

	[20]	[21]	[16]	[112]
Technology	$0.13 \mu\text{m}$	$0.35 \mu\text{m}$	$0.18 \mu\text{m}$	$0.18 \mu\text{m}$
	CMOS	CMOS (Ti/Al/ta/Al)	CMOS	CMOS
Sensitivity, S(dBm)	-14	-14.8	-21.2	-19.4
Data rates (kbps)	40-160	150	71-142	1000
Power consumption ( $\mu\text{W}$ )	N/A	240	3.2	0.6
Typ. range (m)	7	4.5	19.6	15.7
Modulation	ASK PR-ASK	ASK (m=40%)	ASK	impulsive OOK, BPSK

As a proof of concept, we have used NFC and RFID sensors with data logging capabilities, so some data can be taken while the sensor is in sleep state and wakens every once in a while, and the data is saved in the internal memory. Once it is required, the RFID reader can retrieve the stored data from the distance by interrogating the RFID tag. At this time the RFID tag can erase the local memory and start measuring again. The energy required to measure and store data in EEPROM internal memory is taken from the local storage element that is charged using our NFC WPT system.

Table 4.3: EPC CLASS 3 OR 1 GEN 2 UHF RFID ICs AND NFC, WITH SENSING CAPABILITIES

commercial name	EEPROM	Supply	Included sensor	comm's
SL900A Gen2	9kbit	1.5 - 3V	Temp. sensor	SPI
EM4325 Gen2	4kbit	1.25 - 3.6 V	Temp. sensor	SPI
NT3H1101 NTAG	2kbit	1.7 -3.6 V	external	$I^2C$

A common feature for those ICs is that they are active, so require extra supply voltage. Such voltage is used to take measurements while the tag is not being illuminated by the reader, and be stored in the internal memory. For such purpose, some tags require extra MCU functionality that awakens the system, communicates with sensors, takes measurement, stores them and goes to sleep again. Both cases are shown in Fig. 4.4. To show the effectiveness of the NFC-WPT with RFID we have implemented both type of sensors. Using SL900A as UHF tag and sensor, and also using EM4325, which communicates with external MCU unit that performs sensing measurements and stores information in internal EEPROM.

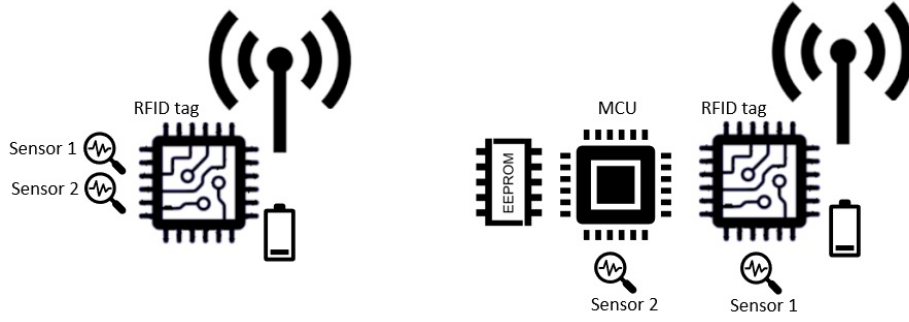


Figure 4.4: Architecture of the RFID sensor tag with and without data logging capabilities.

### 4.3 UHF-RFID electronics design

One of the most important part of RFID reader design is to accomplish a good isolation between transmitter and receiver. Long reading range, means high output power and high sensitivity, and using the described reader architecture, consisting of the one single antenna reader, a good isolation between PA and receiver is mandatory for low coupling. In addition to provide external PA or high isolation coupler in antenna connection, in terms of circuit isolation, we obtain high isolation using Coplanar Waveguide (CPW) layout for transmission lines, because there are always RF grounds between traces. Many examples of high-isolation RF switches have used grounded CPW to get 60 dB isolation or more.

The ground inductance for shunt elements is quite low for CPW, compared to microstrip applications. This is because the RF ground is very close, and it is not necessary to drill a via hole to connect to it (Fig. 4.6). Our intention is to build compact circuits using narrow transmission lines, in this case we have trade off RF loss, and reducing the line length to reduce couplings (coupling increases by 6 dB for each doubling of line length [113]). CPW circuits can have higher losses than comparable microstrip circuits, but on the other hand, we are tracing very short CPW lines, so the losses are reduced.

In terms of circuit size, CPW is at a disadvantage versus a stripline or microstrip circuit, because its effective dielectric constant is lower (half of the fields are in air). There's a rule of thumb for CPW that states that the effective dielectric constant for "classic" CPW is very close to the average of the dielectric constant of the substrate (because the filling factor is 50%), and that of free space. So if we are using FR4 with  $\epsilon = 4.2$ , the effective dielectric constant would be roughly  $(4.2+1)/2=2.6$ . But compromise must be taken since other effects such as Electromagnetic Interference (EMI) or cross-talk are of much important in RF circuits, and also in analog and digital design.

We have placed many ground straps, they are always needed to tie the two grounds together in CPW, to avoid undesirable Modes with possible resonances. These are especially important around any discontinuity, such as a tee junction. So we use differential traces like balun input, in case of the transmitter output signal, or balun output in case of receiver signal, and for the rest just single line Coplanar Wave Guide with Ground (CPWG), see Fig. 4.5.



Figure 4.5: Coplanar wave guide (CPWG) with ground planes used in RF front-end, for transmitting single mode signals (a), or differential signals (b).

In Fig. 4.6 it is shown the layout of top and bottom layer, differentiating the RF ground layer, from the RF digital ground, which are only connected at few locations to reduce couplings and ground loops between DC and RF parts.

The RFID reader is a **monolithic design**, so the antenna is the same for transmitter and receiver. This option is the easiest and most common one for a compact integration. In case more space would be provided, a dual antenna reader could have been designed, in this case the isolation between transmitter and receiver can be higher improve, and also other antennas can be used to activate the RFID tags.

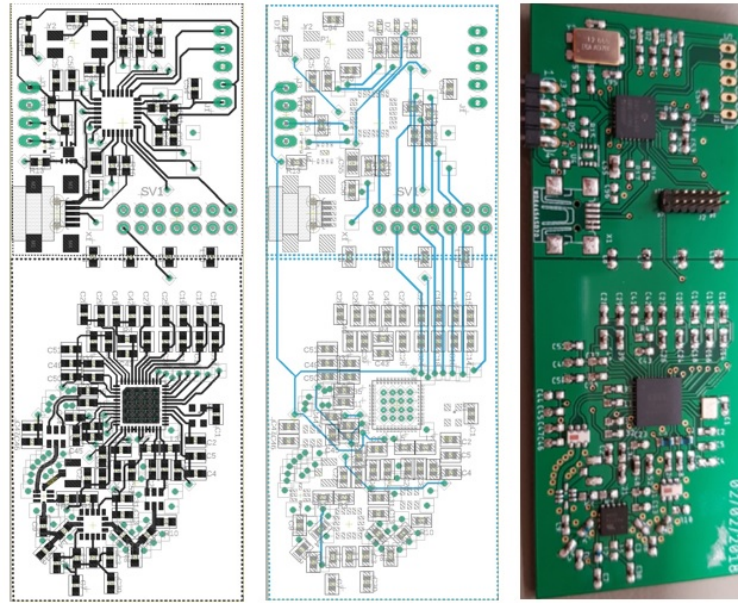


Figure 4.6: Two layer layout (top left and bottom middle) and picture of the PCB for the UHF-RFID front-end.

#### 4.4 UHF-RFID Compact antenna design

We need to design a UHF- antenna working in combination with mobile phone. The backside of mobile phones is characterized by the presence of a battery, which essentially behaves as a metal plane, and consequently, the use of dipoles is not convenient. Thus, a microstrip patch is one of the most suitable configuration to be used as UHF RFID antenna. Moreover, a common characteristic of such antennas is that they are low profile, allowing for a narrow design of the UHF RFID module. The size of the



antenna, namely, 60 mm by 100 mm, was chosen to fit to typical commercial smartphones. Since the above-mentioned size is smaller than half wavelength at the UHF RFID band, a quarter-wavelength patch antenna was considered. To reduce the antenna length even more, the rectangular patch was bent to get a right-angle.

Patch antennas are a type of microstrip antennas, easy to fabricate and integrate because the elements are usually flat, just a conductor over a ground plane. Once feeded on the conductor plane, the electric field distribution is excited in its fundamental mode (TM<sub>10</sub>, electric field in "z" direction and magnetic field in x and y axis parallel to ground plane), being zero at the center of the patch, maximum at one side and minimum at the other side. Such electric field expands beyond the edges of the patch which is known as fringing fields, causing the fields to radiate.

The antenna was designed on a Rogers RO4003 substrate with thickness  $h = 0.8$  mm, dielectric constant  $\epsilon_r = 3.55$ , and loss tangent  $\tan \delta = 0.0022$ . The dimensions of the antenna layout, as shown in Fig. 4.7, are  $w_1 = 0.4$  mm,  $l_1 = 12.6$  mm,  $w_2 = 1.5$  mm,  $l_2 = 9.5$  mm,  $w_3 = 1.5$  mm,  $l_3 = 10.2$  mm,  $w_4 = 5$  mm,  $l_4 = 8.9$  mm,  $w_5 = 3.8$  mm,  $W = 23.8$  mm, and  $L = 45$  mm. It can be observed that a significant size reduction ( $\lambda/7.5$ ) is achieved as compared with typical half-wavelength patch antennas. The radiation efficiency was found to be 20% and the input impedance  $Z_{in_{ANT}} = 1.45 - j22\Omega$  at 867 MHz [8].

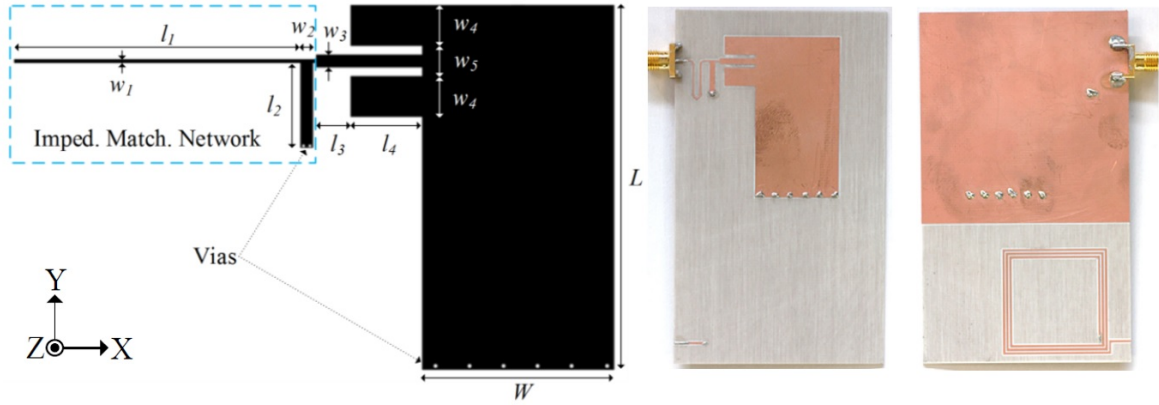


Figure 4.7: Compact HF-UHF antenna design [8].

The return loss  $S_{11}$  of the UHF RFID antenna was measured by means of the E8364B vector network analyzer. As it can be seen in Fig. 4.8 b), a frequency shift of 20 MHz occurred, with a non-significant degradation of the impedance matching. The UHF RFID antenna was scaled a 2% down in order to compensate for the frequency shift.

A link budget was used to measure the RFID antenna radiation patterns of the E-plane (yz-plane) and the H-plane (xz-plane) including co-polar and cross-polar components. The link budget consisted of the above-mentioned vector network analyzer, where the first port was connected to an 83006A amplifier. The output of the amplifier was connected to an ETS-Lindgren 3164-07 horn antenna, which was located inside an anechoic chamber. The antenna prototype under test was also located in the anechoic chamber and connected to the second vector network analyzer port. To measure different angles, an angular sweep was carried out by means of a stepper motor and a controller, and it allowed obtaining the radiation diagram depicted in Fig. 4.8 c). The measured maximum realized gain is  $G = -3.7dB$  (NFC antenna is already explained in section 3).

The electronic components of the RFID reader are placed next to the metal strips of the antenna, not interfering its performance. NFC antenna is also closely connected with the rest of components avoiding interference.

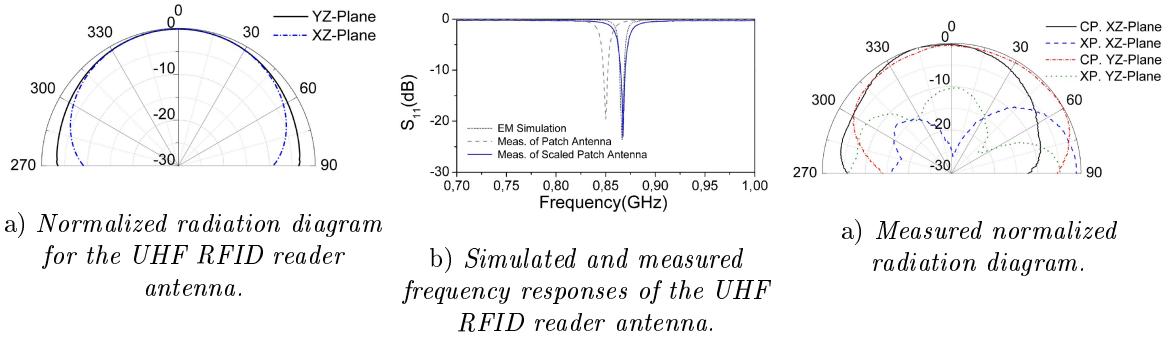


Figure 4.8: Measurements and simulations of the UHF-RFID reader antenna, CP and XP stands for co-polar and crosspolar components respectively. [8].

## 4.5 NFC and WPT circuit design

Operation modes: NFC devices can operate in three different modes based on the ISO/IEC 18092, NFC IP-1 and ISO/IEC 14443 contactless smart card standards.

- **Read / Write:** In this mode, the NFC enabled phone can read or write data to any of the supported tag types in a standard NFC data format.
- **Peer to peer:** In this mode, two NFC-enabled devices can exchange data. For example, you can share Bluetooth or Wi-Fi link set up parameters to initiate a Bluetooth or Wi-Fi link. You can also exchange data such as virtual business cards or digital photos. Peer-to-Peer mode is standardized on the ISO/IEC 18092 standard.
- **Card emulation:** An NFC-enabled phone acts as reader when in contact with tags. In this mode, the phone can act as a tag or contactless card for existing readers.

This section describes the design of the wireless battery charging system composed by elements considered in previous analysis. It consist of a device that uses the electromagnetic field generated by a primary coil in order to induce current to a secondary coil, which is used to charge the battery for our system. Such a way of charging devices, is being already used in some cases such as toothbrush or human body integrated systems under skin, and it is known as inductive charging. But still it is not a well established method, and not yet applied in NFC.

There exists an standard that was created for low power devices (up to 5 W), such as the *Qi* standard, intended to transfer power from a Base Station to a Mobile Device, based on near field magnetic induction between two coils [114]. *Qi* came from the Wireless Power Consortium (WPC) business alliance in 2010. Operating frequency from that system is in the 110 ... 205 kHz range, implementing a simple communication protocol to communicate the two devices.

One of the concerns of WPT is the influence of the electromagnetic fields on the human body. In order to protect against any known kind of health effect, a scientific committee (ICNIRP) [115] has published guidelines (exposure limits) for a maximum exposure. They are based on an extensive number of related scientific publications, and have been reviewed up to today by more than 35 national expert committees. ICNIRP states that: "There is no substantive evidence that adverse health effects, including cancer, can occur in people exposed to levels at or below the ICNIRP limits" The ICNIRP guidelines include basic restrictions for the current density in the body of an exposed human.

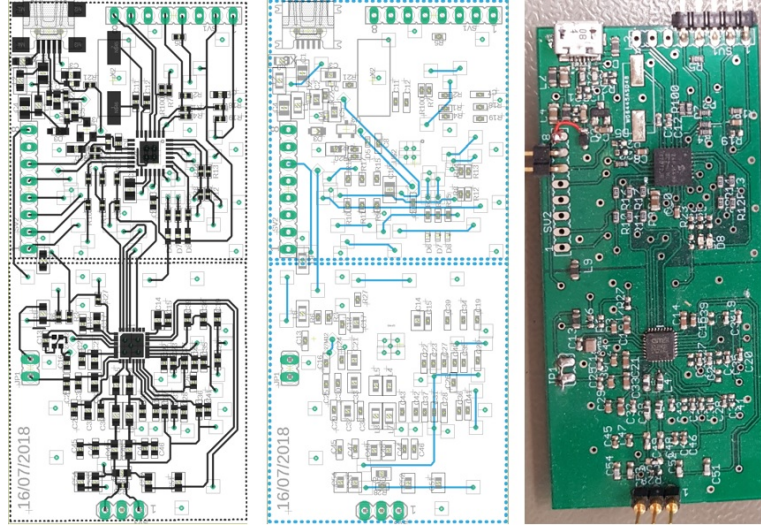


Figure 4.9: Compact NFC circuit layout showing top, bottom layers, and a picture of the PCB board.

As shown in Eq.(3.44), the losses of a wireless power transfer system depends basically of two parameters; the coupling factor  $k$  between the transmitter and receiver coil, and the system quality factor  $Q$ , being the coupling factor depending on the distance between the two coils and their relative size. In addition to optimize these parameters, a good design must comply with very low power consumption. This specification is required by our hand held device, but also applies for any battery powered or energy harvesting device. Some features demanded by our design can be summarized herewith:

- Ultra-low power consumption and high efficiency design.
- The control of charging current even for small magnitudes must be accurate.
- Robust charging method, with the possibility to select between different modes (fast-slow).
- Evaluate the possibility of using different charging frequencies and the use of NFC.

There is no work on the wireless power transfer using NFC, which is our case of interest. The basic wondering would be the liability for this system to transfer information and energy at the same time [116], since such standard is created for data communications and to power-up RFID tags. As it is shown in [117] there exist a clear trade-off between wireless power transfer and communication transfer, showing the need for more work to be done in the optimization between the two processes. Using NFC Personal Area Network (PAN) at 424 kbps, for new applications will be treated here.

Antennas for NFC are electrically small, which implies that for a 1 Mbps broadband NFC link, the required relative bandwidth is over 7%. For a 4 cm NFC antenna, the electrical size is  $ka = 0.011$ , which corresponds to a theoretical lower bound on the quality factor of  $Q_{min} \simeq (ka)^{-3} = 6.8 \times 10^6$ , corresponding to a bandwidth of  $B = 20$  Hz [118]. To increase bandwidth such as required by NFC we need to reduce  $Q$  so to use an antenna with significant resistant loss and low radiation efficiency, which implies high power consumption for the transmitter. Since distance from transmitter and receiver antenna in WPT is very small, the system will operate in strongly coupled regime.

### 4.5.1 Power versus communication trade-off

In a WPT system, the system is designed considering closer proximity for better power coupling, even so, the coils are usually loosely coupled due to the absence of a common magnetic core to confine and guide most of the magnetic flux such as a transformer.

The trade off presented here between using the same circuit for powering or transferring information between devices is the following:

- For proximity wireless communications one has low coupling coefficient ( $k_{low}$ ), and low quality factor ( $Q_{low}$ )
- For WPT one has higher coupling coefficient ( $k_{high}$ ), and higher quality factor ( $Q_{high}$ ).

### 4.5.2 Bandwidth and efficiency tuning circuit

The novelty presented in this work consists on a modification in the matching circuit as in Fig. 4.10, that includes a resistor that reduces the quality factor of the reader inductor, maintaining good matching conditions, accomplishing the conditions of NFC wideband communications. The idea proposed consist of using the same reader for wideband communications and also for power transmission. In this case it is introduced a switchable tuning resistor ( $R_1$  in Fig. 3.10) that will be used to reduce the quality factor of the reader coil for wideband communications, or to increase it for power transfer. The effect of such switchable capability can be seen in the simulation results depicted in Fig. 4.11

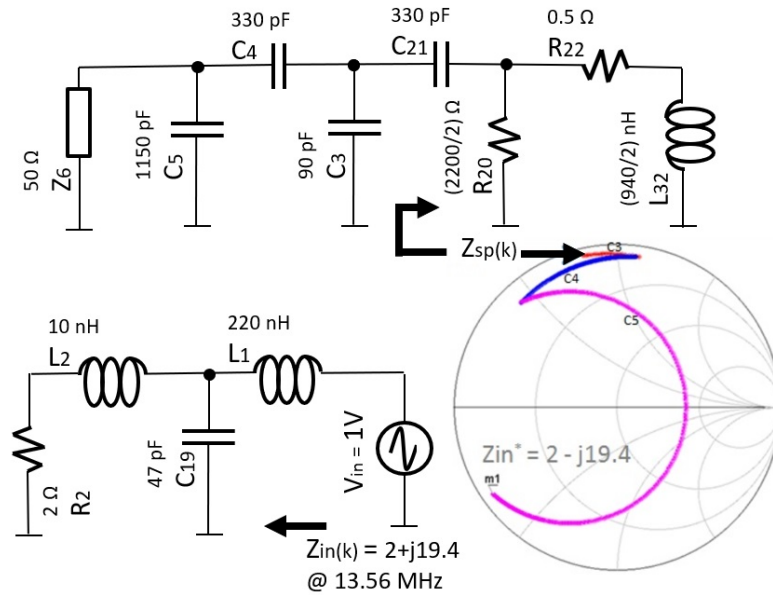


Figure 4.10: Matching network design.

The difficulty on having a good matching network for both cases, results from the fact that the coupling coefficient from both antennas may vary. Not only due to the peculiarity that for WPT the distance between both coils needs to be short to increase the coupling, so the energy transfer efficiency, but also that depending on the distance between reader and tag in a NFC (RFID) system may vary and, so will do the coupling and also the impedance being seeing at the primary antenna coil.

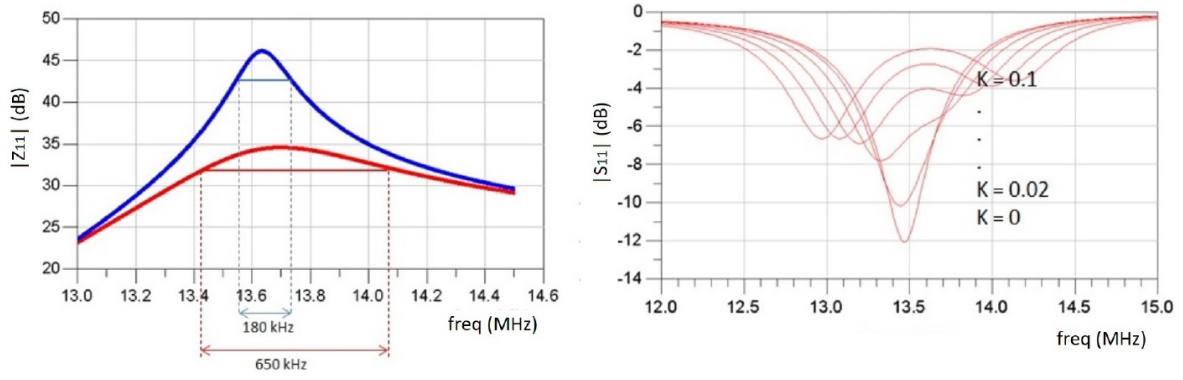


Figure 4.11: Tuning reader antenna quality factor.

At resonance, the imaginary impedance becomes constant, only changing when we move away from resonance. The real part tends to increase by increasing coupling factor as will be deduced next.

Using  $\Re\{Z_r^{pri}(\omega_o)\} = R_r^{pri}$ , as the real part of the impedance seen by the reduced circuit to the primary, the efficiency can be analyzed by using the active components on the equivalent circuit, in our case (Fig. 4.10):

$$\eta^{pri} = \frac{R_r^{pri}(k) [1 - \Gamma^2(k)]}{R_r^{pri}(k) [1 - \Gamma^2(k)] + 2R_{PA}} \quad (4.1)$$

The case of having the system not adapted ( $k \neq k_o$ ), there will be a mismatch that is expressed optimally by the relation:

$$\Gamma(k) = \frac{R_r^{pri}(k) - R_r^{pri}(k_o)}{R_r^{pri}(k) + R_r^{pri}(k_o)} \quad (4.2)$$

which is the reflection coefficient at the primary that will depend on the coupling factor. As can be seen at Fig. 4.11 when varying  $k$ , the resonance peaks will be affected also. The power generated at the receiver (tag or battery from the WPT system), will depend on such matching conditions. In case of WPT the power provided to the battery will become:

$$P_{bat} = \frac{V_L^2}{4R_L} [1 - \Gamma^2(k)] = \frac{V_L^2}{4R_L} \left[ \frac{2R_r^{pri}(k_o)}{R_r^{pri}(k) + R_r^{pri}(k_o)} \right] \quad (4.3)$$

### NFC transformed impedance

In NFC communications, the link between transmitter and receiver is normally achieved by means of using parallel tuning capacitors. The receiver or NFC equivalent impedance for this system can be obtained from (see secondary circuit in Fig. 4.10):

$$Z_{NFC} = R_s + j\omega L_s + \frac{1}{\frac{1}{R_{ic}} + j\omega(C_5 + C_{IC})} \quad (4.4)$$

This impedance being transformed into the primary side of the link (transformer) will become;  $Z_T^{pri} = \frac{(M\omega)^2}{Z_{NFC}}$ , which at the resonance frequency, and taking the real part, will derive in the following expression:

$$\Re\{Z_{NFC}^{pri}(\omega_o)\} = \frac{(M\omega_o)^2(R_{IC} + R_1)}{R_1^2 + (L_s\omega_o)^2} = k^2 \frac{L_1}{L_s} R_{IC} \quad (4.5)$$

when considering  $Q_2 \gg 1$ . It is possible to represent the transformed resistance as a function of the coupling coefficient, expressing  $\Re\{Z_{NFC}^{pri}(\omega_o)\} = R_{NFC_r}$ :

$$R_{NFC_r}(k) = R_1 + k^2 \frac{L_1}{L_s} R_{IC} \quad (4.6)$$

when substituting in expression Eq.(4.2), the reflection coefficient for the NFC system to consider when looking for the circuit efficiency will become:

$$\Gamma_{NFC}(k) = \frac{k^2 - k_0^2}{\frac{2R_2}{R_{IC}} + k^2 + k_0^2} \quad (4.7)$$

#### WPT transformed impedance

In the case of using the reader as a WPT, the receiver part of the charging device is normally designed with series LC circuit. In such a case, the following expression is deduced for the transformed into the primary equivalent impedance:

$$\Re\{R_{WPT_r}(k)\} = \frac{(M\omega)^2}{R_s + R_L} \simeq \frac{k^2 L_1 L_2 \omega_o^2}{R_L} \quad (4.8)$$

when  $R_L \gg R_s$ . In this case one can deduce the transformed resistance part of the impedance as a function of coupling factor as:

$$R_{WPT_r}(k) \simeq R_{WPT_r} + \frac{k^2 L_1 L_2 \omega_o^2}{R_L} \quad (4.9)$$

which when substituting in expression (4.2), the reflection coefficient for the WPT system will become:

$$\Gamma_{WPT}(k) = \frac{k^2 - k_0^2}{\frac{2R_L}{Q_2 Q_{10} R_2} + k^2 + k_0^2} \quad (4.10)$$

where  $Q_{10} = \frac{L_1 \omega_0}{R_1}$ , is the quality factor without any coupling effect from the secondary coil, and  $Q_{11} = \frac{L_1 \omega_0}{R_1 + R_T}$  is the quality factor of the reader with presence of a tag or NFC device.

In all those expressions, there is a dependency on  $k$ , showing the sensitivity to position. For WPT, the position can be much defined by means of mechanical design, but for NFC the position can vary significantly. In Fig. 4.10 one can see how is the input impedance seen at the reader coil, including the matching network depending on  $k$  (distance and misalignment). The matching is done to accomplish the load complex conjugate, that will be coupling  $k$  dependent. The idea is to make the design as robust as possible to coupling variations.

### 4.5.3 Designing the tuning circuit and integration in NFC circuit

One can state that a WPT system is formed by two leakage inductance transformer model tank, and series resonant capacitors, which has a current-source characteristic, so it should be connected to a capacitive filter, having a voltage-source characteristic. In our case a full-bridge rectifier with a capacitive output filter that provides a DC voltage at the output load resistance  $R_L$ .

According to Eq.(4.5) and Eq.(4.8) there is an inverse dependency of primary impedance versus  $R_L$  and  $L_2$ , so in case  $R_L$  increases, the impedance seen by the reader will decrease for the WPT configuration and will increase for NFC. In the case of  $L_2$ , the resistance at the reader trends to increase. Will increase for WPT while for NFC will decrease.

The circuit topology presented in order to compensate for the trade-off is depicted in Fig. 4.12. There is a shunt resistor in parallel with the coil that will be switched ON/OFF accordingly to the functionality. In each case, when the NFC link requires wide bandwidth, it will be of interest to connect the parallel resistor (switch ON), so the quality factor of the antenna is reduced. When transferring power to a remote device for WPT, the resistor will be switched OFF increasing automatically the quality factor to its maximum.

In some applications tuning capacitors are also represented in parallel with the coil inductance in order to tune to the resonance frequency of the RFID system helping in maintaining the resonance frequency versus deviation in the antenna environment, which improves matching stability (Fig. 4.12). This additional feature is justified in NFC since antenna operates in a difficult environment such as smartphone, in close proximity with other devices, and where some parasitic effects due to unknown's for the placement and locations of components within the mobile phone can be relevant.

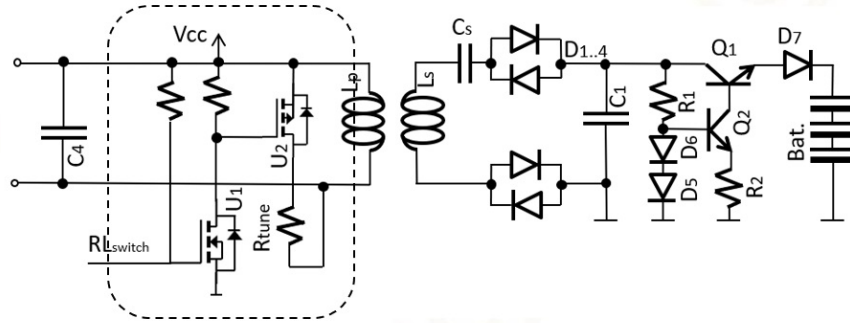


Figure 4.12: Tuning circuit implementation (highlighted) for antenna resonance and quality factor including LPF, Matching Network (MN) and charging circuit.

### Measurement results

A WPT system seen as a series resonant tank has a current-source characteristic, so it should be connected to a capacitive filter having a voltage-source characteristic. In order to use the secondary leaking inductor as charging coil, the adopted solution is to include a full-bridge rectifier, series connected to the leaking inductor by means of a resonance series capacitor, and with a capacitive output filter that provides a DC voltage at the output load resistance  $R_L$ , with filtering functions.

The circuit topology presented in order to compensate for the trade-off is depicted in Fig. 4.12. There is a shunt resistor in parallel with the coil that is switched ON/OFF accordingly to the functionality. In each case, when the NFC link requires wide bandwidth, the parallel resistor is connected (switch ON), so the quality factor of the antenna is reduced. In this case we can communicate with the

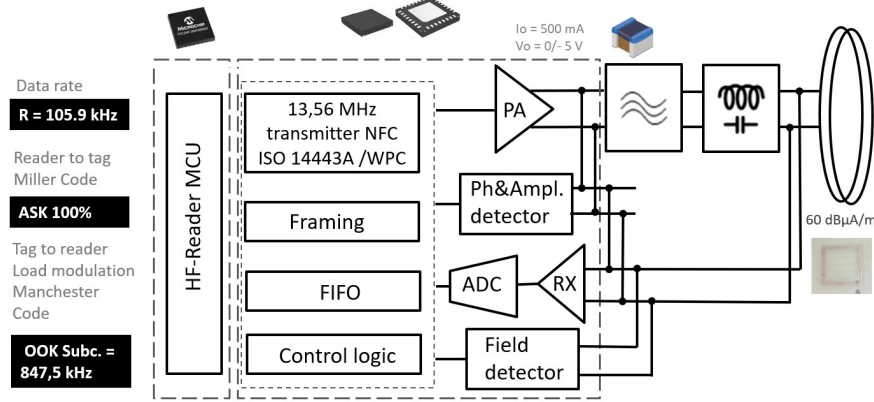


Figure 4.13: HF block diagram including NFC-WPT.

HF tag at high data rates, so one can communicate with other NFC devices at 424 kbps, or can read measurements of a sensor. A sensor that has been programmed as data logger, can provided information data via such NFC communication channel at high speeds.

When transferring power to a remote device for WPT, the resistor will be disconnected, switched OFF, (see Fig. 4.15) increasing automatically the quality factor to its maximum, which reduces the frequency bandwidth, but increases the reactive energy transfer. In this case we can transfer via different secondary coil, power that is stored in the external element, in our case is a Li-Ion battery, but could be another type of battery, capacitor, or ultra-capacitor. This energy will be used for powering the electronics of both HF and UHF sensor electronics part.

In the case presented here, two different coil antennas have been used either for powering transfer and for communications in the HF. Other possibilities would be to combine both features in one coil [119]. As can be seen in the measurement results shown in Fig. 4.15, the current increase when turning OFF the tuning resistor reaches 43 mA, while in the other condition, such current is 34 mA.

The system being tested is using a NFC transmitter that uses the polling tag inventory instruction, in order to detect from the proximity possible tags to be communicated with. Such scan is streaming continuously the information over a carrier in pulses of 130 ms and pause intervals of 75 ms. The receiver uses these pulses in odder to charge the battery, extracting the energy from the HF magnetic field. In order to do so, the bandwidth is switched to narrow band.

The battery charger is applied into 4.2V Li-Io cells. When the cell voltage is lower than 4.2 V, it will be continuously charged by constant current. Once the cell voltage is reached, the cell is being charged at constant voltage until the battery is filled up the full voltage.

Using the resistive impedance from the WPT receiver seeing at the primary Eq.(4.8), the quality factor of a coil and its relation with the bandwidth, one can obtain the following expression that will relate the bandwidth, with load, circuit resistance values, and coupling coefficient:

$$R_r^W(k) = k^2 \left( \frac{f_0}{BW} \right) \omega_0^2 \frac{R_1 R_2}{R_L} \quad (4.11)$$

By extrapolating the results, and combining the interpolation with the relation that the manufacturer of the Li-Ion battery provides, and the charging curves of the cells, it is possible to show the results that would be obtained by time of both, the charging profiles, attending to the current and voltage, and also the power delivered to the load, as a function of load impedance. Such extrapolation results are depicted in Fig. 4.16. The load power curve, is derived from four measurement points, taken using



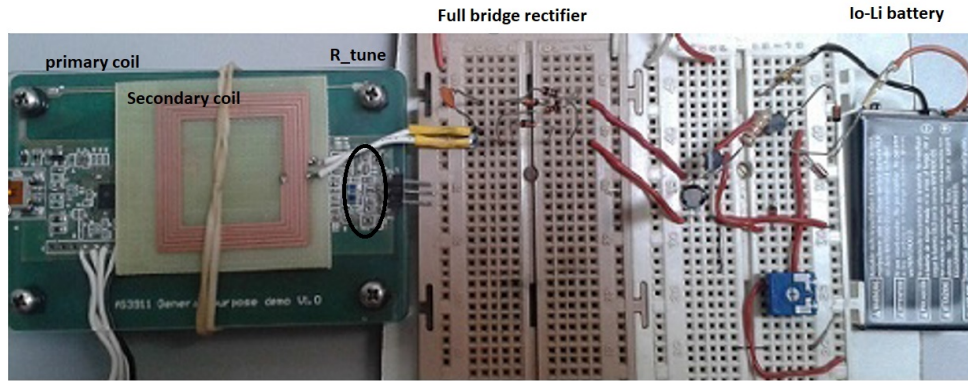


Figure 4.14: Tuning circuit implementation for antenna resonance and quality factor configuration.

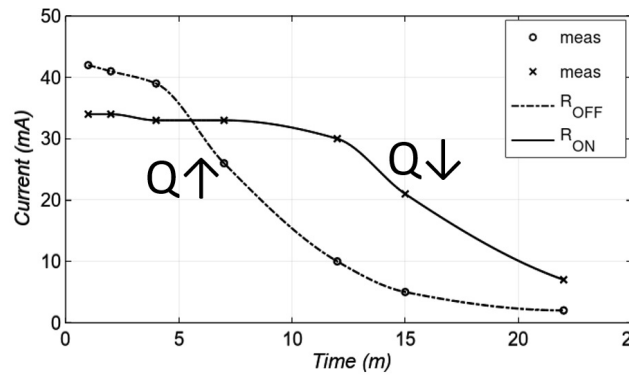


Figure 4.15: Measurement results in case of switching ON/OFF Quality factor  $R_{tune}$ .

the circuit shown in Fig. 4.14, that provides two coils, primary integrated in NFC transmitter PCB, and a second smaller coil located on top of the PCB.

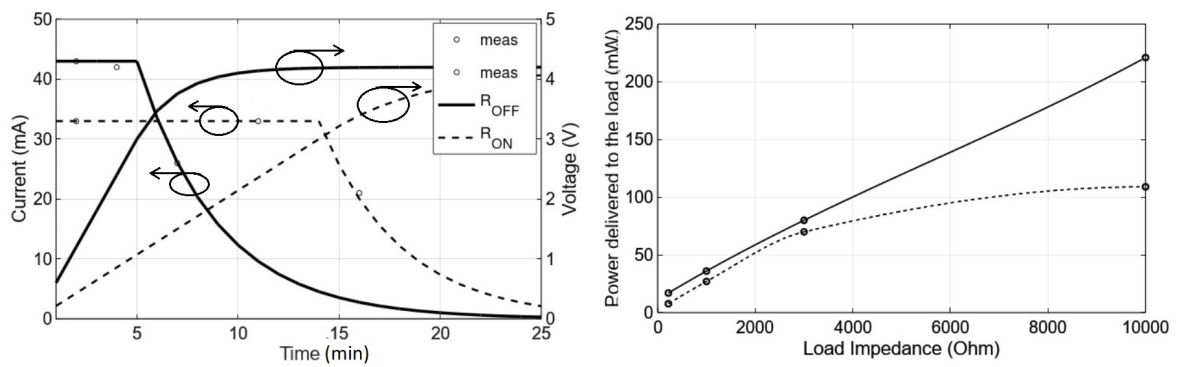


Figure 4.16: Power delivered by the charging device and battery charging response (based on manufacturer and circuit response) with and without optimal design.

## 4.6 Conclusions

An implementation of the tuning circuit for the optimization of both, communications and power transfer link, together with the RFID technology has been implemented. To demonstrate feasibility in a real example, both power transfer for battery charging, with short (NFC) and middle (RFID) range communication, has been implemented using techniques commonly known for low and high frequency electronic design. In addition the UHF-RFID antenna has also been implemented and integrated in a small compact implementation, based on a collaborative work with the research group.

At the end, we show that it is feasible to use the tuning designed circuit to charge a small Li-Ion battery. Such energy transfer, using an already implemented short distance communications channel (NFC), can then be used for different applications, but, at least, it is shown how using state of the art NFC and RFID technologies such topology becomes feasible for some applications.

In the next final chapter, we are going to deep into some real applications and implementations, where the use of the designed topology can be useful for real market applications. A very compact design that can fit in a small hand held portable device is implemented, including all the electronics, baseband and RF circuitry component, and HF-UHF antennas.

This concept presented, opens new means for using the more extended NFC mode of operation that coexist nowadays in all the mobile phones.

## 5 Application in NFC and RFID sensing

### 5.1 NFC and UHF-RFID sensor nodes with WPT

When using WPT feature, we need to program our NFC device for sending continuous carrier (CW) for a period of time, in continuous mode, or in burst (charging time). One way to do that, is by programming the NFC device to send and receive NFC data in the form of NFC Data Exchange Format (NDEF) messages. For that purpose, we need to work on the Android framework APIs that support these features.

Beaming NDEF messages from one device to another is done using Android Beam. The "Android Beam" feature allows a device to push an NDEF message onto another device, by physically tapping the devices together. This interaction, provides an easier way to send data than other wireless technologies like Bluetooth, because with NFC, no manual device discovery or pairing is required. The connection is automatically started when two devices come into range. At this way it is possible to have the NFC device active for long time. This is one way of having active the WPT feature of our NFC-RFID device.

The advantage of NDEF messages, is that, it is a standardized method for a reader to communicate with an NFC device, and contains multiple records with quite a lot of information. The record size can be configured to determine whether it is a short record, one with a payload length less than 256 bytes, or Normal records that can have payload lengths exceeding 255 bytes, with a maximum of  $2^{32} - 1$  bytes = 4 GB, of data. In our test data, using single inventory pulling requests from reader to tag, with bursts of 130ms NFC power packets, and pause intervals of 75 ms (polling tag inventory) can energize storage elements.

Placing the two NFC antennas close together, the energy transferred from primary to secondary is used to charge a battery. For small tags as the ones depicted in Fig. 5.1, we have substituted the Li-Io battery pack by a small button cell battery. The same battery is used by the RFID sensor tag to sense the environment and store the information in an EEPROM. In this way, we can extend the life of the sensor with capabilities of data logging by wirelessly charging its battery.

### 5.2 System energy requirements

#### 5.2.1 Powering the RFID sensor

In the near-field, mutual inductance at HF, both antenna coils act as a loosely (roughly) magnetically coupled transformer, where energy is magnetically induced and propagated from source to destination. Therefore, unlike far-field antennas which are characterized by gain, directivity, and radiation pattern, the coil antennas in near-field are best characterized by the following parameters:

- the coupling coefficient  $k$  between the Reader and the tag coils.

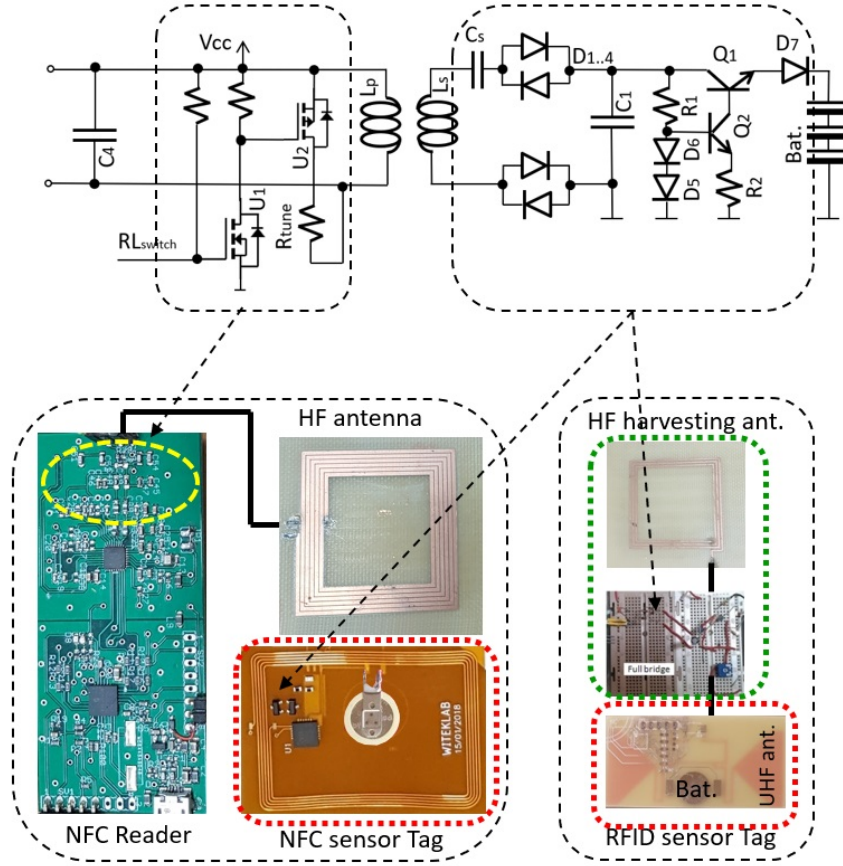


Figure 5.1: Measurements of NFC WPT set-up for RFID and NFC sensor tags.

- $H$ -field at the receiving tag coil.
- inductance  $L$  of the coils.
- unloaded quality ( $Q$ ) factor of the antenna

Conditions for better transferring energy from one coil to another have been analyzed in previous chapters. Some basic conditions are setup on energy demands for RFID sensors, so wireless power transfer is justified.

### 5.2.2 RFID and NFC energy requirements

When dealing with portable RFID reader battery powered, one should estimate the energy required in order to operate with such reader while scanning RFID tags and RFID sensors. For this purpose relevant parameters are defined to analyze such factor.

- $T_m$ : Duration of the measurement (ms)
- $q(m)$ : Average number of reader queires
- $T_{mm}$ : Time between measurements (s)

- $N_m$ : Number of measurements in 1 hour.
- $I_{RD_{tx}}$ : Current consumption of the reader in transmit mode.
- $I_{RD_{sby}}$ : Average current consumption of the reader (mA).
- $I_{MCU}$ : Average micro-controller current consumption (mA).
- $P_{RD}$ : Average power consumption (mW).
- $P_{by}$ : Standby power consumption (mW).
- $E_{rd}$ : Average energy required by the reader (mJ).
- $E_{mcu}$ : Energy required by the microcontroller (mJ).

### Consumption of the sensor

As it is shown in Fig. 4.4, the sensor used corresponds the scheme in the right side, where the RFID is connected to a very low power MCU that takes measurements from external sensor (in our case temperature and humidity sensor), and has its own EEPROM. In case more memory is required, such as de case when having to store more data points as a data logger, an external memory could be also implemented.

The power consumption of the sensor is measured using a circuit made for this purpose as depicted in Fig. 5.2. In particular we use an oscilloscope to view the correct picture of the current consumption in different states of operation. The circuit that converts current to voltage, takes into account the know "burden voltage" problem, the voltage that the internal current shunt resistor drops when the current passes through the circuit. This problem is high for actual electronics that instead of being powered from 5V power supply, for example, are powered to lower supply voltages as 1.2 V and, any voltage drop on shunt resistor affects the measurement. To handle positive and negative power supply, we implement a "virtual ground" that splits the battery supply voltage in half  $\pm 1.5$  V, and is capable of detecting when supply battery voltage from current meter, consisting on 3V lithium coin cell, drops below 2.64V (a RESET is issued).

The output voltage of the circuit, depicted in Fig. 5.2 has output  $mV$  proportional to the  $\mu A$  of current. For very low offset/drift we use the MAX4239 low noise precision amplifier, with almost no offset voltage (0.1 $\mu V$ ). Such operational amplifier has "auto-zero" amplifier, with internal technique to cancel input offset and noise of the amplifier, required to display at the output zero voltage for input zero current. We have implemented three current scales, where the precision limit stays around 300 nA, in the mA range, due to very small shunt resistor ( $R_1$ ):

- For nA range:  $R_2$  (10K $\Omega$ , 0.1%) shunt resistor, with a burden voltage of  $1nA \cdot 10K\Omega = 10 \mu V$ . The scale is 1mV/nA.
- For the  $\mu A$  range:  $R_8$  (10 $\Omega$ , 0.1%) shunt resistor in parallel with  $R_2$ , with a burden voltage of  $1\mu A \cdot 10R = 10 \mu V$ . The scale is 1mV/ $\mu A$ .
- For the mA range:  $R_1$  (10m $\Omega$ , 0.5%) in parallel with  $R_2$ , with a burden voltage of  $1mA \cdot 10m\Omega = 10\mu V$ . The 10m $\Omega$  is a 4 terminal resistor including 2 sense terminals connected across the resistor substrate to eliminate soldering errors. The scale is 1mV/mA.

The use of this current sensing circuit designed for this purpose, allows us to estimate the average current consumption of the sensor tag. A plot of the current measured in the low power consumption RFID tag can be shown in Fig. 5.5. From this analysis we obtain the following consumption:

$$E_{tag} = E_{meas} + E_{wr} + E_{rd} = 2.7\mu A \cdot 3V \cdot 47ms + 1.6\mu A \cdot 3V \cdot 25ms + 1\mu A \cdot 3V \cdot 40ms = 620nJ \quad (5.1)$$

The number of measures in 1 hour is  $N_m$ :

$$N_m = \frac{3600}{T_{mm}} = 12; \quad (5.2)$$

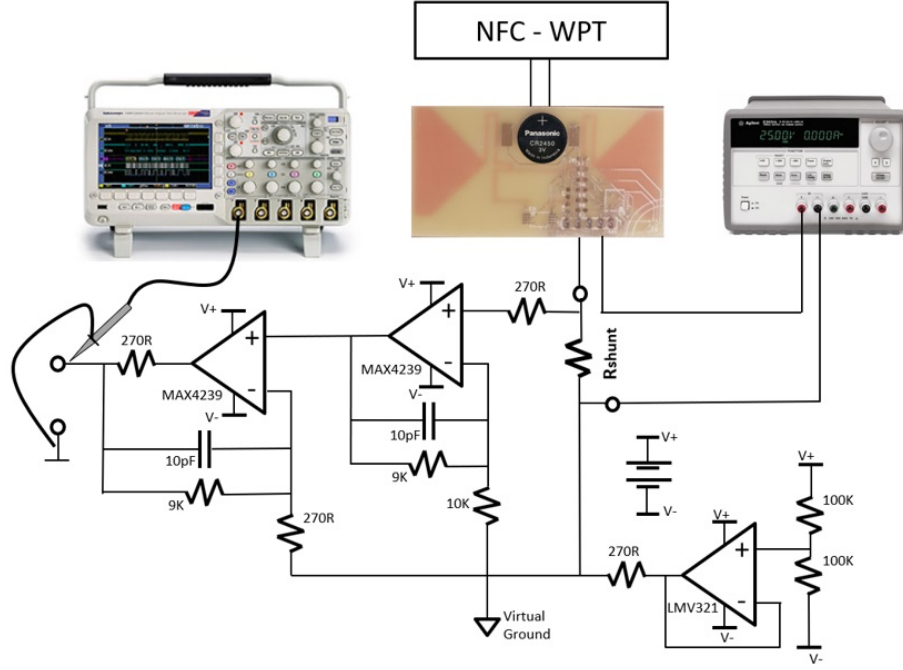


Figure 5.2: Scheme of the measurement circuit for the RFID sensor tag.

### Consumption of the RFID and NFC reader

The NFC reader will be mostly in standby mode, except for transferring data to the mobile phone ( $T_{mb}$ ), or for powering the battery of RFID sensors, sending energy using the NFC coil. This task can be performed few time per day, depending on the power consumption of the sensor, and the application. In our case we have designed a very low power consumption sensor, and the power consumption of the handheld ( $E_{HH}$ ) RFID to NFC system will be:

$$E_{HH} = R_{RD_{tx}} \cdot q(m) \cdot N(m) + E_{RD_{rx}} \cdot H(m) + E_{MCU} \cdot q(m) \cdot [N(m) + 1] \quad (5.3)$$

Table 5.1: CONSUMPTION DATA FOR THE UHF-RFID & NFC READER

$T_m$ (ms)	$T_{mm}$ (min)	$I_{RD_{TX}}$ (mA)	$I_{RD_{SBY}}$ ( $\mu A$ )	$I_{MCU}$ (mA)	$I_{MCU_{SBY}}$ ( $\mu A$ )	$I_{NFC_{TX}}$ mA	$I_{NFC_{SBY}}$ $\mu A$	$V_{ccRF}$ (V)	$V_{ccdig}$ (V)
500	5	180	0.25	0.3	0.6	200	0.7	3	1.8

$$I_{rd} = \frac{I_{tx} T_m}{1000 T_{mm}} = 0.3 \text{ mA} \quad (5.4)$$

The necessary energy by a reader to provide such consumption will become:

$$E_{rd} = P_{rd} \cdot T_{mm} \cdot N_m = I_{rd} \cdot V_{cc} \cdot T_{mm} \cdot N_m = 3240 \text{ mJ} \quad (5.5)$$

The MCU controlling the RF reader part consumes the following:

$$E_{mcu} = I_{mcu} \cdot V_{dd} \cdot T_m \cdot N_m \cdot 1^{-3} = 3.24 \text{ mJ} \quad (5.6)$$

While the reader is not scanning for tags, the power consumption in standby state will correspond to:

$$E_{by} = P_{by} \cdot 3.6 = (I_{by_{mcu}} \cdot V_{dd} + I_{by_{rd}} \cdot V_{cc}) \cdot 3.6 = 6.48 \text{ mJ} \quad (5.7)$$

So the energy required by the NFC reader will become:

$$E_{hf} = \frac{I_{hf} \cdot T_m}{1^3} V_{cc} N_m = 3600 \text{ mJ} \quad (5.8)$$

$$E_{TOT} = E_{by} + E_{mcu} + E_{rd} + E_{hf} = 6850 \text{ mJ}$$

With a total energy required by the reader of 6850 mJ, will correspond to a required battery capacity of 0,63 mAh for a voltage as stated in Table 5.1. So if one has a battery of 220 mAh total capacity, the possible number of working hours for such RFID reader system would be of **347 h**. Depending on RFID sensor type an energy source of capacity between tens of mAh to hundreds may be normal values.

UHF			MCU			NFC			BATERIA			Consum TOTAL UHF+uC			Consum TOTAL		
I_sby (uA) = 1			I_mcu_sby (uA) = 10			I_sby (uA) = 2 (typ. 0,7)			Capacitat de la bateria			# dies			UHF energy		
I_TX (mA) = 180			Actiu I_mcu_on (mA) = 0,3			I_ON (mA) = 200 (typ. 200 mA)			Energia UHF+NFC			UHF energy			NFC energy		
Nm	Energia lectura 1h en 1h	Energia Stby en 1h	Energia MCU ON	Energia MCU stby	Energia NFC Estandby	Energia NFC Estandby	Energia NFC Estandby	Energia NFC Estandby	Capacitat de la bateria	Energia UHF+NFC	Capacitat UHF C. uhf	# hores	# dies		Energia UHF+NFC	Energia NFC	Energia MCU
	(mJ)	(mJ)	(mJ)	(mJ)	(mJ)	(mJ)	(mJ)	(mJ)	(mAh)	(mJ)	(mAh)				(mJ)	(mJ)	(mJ)
12	648	10,8	0,6	64,8	1200,0	36,0	220	1960,2	0,1815	1212	51	658,80	1236	65,43			
8	432	10,8	0,4	64,8	800,0	36,0	220	508,0	0,0470	4677	195	442,80	836	65,22			
6	324	10,8	0,3	64,8	600,0	36,0	220	399,9	0,0370	5941	248	334,80	636	65,11			
4	216	10,8	0,2	64,8	400,0	36,0	220	291,8	0,0270	8142	339	226,80	436	65,01			
2	108	10,8	0,1	64,8	200,0	36,0	220	183,7	0,0170	12934	539	118,80	236	64,90			
1	54	10,8	0,1	64,8	100,0	36,0	220	129,7	0,0120	18326	764	64,80	136	64,85			

Figure 5.3: Considered consumption for the RFID-NFC system

### 5.3 Measurements

We have been using the electronics part developed for the purpose of communicating using NFC device with a mobile phone with NFC, and also to transfer power. Such circuit uses the optimization quality factor feature described above to obtain the maximum power transfer between sensor and activation device. On the other hand we use the RFID-UHF reader to read measurements from the sensor.



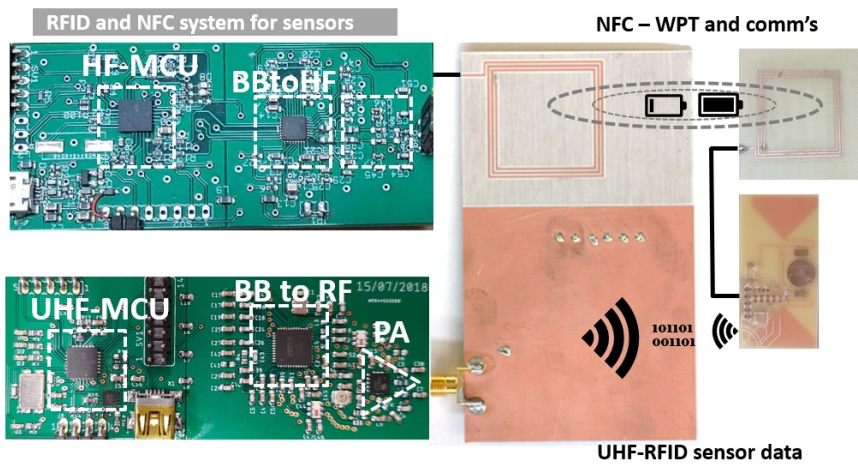


Figure 5.4: Block diagram of the UHF-RFID radio IC, AS3993.

The measurements shown here, depict the current consumption of the wireless sensor, which takes measurements of ambient temperature and humidity, and stores it into the local memory. The sensor is in sleep mode almost all the time, in this time current consumption is in the order of few nano Amperes, which appears in the lower scale of the oscilloscope trace. When local watch dock timer (WDT) wakes the MCU, it starts with the process of measuring, sending the measurement onto the RFID tag so it is available by the UHF-RFID reader, writes it as well into the local memory EEPROM and goes back to sleep.

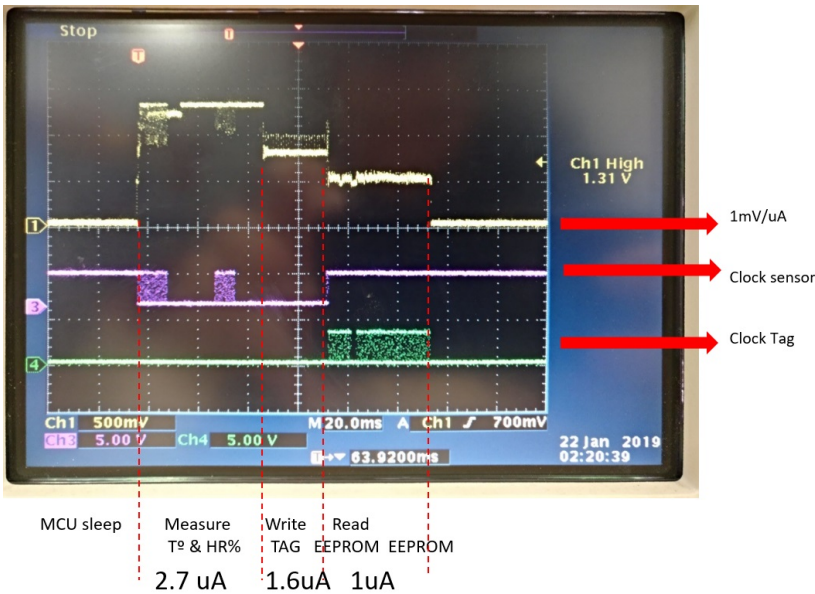


Figure 5.5: Capture of the screenshot of the output current of sensor tag, using the current to voltage converter of Fig. 5.2.

The information stored in the RFID-IC from the sensor, is retrieved every once and a while by the RFID-UHF reader. When this is done, the process is finalized until a new set of measurements is being one by the sensors.



The Fig. 5.6 makes a complete balance budget for the consumption of the system, demonstrating its viability. It will last depending on the number of reading being performed per day as it is shown in the same figure. And of course the battery storage element, will need to be dimension according to such readings requirements made by the system definition.

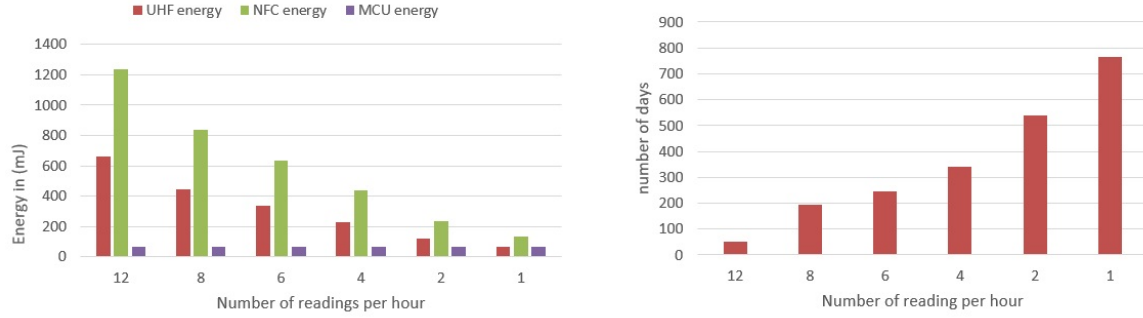


Figure 5.6: Balance of energy consumption per system components, and estimated durability of the system based on system specifications.

## 5.4 Conclusions

This chapter of the thesis, is a justification, using a practical real example, on how the new techniques developed in this work can be applied in reality. Wireless sensors are an important part of the society, where many things need to be monitored, and the IoT needs to be everywhere. In this sense, we have justified this work in a specific set of applications, where monitoring can be implemented even when having difficult access to the sensor,

Using very low power consumption techniques, and optimizing dimension of local storage components, we demonstrate how a sensor, can be charged using a mobile phone from close distance, and have a long durability. During this time the sensor will be able to perform some measurements, in this case from ambient temperature and humidity, store them in local memory according to certain programming timing, and be accessible from a longer distance by a reader. In this case we use UHF-RFID which can reach meter distance readings.

We believe such technique is very practical, and use a different combinations of wireless close proximity devices in order to monitor parameters by the use of minimum power consumption devices. It makes a difference when thinking of having to integrate big batteries in IoT devices (such as AAA or AA or other), if instead, we can apply a rechargeable system in NFC. charging simple small bottom cell batteries, that makes the sensor smaller, lowers the cost, and pollutes less the environment when considered for sensor volumes.

## 6 Conclusions

During the time this work has been done, there has been many ideas that from one starting point looked straight forward or simple in comprehension and implementation, but have become interesting new points of research to investigate. They derive into new concepts, some quite accessible in terms of this thesis, but others for future works, so new horizons have come up.

It has been clear that at this time, people is so much engaged with the use of mobile phones, that has become a normal and useful tool that is carried by everyone. Additionally, some technologies such as IoT are booming, so the work performed in this thesis that concentrates in both topics can be considered of much interest and up to date.

The idea behind the work is to be able to use the smart phone with a new feature that has not been yet integrated by phone manufacturers, probably because the main public is not a vast user of IoT technologies. So, what we have conceived here is a gadget that can convert the smart phone or mobile phone into a device capable of accessing RFID tag at UHF frequencies, and integrate NFC-WPT.

At the beginning the idea was to communicate with passive RFID tags, but due to the increase companies providing RFID tags with sensor, has add some features such as being able not only to access and read passive tags, but also for semi-passive tags, adding the rechargeable function, and additionally to recharge them. So our device has been adapted for such purpose as well.

We have found a way to develop a small form factor RFID and NFC reader in a thin and small size device. Studying the reading range, and the possible interference, has provide us with useful information to choose elements that make the device to become robust in front of such interference. To the knowledge of the author, this is one of the studies that includes more parameters and analysis of radio performance and interference that provide useful information in terms of main functionality, such as reading range.

Some concepts have been theorized, because some extra knowledge was required from other fields, mainly software development, that would have taken to much time to prove, but at least the devices allow to implement some of the ideas conceptualized in this work, such as providing robustness against some interference using RSSI information as it is available now.

Other concepts have been implemented, such as the quality factor tuning device that, as it has been proved, it would allow in a simple manner to develop using the same circuitry a NFC communication device and also capable of charging small batteries. In this regards, some further development could be interesting to follow, such as the implementation of a boost (or step up) converter, to allow charge storage elements at higher voltages. Even combine with a buck (or step down) converter to deliver lower voltages that the ones present in the sencondary circuit when coupling is too high or to much energization is present, and we may use a lower voltage constant value to supply other loads.

The device is integrated in small size, with integrated antennas, communicating with mobile phone via NFC and with RFID passive or semi-passive tags in an efficient manner. Also, it is able to charge some NFC or RFID tags that could not be accessible by the user (here new applications will arise). So, the main purpose of the thesis has been achieved. With this results, new ideas have arise, where

there is the real possibility to implement a new set of devices for the sensor area, using very small powered battery devices, and RF energy harvesting techniques with.

The final implementation of the NFC-WPT and UHF-RFID circuitry, has been achieved using techniques of low power consumption with off the shelf components, small integrable antennas and and small form factory batteries. Such restrictions have been adopted from the beginning because the idea is the be able to integrate all such features, in a hand hekp portable device.

# A ANNEX: Commercial RFID tag performance

In this chapter several RFIC used in passive tags as well as the complete tag are listed. Each tag has been designed with te corresponding antenna to optimize some performances. Sizes are constrained normally to applications, and different antenna concepts to surrounding object, such as metal, wood, water. Some of them are listed from Alien technologies and other as [26, 54].










Tag antenna	Type Ref.	Tag antenna	Type Ref.	Tag antenna	Type Ref.
	ALN9654		AD-110		AD-171
	AD-180		AD-227		AD-233
	AD-318		AD-382		AD-550

Table A.1: List of type of UHF Tags.

## B ANNEX: Magnetic field in coil structures

In the context of loop antennas, one can address the analytic problem from the prospective of antennas or magnetic circuits. Since in the literature it has been seen that depending on the authors different approaches are used, here it is proposed to present both for a deeper and better understanding.

For small loop antennas (dual of the infinitesimal dipole), the analysis of the fields radiated by the loop is performed in the same way as for the linear dipole basic antenna, using the potential function  $\mathbf{A}$  given at any distance  $R$  from any point of the loop antenna with current distribution of  $I$ , considered as constant  $I_0$ , is given by [120]:

$$\mathbf{A} = \frac{\mu}{4\pi} \oint_C \mathbf{I} \frac{e^{-jkR}}{R} \cdot d\mathbf{l} \quad (\text{B.1})$$

The potential vector  $\mathbf{A}$  is useful in solving electromagnetic problems to find fields generated by a given electric current, and is justified by the fact that since the magnetic flux  $\mathbf{B}$  is always sinusoidal; that is,  $\nabla \cdot \mathbf{B} = 0$ , then it can be represented by the curl of another vector because:  $\nabla \cdot \nabla \times \mathbf{A} = 0$ , where  $\mathbf{A}$  is an arbitrary vector. Thus one can define:

$$\mathbf{B} = \mu \mathbf{H} = \nabla \times \mathbf{A} \quad \rightarrow \quad \mathbf{H} = \frac{1}{\mu} \nabla \times \mathbf{A} \quad (\text{B.2})$$

The integration of B.1, for very thin circular loop of any radius is being treated in detail in [120], and the final expressions are presented bellow:

$$H_r = j \frac{kR_1^2 I_0 \cos(\theta)}{2r^2} \left[ 1 + \frac{1}{jkr} \right] e^{-jkr} \quad (\text{B.3})$$

$$H_\theta = - \frac{(kR_1)^2 I_0 \sin(\theta)}{4r} \left[ 1 + \frac{1}{jkr} - \frac{1}{(kr)^2} \right] e^{-jkr} \quad (\text{B.4})$$

$$H_\phi = 0 \quad (\text{B.5})$$

$$E_r = E_\theta = 0 \quad (\text{B.6})$$

$$E_{phi} = \eta_0 \frac{(kR_1)^4 I_0 \sin \theta}{4r} \left[ 1 + \frac{1}{jkr} \right] e^{-jkr} \quad (\text{B.7})$$

where

- $I_0$  is the loop current
- $r$  is the distance from the center of the loop
- $k$  is the wave number
- $\eta_0$  is the intrinsic impedance of the air
- $R_1$  is the radius of the loop.

The total radiated power over a closed spherical area follows the following expression:

$$P = \int \frac{1}{2} (\mathbf{E} \times \mathbf{H}^*) dS = \eta_0 \frac{\pi}{12} (kR_1)^4 |I_0|^2 \left[ 1 + j \frac{1}{(kr)^3} \right] \hat{\mathbf{r}} \quad (\text{B.8})$$

For near field zone ( $kr \ll 1$ ) the second imaginary term is dominant, so the radiated power is reactive and inductive, while for far field zone ( $kr \gg 1$ ) the real term is dominant.

Which are reduced to the following expressions for the case of application of near field ( $kr \ll 1$ ) which corresponds to the case of RFID:

$$H_r \simeq \frac{R_1^2 I_0 e^{-jkr}}{2r^3} \cos(\theta) \quad (\text{B.9})$$

$$H_\theta \simeq \frac{R_1^2 I_0 e^{-jkr}}{4r^3} \sin(\theta) \quad (\text{B.10})$$

Based on the previous results, it is direct to obtain the expression for the magnetic field produced by a circular loop antenna of radius  $R_1$  at any point of the axis of the antenna, which is given by:

$$B_z = \frac{\mu_0 I_0 N R_1^2}{2(R_1^2 + r^2)^{3/2}}; \quad \text{for } r^2 \gg R_1^2, \quad B_z = \frac{\mu_0 I_0 N R_1^2}{2} \left( \frac{1}{r^3} \right) \quad (\text{B.11})$$

where

- $\mu_0$  is the permeability of free space and given as:  $4\pi 10^{-7} \text{Vs/Am}$ .

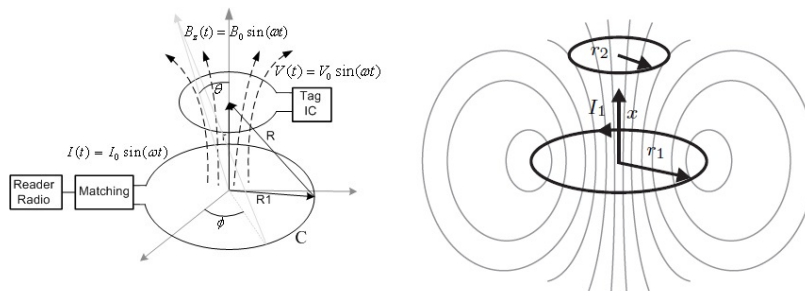


Figure B.1: Coupling between two coils

When placing another coil in the influence of a tie varying magnetic field  $B$ , Faraday's law states that through the surface bounded by a closed path (with surface  $S$ ), induces a voltage around the loop

(electromotive force) proportional to the rate change of the magnetic flux  $\Psi$  and the number of turn  $N$ :

$$V = -N \frac{d\Psi}{dt} \quad \text{where} \quad \Psi = \int B \cdot dS \quad (\text{B.12})$$

Lenz's law emphasizes that the direction of current flow in the circuit is such that the induced magnetic field produced by the induced current will oppose the original magnetic field. By substituting in the previous equations we can find an expression of the voltage generated in the induced coil depending on current flowing and geometrical parameters.

$$\begin{aligned} V &= -N_2 \frac{d\Psi_{21}}{dt} = -N_2 \frac{d}{dt} \left( \int B \cdot dS \right) = -N_2 \frac{d}{dt} \left[ \int \frac{\mu_0 i_1 N_1 a^2}{2(a^2 + r^2)^{(3/2)}} \cdot dS \right] \\ &= - \left[ \frac{\mu_0 N_1 N_2 a^2 (\pi b^2)}{2(a^2 + r^2)^{(3/2)}} \right] \frac{di_1}{dt} = -M \frac{di_1}{dt} \end{aligned} \quad (\text{B.13})$$

where the last term indicates the mutual coupling between the two coils, which is a dependent on coil geometry such as the total number of turns of each of the coils and the spacing between them.

$$M = \left[ \frac{\mu_0 \pi N_1 N_2 (ab)^2}{2(a^2 + r^2)^{(3/2)}} \right] \quad (\text{B.14})$$

When the coils are used for sending information or energy between them, a good particularity is being tuned at the same frequency to maximize mutual coupling. The voltage induced in the tuned coil with quality factor  $Q$  can be obtained from:

$$u_0(t) = - \frac{d\Phi(t)}{dt} \quad (\text{B.15})$$

the phase shift ( $90^\circ$ ) of the carrier is not relevant, but the angle orientation between the two coils ( $\alpha$ ) is interesting to be considered, then the root mean square value (RMS) is given by:

$$V_0 = \Phi \cdot \cos(\alpha) \cdot \omega = B \cdot \cos(\alpha) \cdot A_{tot} \omega = (\mu_0 H)(NA)Q2\pi f \cdot \cos(\alpha) \quad (\text{B.16})$$

The quality factor  $Q$  is one of the most important parameters in resonant circuits, that is introduced in the voltage equation since it is considered the resonance frequency  $f_{res}$  is equal to carrier frequency  $f_{car}$  in our case just  $f$ .

## C ANNEX: Losses in a HF-coupled loop-based system

In analyzing the losses for the coil coupled circuit depicted in Fig.C, we can define a **Loss Factor** (LF) that will be the sum of the transmit coil circuit loss factor and the receive coil circuit loss factor. All of them can be obtained from the equivalent circuit reduced to one side of the transforming equivalent circuit, for example it can be transformed to the to the receiving circuit for calculation simplification.

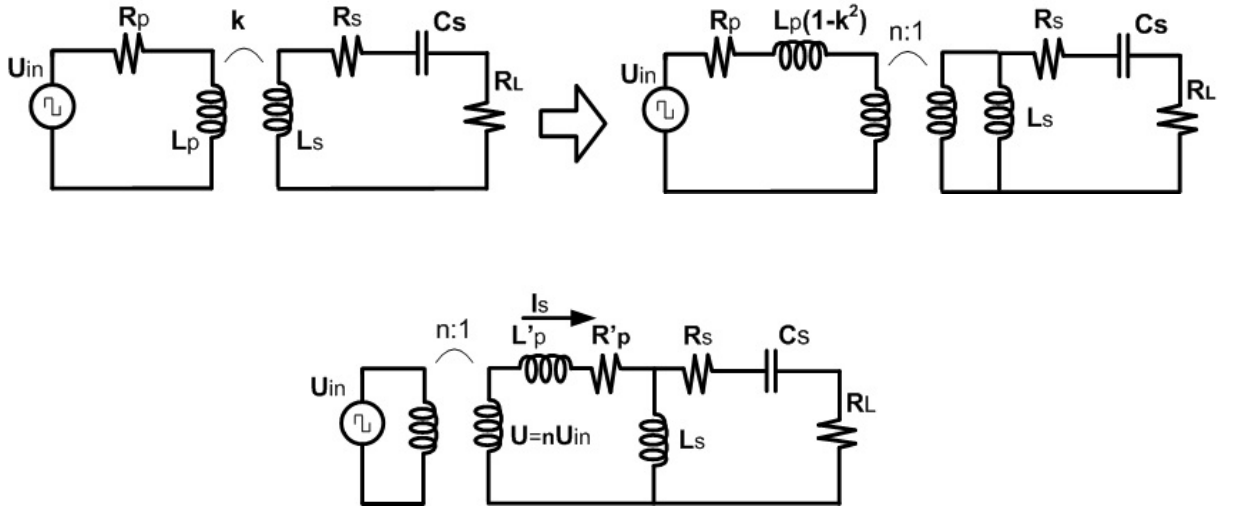


Figure C.1: Equivalent circuit of the coupling between transmitter and receiving coil reduced to the secondary coil.

The following table C.1 uses some basic definitions from parameters extracted from the equivalent circuit and some that will be used for simplification purposes of the expressions.

Table C.1: EQUIVALENT CIRCUIT PARAMETER DEFINITION

Matching Factor ( $\gamma$ )	Tx. Quality factor ( $Q_p$ )	Rx. Quality factor ( $Q_s$ )	System $Q$	Quality factor ratio $q$	$R'_p$	$L'_p$	Transf. ratio $n$
$\frac{R_L}{\omega L_s}$	$\frac{\omega L_p}{R_p}$	$\frac{\omega L_s}{R_s}$	$\sqrt{Q_p Q_s}$	$\sqrt{\frac{Q_s}{Q_p}}$	$R_p n^2$	$L_p n^2 (1 - k^2)$	$\sqrt{\frac{L_s}{k^2 L_p}}$



Starting from the receiving coil, the loss factor can be expressed as the relation between the power dissipated in the receiving coil resistance and the power dissipated at the receiver output:

$$LF_s = \frac{P_s}{P_{out}} = \frac{R_s}{R_L} \quad (C.1)$$

To derive the loss factor in the transmitter, let's start by looking at the power being dissipated in the transmit coil:

$$LF_p = \frac{P_p}{P_{out}} \quad (C.2)$$

Let's start with the transmit power expression:

$$\begin{aligned} P_p &= \left| \frac{V_m}{jX_{Ls}} + \frac{V_m}{R_s + R_L + jX_{Cs}} \right|^2 R'_p = V_m^2 R'_p \left| \frac{-j}{X_{Ls}} + \frac{(R_s + R_L) - jX_{Cs}}{(R_s + R_L)^2 + X_{Cs}^2} \right|^2 = \\ &= \frac{V_m^2 R'_p}{X_{Ls}^2 [(R_s + R_L)^2 + X_{Cs}^2]^2} \left| (-j) [(R_s + R_L)^2 + X_{Cs}^2] + X_{Ls} [(R_s + R_L) - jX_{Cs}] \right|^2 = \\ &= \frac{V_m^2 R'_p}{X_{Ls}^2 [(R_s + R_L)^2 + X_{Cs}^2]^2} \left\{ X_{Ls}^2 (R_s + R_L)^2 + [(R_s + R_L)^2 + X_{Cs}^2 - X_{Cs} X_{Ls}]^2 \right\} \end{aligned} \quad (C.3)$$

The output power, will depend on the load resistance  $R_L$ , and will become:

$$P_{out} = \left| \frac{V_m}{R_s + R_L + jX_{Cs}} \right|^2 R_L = \frac{V_m^2 R_L}{(R_s + R_L)^2 + X_{Cs}^2} \quad (C.4)$$

Taking the previous two expressions the loss factor for the transmitter part will be:

$$\begin{aligned} LF_p &= \frac{R'_p}{R_L} \frac{\left\{ X_{Ls}^2 (R_s + R_L)^2 + [(R_s + R_L)^2 + X_{Cs}^2 - X_{Cs} X_{Ls}]^2 \right\} [(R_s + R_L)^2 + X_{Cs}^2]}{X_{Ls}^2 [(R_s + R_L)^2 + X_{Cs}^2]^2} = \\ &= \frac{R'_p}{R_L} \left[ \frac{(R_s + R_L)^2}{(R_s + R_L)^2 + X_{Cs}^2} + \frac{[(R_s + R_L)^2 + X_{Cs}^2]^2 - 2[(R_s + R_L)^2 + X_{Cs}^2] X_{Cs} X_{Ls} + X_{Cs}^2 X_{Ls}^2}{X_{Ls}^2 [(R_s + R_L)^2 + X_{Cs}^2]} \right] = \\ &= \frac{R'_p}{R_L} \left[ \frac{(R_s + R_L)^2 + X_{Cs}^2}{X_{Ls}^2} - \frac{2X_{Cs}}{X_{Ls}} \right] = \frac{R'_p}{R_L} \left[ \frac{(R_s + R_L)^2}{X_{Ls}^2} + \frac{(X_{Ls} - X_{Cs})^2}{X_{Ls}^2} \right] \end{aligned} \quad (C.5)$$

at this point, it is interesting to reduce the previous expressions using the parameter definition in C.1 so one can obtain a similar expression as derived from [121]. Before that it will be assumed the ideal case of minimum losses ( $\frac{\delta LF}{\delta \omega_{res}}$ ), so in the case of  $X_{Ls} = X_{Cs}$ .

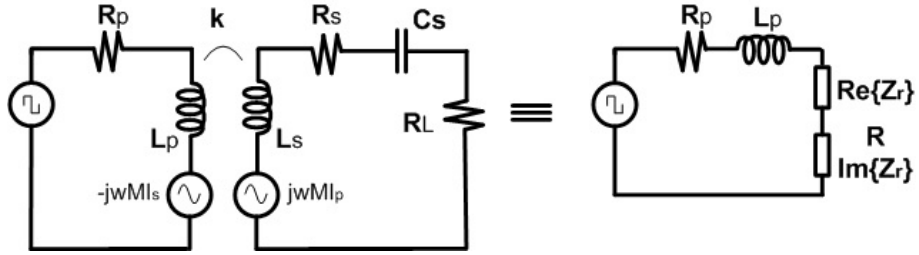
$$\begin{aligned} LF_p &= \frac{R'_p}{R_L} \left( \frac{R_s + R_L}{X_{Ls}} \right)^2 = \frac{X_{Ls}}{Q_p \cdot k^2} \frac{1}{\gamma \cdot X_{Ls}} \left( \frac{\frac{X_{Ls}}{Q_s} + \gamma X_{Ls}}{X_{Ls}} \right)^2 = \frac{q}{Q k^2 \gamma} \left( \frac{1}{qQ} + \gamma \right)^2 = \\ &= \frac{q\gamma}{Q k^2} \left( \frac{1}{q\gamma Q} + 1 \right)^2 = \frac{q\gamma}{Q k^2} \left[ \frac{1}{\sqrt{q\gamma Q}} \left( \frac{1}{\sqrt{q\gamma Q}} + \sqrt{q\gamma Q} \right) \right]^2 = \frac{1}{(Qk)^2} \left( \frac{1}{\sqrt{q\gamma Q}} + \sqrt{q\gamma Q} \right)^2 \end{aligned} \quad (C.6)$$

The total loss factor will be obtained by adding the previous two expressions.

$$LF = LF_s + LF_p = \frac{1}{qQ\gamma} + \frac{1}{(Qk)^2} \left( \frac{1}{\sqrt{q\gamma Q}} + \sqrt{q\gamma Q} \right)^2 \quad (\text{C.7})$$

#### *Efficiency based on induced voltages equivalent circuit*

Another possibility that is solved, is the use of circuit c) from Fig.C. In this case it is used the primary and secondary antenna coils with their losses associated to resolve the power efficiency. The total efficiency is presented in 3.47 and deduced herewith:



$$Z_s = j\omega L_s + \frac{1}{j\omega L_s} + R_L + R_s \quad (\text{C.8})$$

The reflected impedance from the secondary to the primary is obtained from this equivalent circuit:

$$Z_s = \frac{(M\omega)^2}{Z_s} = \frac{(M\omega)^2}{R_s + R_L + j(j\omega L - \frac{1}{C_s\omega})} = \frac{(M\omega)^2 \left[ R_s + R_L - j(L_s\omega - \frac{1}{C_s\omega}) \right]}{(R_s + R_L)^2 + (L_s\omega - \frac{1}{C_s\omega})^2} \quad (\text{C.9})$$

The efficiency in transferring power from the primary winding antenna to the secondary winding antenna can be expressed as:

$$\eta = \eta_p \cdot \eta_s; \quad \eta_p = \frac{\Re\{Z_r\}}{\Im\{Z_r\} + R_p}; \quad \eta_s = \frac{R_L}{R_L + R_s} \quad (\text{C.10})$$

$$\eta_p = \frac{(M\omega)^2(R_s + R_L)}{(M\omega)^2(R_s + R_L) + R_p(R_s + R_L)^2 + R_p(L_s\omega - \frac{1}{C_s\omega})^2} \quad (\text{C.11})$$

$$\eta_T = \eta_p \cdot \eta_s = \frac{(M\omega)^2 R_L}{(M\omega)^2(R_s + R_L) + R_p(R_s + R_L)^2 + R_p(L_s\omega - \frac{1}{C_s\omega})^2} \quad (\text{C.12})$$

## D ANNEX: Probability Distribution functions

In general if the real and imaginary part of a PM signal is corrupted by Gaussian noise, then the statistics of the signal will follow Rician distribution. The difference from the case of Rayleigh distribution is:

### ***Rayleigh Distribution***

Considering a noise process  $n(t) = r(t)e^{j\Phi(t)} = x(t) + jy(t)$ , where  $r(t)$  is the magnitude or envelope and  $\Phi(t)$  the phase,  $x(t)$  is the in-phase, and  $y(t)$  is the quadrature component. If both random processes  $x(t)$  and  $y(t)$  are statistically independent Gaussian distributed, with the same variance and zero mean, then their joint probability density function is:

$$P(x, y) = P(x)P(y) = \frac{1}{2\pi\sigma^2} e^{-\frac{x^2+y^2}{2\sigma^2}} \quad (\text{D.1})$$

Transforming differential areas by using  $dx dy = r dr d\Phi$ , gives the joint probability density function of  $r(t)$  and  $\Phi(t)$  as;

$$P(r) = \int_{-\pi}^{\pi} \frac{r}{2\pi\sigma^2} e^{-\frac{r^2}{2\sigma^2}} d\Phi = \boxed{\frac{r}{\sigma^2} e^{-\frac{r^2}{2\sigma^2}}} \quad \text{Rayleigh distribution} \quad (\text{D.2})$$

$$P(\Phi) = \int_0^{\infty} \frac{r}{2\pi\sigma^2} e^{-\frac{r^2}{2\sigma^2}} dr = \boxed{\frac{1}{2\pi}} \quad \text{Uniform distribution} \quad (\text{D.3})$$

with the random variables  $t$  and  $\Phi$  that are statistically independent,  $P(r, \Phi) = P(r)P(\Phi)$ .

### ***Rice Distribution***

Considering a noise process  $n(t) = r(t)e^{j\Phi(t)} = x(t) + jy(t)$  where  $r(t)$  is the magnitude or envelope and  $\Phi(t)$  the phase,  $x(t)$  is the in-phase, and  $y(t)$  is the quadrature component ( $X$  is from  $N(\mu_x, \sigma^2)$  and  $Y$  is from  $N(\mu_y, \sigma^2)$ ). If both processes are statistically independent Gaussian distributed with the same variance  $\sigma^2$  and means  $\mu_x$  and  $\mu_y$ , then the probability density function of  $r$  is the Rician probability density function given by;

$$p(r) = \frac{r}{\sigma^2} e^{-\frac{r^2+m^2}{2\sigma^2}} I_0\left(\frac{rm}{\sigma^2}\right) \quad (\text{D.4})$$

where  $m^2 = \mu_x^2 + \mu_y^2$  and  $I_0$  is the modified 0-th order Bessel function of the first kind given by:

$$I_0(x) \equiv \frac{1}{\pi} \int_0^\pi e^{x \cos \theta} d\theta \quad (\text{D.5})$$

While Rayleigh and Nakagami distributions are used to model dense scatters, the Rician models fading with a stronger LoS component. A parameter to describe such scattering is the  $K$  value, that defines the importance of the LoS component between transmitter and receiver, defined as:

$$K = \frac{\text{LoS component}}{\text{Difuse power}} = \frac{m^2}{2\sigma^2} \quad (\text{D.6})$$

The value of the Rician  $K$  factor is a measure of the severity of fading, with  $K=0$  ( $-\infty$  dB) being the most severe fading case (Rayleigh fading), and  $K = \infty$  representing no fading (for  $K \gg 1$ , tends to Gaussian distribution).

## E ANNEX: DC induced voltage

A coil structure is sensible to the magnetic field that crosses the loop, inducing a voltage at its terminals that will depend on the uniform sinusoidal external magnetic field crossing the loop. In our design case, with rectangular geometries, it is convenient such geometry because on one hand produces greater volume of nearly uniform magnetic field than a circular Helmholtz coil of comparable dimensions [122], the expressions for the three spatial components of the flux density are in close form.

In order to come with the expressions of magnetic flux density, it is considered static and time varying fields that are quasi-static [123], so one can solve the static field problem first and, with negligible error, introduce the time dependence as multiplicative factor.

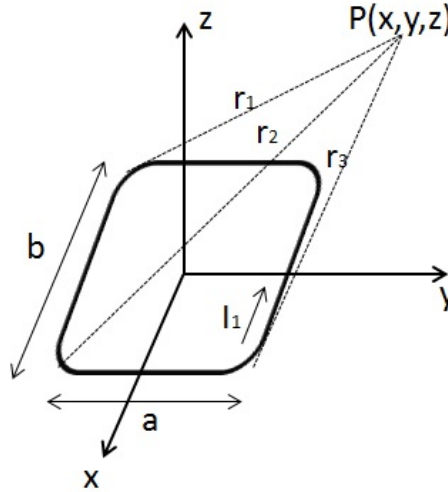


Figure E.1: Geometry for a single rectangular loop of wire in the x -y plane.

The (x,y,z) components for the magnetic flux density at the point of space P(x,y,z) will be obtained by deriving the vector potential (**A**) [123], multiplied by the number of turns N. In the case of having an alternating current  $I_o$  circulating at the rectangular loop of antenna of area  $a \times b$ , it will be;

$$B_x = \frac{\mu_o I_1}{4\pi} \sum_{i=1}^4 \left[ \frac{(-1)^{i+1} z}{r_i(r_i + d_i)} \right]; \quad B_y = \frac{\mu_o I_1}{4\pi} \sum_{i=1}^4 \left[ \frac{(-1)^{i+1} z}{r_i(r_i + d_i)} \right] \quad (\text{E.1})$$

$$B_z = \frac{\mu_o I_1}{4\pi} \sum_{i=1}^4 \left[ \frac{(-1)^i d_i}{r_i[r_i + (-1)^{i+1} C_i]} - \frac{C_i}{r_i(r_i + d_i)} \right] \quad (\text{E.2})$$

where  $I$  is the current in the loop, the parameters  $r_i$  are the distances from the corners of the loop to the point  $P(x,y,z)$

$$\begin{aligned} r_1 &= \sqrt{(a_1 + x)^2 + (y + b_1)^2 + z^2}; & r_2 &= \sqrt{(a_1 - x)^2 + (y + b_1)^2 + z^2}; \\ r_3 &= \sqrt{(a_1 - x)^2 + (y - b_1)^2 + z^2}; & r_4 &= \sqrt{(a_1 + x)^2 + (y - b_1)^2 + z^2}; \end{aligned} \quad (\text{E.3})$$

and the rest of parameters we have also  $C_1 = -C_4 = a_1 + x$ ,  $C_2 = -C_3 = a_1 - x$ , and for the rest;  $d_1 = d_2 = y + b_1$  and also  $d_3 = d_4 = y - b_1$ . Similarly the the other components of the magnetic flux density we have:

Adding the different components of the magnetic flux density linearly polarized (oscillatory motion along a straight line) we can obtain the magnitude of such vector. Such value is represented in Fig. E.2.

$$|\mathbf{B}| = \sqrt{B_x^2 + B_y^2 + B_z^2} \quad (\text{E.4})$$

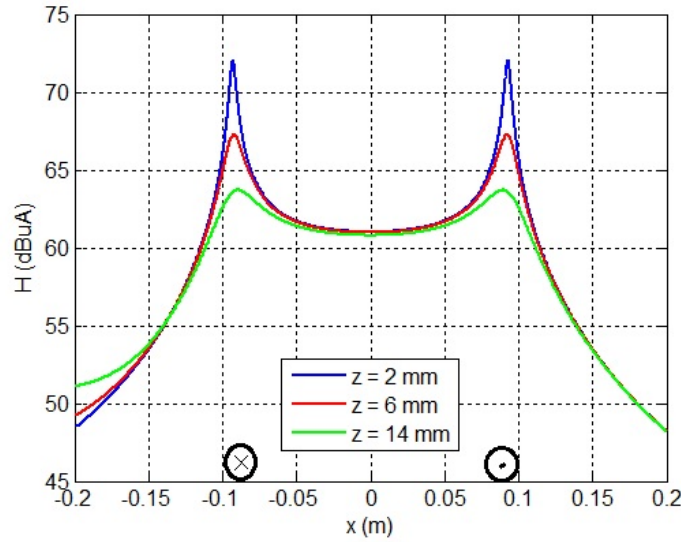


Figure E.2: Magnetic flux density at different distances  $z$  (2, 6, 8 mm) from the plane XY ( $Z = 0$ ) of the loop antenna at its center ( $y = 0$ ) and current  $I_o = 100$  mA.

The loop will induce a voltage at its terminals, that will depend on the electromotive force induced  $E = \omega AB e^{\omega t - \pi/2}$ . If we connect a load resistance  $R_L$  at the terminal of the resonant coil, the potential across the terminating resistance is:

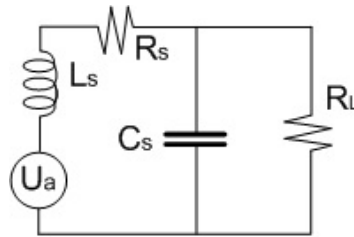


Figure E.3: Coil with induced voltage attached to a load  $R_L$ .

$$V_p = \frac{2\pi A}{\sqrt{\left(1 + \frac{R}{R_L}\right)^2 \left[ (CR)^2 + \left(\frac{L}{R_L}\right)^2 - 2LC \right] \omega^2 + (LC)^2 \omega^4}} f B_e e^{\{-j(\omega t + \theta)\}} \quad (\text{E.5})$$

that according to [124];

$$\theta = \tan^{-1} \left[ \frac{\omega(CR + L/R_L)}{(1 + R/R_L) - \omega^2 LC} \right] \quad (\text{E.6})$$

If one defines the sensibility of the coil by  $S = V_p/H$ , the frequency response of such magnitude would vary according to a low-pass characteristics as shown in Fig.E.4. Also shown the response dependence on the value of the capacitor from the resonant circuit.

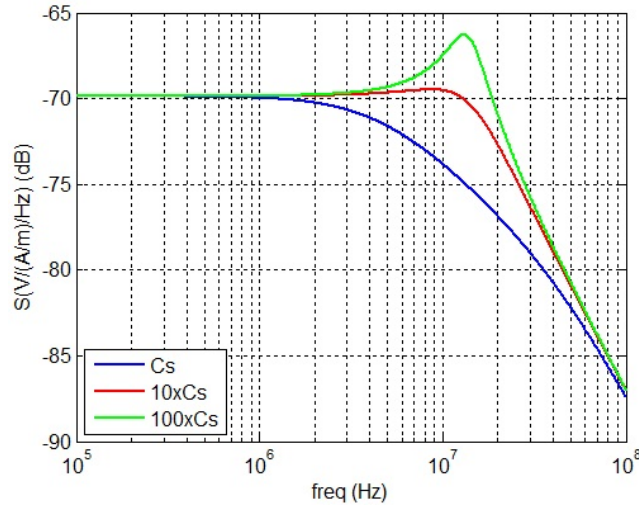


Figure E.4: Frequency response for the sensibility of the magnetic loop.

The magnetic induction that crosses the coil has been obtained from the previous analysis, thus depending upon the distance between the two coils, and the current circulating at the primary coil, one could monitor the induced voltage. In case we would account for discrete values of  $\mathbf{B}$ , around all the perimeter of

### Power to the load

For the WPT circuit, the important part is the amount of power that is transferred to the load (battery) from the secondary coil. So we must deduce an analytical expression that would help in predicting such power. A first step is to use the two-leakage inductance transformer equivalent model (Fig.E.5 b), and transform this initial circuit into an easier one to make the analysis.

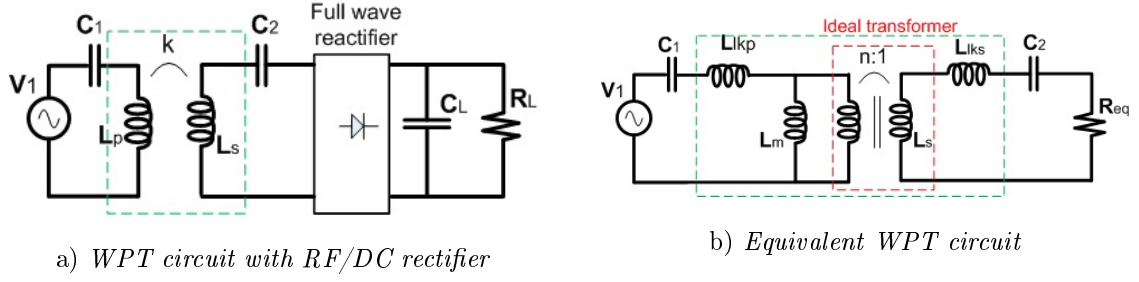


Figure E.5: Electrical circuit for the WPT system including full-wave rectifier.  $L_{lkp} = (1 - k)L_p = (1 - k)n^2L_s$ ,  $L_{lks} = (1 - k)L_s$  and  $L_m = k \cdot L_p$ .

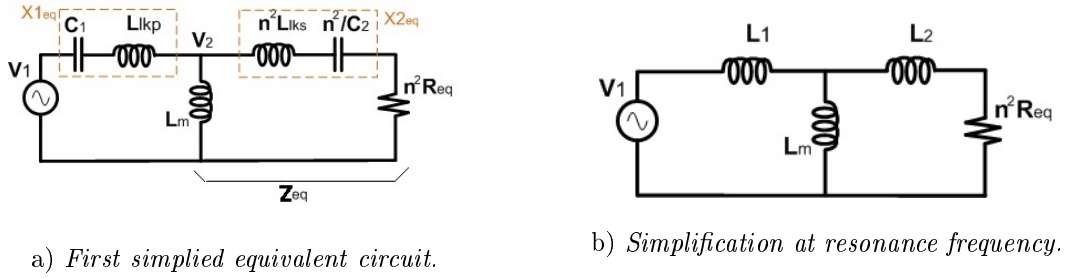


Figure E.6: Simplification on the previous WPT system.  $L_1 = L_{lkp}$ ,  $L_2 = -kn^2L_p$ .

From this first circuit it is possible even to reduce further by transforming the secondary into the primary side such as Fig.E.6 a), and finally if we considering the working conditions at the resonant frequency, with ideal matching and efficiency conditions, it is possible to reduce even further the circuit to the one depicted in Fig.E.6 b).

$$P_L = \frac{V_L^2}{R_L}; \quad \text{where} \quad V_L \Big|_{f_o} = V_2 \frac{n^2 R_{eq}}{|n^2 R_{eq} - j\omega L_p(1 - k - n^2)|}; \quad V_2 = V_1 \frac{Z_{eq}}{|Z_{eq} - j\omega L_p k|} \quad (\text{E.7})$$

$$Z_{eq} \Big|_{f_o} = \frac{j\omega k L_p [(n^2 R_{eq} + j\omega L_p(1 - k - n^2))]}{j\omega k L_p + n^2 R_{eq} + j\omega L_p(1 - k - n^2)} = \frac{j\omega k L_p [n^2 R_{eq} + j\omega L_p(1 - k - n^2)]}{n^2 R_{eq} + j\omega L_p(1 - n^2)} \quad (\text{E.8})$$

$$V_L \Big|_{f_o} = \frac{V_1 \cdot n^2 R_{eq}}{|n^2 R_{eq} + j\omega L_p(1 - k - n^2)|} \cdot \frac{j\omega L_p k [n^2 R_{eq} + j\omega L_p(1 - k - n^2)]}{|j\omega k L_p [n^2 R_{eq} + j\omega L_p(1 - k - n^2)] - j\omega L_p k [n^2 R_{eq} + j\omega L_p(1 - n^2)]|} \quad (\text{E.9})$$

$$V_L \Big|_{f_o} = V_1 \frac{L_p \omega (n^2 + k - 1) + j n^2 R_{eq}}{\omega L_p k} \quad (\text{E.10})$$

where  $V_L$  is the load voltage. In a symmetric WPT circuit, with equal values for the coils in the primary and secondary, the values have been simplified using;  $L_1 = -kL_p$ ,  $L_2 = -L_p(1 - k - n^2)$ , and  $L_m = kL_p$ , and in the case  $L_1 = L_2$  we would have  $n = 1$ .



# Bibliography

- [1] Z. Rashid, E. Peig, and R. Pour, “Bringing online shopping experience to offline retail through augmented retail and rfid,” *5th Int’l conference on Internet of Things (IoT)*, pp. 45–51, April 2015.
- [2] S. Pais and J. Symonds, “Data storage on a rfid tag for a distributed system,” *International Journal of UbiComp (IJU)*, vol. 2, April 2011.
- [3] B. Bacheldor, “Tego launches 32-kilobyte epc rfid tag,” <http://www.rfidjournal.com/article/view/4578>, 2009.
- [4] Ward, M. Kraneneburg, and R. Backhouse, “Rfid: Frequency, standards, adoption and innovation,” *JISC Technology and standards Watch*, <http://www.rfidconsultation.eu/docs/ficheiros/TSW0602.pdf>, pp. 1–36, 2007.
- [5] *Electromagnetic compatibility and Radio spectrum Matters (ERM); Radio Frequency Identification Equipment operating in the band 865 MHz to 868 MHz with power levels up to 2 W: Part 1: Technical requirements and methods of measurements*. ETSI EN 302 208: (V1.1.2).
- [6] “Operation within the bands 902-928 mhz, 2435-2465 mhz, 5785-5815 mhz, 10500-10550 mhz, and 24075-24175 mhz,” *FCC Title 47, Part 15*,.
- [7] J.-I. Cairo, J. Bonache, F. Paredes, and F. Martin, “Review of interference sources in congested environments and its effects in uhf-rfid systems,” *IEEE Journal of Radio Frequency Identification*, vol. 2, pp. 1–8, March 2018.
- [8] F. Paredes, J.-I. Cairo, S. Zuffanelli, G. Zamora, J. Bonache, and F. Martin, “Compact design of uhf rfid and nfc antennas for mobile phones,” *IET Microwaves, Antennas and Propagation*, vol. 11, pp. 1016–1019, May 2017.
- [9] J.-I. Cairo, J. Bonache, F. Paredes, and F. Martin, “Reconfigurable system for wireless power transfer (wpt) and near field communications (nfc),” *IEEE Journal of Radio Frequency Identification*, vol. 1, pp. 253–259, Dec. 2017.
- [10] J.-I. Cairo, J. Bonache, F. Paredes, and F. Martin, “Nfc system optimization for simultaneous powering and communication with wireless sensors,” *2019 European Microwave Conference in Central Europe (EuMCE)*, Oct. 2019.
- [11] S. Mou, Wu, J. R. Yang, and T. Y. Liu, “A transponder ic for wireless identification systems,” *Proc. 7th Int. Symp. Personal Indoor and Mobile Radio Commun. (PIMRC’96)*, vol. 1, pp. 238–241, 1996.
- [12] D. M. Dobkin, *The RF in RFID. Passive UHF RFID in Practice*. Elsevier, 2008.
- [13] A. Ghahremani, V. D. Rezaei, and M. S. Bakhtiar, “A uhf-rfid transceiver with a blocker-canceller feedback and +30 dbm output power,” *IEEE Transactions on Circuits and Systems*, Feb. 2013.

- [14] A. D. Droitcour, O. B. Lubecke, V. M. Lubecke, J. Lin, and G. T. A. Kovac, "Range correlation and i/q performance benefits in single-chip silicon doppler radars for non-coherent cardiopulmonary monitoring," *IEEE Transactions on Microwave Theory and Techniques*, vol. 52, pp. 838–848, March 2004.
- [15] V. Najafi, M. Jenabi, S. Mohammadi, and A. F. Ahmady, "A dual mode epc gen 2 uhf rfid transponder in 0.18 $\mu$ m cmos," *IEEE Int'l. Conference on Electronics, Circuits and Systems (ICECS)*, pp. 1135–1138, Aug. 2008.
- [16] C. Y. Yao and W. C. Hsia, "A -21.2-dbm dual-channel uhf passive cmos rfid tag design," *IEEE Transactions on Circuits and Systems*, vol. 61, pp. 1269–1279, April 2014.
- [17] N. E. Roberts and D. D. Wentzloff, "915mhz ultra low power receiver using sub-vt active rectifiers," *IEEE Subthreshold Microelectronics Conference (SubVT)*, pp. 1–3, 2012.
- [18] S. C. nad Hartmann and L. T. Claiborne, "Fundamental limitations on reading range of passive ic-based rfid and saw-based rfid," *IEEE International Conference on RFID*, pp. 41–48, March 2007.
- [19] N. M. Pletcher, S. Gambini, and J. M. Rabaey, "A 52 uw wake-up receiver with -72 dbm sensitivity using uncertain-if architecture," *IEEE International Solid State Circuits Conference (ISSCC)*, pp. 524–533, Feb. 2008.
- [20] R. Barnett, G. Balachandran, S. Lazar, B. Kramer, G. Konnail, S. Rajasekhar, and V. Drobny, "A passive uhf rfid transponder for epc gen 2 with -14dbm sensitivity in 0.13 $\mu$ m cmos," *IEEE International Solid-State Circuits Conference*, 2007.
- [21] J. W. Lee and B. Lee, "A long.range uhf-band passive rfid tag ic based on high-q design approach," *IEEE Transactions on Industrial Electronics*, vol. 56, pp. 708–714, July 2009.
- [22] C. Chelho, K. Y. Ham, K. T. Hun, B. K. Bae, and K. Jongbae, "Fully integrated ultra-low-power passive uhf rfid transponder ic," *IEEE International Symposium on Radio-Frequency Integration Technology*, pp. 77–80, Nov. 2011.
- [23] L. J. Wook, P. D. Ngoc, V. H. Thai, and D. V. Hao, "A fully integrated epc gen-2 uhf-band passive tag ic using an efficient power management technique," *IEEE Transactions on Industrial Electronics*, vol. 61, pp. 2922–2932, June 2014.
- [24] Q. Guo, Y. Zhai, X. Tan, and H. Min, "An on-chip configurable receiver with >55-db tx leakage suppression for uhf rfid reader," *IEEE Microwave and wireless components letters*, vol. 29, pp. 357–359, May 2019.
- [25] ETSI, EN, and 302-208-1, "Electromagnetic compatibility and radio spectrum matters (erm): Radio frequency identification equipment operating in the band 865 mhz to 868 mhz with power levels up to 2 w, part 1: Technical requirements and methods of measurement," July 2007.
- [26] M. S. Trotter and G. D. Durgin, "Survey of range improvement of commercial rfid tags with power optimized waveforms," *IEEE International Conference on RFID*, pp. 195–202, 2010.
- [27] K. Daeyoung, M. A. Ingram, and W. W. Smith, "Measurements of small-scale fading and path loss for long range rf tags," *IEEE Transactions on Antennas and Propagation*, vol. 51, pp. 1740–1749, Nov. 2003.
- [28] H. H. Xia, H. L. Bertoni, L. R. Maciel, A. L. Stewart, and R. Rowe, "Radio propagation characteristics for line-of-sight microcellular and personal communications," *IEEE Transactions on Antennas and Propagation*, vol. 41, pp. 1439–1447, Oct. 1993.
- [29] W. C. Jakes, *Microwave Mobile Communications*. New York: Wiley, 1974.

- [30] H. Yifeng, L. Qiang, and M. Hao, "System modeling and simulation of rfid," *Autoidlabs WP hardware 010*, 2005.
- [31] V. Pavel and K. V. S. Rao, "Theory and measurement of backscattering from rfid tags," *IEEE Antennas and Propagation Magazine*, pp. 212–218, Dec. 2006.
- [32] P. V. Nikitin, K. V. S. Rao, S. F. Lam, V. Pillai, R. Martinez, and H. Heinrich, "Power reflection coefficient analysis for complex impedances in rfid tag design," *IEEE Transactions Microwave Theory Techniques*, vol. 53, pp. 2721–2725, Sep. 2005.
- [33] U. Karthaus and M. Fisher, "Fully integrated passive uhf rfid transponder ic with 16.7 uw minimum rf input power," *IEEE Journal of Solid-State Circuits*, vol. 38, pp. 1602–1608, Oct. 2003.
- [34] H. M. Ouda, K. Waleed, and N. K. Salama, "Wide-range adaptive rf-to-dc power converter for uhf rfids," *IEEE Microwave and wireless components letters*, vol. 26, pp. 634–636, Aug 2016.
- [35] L. Zöschner, P. Herkees, J. Grosinger, U. Muehlmann, D. Amschl, and W. Bösch, "A differential threshold voltage compensated rf-dc power converter for rfid tag ics," *2017 International Workshop on Integrated Nonlinear Microwave and Millimeter-Wave Circuits INMMiC*, April 2017.
- [36] P. Nikitin and K. Rao, "Antennas and propagation in uhf rfid systems," *IEEE RFID conference*, April 2008.
- [37] "Alien homepage [online]." <http://www.alientechnology.com>.
- [38] M. White, "Radar cross-section: Measurement, prediction, control," *Journal of Electronics and Communication Engineering*, vol. 2, Nov. 2007.
- [39] G. D. Durgin, C. R. Valenta, B. M. Akbar, M. M. Morys, B. R. Marshall, and L. Yenpao, "Modulation and sensitivity limits for backscatter receivers," *IEEE International Conference on RFID*, pp. 124–130, 2013.
- [40] Yen, C. Chuan, A. E. Gutierrez, and D. Veeramani, "Radar cross-section analysis of backscattering rfid tags," *IEEE Antennas and Wireless Propagation Letters*, vol. 6, pp. 279–281, 2007.
- [41] L. Liu, B. You, and X. Wen, "An improved rf front-end of uhf rfid," *2010 International Conference on Microwave and Milimeter Wave Technology (ICMMT)*, pp. 1450–1452, May 2010.
- [42] J. G. Kim, S. Ko, S. Jeon, J. W. Park, and S. Hong, "Balanced topology to cancel tx leakage in cw radar," *IEEE Microwave and wireless components letters*, vol. 14, pp. 443–445, Sep 2004.
- [43] J. Lee, J. Choi, K. H. Lee, B. Kim, S. M. Moon, J. Y. Lee, S. Park, W. Kong, J. Kim, T. J. Lee, B. E. Kim, and B. K. Ko, "A uhf mobile rfid reader ic with self-leakage canceller," *IEEE Radio Frequency integrated Circuits (RFIC) Symposium*, pp. 273–276, 2007.
- [44] E. Global, *EPC radio-frequency identity protocols: Class-1 Generation-2 UHF RFID protocol for communications at 860 MHz - 960 MHz ver 1.0.9*. 2005.
- [45] AN2, *AN2 - Reflected RF level indicator*. AMS, 2012.
- [46] M. Soer, E. Klumperink, Z. Ru, F. E. van Vliet, and B. Nauta, "A 0.2-to-2.0 ghz 65 nm cmos receiver without lna achieving 11 dbm iip3 and 6.5 db nf," *IEEE International Solid State Circuits Conference (ISSCC)*, vol. 52, pp. 222–223, Feb. 2009.
- [47] L. Zhiheng, X. Tan, and H. Min, "A cmos passive mixer-first receiver front-end for uhf rfid reader," *IEEE 10th International COnference on ASIC (ASICON)*, pp. 1–4, Oct. 2013.

- [48] R. Chakraborty, S. Roy, and V. Jandhyala, "Revisiting rfid link budgets for technology scaling: Range maximization of rfid tags," *IEEE Transactions on Microwave Theory Tech.*, pp. 496–503, Feb. 2011.
- [49] *M66 05R1 SE24 LTE unwanted emissions vs. adjacent 863-870 MHz band*. 2012.
- [50] D. A. Cormos, T. Letertre, A. Diet, and A. Azoulay, "Electromagnetic environment of rfid systems," *IEEE Proceedings of the 37th European Microwave Conference (EuMA)*, pp. 1652–1655, Oct.. 2007.
- [51] *LTE; Evolved Universal Terrestrial Radio Access (E-UTRA); User Equipment (UE) radio transmission and reception*. ETSI TS 136 101, V10.7.0, 2012-07.
- [52] Ofcom, *LTE User Equipment coexistence with 862 - 870 MHz*. Research document, 2012.
- [53] H. C. Baker and A. H. Grone, "Digital computation of the mutual impedance between thin dipoles," *IRE Transactions on Antennas Propagation*, vol. 10, pp. 172–178, Mar. 1962.
- [54] Pavel, V. Nikitin, and K. V. S. Rao, "Effect of gen2 protocol parameters on rfid tag performance," *IEEE International Conference on RFID*, pp. 117–122, 2009.
- [55] Y. Tanaka, Y. Umeda, O. Takyu, M. Nakayama, and K. Kodama, "Change of read range for uhf passive rfid tags in close proximity," *IEEE International Conference on RFID*, pp. 338–345, 2009.
- [56] H. Yohima, Y. Tanaka, Y. Umeda, and O. Takyu, "Analysis of read range for uhf passive rfid tags in close proximity with dynamic impedance measurement of tag ics," *IEEE Radio and Wireless Symposium (RWS)*, pp. 110–113, Jan. 2001.
- [57] F. Fuschini, C. Piersanti, F. Paolazzi, and G. Falciasacca, "On the efficiency of load modulation in rfid systems operating in real environment," *IEEE Antennas and Wireless Propagation Letters*, vol. 7, pp. 243–246, 2008.
- [58] D. Gokhale, S. Sen, K. Chebrolu, and B. Raman, "On the feasibility of the link abstraction in (rural) mesh networks," *IEEE Proceedings in FOCOM*, pp. 61–65, April 2008.
- [59] S. Woo and H. Kim, "An empirical interference modeling for link reliability assessment in wireless networks," *IEEE Transactions on networking*, pp. 272–282, Feb. 2013.
- [60] AMS, *AS3993 UHF Single Chip Reader EPC Class 1 Gen2 Compatible*. AS3993 Datasheet EN v1: <http://www.maruwa-g.com/e/products/electronic-parts/000340.html>, 2014.
- [61] P. R. Foster and R. A. Burberry, "Antenna problems in rfid systems," *IEE Colloq. RFID Technolo.*, pp. 31–35, 1999.
- [62] P. Raumonon, "Folded dipole antenna near metal plate," *Proc. IEEE Antennas Propagat. Soc. Int. Symp.*, vol. 1, pp. 848–851, 2003.
- [63] J. D. Griffin, G. D. Durgin, A. Haldi, and B. Kippelen, "Rf tag antenna performance on various materials using radio link budgets," *IEEE Antennas and Wireless Propagation Letters*, vol. 5, pp. 247–250, 2006.
- [64] A. R. V. Hippel, *Dielectric Materials and Applications*. New York: Wiley, 1954.
- [65] H. Lehpamer, *RFID Design Principles*. 685 Canton Street, Norwood, MA 02062: Artech House Inc., 2008.
- [66] D. Dobkin and S. Weigand, "Environmental effects on rfid tag antennas," *IEEE Microwave Symposium Digest International (MTT-s)*, pp. 135–138, 2005.

- [67] K. Kurokawa, "Power waves and scattering matrix," *IEEE Transactions on Microwave Theory Tech.*, vol. 2, pp. 194–202, Mar. 1964.
- [68] K. Finkenzeller, *RFID Handbook: Fundamentals and Applications in Contactless Smart Cards and Identification*. John Wiley and Sons Inc. 2nd Ed., 1999.
- [69] M. Simon and D. Divsalar, "Some interesting observations for certain line codes with application to rfid," *IEEE Transactions on Communication*, vol. 54, pp. 583–586, 2006.
- [70] A. Lazaro, D. Girbau, and R. Villarina, "Effects of interferences in uhf rfid systems," *Progress in Electromagnetics Research*, pp. 425–443, 2009.
- [71] A. Piche, R. Perraud, and G. Peres, "Prediction by simulation of performances of rfid systems in aeronautic environments," *9th European Conference on Antennas and Propagation (EuCAP)*, pp. 1–5, 2015.
- [72] V. Lalitha and S. Kathiravan, "A review of manchester, miller, and fm0 encoding techniques." *Smart Computing Review*, vol. 4, no. 6, pp. 75–77, Dec. 2014.
- [73] M. C. Ltd, *FSF Series for NFC, Wireless Charger, RFID (Ferrite Foil FSF161)*. assessed 14, 2: <http://www.maruwa-g.com/e/products/electronic-parts/000340.html>, 2013.
- [74] B. Jiang, J. R. Smith, M. Philipose, S. Roy, K. S. Rajan, and A. V. Mamishev, "Energy scavenging for inductively coupled passive rfid systems," *IEEE Transactions on Instrumentation Measurement*, vol. 56, pp. 118–125, Feb. 2007.
- [75] A. Sharma, I. J. Zuazola, A. Gupta, A. Perallos, and J. C. Batchelor, "Non-uniformly distributed-turns coil antenna for enhanced h-field in hf-rfid," *IEEE Transactions on Antennas and Propagation*, vol. 61, pp. 4900–4907, Oct. 2013.
- [76] G. Vandevoorde and R. Puers, "Wireless energy transfer for standalone systems a comparison between low and high energy applicability," *Elsevier, Sensors and Actuators Annals of Physics*, vol. 92, pp. 303–311, Aug. 2001.
- [77] S. V. Georgakopoulos and O. Jonah, "Optimized wireless power transfer to rfid sensors via magnetic resonance," *IEEE Int'l Symposium on Antennas and Propagation (APSURSI)*, pp. 1421–1424, July 2011.
- [78] Karalis, J. D. Joannopoulos, and M. Solijacic, "Efficiency wireless non-radiative mid-range energy transfer," *Elsevier Annals of Physics*, pp. 34–48, Aug. 2008.
- [79] N. Kurs, A. Karalis, R. Moffat, and M. Soljagic, "Simultaneous midrange power transfer to multiple sevicees," *Applied Physics Letters*, vol. 96, 2010.
- [80] F. H. Raab, "Idealized operation of the class e tuned power amplifier," *IEEE Transactions on Circuits and Systems*, vol. 24, pp. 725–735, Dec. 1977.
- [81] N. O. Sokal and D. A. Sokal, "Class-e new class of high efficiency tuned single-ended switching power amplifiers," *IEEE Journal of Solid-State Circuits*, vol. 10, pp. 168–176, Oct. 1975.
- [82] H. Ali, T. J. Ahmad, and S. A. Khan, "Inductive link design for medical implants," *IEEE Symposium on Industrial Electronics and Applications (ISIEA)*, pp. 694–699, Oct. 2009.
- [83] W. L. Stutzman and G. A. Thiele, *Antenna Theory and Design*. New Jersey: Wiley, 2005.
- [84] L. C. Maxwell, *A Treatise on Electricity and Magnetism*. Osford: Clarendon, 3rd ed., 1892.
- [85] L. Youbok, *Antenna Circuit Design for RFID Applications - AN710*. Microchip, 2003.

- [86] C. Reinhold, P. Scholtz, W. John, and U. Hilleringmann, "Efficient antenna design of inductive coupled rfid systems with high power demand," *Journal of Communications*, vol. 2, Nov. 2007.
- [87] C. M. Zierhofer and E. S. Hochmair, "Geometric approach for coupling enhancement of magnetically coupled coils," *IEEE Transactions Biomedical Engineering*, vol. 43, pp. 2308–2316, 1996.
- [88] X. Chen, W. G. Yeoh, Y. B. Choi, H. Li, and R. Singh, "A 2.45-ghz near-field rfid system with passive on-chip antenna tags," *IEEE Transactions on Microwave Theory Tech.*, vol. 56, pp. 1397–1404, 2008.
- [89] K. Fotopoulou and B. W. Flynn, "Optimum antenna coil structure for inductive powering of passive rfid tags," *Proc. IEEE International Conference on RFID*, pp. 71–77, 2007.
- [90] C. Peters and Y. Manoli, "Inductance calculation of planar multi-layer and multi-wire coils: An analytical approach," *Elsevier*, pp. 394–404, 2007.
- [91] F. Grover, *Inductance calculations: Working Formulas and Tables*. New York: Dover Publications Inc., 1946.
- [92] M. Gebhart and R. Szoncsó, "Optimizing design of smaller antennas for proximity transponders," *IEEE Computer society, 2nd International Workshop on Near Field Communication*, pp. 77–82, 2010.
- [93] M. Drakaki, A. A. Hatzopoulos, and S. Siskos, "Cmos inductor performance estimation using z-and s-parameters," *IEEE International Symposium on Circuits and Systems*, pp. 2256–2259, 2007.
- [94] D. Rinner, H. Witschnig, and E. Merlin, "Broadband nfc - a system analysis for the uplink," *Communication systems, Networks and Digital Signal Processing, 2008 CNSDSP 6th International Symposium*, pp. 292–296, July 2008.
- [95] W. S. Lee, H. L. Lee, K. S. Oh, and J. W. Yu, "Switchable distance-based impedance matching networks for a tunable hf system," *Progress In Electromagnetic Research*, vol. 128, pp. 19–34, May 2012.
- [96] M. Gebhart, T. Baier, and M. Facchini, "Automated antenna impedance adjustment for near field communication (nfc)," *IEEE 12th International Conference on Telecommunications*, pp. 235–242, June 2013.
- [97] M. Waqas, A. Khan, L. Sydänheimo, T. Björninen, and L. Ukkonen, "Wirelessly poowered implantable system for wireless long-term monitoring of intracranial pressure," *2017 International Workshop on Antenna Technology (WAT)*, pp. 1–3, May 2017.
- [98] K. Sunkyu, K. Myunghoi, K. Kyoungchoul, A. Seungyoung, B. Bumhee, and K. Joungho, "Analytical expressions for maximum transferred power in wireless power transfer systems," *IEEE International Symposium on Electromagnetic Compatibility (EMC)*, pp. 379–383, Aug. 2011.
- [99] *System description wireless power transfer, Volume I: Low Power, Part 1: Interface definition*. Wireless Power Consortium, V1.1.2, June 2013.
- [100] L. Xun, C. K. Lee, and S. Y. Hui, "Optimal operation of contactless transformers with resonance in secondary circuits," *IEEE Applied power electronics conference and exposition APEC 2008*, pp. 645–650, Feb. 2008.
- [101] Nathao, O. Sokal, and A. D. Sokal, "Class e - a new class of high efficiency tuned single-ended switching power amplifiers," *IEEE Journal Solid State Circuits*, Jun. 1975.

- [102] R. R. Harrison, "Designing efficient inductive power links for implantable devices," *IEEE International Symposium on Circuits and Systems (ISCAS)*, pp. 2080–2083, May 2007.
- [103] T. H. Lee, *The Design of CMOS Radio-Frequency Integrated Circuits*, 2nd ed. Cambridge: Cambridge University Press, 2004.
- [104] *EPC Radio-Frequency Identification Protocols Class-1 Generation-2 UHF RFID Protocol for Communications at 860 MHz - 960 MHz, Version 1.2.0*. EPCglobal Inc., 2008.
- [105] I. Aoki, S. Kee, D. Rutledge, and A. Hajimiri, "Fully integrated cmos power amplifier design using the distributed active-transformer architecture," *IEEE Journal of Solid-State Circuits*, vol. 37, pp. 371–383, Mar. 2002.
- [106] S. Chiu, I. Kipnis, M. Loyer, J. Rapp, D. Westberg, J. Johansson, and P. Johansson, "A 900 mhz uhf rfid reader transceiver ic," *IEEE Journal of Solid-State Circuits*, vol. 42, pp. 2822–2833, Dec. 2007.
- [107] I. Kwon, Y. Eo, H. Bang, K. Choi, S. Jeonand, S. Jung, D. Lee, and H. Lee, "A single-chip cmos transceiver for uhf mobile rfid reader," *IEEE Journal of Solid-State Circuits*, vol. 43, pp. 729–738, March 2008.
- [108] P. B. Khannur, X. Chen, D. L. Yan, D. Shen, B. Zhao, M. K. Raja, Y. Wu, R. Sindunata, W. G. Yoeh, and R. A. Singh, "A universal uhf rfid reader ic in 0.18-um cmos technology," *IEEE Journal of Solid-State Circuits*, vol. 43, pp. 1146–1155, May 2008.
- [109] W. Wang, S. Lou, K. W. Chui, R. Rong, C. F. Lok, H. Zheng, H. T. Chan, S. W. Man, H. C. Luong, V. K. Lau, and C. Y. Tsui, "A single-chip uhf rfid reader in 0.18um cmos process," *IEEE Journal of Solid-State Circuits*, vol. 43, pp. 1741–1754, August 2008.
- [110] R. Zhang, C. Shi, and Z. Lai, "A single-chip uhf rfid reader transceiver for mobile applications," *IEEE International Wireless Symposium*, pp. 1–4, 2014.
- [111] L. Ye, H. Liao, F. Song, J. Chen, C. Shi, C. Li, J. Liu, R. Huang, J. Zhao, H. Xiao, R. Liu, and X. Wang, "A single-chip cmos uhf rfid reader transceiver for mobile applications," *Proceeding of ESSCIRC*, pp. 228–231, 2009.
- [112]
- [113] T. W. Rider, *Crosstalk and EMI on microwave circuit boards*. Manhattan, Kansas: Kansas State University, Thesis, 2017.
- [114] D. Wageningen and T. Staring, "The qi wireless power standard," *EPE 14th International power electronics and motion control conference*, pp. 25–32, 2010.
- [115] "Guidelines for limiting exposure to time-varying electric, magnetic, and electromagnetic fields," *International Commission on Non-Ionizing Radiation Protection [ICNIRP] Health Physics*, vol. 74, April 1998.
- [116] E. Strömer, M. Jurvansuu, T. Tuikka, A. Ylisaukko-oja, H. Rapakko, and J. Vesterinen, "Nfc-enabled wireless charging," *IEEE Computer society, 4th International Workshop on Near Field Communication*, pp. 36–41, 2012.
- [117] T. Sarkar, E. P. Caspers, M. S. Palma, and M. A. Lagunas, "Wireless power transfer versus wireless information transfer," *IEEE Microwave Symposium Digest International (MTT-s)*, pp. 1–3, June 2012.
- [118] D. Sievenpiper, "Experimental validation of performance limits and design guidenes for small antennas," *IEEE Transactions on Antennas and Propagation*, vol. 60, pp. 8–19, Jan. 2012.

- [119] M. Dionigi and M. Mongiardo, "Multi band resonators for wireless power tranfer and near field magnetic communications," *Proc. IEEE MTT-S International Microwave Workshop Series on Innovative Wireless Power Transmission: Technologies, Systems, and Applications*, pp. 61–64, 2012.
- [120] C. A. Balanis, *Antenna Theory Analysis and Design*. New York: John Wiley and Sons, Inc. 3rt Ed., 1998.
- [121] E. Waffenschmidt and T. Staring, "Limitation of inductive power transfer for consumer applications," *EPE 13th European Conference on Power Electronics and Applications*, pp. 1–10, Sep. 2009.
- [122] W. M. Frix, G. G. Karady, and B. A. Venetz, *Comparison of calibration systems for magnetic field measurement equipment*, vol. 9. 1994.
- [123] M. Misakian, "Equations for the magentic field produced by one or more rectangular loops of wire in the same plane," *Journal of Research of the National Institute of Standards and Technology*, vol. 105, pp. 557–564, Aug. 2000.
- [124] H. Ueda and T. Watanabe, "Several problems about sensitivity and frequency response of an induction magnetometer," *Science Report Tohoku University Geophysics*, vol. 22, pp. 107–127, 1975.